



Cape Peninsula
University of Technology

AN ASSESSMENT OF UAV-GENERATED DIGITAL ELEVATION MODEL USING GROUND SURVEYING TECHNIQUES

by

Thabani Thuse

Thesis submitted in fulfilment of the requirements for the degree:

MTech: Cartography

**Department of Civil Engineering and Geomatics
in the Faculty of Engineering & the Built Environment**

at the Cape Peninsula University of Technology

Supervisor: Mr. K. Musungu (CPUT)

Co-supervisor: Associate Professor P. A. Odera (UCT)

Bellville

February 2023

CPUT copyright information

The dissertation may not be published either in part (in scholarly, scientific or technical journals), or as a whole (as a monograph), unless permission has been obtained from the Cape Peninsula University of Technology.

Declaration

I declare that this research dissertation is my unaided work. It is being submitted for the MTech Degree at Cape Peninsula University of Technology, Cape Town. It has not been submitted before for any degree or examination at any other University.



(Signature)

Signed in Cape Town this ____20th____ day of ____February____ 2023

Abstract

The use of traditional surveying methods and instruments is common for the geodetic survey of the terrain surface. New technologies are currently being developed and utilised, for example, Unmanned Aerial Vehicles (UAVs) and their combination with a digital camera, also bring new opportunities to document earth's surface. This combination of technologies allows for low-cost digital photogrammetry to document the earth's surface in relation to already tested and adopted technologies. This thesis aims to evaluate the accuracy of the Digital Elevation Model (DEM) generated from aerial imagery obtained using low-cost UAVs by comparing it with the results for ground surveying techniques. The open field in the District 6 area in Cape Town was chosen as the test area. This open space field with its morphologically dissected surface and undulating terrain is ideal for testing the use of UAV photogrammetry to capture intricate surface details. The drone-based elevations were derived using UAV drone computer vision techniques. Using the UAV drone, the re-constructed camera positions and terrain features were used to derive ultra-high-resolution point clouds, ortho-photos and digital surface models from the multi-view UAV camera photos. A total number of 159 common points were compared, and a Root Mean Square Error (RMSE) of 0.338m (at 100m flight height), 0.078m (at 120m flight height) and 0.265m (at 140m flight height) for the vertical differences between the co-ordinates measured with the total station and the co-ordinates measured with a UAV drone were obtained. These residuals varied based on the elevations of the selected test points. It was found that the same points gave a RMSE of 0.050m (at 100m flight height), 0.046m (at 120m flight height) and 0.051 (at 140m flight height) on the X positions and a RMSE of 0.040m (at 100m flight height), 0.038m (at 120m flight height) and 0.052m (at 140m flight height) on the Y position for horizontal differences. The research conducted demonstrated that the accuracy of the model created from UAV photogrammetric data is similar to that of traditional ground survey techniques. From the selection of the test consisting of 159 points, nine points across all the 3 flights (100, 120 and 140 m) failed the conditions for the accuracy of the detailed points. These results indicate that combining a low-cost UAV and a digital camera may be a viable alternative for collecting data to document surface structures and form three-dimensional (3D) models. It is evident that several factors, including the terrain under investigation, flight configuration, flying height, sensor specifications, ground control distribution have a role to play in the final survey accuracy.

Acknowledgements

I would like to thank the following institutions and people for their contributions to this research project:

CPUT Civil Engineering and Geomatics Department made this study possible through the support and use of all the instruments and the software provided.

Mr. K. Musungu (Supervisor) for all the advice given throughout the years spent on this research project.

Associate Prof P. A. Odera (External Supervisor) for his technical guidance, help and advice with this project.

Mr Colin Geel (Pilot/Drone operator) and student assistants for all the help and time spent with the data acquisition and processing.

The City of Cape Town, GIS Department, for all the invaluable data necessary to execute this research.

Dr Gerald Du Preez for editing the thesis for submission to maintain the standard and quality as required by CPUT.

A special thank you to Luvo Maduna, Garth Chandler and Karabo Mothwagae for their invaluable assistance with the writing of this thesis.

My partner, "MaNgxabane", for all the support and understanding during this study.

My friends and family (special mention to my mom) for their support and encouragement during this study.

Most importantly, I would like to thank GOD for giving me the resources and energy to complete this study.

Table of Contents

DECLARATION	I
ABSTRACT.....	II
ACKNOWLEDGEMENTS	III
TABLE OF CONTENTS.....	IV
LIST OF TABLES	VIII
LIST OF FIGURES.....	IX
NOMENCLATURE.....	XI
<i>Greek letters</i>	<i>xi</i>
<i>Subscripts/superscripts</i>	<i>xi</i>
TERMS AND CONCEPTS	XII
CHAPTER 1 INTRODUCTION	1
1.1 CONTEXT AND MOTIVATION	1
1.2 RESEARCH PROBLEM	2
1.3 RESEARCH AIM, OBJECTIVES, AND OUTCOMES	2
1.3.1 <i>Objectives</i>	2
1.3.2 <i>Outcomes</i>	3
1.4 RESEARCH QUESTION	3
1.5 SIGNIFICANCE.....	3
1.6 DELINEATION	3
1.7 ORGANISATION OF THE DISSERTATION.....	4
CHAPTER 2 LITERATURE REVIEW AND THEORY	5
2.1 INTRODUCTION.....	5
2.2 DIGITAL ELEVATION MODEL.....	5
2.3 SATELLITE-BASED DEMS IN SOUTH AFRICA.....	7
2.3.1 <i>Global DEMS</i>	7
2.3.1.1 Shuttle Radar Topography Mission (SRTM).....	7
2.3.1.2 Advanced Spaceborne Thermal Emission and Reflection Radiometer (ASTER GDEM)	7
2.3.1.3 WorldDEM and Height10	8
2.3.1.4 Satellite Pour L’Observation de la Terre (SPOT DEM) (Elevation30)	8
2.3.1.5 Elevation8.....	9
2.3.1.6 TomTom DEM	9
2.3.2 <i>National DEMS</i>	9
2.3.2.1 Chief Directorate: National Geo-spatial Information (CD: NGI) 25 m DEM.....	9
2.3.2.2 SUDEM	9
2.3.2.3 SANSA 20 m DEM	10
2.3.2.4 ComputaMaps DEM	10

2.3.2.5	GISCOE 20 m DEM	10
2.3.3	Local and small area DEMs	10
2.3.3.1	Metropolitan DEMS.....	10
2.3.3.2	Eskom lidar data	10
2.4	WHAT ARE UAVS?	11
2.5	UAV PLATFORMS	12
2.6	UAV APPLICATIONS IN GEOMATICS.....	14
2.6.1	UAV Photogrammetry.....	14
2.7	HISTORICAL FRAMEWORK AND REGULATIONS.....	16
2.8	DRONE REGULATIONS: SOUTH AFRICA – CIVIL AVIATION REGULATION 101	18
2.8.1	Applications.....	18
2.8.1.1	Private RPA Operations	19
2.8.2	Commercial, Corporate, and Non-profit Operations	20
2.9	DATA ACQUISITION AND PROCESSING	21
2.10	FLIGHT PLANNING AND IMAGE ACQUISITION	21
2.11	PHOTOGRAMMETRIC UNMANNED AERIAL VEHICLES	23
2.11.1	Varieties of UAVs employed in photogrammetry.....	23
2.11.2	Flight Planning for UAV photogrammetry.....	23
2.12	GROUND CONTROL POINTS	26
2.13	UAV PHOTOGRAMMETRIC MEASUREMENTS UTILIZING UAVS FOR SURVEYING	26
2.14	UAV ACCURACIES APPLICATIONS.....	27
2.15	INSTRUMENTS/EQUIPMENT	27
2.16	DATA ACQUISITION, PROCESSING AND RESULTS	28
2.17	IMAGE/DATA ACQUISITION.....	31
2.17.1	Processing and validation of data	33
2.17.2	Results and analysis	33
2.18	DTM CREATION	38
2.19	TRADITIONAL SURVEYING METHODS.....	38
2.19.1	The theodolite and the evolution of the contemporary 'total station'	38
2.19.2	GPS techniques for DEM generation	39
2.20	ACCURACY ASSESSMENT OF A DEM.....	40
2.20.1	Deciding on sample points	40
2.20.2	Accuracy measures.....	41
2.21	DATA INTERPOLATION.....	41
2.21.1	Residual analysis and DEM accuracy.....	41
2.22	SUMMARY	43
CHAPTER 3	RESEARCH METHODOLOGY	45

3.1	INTRODUCTION.....	45
3.2	INSTRUMENTS AND SOFTWARE USED FOR RESEARCH	46
3.3	FIELD TESTING SITE DESCRIPTION.....	47
3.3.1	<i>Site Location</i>	47
3.4	PLANNING FIELD TESTING.....	48
3.4.1	<i>Control Planning</i>	48
3.4.2	<i>Establishment of RTK GPS Control at the Site</i>	49
3.4.3	<i>Test points</i>	51
3.4.4	<i>Preparation for the Total Station Survey</i>	52
3.4.5	<i>Flight Planning</i>	52
3.5	FIELD METHODOLOGY (DATA).....	56
3.5.1	<i>Traditional Survey</i>	56
3.5.2	<i>Flight</i>	57
3.5.3	<i>Processing and analysis of the data</i>	59
3.5.3.1	Trimble M3 Total Station and 5700 & 5800 series Trimble GPS base and rover data.....	59
3.5.3.2	UAV drone data (Image processing).....	59
3.6	DATA REDUCTION AND CALCULATIONS FOR TOTAL STATION AND GPS FIELD DATA.....	59
3.7	PHOTO ORTHO-RECTIFICATION, MOSAIC, DSM AND DEM OF UAV DATA.....	60
3.8	SHUTTLE RADAR TOPOGRAPHY MISSION DATA	64
3.9	LIDAR DATA	65
3.10	PRODUCT SPECIFICATION AND EXPECTED ACCURACIES	65
3.10.1	<i>DJI Phantom 4 Pro drone</i>	65
3.10.2	<i>Trimble M3 total station specifications</i>	67
3.10.3	<i>Trimble R8 GNSS Receiver</i>	68
3.11	SOFTWARE	69
3.12	PIX4D MAPPER.....	69
3.13	ARCGIS PRO.....	70
3.14	SUMMARY	70
CHAPTER 4	RESULTS.....	71
4.1	INTRODUCTION.....	71
4.2	TRADITIONAL SURVEY.....	71
4.2.1	<i>Total station field data</i>	71
4.2.2	<i>Results of Total Station Surveys</i>	73
4.3	PHOTOGRAMMETRIC DATA FROM UAV SURVEYS.....	74
4.3.1	<i>Image Processing</i>	74
4.3.2	<i>Point Cloud, Ortho-mosaic, and Digital Surface Model</i>	76
4.3.3	<i>Surface Model Points Extraction</i>	77

4.3.4	Results of the model accuracy assessment for the generated DEM.....	80
4.3.5	Results of the slope variation accuracy assessment.....	81
4.3.6	Results of the elevation variation accuracy assessment	87
4.4	ACCURACY ASSESSMENT OF UAV DEM AND OTHER SATELLITE-BASED DEMs.....	91
4.4.1	Absolute differences in height:.....	91
4.4.2	Relative differences in height:	95
4.5	POTENTIAL ERRORS IN THE COLLECTED DATA.....	99
4.6	SUMMARY	103
CHAPTER 5	DISCUSSION	104
5.1	INTRODUCTION.....	104
5.2	ACCURACY OF UAV-GENERATED DEM	104
5.3	THE EFFECT OF FLYING HEIGHT, SLOPE, AND TERRAIN VARIATIONS ON THE ACCURACY OF UAV DEM	105
5.3.1	Variation of flying height.....	105
5.3.2	Slope variations	106
5.3.3	Elevation variations.....	107
5.4	OUTLIERS	108
5.5	COMPARATIVE ANALYSIS OF UAV AND OTHER SATELLITE-BASED DEMs.....	109
5.5.1	Absolute comparisons of UAV, LiDAR and SRTM based on total station data	109
5.5.2	Relative comparisons between UAV, LiDAR and SRTM DEMs.....	109
5.6	CONCLUSIONS	110
CHAPTER 6	CONCLUSIONS AND RECOMMENDATIONS	111
6.1	FINAL CONCLUSIONS.....	111
6.2	RECOMMENDATIONS	112
6.2.1	Possible areas and outcomes for future research	112
REFERENCES.....		114
APPENDICES.....		121
APPENDIX A	DJI PHANTOM 4 DRONE UAV	121
APPENDIX B	TOTAL STATION DATASHEET	127
APPENDIX C	TRIMBLE GPS BASE AND ROVER 5700 & 5800 SERIES DATASHEET	128
APPENDIX D	M3 TOTAL STATION SURVEY REPORT.....	129
APPENDIX E	PIX4D REPORT 100M	221
APPENDIX F	PIX4D REPORT 120M	237
APPENDIX G	PIX4D REPORT 140M.....	252
APPENDIX H	EDITOR’S CERTIFICATE.....	267
APPENDIX I	PLAGIARISM REPORT.....	268

List of Tables

TABLE 2.1 FEATURES OF AERIAL, CLOSE RANGE AND UAV PHOTOGRAMMETRY	16
TABLE 2.2 COMPARISON BETWEEN GPS SURVEY AND UAV SURVEY	29
TABLE 3.1 MEASURED GROUND CONTROL POINTS	50
TABLE 3.2 PHANTOM 4 PRO SPECIFICATIONS	66
TABLE 3.3 TRIMBLE M3 DATASHEET	67
TABLE 3.4 TRIMBLE R8 GNSS RECEIVER	68
TABLE 4.1 DIFFERENCES IN X, Y AND Z BETWEEN TOTAL STATION AND UAV DEM DATA AT 100, 120 AND 140 FLIGHT HEIGHTS (ABSOLUTE)	81
TABLE 4.2 VARIATION OF DIFFERENCES BETWEEN TOTAL STATION AND UAV DEM DATA AT VARYING SLOPES AT 100 M FLIGHT HEIGHT	83
TABLE 4.3 VARIATION OF DIFFERENCES BETWEEN TOTAL STATION AND UAV DEM DATA AT VARYING SLOPES AT 120 M FLIGHT HEIGHT	85
TABLE 4.4 VARIATION OF DIFFERENCES BETWEEN TOTAL STATION AND UAV DEM DATA AT VARYING SLOPES AT 140 M FLIGHT HEIGHT	87
TABLE 4.5 VARIATION OF DIFFERENCES BETWEEN TOTAL STATION AND UAV DEM DATA AT VARYING ELEVATIONS AT 100 M FLIGHT HEIGHT	88
TABLE 4.6 VARIATION OF DIFFERENCES BETWEEN TOTAL STATION AND UAV DEM DATA AT VARYING ELEVATIONS AT 120 M FLIGHT HEIGHT	89
TABLE 4.7 VARIATION OF DIFFERENCES BETWEEN TOTAL STATION AND UAV DEM DATA AT VARYING ELEVATIONS AT 140 M FLIGHT HEIGHT	90
TABLE 4.8 ABSOLUTE DIFFERENCES IN HEIGHT BETWEEN TOTAL STATION, UAV DEM, LiDAR DEM AND SRTM DEM DATA AT 100, 120 AND 140M FLIGHT HEIGHTS AT GROUND SURVEYED POINTS.....	94
TABLE 4.9 RELATIVE DIFFERENCES IN HEIGHT BETWEEN UAV, LiDAR AND SRTM DEMS AT GRID POINTS AT 100, 120 AND 140M FLIGHT HEIGHTS	96
TABLE 4.10 VARIATION OF RELATIVE DIFFERENCES BETWEEN UAV, LiDAR AND SRTM DEMS AT VARYING SLOPES USING GRID POINTS 120M FLYING HEIGHT	97
TABLE 4.11: VARIATION OF RELATIVE HEIGHT DIFFERENCES BETWEEN UAV, LiDAR AND SRTM DEMS AT VARYING ELEVATIONS USING GRID POINTS 120M FLYING HEIGHT	98
TABLE 4.12: RELATIVE DIFFERENCES IN HEIGHT BETWEEN UAV, LiDAR AND SRTM DEMS AT GRID POINTS AT 100, 120 AND 140M FLIGHT HEIGHTS (RE-CALCULATED)	100
TABLE 4.13: VARIATION OF RELATIVE DIFFERENCES BETWEEN UAV, LiDAR AND SRTM DEMS AT VARYING SLOPES USING GRID POINTS 120M FLYING HEIGHT (RE-CALCULATED).....	101
TABLE 4.14 VARIATION OF RELATIVE HEIGHT DIFFERENCES BETWEEN UAV, LiDAR AND SRTM DEMS AT VARYING ELEVATIONS USING GRID POINTS 120M FLYING HEIGHT (RE-CALCULATED)	102

List of Figures

FIGURE 2.1: DEM AND DSM.....	6
FIGURE 2.2: AVAILABLE GEOMATICS TECHNIQUES, SENSORS AND PLATFORMS FOR 3D RECORDING PURPOSES, ACCORDING TO THE SCENE’ DIMENSIONS AND COMPLEXITY	12
FIGURE 2.3: TYPICAL ACQUISITION AND PROCESSING PIPELINE FOR UAV IMAGES	17
FIGURE 2.4: DIFFERENT MODALITIES OF THE FLIGHT EXECUTION DELIVER DIFFERENT IMAGE BLOCK’S QUALITY: A) MANUAL MODE AND IMAGE ACQUISITION WITH A SCHEDULED INTERVAL; B) LOW-COST NAVIGATION SYSTEM WITH POSSIBLE WAYPOINTS BUT IRREGULAR IMAGE OVERLAP; C) AUTOMATED FLYING AND ACQUISITION MADE ACHIEVED WITH A HIGH QUALITY NAVIGATION SYSTEM.....	22
FIGURE 2.5: A SCREENSHOT FROM EMOTION 2.0 FLIGHT PLANNING SOFTWARE UTILISED WITHIN FIELD TESTING	24
FIGURE 2.6: UAV FLIGHT METHODOLOGY: PREPARATION, RECORDING, POST-FLIGHT DATA PROCESSING, AND INFORMATION GENERATION.....	25
FIGURE 2.7: GROUND CONTROL AND CHECK POINT TARGET	28
FIGURE 2.8: CONTROL POINTS WHEN USED FOR IDENTIFICATION IN PHOTO SCAN SOFTWARE	29
FIGURE 2.9: COMPARISON BETWEEN GPS SURVEY AND UAV SURVEY	30
FIGURE 2.10: DISTRIBUTION OF THE USED GCPS	31
FIGURE 2.11: FLIGHT PLAN.....	32
FIGURE 2.12: SPARSE POINT CLOUD	34
FIGURE 2.13: DENSE POINT CLOUD.....	35
FIGURE 2.14: DIGITAL ORTHOPHOTO	36
FIGURE 2.15: GENERATED DIGITAL SURFACE MODEL	37
FIGURE 3.1: PROJECT WORKFLOW: PREPARATION, DATA COLLECTION, POST-FLIGHT DATA PROCESSING, AND INFORMATION GENERATION	45
FIGURE 3.2: AREA OF STUDY	47
FIGURE 3.3: EXISTING CONTROL POINTS OF THE STUDY AREA.....	48
FIGURE 3.4: STUDY AREA WITH GROUND CONTROL POINTS (GCP).....	49
FIGURE 3.5: TARGET PRE-MARKS	50
FIGURE 3.6: CHECK POINTS DISTRIBUTION, DIGITISED CONTOUR LINES.....	51
FIGURE 3.7: UAV FORECAST (FLIGHT PLANNER)	53
FIGURE 3.8: FLIGHT PLANNER - FLIGHT LINES, ANGLES, OVERLAPS (100M).....	55
FIGURE 3.9: FLIGHT PLANNER - FLIGHT LINES, ANGLES, OVERLAPS (120M).....	55
FIGURE 3.10: FLIGHT PLANNER - FLIGHT LINES, ANGLES, OVERLAPS (140M).....	56
FIGURE 3.11: LOCATION OF GROUND CONTROL POINTS USING GPS.....	58
FIGURE 3.12: SCREENSHOT OF THE PROCESSING OPTIONS FOR INITIAL PROCESSING WITHIN PIX4D	60

FIGURE 3.13: THE IMAGES IMPORTED IN PIX4D SOFTWARE (NB, THESE ARE APPROXIMATE COORDINATES)	61
FIGURE 3.14: SCREENSHOT OF THE PROCESSING OPTIONS FOR THE POINT CLOUD AND MESH CREATION.....	62
FIGURE 3.15: SCREENSHOT OF THE PROCESSING OPTIONS FOR THE DSM & ORTHO-MOSAIC CREATION.....	63
FIGURE 3.16: POINT CLOUD GENERATION FROM THE PIX4D SOFTWARE INITIAL ANALYSIS	64
FIGURE 4.1: SCREENSHOT OF THE POINT DATA FROM THE TOTAL STATION SURVEY AFTER BEING REDUCED INTO ARCGIS.....	71
FIGURE 4.2: SCREENSHOTS OF THE 3D TRIANGLE TIN AND CONTOUR DATA FROM THE TOTAL STATION SURVEY AFTER BEING COMPUTED INTO ARCGIS.....	72
FIGURE 4.3: SCREENSHOTS OF THE 3D TRIANGLE TIN AND CONTOUR DATA FROM THE TOTAL STATION SURVEY AFTER BEING COMPUTED INTO ARCGIS.....	73
FIGURE 4.4: DIGITAL TERRAIN MODEL OF THE TOTAL STATION	74
FIGURE 4.5: COMPARISON SECTION SCREENSHOT OF THE POINT CLOUD EDITOR SECTION OF THE PIX4D SOFTWARE PACKAGE	75
FIGURE 4.6: (A) ORTHO-MOSAIC OF THE COMPARISON AREA AT FLIGHT HEIGHT 100 M AND (B) DIGITAL SURFACE MODEL OF THE COMPARISON AREA AT FLIGHT HEIGHT 100M	76
FIGURE 4.7: (A) ORTHO-MOSAIC OF THE COMPARISON AREA AT FLIGHT HEIGHT 120 M AND (B) DIGITAL SURFACE MODEL OF THE COMPARISON AREA AT FLIGHT HEIGHT 120M	76
FIGURE 4.8: (A) ORTHO-MOSAIC OF THE COMPARISON AREA AT FLIGHT HEIGHT 140 M AND (B) DIGITAL SURFACE MODEL OF THE COMPARISON AREA AT FLIGHT HEIGHT 140M	77
FIGURE 4.9: SCREENSHOT OF DIGITISING OF POINTS PROCESS FROM ORTHOMOSAICS.....	78
FIGURE 4.10: DSM ELEVATION RANGES FOR FLIGHT 100M (10.0016M – 110.344M).....	78
FIGURE 4.11: DSM ELEVATION RANGES FOR FLIGHT 120M (11.1555M – 115.285M).....	79
FIGURE 4.12: DSM ELEVATION RANGE FOR FLIGHT 140M (13.1948M – 117.103M)	79
FIGURE 4.13: SLOPE MAP SHOWING 100M FLYING HEIGHT POINT VALUES.	82
FIGURE 4.14: SLOPE MAP SHOWING POINT VALUES, 120M FLYING HEIGHT	84
FIGURE 4.15: SLOPE MAP SHOWING POINT VALUES, 140M FLYING HEIGHT	86
FIGURE 4.16: SCREENSHOT OF SRTM DATA DOWNLOAD	92
FIGURE 4.17: SRTM ELEVATION DATA.....	93
FIGURE 4.18: LIDAR ELEVATION DATA.....	93
FIGURE 4.19: 30MX 30M GRID POINTS (FISHNET)	95
FIGURE 4.20: EXAMPLE OF OUTLIERS FROM THE 30X30M GRID FOR RELATIVE ACCURACY	99

Nomenclature

Greek letters

ω	omega – heading about the x axis
κ	Kappa - Rotation about the Z axis
ϕ	Phi - Rotation about the Y axis

Subscripts/superscripts

m/s	Meters Per Second
Cm	Centimetres
M	Metres
Km/h	Kilometres Per Hour
Mm	Millimetres
Kg	Kilograms
X & Y	Position on projected plane
Z	Height
Ha	Hectare

Terms and concepts

CP	Check Points
DEM	Digital Elevation Model
DSM	Digital Surface Model
DTM	Digital Terrain Model
EDM	Electronic Distance Measure
GCP	Ground Control Point
GCS	Ground Control Station
GNSS	Global Navigational Satellite Systems
GPS	Global Positioning System
GSD	Ground Sample Distance
IMU	Inertial Measurement Unit
LiDAR	Light Detection and Ranging
MSL	Mean Sea Level
RC	Remote Control
RMSE	Root Mean Square Error
RPAS	Remotely Piloted Aircraft Systems
RTK	Real Time Kinematic
SfM	Structure from Motion
TS	Total Station
UAS	Unmanned Aerial Structure
UAV	Unmanned Aerial Vehicle

CHAPTER 1

INTRODUCTION

Digital Elevation Model (DEM) is an essential topographic product and a requirement for various applications. However, traditional methods for obtaining DEM are expensive and time-consuming due to land surveys. Therefore, photogrammetry has been one of the primary technologies for generating DEM over time (Uysal et al., 2015). Recently, the airborne Light Detection and Ranging (LiDAR) system has become an excellent approach to creating a digital elevation model (DEM) due to its ability to capture three-dimensional data over a broad region with great precision and speed (Polat and Uysal, 2015). However, the primary disadvantage of human aerial platforms such as aeroplanes is that they are costly, particularly for small research regions. In recent decades, inexpensive Unmanned Aerial Vehicles (UAVs) have been employed to overcome this obstacle (Remondino et al., 2011). Due to their affordability, inspection, surveillance, reconnaissance, and mapping benefits, the use of UAVs is increasing (Remondino et al., 2011). As a result, the term UAV is extensively used in the fields of computer science and artificial intelligence. Nevertheless, terms such as Remotely Piloted Vehicle (RPV), Remotely Operated Aircraft (ROA), Remote Controlled (RC) Helicopter, Unmanned Vehicle Systems (UVS), and Model Helicopter are frequently employed (Eisenbeiss, 2004). In accordance with their size, endurance, range, and flying altitude, the Unmanned Vehicle Systems International Associations classify RC and model helicopters as tiny, close, short, and medium-range UAVs (Eisenbeiss, 2004, Remondino et al., 2011).

Due to their ability to accomplish complicated tasks in constrained locations, UAVs have experienced exponential growth in recent decades (Ruzgiene et al., 2015). The scientific community has made significant efforts to utilise their potential in applications like remote sensing, disaster response, surveillance, search and rescue, and atmospheric survey. Recent research has also been focused on the automatic creation of DEMs, including Digital Terrain Model and Digital Surface Model (DTM and DSM). Multiple variables, such as overlapping, flying altitude, and camera resolution, influence the typical processing pipeline for DEM creation. Variations in these parameters affect the model's final precision created, and numerous studies have examined this phenomenon (Hudzietz and Saripalli, 2011).

1.1 Context and Motivation

With the debut of UAVs and attempts to employ them as devices for topographical data collection, a discussion has emerged over the quality of derived products and the potential for their further use in geomatics applications. The DEM, which portrays the bare earth surface, is

one of the intended outputs. To extract DEM from drone photos, the point cloud must be filtered to exclude all points above the surface of the earth, according to (Zietara, 2014). Most available software packages accomplish this with cloud-based categorisation algorithms (Zietara, 2014). However, outcomes are frequently unsatisfactory, resulting in inaccurate DEM. (Ruiz et al., 2013) found that the final DEM accuracy depends on the positioning information, as the state-of-the-art DEM generating algorithms are susceptible to inaccuracies caused by Global Navigational Satellite Systems (GNSS) devices in the position measurements linked with each generated image. (Fonstad et al., 2013) found that developing topographic datasets has long been of interest and utility in the geomorphic sciences, including river sciences.

As a result, a variety of topographic measurement techniques have evolved. However, despite the variety of available techniques, creating a high-resolution, high-quality digital elevation model necessitates a substantial investment in staff time, technology, and software. Therefore, UAVs are widely utilised in land surveying (geomatics) to acquire DEMs and other information regarding the earth's surface (El Meouche et al., 2016). We will explore the applicability of an unmanned aerial vehicle (UAV) on an undulating terrain by capturing multiple aerial photographs with a DJI Phantom 4 drone. This study aims to assess the accuracy of the DEM generated from aerial imagery captured with a UAV by comparing ground surveying techniques and UAV drone aerial surveys for both horizontal and vertical precision.

1.2 Research Problem

A DEM comprises inherent errors resulting from the primary data collecting technique and processing methods for specific terrain and land cover type (Mukherjee et al., 2013). The accuracy of these datasets is frequently uncertain and inconsistent within each dataset. In South Africa, these UAV accuracies have not yet been compared to the traditional ground surveying techniques and conventional aerial photogrammetric standards.

1.3 Research Aim, Objectives, and Outcomes

1.3.1 Objectives

- To determine the accuracy of UAV-generated DEM using ground surveying techniques.
- To analyse the effect of slope, terrain, and flying height variations on the accuracy of UAV DEM.
- To compare UAV-generated DEM and freely available satellite and airborne-based DEMs.

1.3.2 Outcomes

- Accuracy of a UAV-generated DEM for both horizontal (x, y) and vertical position (Z) and potential applications based on the ranges.
- An optimal flying height for the UAV drone for enhanced accuracy & precision in various mapping applications.
- Appropriate slope, terrain, and land cover for improved accuracy in general applications.

1.4 Research Question

- What is the accuracy of UAV-generated DEMs?
- How does the slope of the survey area influence the accuracy of the DEM generated by a UAV for land surveying or general applications?
- Given the accuracy ranges, what are the possible applications of a UAV-generated DEM?
- How does the flight height change influence a UAV-generated DEM's accuracy?
- What are the key data collecting technologies currently employed for DEM creation, and what are their limitations?

1.5 Significance

A point cloud and a DEM created from imagery obtained with a DJI Phantom Drone has not yet been compared to conventional ground survey parameters. Two different points of the same position will be used to determine the accuracy and precision of a UAV-generated DEM compared to traditional ground survey techniques and to conclude if DJI Phantom UAV drone is a feasible instrument for the DEM generation. Three different flying heights were employed to identify the optimal flying height for achieving acceptable accuracy.

1.6 Delineation

In determining the accuracy of a DEM utilising a UAV DJI Phantom 4 professional drone, the following variables were not taken into account: Multiple factors, including camera resolution, GPS/INS device deviations, the change in temperature during the flight's time of day, wind speed, the influence of air pressure, the different seasons, and the differences between cameras with varying Ground Sample Distances, these have already been investigated by (Ruiz et al., 2013). However, the fundamental objective of this dissertation is to determine whether the workflow of the equipment, as mentioned above, is adequate for creating accurate and reliable DEMs, as well as how varying flight height affect the DEMs accuracy.

1.7 Organisation of the dissertation

The existing literature on UAVs and DEMs is described in Chapter 2 to assist this study. First, the history of UAVs is addressed, followed by the many UAV uses and platforms. Next, applications of UAV accuracy are examined, followed by the historical context and regulations. Data collection and processing are then addressed. Following this, apparatus and equipment utilised in prior experiments are discussed. The findings of earlier examinations are then discussed. Afterwards, a discussion of some experimental projects attempted in prior research follows. The supporting literature for model building and DTM creation is then discussed. Next, the merits, limits, and prospects of DTMs obtained using photogrammetric approaches are reviewed, and the evaluation of DTMs is derived from earlier research. In the final chapter, the prior research's conclusions are discussed. The third chapter discusses the approach and design for data collection. The statistical data and analysis of the study are presented in chapter 4. Chapter 5 discusses the results and analyses presented in chapter 4. Finally, the study's conclusions and recommendations are presented in the sixth chapter.

CHAPTER 2

LITERATURE REVIEW AND THEORY

2.1 Introduction

As part of this research, a literature review was conducted on several crucial aspects pertinent to evaluating a Digital Elevation Model generated by a UAV using ground surveying techniques. As reflected below, these key aspects include, among others: the definition of UAVs, uses in photogrammetric measurements, use in survey applications, traditional survey techniques, among others. These key aspects will allow for a better overall understanding of the topic area, which will assist in the field-testing approach and design

2.2 Digital Elevation Model

A DEM is an essential topographic product and a requirement for various applications. It is one of the most vital components of the GIS database. Traditional methods for creating DEMs are expensive and time-consuming due to the necessity of collecting ground data. Photogrammetry has become one of the primary methods for generating DEM over time (Uysal et al., 2015). Recently, the airborne Light Detection and Ranging (LiDAR) system has become an effective way to create a DEM due to its ability to collect three-dimensional data over a large area with great precision and time (Uysal et al., 2015). A DEM is a stereoscopic representation of the earth's surface that provides essential information about the terrain elevations (Gilani et al., 2014). Therefore, DEM may be regarded as the most effective method of terrain modelling as it is a grid-based matrix structure that implicitly illustrates the topological connections between data points (Guth, 2006). Terrain analysis utilises significant DEM-derived parameters, such as aspect, topographic index, slope, drainage area, and network, to extract spatial information (Ozturk et al., 2011). These are essential for numerous applications, including landform investigation, relief map creation, territory representation and mapping, and weather and meteorological research (Ozturk et al., 2011). The models' results rely on the accuracy of the DEM (Mukherjee et al., 2013). DEMs are created using photogrammetry, airborne laser scanning, radar interferometry, and topographic surveys (Muhadi et al., 2020). As with any spatial dataset, DEM is susceptible to various errors, such as gross error during data collection, inadequate orientation of stereo images with photogrammetrically determined elevation values, and obscure blends of errors (Blunders), which are inevitable (Mukherjee et al., 2011). Geographically, these errors depend on the terrain's status. Other aspects of DEM accuracies comprise grid spacing and interpolation modes (Patel et al., 2016)

A DEM depicts the variations on the earth's surface. The data can be stored in either raster or vector format, making it compatible with GIS integration. Levelling (surveying) or, more commonly, remote sensing techniques can be used to collect DEM data. Methods for remote sensing include LiDAR, synthetic aperture radar (SAR), and photogrammetry. A DEM can be divided into a digital surface model (DSM) or a digital terrain model (DTM). A DSM depicts elevations on the earth's surface, such as the tops of buildings and trees, whereas a DTM follows the natural terrain and disregards features (Verhulp, 2015).

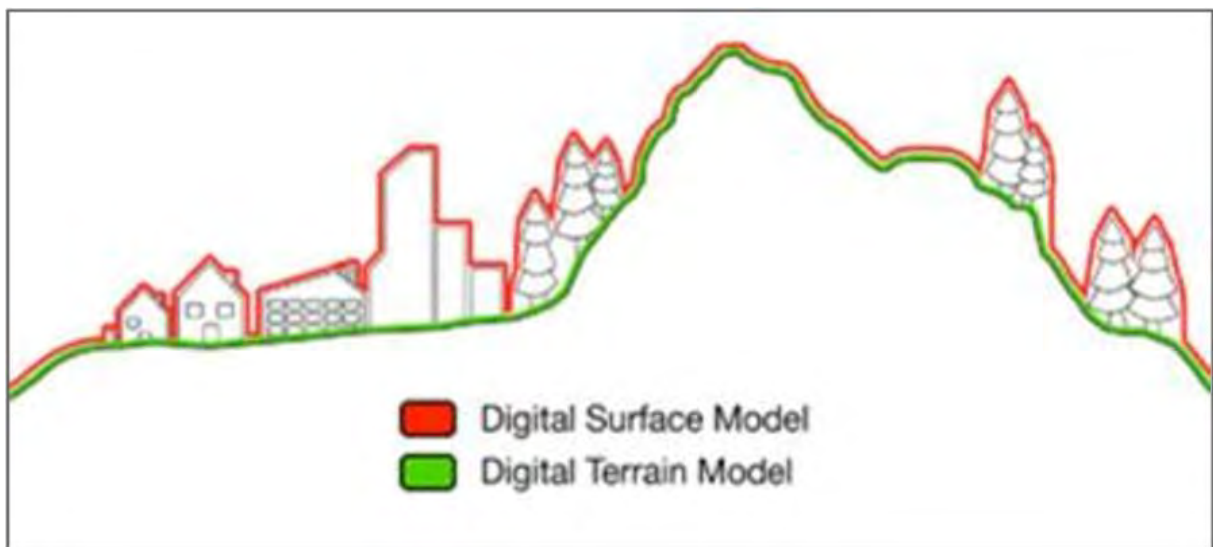


FIGURE 2.1: DEM AND DSM

SOURCE: GEOIMAGE.COM.AU

A DEM has primarily been used for ortho-rectification or as contours for the topographic maps. Thus, the DEM's accuracy, currency and resolution were determined to meet ortho-rectification standards (Singh et al., 2010).

2.3 Satellite-Based DEMs in South Africa

2.3.1 Global DEMS

2.3.1.1 Shuttle Radar Topography Mission (SRTM)

The National Geospatial-Intelligence Agency (NASA) and the German and Italian space agencies worked together to create the SRTM, (Bamler, 1990). The project aimed to create a free global (or near-global) DEM using radar interferometry. The original SRTM was available in the United States with a 30 m resolution and a 90 m resolution everywhere else. NASA released the global 30-m resolution (1-arcsecond) DEM in 2014; a report found that the current 1-arcsecond Level-2 product had an absolute (vertical) accuracy of 16 m and a relative (horizontal) accuracy of 6 m at a 90% confidence level (Bamler, 1990). Access the SRTM at <http://earthexplorer.usgs.gov/>.

The National Imagery and Mapping Agency (NIMA) and NASA collaborated on the Shuttle Radar Topography Mission (SRTM) to collect global elevation data sets (Rabus et al., 2002). STRM provides the highest available DEM resolution of the earth. It is based on the standard of interferometry Synthetic Aperture Radar SAR or Interferometric Synthetic Aperture Radar InSAR, which uses phase-difference estimates derived from two radar images. Quantitatively, the SRTM data's cartographic elements are examined over a roughly 30-by-30-meter grid. In addition, the product includes raster information that is consistent across a user-specified coverage region. As determined by the mission, the horizontal accuracy of the SRTM data is 20 metres, and the vertical accuracy is 16 metres, with a 90% confidence level. It applies to various monographs on geomorphology, topography, vegetation cover, tidal assessment, and urban investigations (Patel et al., 2016). SRTM data verification was performed utilising various altimetry data and DEMs. The SRTM data for this study were downloaded from <http://srtm.csi.cgiar.org>.

2.3.1.2 Advanced Spaceborne Thermal Emission and Reflection Radiometer (ASTER GDEM)

The Advanced Spaceborne Thermal Emission Reflection Radiometer Global DEM is a partnership between the Japanese Ministry of Economy, Trade, and Industry and NASA. Data from the ASTER are used to generate the DEM. The original DEM was released in 2009, followed by a second version in 2011, with a resolution of 1 arcsecond (30 m). Depending on the terrain, Version 2's RMSE vertical accuracy is between 6 and 15 metres, according to a study (Tachikawa et al., 2003). ASTER GDEM is available for free download at <http://gdem.ersdac.jspacesystems.or.jp/>.

The Japanese Ministry of Economy, Trade, and Industry (METI) and NASA developed the ASTER. It can acquire stereo images using its near-infrared spectral band for an along-track stereoscopic vision. The spatial resolution is 15 m, while the DEM created is 30 m. It encompasses areas between 83 N and 83 S. ASTER's absolute vertical accuracy is 20 metres with 95% confidence level (JPL, 2019). The improved vertical precision of ASTER, which was launched on October 17, 2011, is 8.86 metres (Mukherjee et al., 2013).

2.3.1.3 WorldDEM and Height10

A public-private partnership between the German Aerospace Centre and Airbus Defence and Space produced the WorldDEM. The DEM is derived from TerraSAR-X and TanDEM-X, two high-resolution Interferometric SAR satellites. WorldDEM offers three distinct products: an unedited DSM, an edited DSM, and a DTM. The DTM and edited DSM have a resolution of 12 m, with a vertical accuracy of 2 - 5 m relative and 10 m absolute at a 90% confidence level. The unrevised DSM is less accurate and frequently contains artefacts and voids. The DSM costs between €8 and €10 per kilometre (depending on whether it has been edited), while the DTM's price is unknown. Elevation10 is also derived from TerraSAR-X, but its resolution and accuracy are slightly higher at 10 m and 5 m, respectively. Depending on the product level, the price per kilometre for Elevation10 ranges from €16 to €30 (Verhulp, 2015).

The WorldDEM can be accessed at www.geo-airbusds.com/worlddem, and Elevation10 can be accessed at www.geo-airbusds.com/en/119-elevation10-custom-tailored-10-m-elevation-models-even-in-difficult-areas.

2.3.1.4 Satellite Pour L'Observation de la Terre (SPOT DEM) (Elevation30)

Elevation30 consists of three SPOT-5 satellite-derived elevation products. SPOT DEM and SPOT DEM Precision are level 1 and 2 DEMs derived from the satellite's high-resolution stereoscopic (HRS) instrument. Reference 3-D is a database that contains orthoimages in addition to a DEM. The SPOT DEM product has a resolution of 1 arcsecond (or 20 m after resampling) and an absolute vertical accuracy of 10 to 20 m with a 90% confidence level. SPOT DEM Precision has the same resolution but a 10 to 30 m accuracy (Verhulp, 2015). The Elevation30 DEM is available for purchase at www.geo-airbusds.com/en/6073-elevation30-products.

2.3.1.5 Elevation8

Another Airbus product, Elevation8, is a DEM derived from SPOT 6 and SPOT 7 optical satellites. The DEM is computed using tri-stereo acquisition to capture data in steep terrains. The DEM has an 8 m resolution, 2 to 10 m absolute vertical accuracy, and 3 m relative accuracy (Verhulp, 2015). Airbus offers Elevation8 at www.geo-airbusds.com/en/5409-elevation8.

2.3.1.6 TomTom DEM

TomTom sells a global DEM derived from SRTM and GTOPO data, with resolutions ranging from 20 to 300 metres. Unfortunately, no accuracy statement is available, but according to TomTom, the DEM can be used for mapping at a scale of 1:100,000 to 1:50,000 or smaller. While the DEM's primary purpose is to improve their maps' visual orientation and aesthetics, the DEM also has applications in analysis and planning (Verhulp, 2015). TomTom's website can be accessed at www.tomtom.com.

2.3.2 National DEMS

2.3.2.1 Chief Directorate: National Geo-spatial Information (CD: NGI) 25 m DEM

DEM covers approximately 66% of the country according to the CD: NGI. At a confidence level of 95%, a DEM derived from photogrammetric applications (i.e. stereo digital imagery) with a 25 m resolution (and 5 m contours) is accurate to within 3 m. There are also digitally captured 20 m contours from old hardcopy topographic maps, which are accurate to 11 m with a 95% confidence level (Verhulp, 2015). Both are freely accessible at www.ngi.gov.za.

2.3.2.2 SUDEM

Stellenbosch University has created the SUDEM, a national DEM. The DEM was produced by combining multiple sources of elevation data, namely large-scale contours, and spot heights. The SUDEM is available in three product grades. Levels 1 and 2 have a resolution of 5 m and an RMSE of 10,1 and 10,2 metres, respectively. Level 3 is a 2 m DSM whose absolute accuracy is estimated to be less than 1 m. (Van Niekerk, 2014). The price of the SUDEM varies based on product level and size. The SUDEM can be purchased through the website www.innovus.co.za/pages/english/technology/sudem.php.

2.3.2.3 SANSa 20 m DEM

This DEM was acquired through ComputaMaps in 2000 and is primarily used for orthorectification, hydrological modelling, and defining topographic variables (DEM derivatives). It was interpolated from contour vector lines and spot heights at a scale of 1:50 000 (20 m) and patched with SRTM90 (De Lemos, 2014). Limitations include artefacts caused by incorrectly assigned contour heights and unknown/undefined elevation accuracy (De Lemos, 2014). SANSa is accessible at www.sansa.org.za.

2.3.2.4 ComputaMaps DEM

In addition, ComputaMaps offers DTM and DSM products that can be generated on demand. Derived from Worldview and GeoEye stereo imagery, both DEMs have a 1 m resolution and an absolute vertical accuracy of 1 m (Verhulp, 2015). DEM can be ordered directly from ComputaMaps at www.computamaps.com.

2.3.2.5 GISCOE 20 m DEM

GISCOE was formerly referred to as GIMS. Using contours, spot heights, and trigonometric beacons digitised from the 1:50 000 map series, a 20 m DEM was created in 2000. The product contains no accuracy statement (Verhulp, 2015). The contact page for GISCOE is located at www.giscoe.com/contact.htm.

2.3.3 Local and small area DEMs

2.3.3.1 Metropolitan DEMS

Various provincial departments or metropolitans may have DEMs. An example is the 2700 km² DTM and DSM created from lidar data for the City of Cape Town. Nevertheless, very little is understood about regional DEMs in other metropolitan areas (Verhulp, 2015). The CD: NGI is currently investigating this matter.

2.3.3.2 Eskom lidar data

Eskom has collected elevation data from approximately 10,000 kilometres of lidar strips across the country. The LiDAR was captured with a vertical accuracy of 0.15 m and at least two points per m² (Verhulp, 2015). However, unknown is the precise location of the coverage.

2.4 What are UAVs?

Unmanned Aerial Vehicle (UAV) is a generic aircraft designed to fly without a pilot. Drone, Remotely Piloted Vehicle (RPV), Remotely Operated Aircraft (ROA), Micro Aerial Vehicles (MAV), Unmanned Combat Air Vehicle (UCAV), Small UAV (SUAV), Low Altitude Deep Penetration (LADP) UAV, Low Altitude Long Endurance (LALE) UAV, Medium Altitude Long Endurance (MALE) UAV, Remote Controlled (RC) Helicopter, and Model Helicopter are also terms frequently used. UAS (Unmanned Aerial System) refers to the entire system consisting of the aerial vehicle/platform (UAV) and the Ground Control Station (GCS). (Blyenburg, 1999) defines UAVs as uninhabited and reusable motorised aerial vehicles. (Sanna, 2005) defines UAVs as Uninhabited Air Vehicles. In the past, military objectives and applications primarily drove the development of UAV systems and platforms. The primary military objectives were unmanned inspection, surveillance, reconnaissance, and mapping of hostile territory (Watts et al., 2012). The first experience with Geomatics applications was conducted three decades ago, but only recently have UAVs in the Geomatics field become a common platform for data acquisition, figure. 2.2.

As (Colomina, 2008) and (Eisenbeiss, 2009) state, UAV photogrammetry offers a low-cost alternative to conventional manned aerial photogrammetry for large-scale topographic mapping or precise 3D ground data recording, in addition to being a valid supplement to terrestrial acquisitions. The recent success and advancements of unmanned aerial vehicles can be attributed to the proliferation of low-cost platforms coupled with amateur or Single Lens Reflex (SLR) digital cameras and GNSS/INS systems required to navigate the platforms, predict the acquisition points, and potentially perform direct geo-referencing. Although conventional airborne remote sensing still has some advantages and the tremendous advances in extremely high-resolution satellite imagery is closing the mapping gap between airborne and satellite applications, unmanned aerial vehicle (UAV) platforms are an essential alternative and solution for studying and exploring our environment, particularly for heritage sites or emergency response applications. Private companies are now investing in and offering photogrammetric products (primarily Digital Surface Models – DSM – and ortho-images) derived from UAV-based aerial images due to the use of flying unmanned platforms with variable dimensions and light weight. In addition, the high ground resolution enables flight operations to be conducted at a lower cost than conventional aircraft. Of course, there are still issues and limitations, but UAVs are a viable source of imaging data for various applications (Colomina and Molina, 2014).

2.5 UAV Platforms

The primary airframe types are fixed and rotary wings, and the most common launch/take-off methods, in addition to autonomous mode, are, air-, hand-, car/track-, canister-, and bungee cord launches. Depending on the on-board instrumentation, payload, flight autonomy, type of platform, and level of automation required for its applications, a typical UAV platform for geomatics can range in price from 1000 to 50,000 Euros (Remondino, 2009).

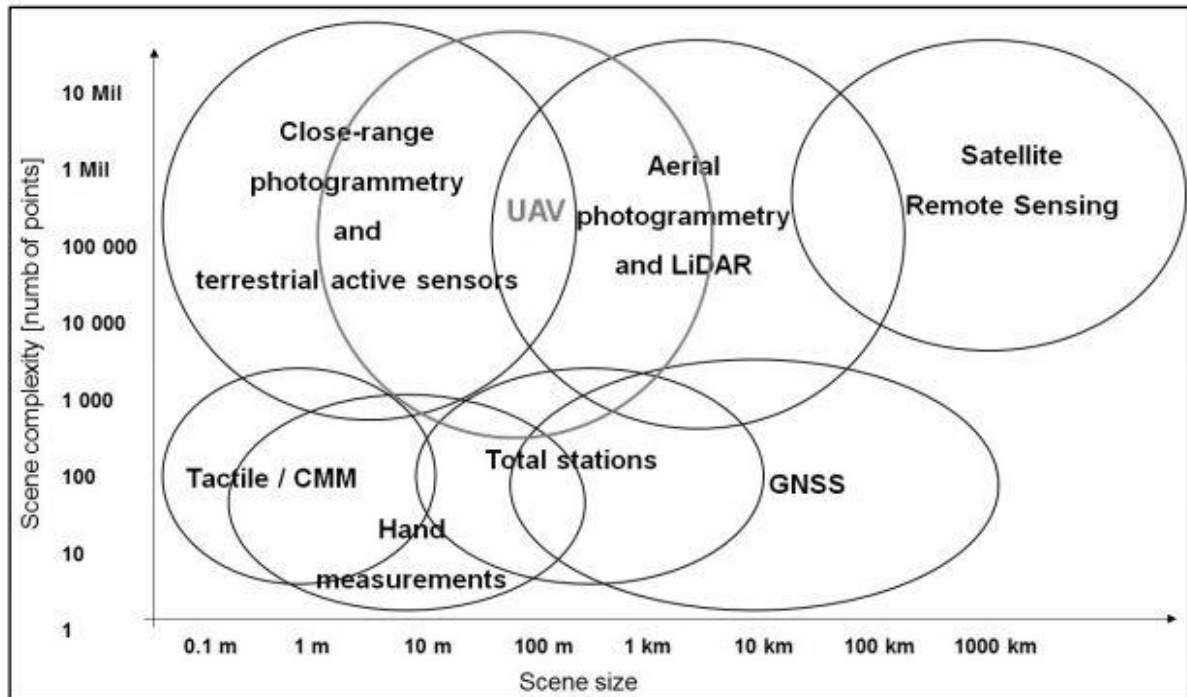


FIGURE 2.2: AVAILABLE GEOMATICS TECHNIQUES, SENSORS AND PLATFORMS FOR 3D RECORDING PURPOSES, ACCORDING TO THE SCENE' DIMENSIONS AND COMPLEXITY
SOURCE: REMONDINO ET AL., 2011

Typically, low-cost solutions are incapable of autonomous flight and require human assistance during take-off and landing, (Vallet, 2011). In previous research, inexpensive and open-source platforms and toolkits were presented (Remondino et al., 2011). Simple and hand-launched UAVs that perform autonomous flights using MEMS-based (Micro-Electro-Mechanical Systems) or Coarse Acquisition (CA) code GPS for the autopilot are the cheapest systems, according to (Vallet, 2011), although stability in windy areas may be an issue. Larger and more stable systems, typically based on an Internal Combustion Engine (ICE), have longer endurance than electric engine UAVs and, due to their higher payload, can carry format (reflex) cameras, LiDAR, or SAR instruments, (Grenzdoffer, 2012). In the robotics, aeronautical, and optical communities, breakthrough solutions are sought to miniaturise optical systems, increase payload, achieve fully autonomous navigation, and enhance flying performances,

(Schaeffer, 2009). Researchers have also examined flying invertebrates to comprehend their mobility, obstacle avoidance, and autonomous landing and take-off capabilities, (Moore et al., 2007).

UAV International defines three primary UAV categories based on size, weight, endurance, range, and flying altitude, (Remondino et al., 2020)

- *Tactical unmanned aerial vehicles* consist of micro, mini, close-, short-, medium-, and medium-range endurance, low-altitude deep penetration, low-altitude long endurance, and medium-altitude long-endurance systems. The mass ranges from a few kilogrammes to one thousand kilogrammes, the range from a few kilometres to five hundred kilometres, the flight altitude from a few hundred metres to five kilometres, and the endurance from a few minutes to two or three days.
- *Strategic UAVs*, including high altitude long endurance, stratospheric and exo-stratospheric systems that fly above 20,000 m altitude and have a 2 to 4-day endurance.
- *UAVs designed for special tasks*, such as unmanned combat autonomous vehicles and lethal and decoy systems.

According to their engine/propulsion system, UAVs for geomatics applications can be categorised briefly as:

- Non-powered platforms, such as balloons, kites, gliders, and paragliders.
- Powered platforms, such as airships, gliders, propellers, electric motors, and internal combustion engines.
- Alternately, they could be categorised based on their aerodynamic and "physical" characteristics as:
 - lighter-than-air, such as a balloon or an airship
 - rotary-wing, either electric or powered by an internal combustion engine, such as single-rotor, coaxial, Quadrocopter, and multi-rotor aircraft.
 - fixed-wing aircraft, either unpowered, electric, or powered by a combustion engine, such as gliders or high-wing aircraft (Zhang et al., 2022).

2.6 UAV Applications in Geomatics

Civil UAV applications are discussed in reports on UAV projects, regulations, classifications, and mapping applications. Typical applications for UAV images and photogrammetrically derived DSM or orthoimages include the following:

Agriculture: producers can make dependable decisions to save money and time (e.g., precision farming), obtain a quick and accurate record of damages or identify potential issues in the field Newcombe (2007).

Forestry: accurate assessments of woodlots, fire surveillance, vegetation monitoring, species identification, volume computation, and silviculture, (Berni et al., 2009).

Archaeology and architecture: Low-altitude image-based methods can be used for 3D surveying and mapping of sites and man-made structures. (Rinaudo, 2012).

Environment: rapid and inexpensive regular flights enable land and water monitoring at multiple epochs, road mapping, cadastral mapping, thermal analyses, excavation volume computation, and volcano monitoring. (Smith, 2009) or natural resource documentations for geological analyses are also viable options.

Emergency management: Unmanned aerial vehicles (UAVs) can rapidly acquire images for early impact assessment and rescue planning. (Molina, 2012). The flight can be conducted over contaminated regions without endangering pilots or necessitating extensive pre-flight operations.

Traffic monitoring: surveillance, travel time estimation, trajectories, lane occupancy, and incident response data are the most crucial, (Puri, 2007).

Frequently, UAV images are combined with terrestrial surveying to create orthoimages and close any potential 3D modelling gaps. (Remondino, 2009).

2.6.1 UAV Photogrammetry

Since the early 2000s, the use of UAVs to capture photogrammetric images has expanded rapidly. (Esenbein, 2009) enumerates various UAVs capable of capturing photogrammetric images, such as balloons, hang gliders, paragliders, kites, gliders, rotor-kites, airships, propellers, jet engines, single rotors, coaxial, quad-rotors, and multi-rotors. Since the turn of the 21st century, fixed-wing and multi-rotor UAVs have been the most utilised and developed for photogrammetric purposes (Haarbrink, 2011). The advantages of fixed-wing UAVs are their durability, simplicity of design, and extended flight duration (usually around 40-60 minutes). However, fixed-wing UAVs have the disadvantage that photographs can only be taken from a vertical (or plane view) perspective and that high wind speeds will affect the flight path and

may cause the captured image to tilt off vertical. With recent advancements in electronic motor technology, multi-rotor UAVs have advanced rapidly. They may have four or more rotor blades, with half spinning in a clockwise direction and the other half in a counter-clockwise direction. Reducing a specific rotor's engine speed will give the operator precise control over the UAV. The camera is mounted to the bottom of the UAV with a camera mount, and this mount can be adjusted so that the camera always faces directly down, or it can be moved to take photographs from various angles, allowing the sides of objects to be captured more precisely. Among the disadvantages of multirotor UAVs is the short battery life of the rotor engines, which limits flight duration.

UAVs have become a substitute for traditional photogrammetry. Many changes have occurred in the photogrammetry field due to replacing traditional aircraft with a pilot with unmanned aircraft. First, photographing has evolved significantly. Considering flight height, endurance, higher platform instability, and the type of onboard camera as its numerous benefits, disadvantages could be identified compared to conventional methods. It is believed that UAV photogrammetry bridges the gap between traditional and terrestrial close-range photogrammetry enabled by laser scanners. Nonetheless, a sizeable minority views UAV platform as the sole supplement to conventional methods. The comparison between close-range, aerial, and UAV photogrammetry is presented in Table 2.1.

TABLE 2.1 FEATURES OF AERIAL, CLOSE RANGE AND UAV PHOTOGRAMMETRY

Source: (Eisenbein, 2009)

	Aerial	Close Range	UAV
Planning	automatic, semi-automatic	manual	automatic, semi-automatic, manual
Data acquisition/flight	assisted, manual	autonomous, assisted, manual	autonomous, assisted, manual
Size of the area	km ²	mm ² - m ²	m ² - km ²
Image resolution/GSD	cm - m	mm - dm	mm - m
Distance to the object	100 m – 10 km	cm – 300 m	m - km
Orientation	normal, (oblique)	normal, oblique	normal, oblique
Absolut accuracy of the initial orientation values	cm - dm	mm - m	cm -10 m
Image block size/number of scans	10-1000	1-500	1-1000
Special applications	large scale areas (mapping, forestry, glaciology, 3D city modelling)	small scale areas and objects (architectural and industrial photogrammetry)	small and large scale areas, also inaccessible areas and dangerous objects)

In addition to the table, it could be stated that UAV flights appear to be more cost-effective, accessible, and simple to deploy than conventional measurement techniques. They are less reliant on the weather and enable the acquisition of vertical, oblique, and targeted images during a single flight mission. However, due to the lower flight altitude and the smaller size of the CCD matrices in the camera, many more photographs are required to cover the same area as aerial imagery, (Eisenbein, 2009).

2.7 Historical Framework and Regulations

UAVs were initially designed for military applications, with flight recognition in enemy territory and without risk to pilots. The first experiments with civil and Geomatics applications were conducted at the end of the 1970s. Their use has increased dramatically over the past decade due to rapid advancements in platforms, communication technologies, and software and the expansion of possible applications. Thus, using such flying platforms in civil applications is mandated to increase the safety of UAV flights and protect humans from harm. Consequently, the international community began defining UAV security criteria several years ago. Several national and international associations are analysing the operational safety of UAVs due to the widespread adoption and commercialization of new UAV systems. One or more autonomous authorities administer each country's UAV regulations. Due to the lack of cooperation between these authorities, it is challenging to describe the specific objectives of each of them without

sacrificing generality. The primary objective of the elements of UAV regulations is to increase the dependability of the platforms, emphasising the need for safety certifications for each platform and ensuring public safety. In most countries, these regulations are continually evolving. As technological advancements and safety standards condition them, the same rules and certifications should be applied to comparable manned aircraft. Due to the unmanned nature of UAVs, however, the citizens' security in the event of an impact is the most pressing concern. Figure 2.3 depicts a unique image acquisition and processing procedure for UAVs.

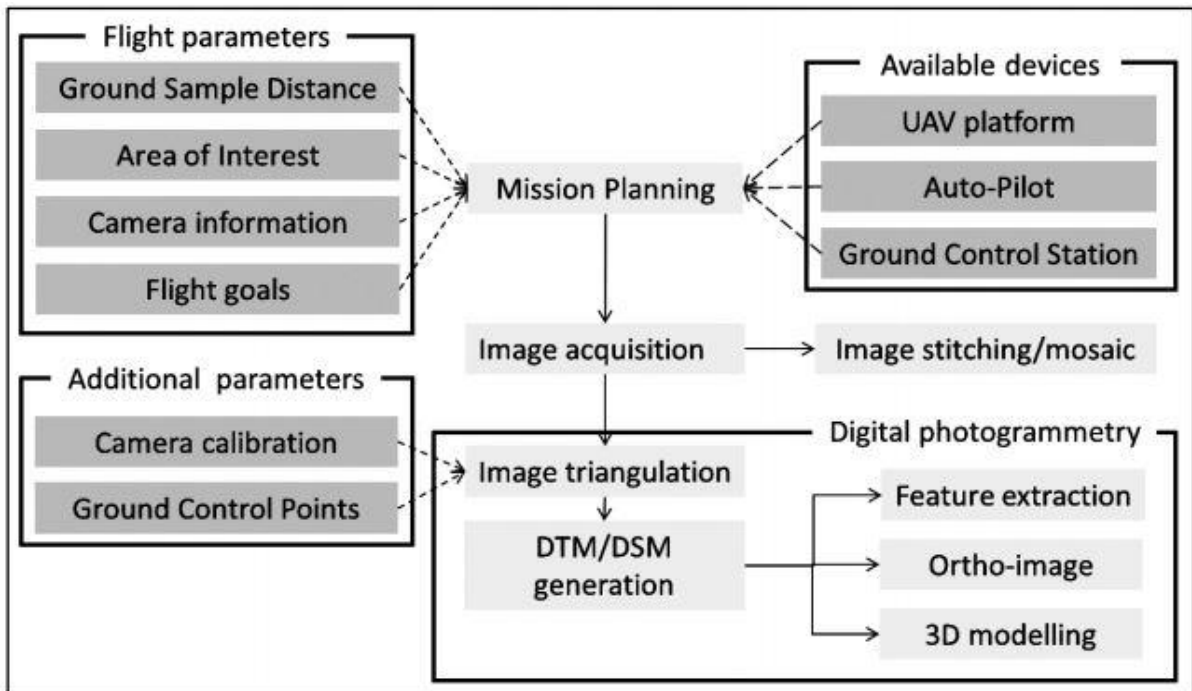


FIGURE 2.3: TYPICAL ACQUISITION AND PROCESSING PIPELINE FOR UAV IMAGES

Source: Remondino et al., 2011

UAVs' safety levels vary based on size, weight, and onboard technology. Due to this, the rules applicable to each UAV cannot be identical across all platforms and categories. For instance, in the United States, safety is defined by its use (public or civic), whereas in Europe, it is defined by its weight; this parameter is directly related to the amount of damage it can cause in a collision. Other restrictions include minimum and maximum altitude, maximum payload, and surveying area. In addition, the indirect control of a pilot by the GCS may increase the number of accidents caused by human error. For this reason, UAV operators must have training and credentials in several nations.

2.8 Drone regulations: South Africa – Civil Aviation Regulation 101

South Africa's Ministry of Transportation and Civil Aviation Authority (CAA) recently added a chapter on remotely piloted aircraft systems (RPAS) to the Civil Aviation Regulations and issued supplementary documents, such as technical standards and aeronautical information circulars. Under these laws and standards, South Africa permits private, commercial, corporate, and non-profit RPAS operations. While some rules and restrictions are universally applicable, the level of technical and operational requirements appears to be partially dependent on the form of operation, with private operation on one end and all other forms on the other. For example, conducting a private operation is only permitted with a Class-1A or Class-1BRPAS, 400 feet above the ground, and within the line of sight of the operator; these rules do not apply to or may be waived for other types of operations. These private operations are exempt from various requirements applicable to other operations, such as obtaining a letter of approval and a registration certification, a remote pilot licence, and an RPA operator certificate. The level of restrictions is also proportional to the operation's complexity. Operations are subject to stricter regulations in a controlled airspace and beyond the visual line of sight.

The CAA is the regulatory agency for RPAS. Its responsibilities include acting on aviation regulations, establishing safety and security standards, issuing all necessary licences and permits, and developing enforcement mechanisms to ensure compliance with applicable laws and regulations.

2.8.1 Applications

The Civil Aviation Regulations apply to Class-1 and Class-2 RPA, as well as their owners, operators, pilots, and those responsible for their maintenance. An RPA is "an unmanned aircraft piloted remotely, excluding model and toy aircraft." The SA-CATS defines these RPA classes, including their weight. Class-1 and Class-2 RPAs are further subdivided into subclasses: Class-1A (weighing less than 1.5 kilograms/3.3 pounds), Class-1B (weighing less than 7 kilograms/15.4 pounds), and Class-1C and Class 2A (weighing less than 20 kilograms/44 pounds). The regulations do not apply to the following:

- autonomous unmanned aircraft, unmanned free balloons and their operations, and other types of aircraft that cannot be managed in real-time during flight
- aircraft operated following Part 94 of the Civil Aviation Regulations (which governs the operation of "Non-type Certified Aircraft");
- model aircraft;
- toy aircraft

The regulations authorise different uses of RPA. RPA can be utilised for private, commercial, corporate, and charitable purposes.

2.8.1.1 Private RPA Operations

A private operation is "using an RPA for a person's personal and private purposes in the absence of any commercial outcome, interest, or profit." Private operations are subject to particular constraints. They may only be conducted with a Class-1A RPA (weighing less than 1.5 kilogrammes) or Class-1B RPA (weighing less than 7 kilogrammes), which may exceed 400 feet above the ground. All private operations must be conducted within a restricted visual line of sight (R-VLOS), which is defined as "within 500 metres of the remote pilot and below the height of the tallest obstacle within 300 metres of the RPA, in which the remote pilot maintains direct unaided visual contact with the RPA to manage its flight and meet separation and collision avoidance responsibilities." In addition, RPA may only be operated over the operator's property or with the owner's permission over other property. The Regulations also impose restrictions on particular RPA applications. An RPA is not permitted to tow another aircraft, perform aerobatic or aerial displays, or fly in formation or swarm. It may not be flown within a 10-kilometre (6.2-mile) radius of an airfield, within restricted or prohibited airspace, or above or near a sensitive area, such as a nuclear power plant, a correctional facility, a police station, a crime scene, or a court. No RPA may be flown directly overhead or within a person's 50 metres (164 feet). It cannot be utilised to release, dispense, drop, deliver, or deploy an object or substance. Its use is confined to daytime and in good weather. Private RPA operations are exempt from several regulations that apply to other RPA operations. For example, rules regarding the need for approval and registration of an RPA prior to operation, personnel licencing requirements, and RPA operator certificate and maintenance requirements do not apply to private RPA operations (for more information on these requirements, see Part II(C) below). In addition, they are exempt from regulations governing the transport of dangerous goods and safety considerations (such as ensuring that an RPA is in a "flyable condition").

In addition, they are exempt from regulations regarding the recording and reporting of flight time, as well as the use of flight logbooks, power reserves, first-aid kits, and hand-held fire extinguishers.

2.8.2 Commercial, Corporate, and Non-profit Operations

There are numerous restrictions on commercial, corporate, and non-profit RPA operations.

1. Authorization and Registration

In South Africa, an RPA may not be used for non-private purposes unless the CAA Director has issued the operator an RPA letter of approval (RLA) and a registration certificate. For the Director to issue an RLA, the applicant must submit

- documentation regarding the standard to which the RPAS was designed,
- equivalent documentation demonstrating a level of safety acceptable to the Director; or
- documentation demonstrating system safety following Document SA-CATS 101.

Initial approval of an RPA requires the submission of the manufacturer's operating manual and the following information for Class-1 and Class-2 operations:

- RPAS type
- RPA structure
- RPA composition
- flight envelope capability
- RPA dimensions/measurements and weight in addition to drawings
- mass and balance
- specific or generic payloads
- utilisation of frequencies
- ground support equipment
- flight recovery system
- remote pilot station

The submission must also contain the following information regarding the RPA's performance characteristics:

- maximum altitude
- maximum endurance
- maximum range
- Airspeed (take-off, cruise, landing, stall, maximum)

- maximum rate of climb
- maximum rate of descent
- maximum bank angle
- turn rate limits

propulsion system such as engine/motor, fuel, electrical, hydraulic, pneumatic, gas, solar
<http://www.sacaa.co.za>

2.9 Data Acquisition and Processing

A typical image-based aerial surveying with a UAV platform requires flight or mission planning and the measurement of GCPs (Ground Control Points) for georeferencing purposes (if not already available). After acquisition, images can be utilised for stitching, mosaicking, or as input for the photogrammetric process. In this instance, camera calibration and image triangulation are performed first to generate a Digital Surface Model (DSM) or Digital Terrain Model (DTM). These products can ultimately be utilised to generate ortho-images, 3D modelling applications, or extract additional metric data. The workflow is depicted in Figure 2.3, while the individual steps are described in the following sections.

2.10 Flight Planning and Image Acquisition

Typically, the mission (flight and data acquisition) is planned in the lab using specialised software, beginning with knowledge of the area of interest (AOI), the required Ground Sample Distance (GSD) or footprint, as well as the intrinsic parameters of the digital camera onboard. First, the camera's desired image scale and focal length are generally fixed to determine the mission flying height. Next, the camera perspective centres ("waypoints") are computed to fix the longitudinal and transversal overlap of the strips (e.g., 80 - 60%). These parameters vary depending on the purpose of the flight: To achieve small GSDs, missions for the generation of detailed 3D models typically require high overlaps and low-altitude flights. On the other hand, quick flights for emergency surveying and management require more expansive areas to be recorded in a few minutes at a lower resolution. The onboard presence of GNSS/INS navigation devices is typically utilised for autonomous flight (take off, navigation, and landing) and image acquisition guidance. Figure 2.4(a) demonstrates that the flight type significantly impacts the image network quality; in manual mode, the image overlap and acquisition geometry is typically highly irregular, whereas the presence of GNSS/INS devices and a navigation system can guide and improve the acquisition. The navigation system, commonly called the autopilot, consists of hardware (often in miniature form) and software devices. An autopilot enables adherence to the flight plan and communication with the platform throughout the mission.

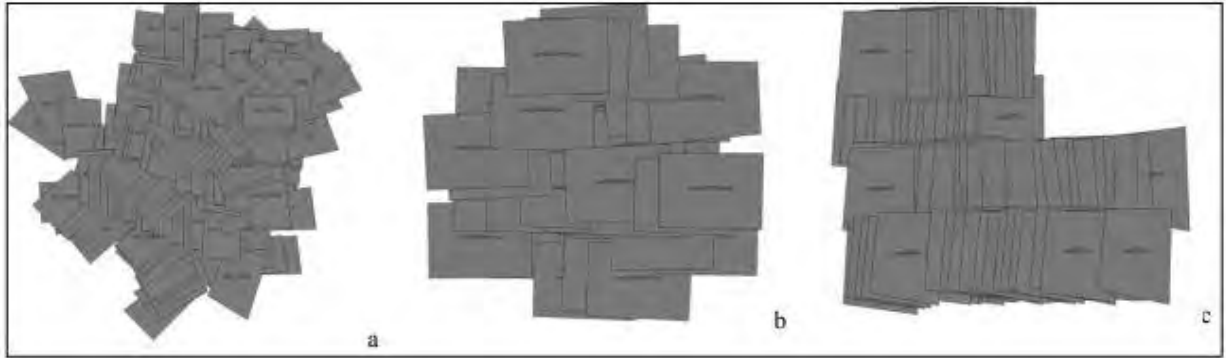


FIGURE 2.4: DIFFERENT MODALITIES OF THE FLIGHT EXECUTION DELIVER DIFFERENT IMAGE BLOCK'S QUALITY: A) MANUAL MODE AND IMAGE ACQUISITION WITH A SCHEDULED INTERVAL; B) LOW-COST NAVIGATION SYSTEM WITH POSSIBLE WAYPOINTS BUT IRREGULAR IMAGE OVERLAP; C) AUTOMATED FLYING AND ACQUISITION MADE ACHIEVED WITH A HIGH QUALITY NAVIGATION SYSTEM

Source: Remondino & Campana, 2014

The cheapest solution relies on MEMS-based inertial sensors, which have significantly reduced weight but, to our knowledge, insufficient precision for direct geo-referencing. More sophisticated and costly sensors, possibly based on single/double frequency positioning mode or RTK, would improve positioning accuracy to the decimetre level, but they are still too costly to be widely implemented in low-cost solutions. During the flight, the autonomous platform is typically monitored by a Ground Control Station (GCS) that displays real-time flight data such as position, speed, attitude, distances, GNSS observations, battery or fuel status and rotor speed. In contrast, the operator remotely piloted systems from a ground station. Most systems permit image data acquisition based on computed waypoints, whereas low-cost systems acquire images at predetermined intervals. The utilised devices (platform, auto-pilot, and GCS) are crucial to the quality and dependability of the final product: low-cost instruments may suffice for short durations and low-altitude flights, whereas more expensive instruments are required for long-duration flights over vast areas. In the case of lightweight and low-cost platforms, a regular overlap in the image block cannot be guaranteed due to the presence of wind, piloting abilities, and GNSS/INS quality, all of which influence the attitude and location of the platforms randomly during flight. Keeping these issues in mind, increasing the overlap between flights performed by human-crewed vehicles or extremely expensive UAVs is generally advised.

2.11 Photogrammetric Unmanned Aerial Vehicles

Since the early 2000s, the use of UAVs to capture photogrammetric images has expanded rapidly. (Esienbein, 2009) enumerates various UAVs capable of capturing photogrammetric images, such as balloons, hang gliders, paragliders, kites, gliders, rotor-kites, airships, propellers, jet engines, single rotors, coaxial, quad-rotors, and multi-rotors. Since the turn of the 21st century, fixed-wing and multi-rotor UAVs have been the most utilised and developed for photogrammetric purposes (Haarbrink, 2011). The advantages of fixed-wing UAVs are their durability, simplicity of design, and extended flight duration (usually around 40-60 minutes). However, fixed-wing UAVs have the disadvantage that photographs can only be taken from a vertical (or plane view) perspective and that high wind speeds will affect the flight path and may cause the captured image to tilt off vertical. With recent advancements in electronic motor technology, multi-rotor UAVs have advanced rapidly. They may have four or more rotor blades, with half spinning in a clockwise direction and the other half in a counter clockwise direction. Reducing a specific rotor's engine speed will give the operator precise control over the UAV. A camera mount secures the camera to the underside of the UAV. This mount can be adjusted so that the camera always faces directly down, or it can be moved to take photographs from various angles, allowing for more precise photography of the sides of objects. Among the disadvantages of multirotor UAVs is the short battery life of the rotor engines, which limits flight duration.

2.11.1 Varieties of UAVs employed in photogrammetry

According to (Esienbein, 2009), balloons, fixed wings, rotary-wing, airships, and kites were used as UAVs for photogrammetry in the late 20th century. Various balloon, airship, and kit-based experiments were conducted with varying degrees of success. Due to the difficulty in controlling the flight path of the UAVs, however, all three methods were found to have limitations. Because they can be remotely controlled and fly more precise flight paths, fixed-wing and rotary-wing UAVs have been further developed for image capture for photogrammetric measurements in the 21st century.

2.11.2 Flight Planning for UAV photogrammetry

During the 20th century, photogrammetric UAVs relied primarily on radio link-based remote controls for their flight path, altitude, heading, and image acquisition. Prior flight planning must precede all UAV photogrammetric work to ensure sufficient image overlap for photogrammetric purposes; however, when using radio link-based remote controls, the specific accuracy of flight paths is ultimately dependent on the skills of the operator and navigator. In most cases, the navigator is responsible for operating the camera and taking photos at the appropriate time

and location. Due to the automation of flight controls in fixed-wing and rotary UAVs of the twenty-first century, operator errors in this process have been mitigated. Before conducting fieldwork, these automated UAVs utilise flight planning software to map the UAV's flight path. As shown in Figure 2.5, the operator then launches the UAV, which will automatically fly the route to the best of its abilities under weather conditions.



FIGURE 2.5: A SCREENSHOT FROM EMOTION 2.0 FLIGHT PLANNING SOFTWARE UTILISED WITHIN FIELD TESTING

Source: Smeaton, 2015

Lab-based flight planning utilises specialised software. Inputting the required ground sample distance and the parameters of the digital camera mounted on the UAV into the software determines the image scale, flying height, and focal length of the camera. Determining the side and forward overlap of the images in the strips fixes the image centres. An onboard GNSS/INS governs image acquisition. Control stations are used to monitor the flight of platforms. The control stations display flight data in real-time. This data includes distance, position, altitude, rotor speed, battery strength or fuel status, and GNSS observations (Remondino et al., 2011). The mission (flight and data acquisition) is planned in the laboratory using specialised software, beginning with the area of interest (AOI), the required ground sample distance (GSD), or footprint, and the intrinsic parameters of the mounted digital camera. The flying height can be calculated with the image scale and camera focal length fixed. The camera perspective centres ('waypoints') are computed by fixing the longitudinal and transversal overlap of strips, and the

onboard GNSS/INS is typically utilised to guide the image acquisition. The take-off and landing operations are strictly related to the employed vehicle and its characteristics but are typically managed by a pilot on the ground (e.g., with a remote controller). During flight, the platform is typically monitored by a control station that displays real-time flight data including position, speed, altitude, distance, GNSS observations, battery or fuel status, and rotor speed. Most systems permit image data acquisition based on computed 'waypoints,' whereas low-cost systems acquire images at predetermined intervals. Figure 2.6 illustrates a typical process flow diagram for generating an elevation model using a UAV.

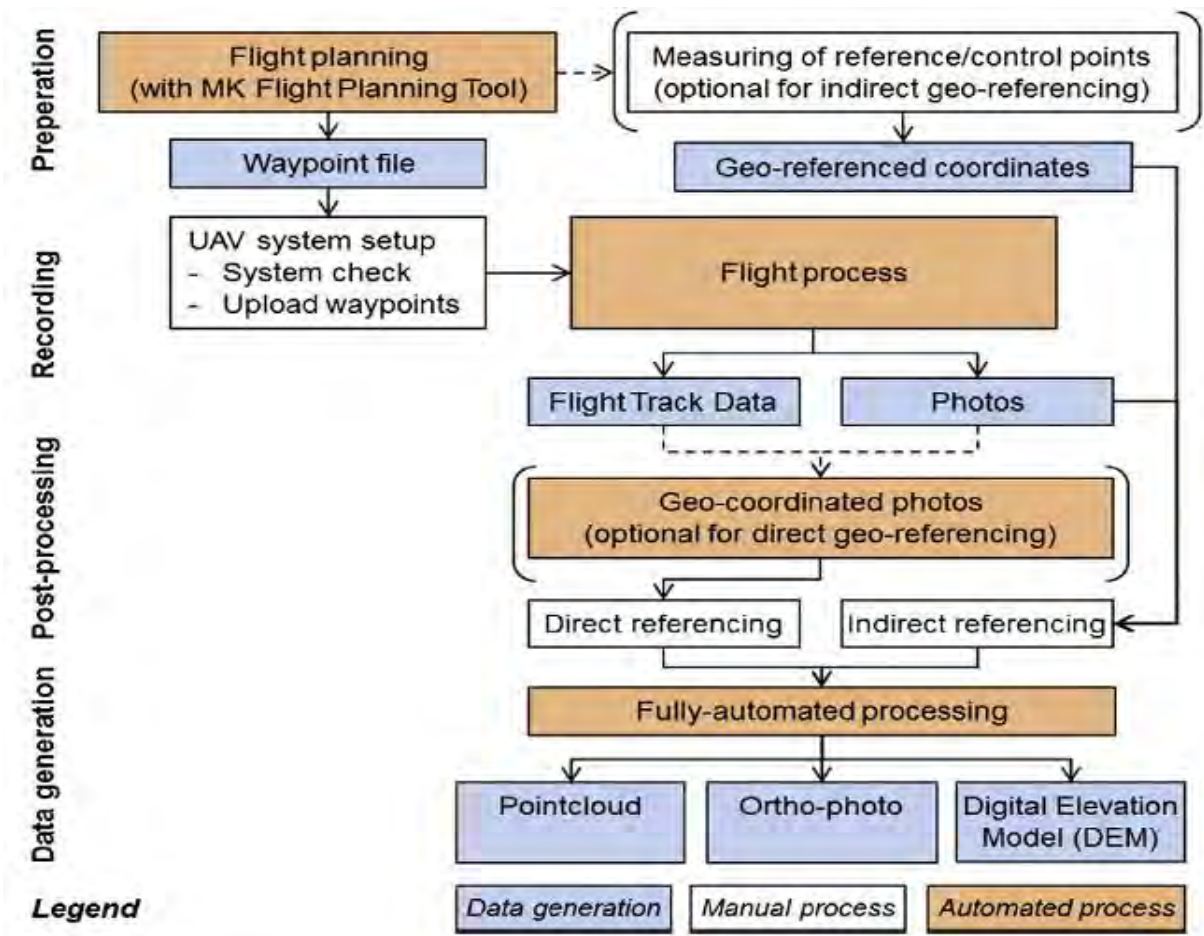


FIGURE 2.6: UAV FLIGHT METHODOLOGY: PREPARATION, RECORDING, POST-FLIGHT DATA PROCESSING, AND INFORMATION GENERATION.

Source: Siebert and Teizer, 2014

2.12 Ground Control Points

Ground Control Points (GCP) are terrain-marked points with known coordinates. As their values must be precisely determined, they are typically measured using conventional survey techniques. Then, they are used to geo-reference photographs, which involve calculating the products' scale, orientation, and absolute position within a preferred coordinate system (Madawalagama et al., 2016). They could be natural, like the centres of sewer drains, or artificial, like crosses or circles painted on the road. Depending on their dimension, they could be 3D, 2D, or 1D.

In addition, depending on their function, they may account for the adjustment or serve as checkpoints to validate the final product's accuracy. GCPs should be positioned on a flat surface within the study area, particularly in the corners of the image block. The GNSS system mounted on the drone can also acquire the coordinates of photographs and geo-reference products in a given area. Due to the low price and diminutive size of drones, the accuracy of these GNSS receivers is unsatisfactory; therefore, GCPs are required to improve accuracy and obtain reliable products placed on precise Earth. Using CV software, a few GCP (but more than three) evenly distributed across the study area are sufficient to geo-reference an image block. Check Points are typically a subset of Ground Control Points (CP). These points with known coordinates serve as image processing validation. It indicates that their coordinates are not included in the computations for bundle block adjustment, but the difference between their coordinates and the interpolated surface determines the precision of adjustment. Global positioning system (GPS) control points must be established to acquire data with high precision if a UAV system is used for surveying.

Before the UAV takes flight, these control points are manually set to generate a Geographic coordinate system. They are used to correct the orientation of the image. In the survey area containing natural features, trees and rocks cannot be used as control points; therefore, artificial points must be placed on the surface of the ground. Before GPS operation and UAV photography, man-made features must be sufficiently delineated and securely fastened to prevent damage.

2.13 UAV Photogrammetric Measurements Utilizing UAVs for Surveying

Few studies have been done on UAVs for specific survey applications. The studies conducted have yielded positive results for the accuracy and precision required for survey work conducted in the field for this dissertation's fieldwork. (Manyoky et al., 2011) suggest that "the UAV method with appropriate photogrammetric evaluation methods offers a significant opportunity to extract useful information from the captured cadastral data. (Manyoky et al.,2011) also

concluded that UAVs are capable of survey applications with the same precision as GNSS and tachymetry techniques. UAV flights can generate photogrammetric models that can be used to create a digital elevation model (DEM). For the DEM to relate to real-world applications, the photographs must contain geo-located ground control points (GCPs) with three-dimensional coordinates. (Rock et al., 2011) examined the relationship between the quality of DEMs generated by UAVs and the number of GCPs. They discovered that "a compromise must be reached between high-resolution images and the susceptibility to outliers in response to shadow movement" (Rock, 2011). Ultimately, the study concluded that the placement of GCPs would be time-consuming if high-resolution images were required. (Kung et al., 2011) evaluated the precision of UAV photogrammetric techniques utilising the same and comparable fixed-wing UAV models as those used in this dissertation. The study found that the ground resolution of the photogrammetric models produced had field accuracies ranging from 57 to 338 mm/pixel. With 12 to 19 ground control points on each tested photogrammetric model.

2.14 UAV Accuracies Applications

UAVs have been utilised for a vast array of purposes in the past. Surveying archaeological sites, excavations, and agricultural areas are a few examples of applications (Remondino et al., 2011). Different techniques for determining the precision of UAVs have been investigated. Checking the DTM with RTK GPS points was a previous method for determining the accuracy of a digital terrain model created by an unmanned aerial vehicle. Then, a C-Astral Bramor UAV was used to acquire the imagery, and photogrammetric techniques were utilised to create the digital terrain model (Barry & Coakley, 2013). Various methods have been implemented to test the accuracy of UAVs' DTM models. For instance, digital elevation models derived from UAV imagery and digital elevation models derived from laser scanning were compared. The project's objective was to examine the applicability of modern surveying techniques to archaeological documentation studies in terms of precision, efficiency, speed, and detail resolution.

2.15 Instruments/Equipment

(Barry and Coakley, 2013) utilised the C-Astral Bramor due to its superior stability in their research. The C-ASTRAL Bramor utilises the 24MP Sony next-7 camera. Ten photo control points were placed in a 2 ha area where two ha were used. Identifying targets was black and white, as shown in Figure 2.7.



FIGURE 2.7: GROUND CONTROL AND CHECK POINT TARGET

Source: Barry & Coakley, 2013

The flight was planned with an 80 per cent forward lap and an 80 per cent side lap, and the altitude was set at 90 metres to achieve the required GSD of 10 millimetres. A Trimble GeoXR Network RTK GPS and a C-ASTRAL Bramor UAV were utilised to collect the data as part of an integrated system. The GPS's accuracies range between 10 and 25 mm horizontally and vertically.

2.16 Data acquisition, processing and results

(Barry and Coakley, 2013) imported ten control points and forty-five checkpoints surveyed by Network RTK GPS in the Irnet95 coordinate system in their data processing procedures to determine the accuracy of UAVs compared to RTK GPS. Next, the 1601 images were downloaded. Using this software, redundant images could be eliminated by deleting images with excessively high roll values. These occurred in succession. After this process, they were left with 728 images to use for photo alignment. As depicted in Figure 2.8, they then imported the ten photo control points into the Photoscan software and identified the centre of each control point. In this manner, a georeferenced model was created.

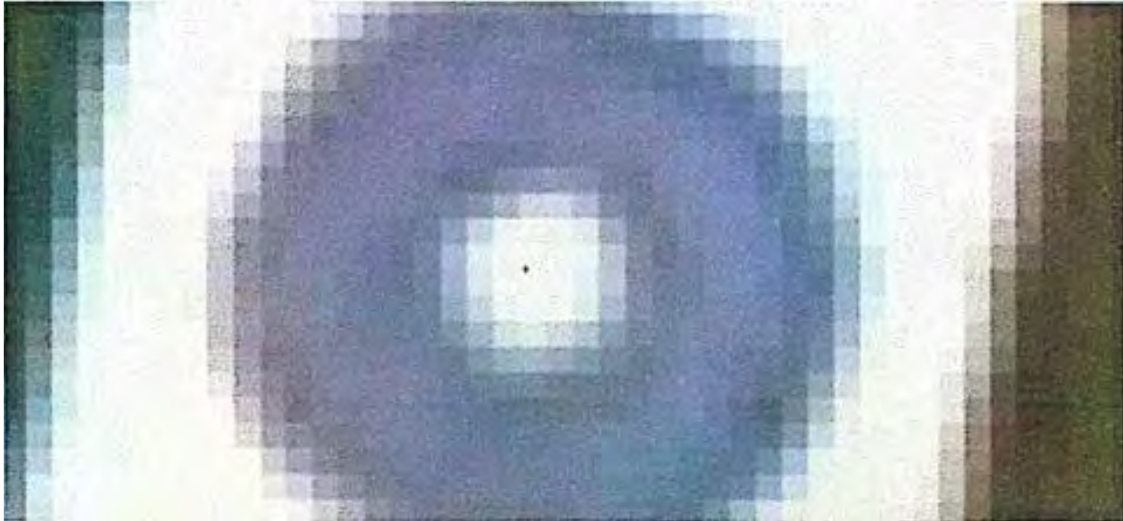


FIGURE 2.8: CONTROL POINTS WHEN USED FOR IDENTIFICATION IN PHOTO SCAN SOFTWARE

Source: Barry & Coakley, 2013

According to (Barry and Coakley, 2013), various methods were used to determine previously mentioned research outcomes. First, the ITM geo-referenced orthophoto and DEM data and the GPS CAD data were imported into ArcGIS. Then, measurements were taken between the centres of the targets as depicted on the orthophotos and the centres of the targets as measured by GPS. This was accomplished using the ArcGIS measuring tool. Then, the GPS point data was compared to the corresponding DEM readings.

TABLE 2.2 COMPARISON BETWEEN GPS SURVEY AND UAV SURVEY

Source: Barry & Coakley, 2013

Accuracy Results	XY (m)	Z (m)
Mean	0.021	0.031
RMSE	0.023	0.035
Accuracy 95%	0.041	0.068

If the UAV photogrammetric scale is within 1:200, it would be possible to generate 0.2m contour intervals based on table 2.2 results (Barry and Coakley, 2013). This DTM model was created using a single image collection. Unfortunately, only the accuracy at this particular flying height was determined. Therefore, the accuracies of these DTM models must be evaluated using imagery captured at varying altitudes and then independently surveyed checkpoints to determine each model's precision.

The effect of different positioning systems on the accuracy of Digital Elevation Models (DEMs) generated from aerial imagery collected by Unmanned Aerial Vehicles was the subject of a second study (Ruiz et al., 2013).

Ascending Technologies GmbH conducted their experiments utilising a Pelican quadrotor as an aerial platform. The platform has a payload of approximately 600 grammes and up to 15 minutes. Canon PowerShot G10 was the camera used to capture the images.

Figure 2.9 illustrates the results obtained for the horizontal and vertical accuracies of the generated DEM using various GPS receivers to obtain positioning data. Note that the scenario involves typical UAV flights of (1:100). In a real-world scenario, the precisions expressed in millimetres correspond to decimetres. Horizontal and vertical accuracies tend to follow two exponential distributions because they increase dramatically for GPS deviations greater than 100 GSD. However, smaller deviation values result in less accuracy improvement.

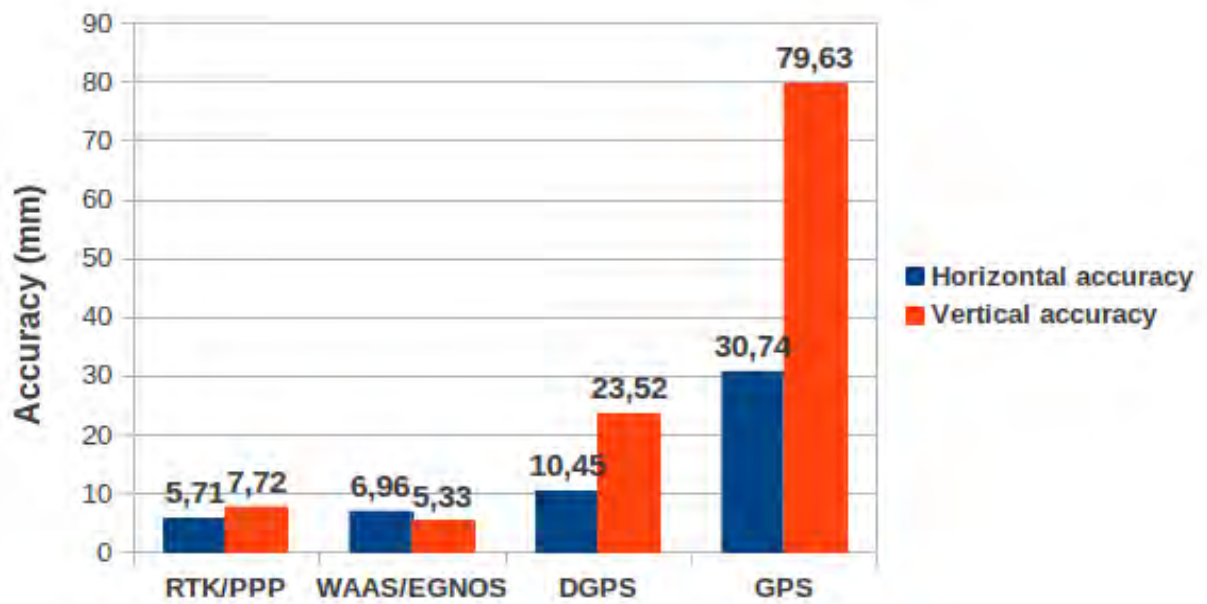


FIGURE 2.9: COMPARISON BETWEEN GPS SURVEY AND UAV SURVEY

Source: Ruiz et al., 2013

The results demonstrate a correlation between position errors and the DEM accuracy, which proliferates with standard GPS receivers. In addition, the results demonstrated that DEM accuracy depends on positioning information.

In the research conducted by (Ajayi et al., 2018), the following procedure was used for the overall data collection process.

2.17 Image/Data Acquisition

Before conducting the flight mission, two Hi-Target Differential Global Positioning System (DGPS) receivers, one of which served as a base station, were used to position GCPs marked during reconnaissance (permanently stationed). Simultaneously, the other roved over the GCPs and acquired positional data in Real-Time Kinematic (RTK) mode. The approximate distance between the base station and the rover is 900 metres. Twenty GCPs were established throughout the imaging region (see Fig. 2.10).

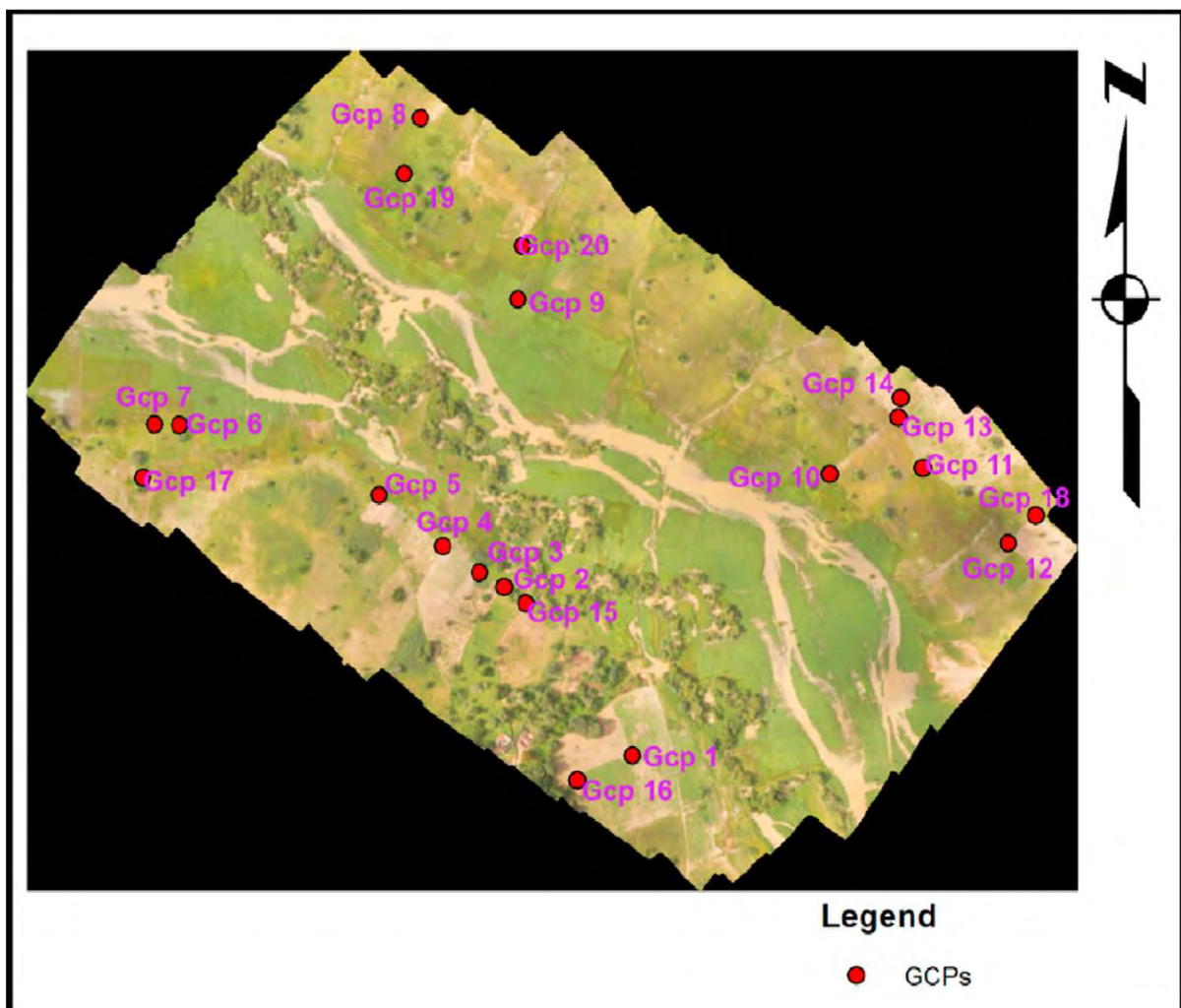


FIGURE 2.10: DISTRIBUTION OF THE USED GCPs

Source: Ajayi et al., 2018

These GCPs are essential for accurate geo-referencing of the images (to ensure precise alignments), elimination of bowing effects in the UAV data (Mesas-Carrascosa et al., 2015), and qualitative analysis of the anticipated 3D model. The area to be mapped was determined after calibrating the UAV and ensuring that all its components were in perfect working order. Setting all parameters on the DJI GO mapping made it easy to map the pilot app. Finally, the controller was connected to the drone, and the nadir images were captured autonomously using a DJI Phantom 2 quadcopter equipped with a GoPro 3 camera model, with a camera focal length of 3.61mm at a flying height of 120 metres and a camera sensor width of 6.25 mm. To ensure stereoscopic imaging, the camera frame pixel size of each acquired overlapping image is 40003000 mm, covering approximately 34,090.68m² (0.0341 km²) on the ground with approximately 65% overlap.

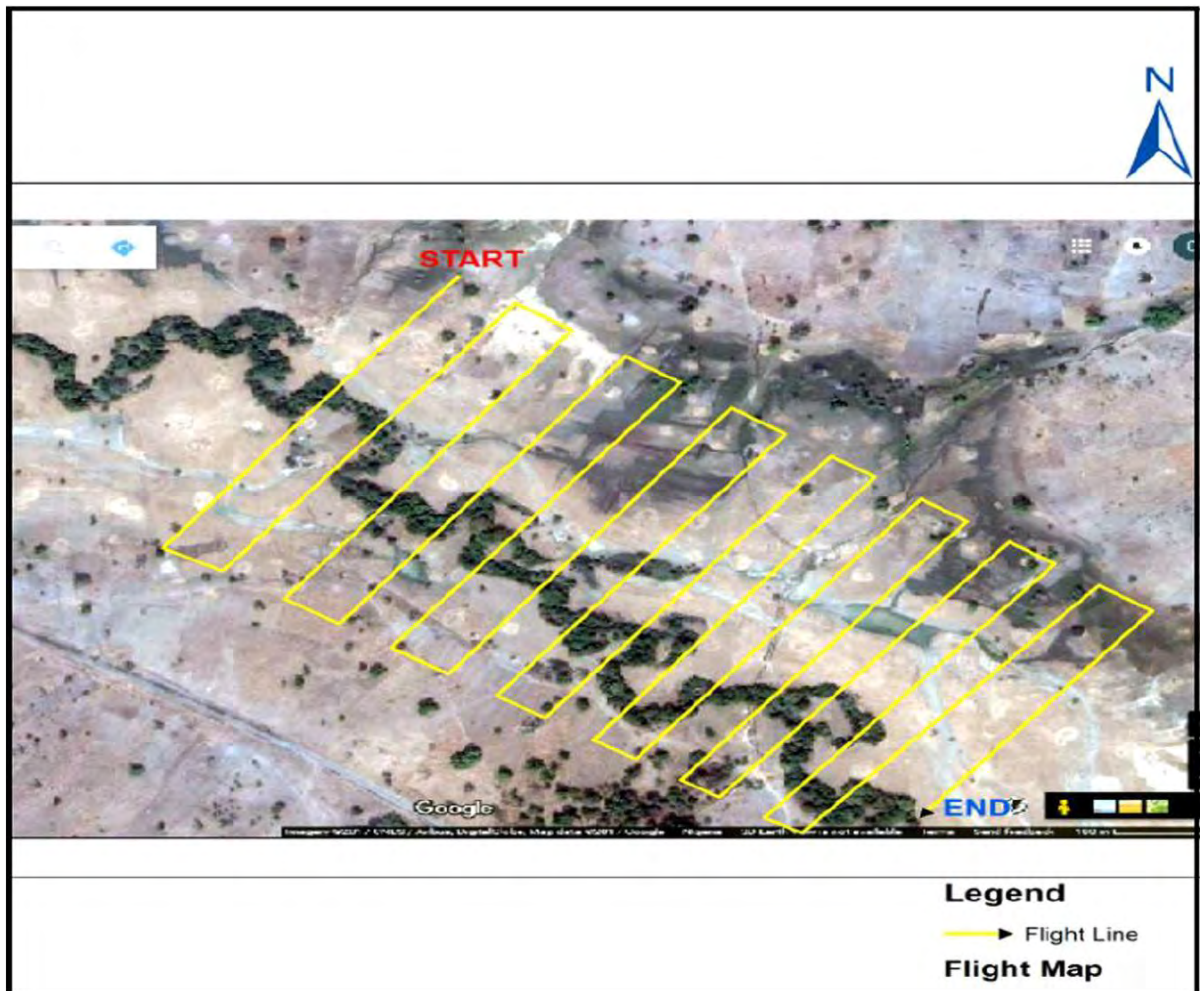


FIGURE 2.11: FLIGHT PLAN

Source: Ajayi et al., 2018

2.17.1 Processing and validation of data

All acquired overlapping images were processed using the digital photogrammetric software Agisoft Photoscan. The processing includes relative orientation/external orientation, interior orientation, and absolute orientation, as well as the generation of 3D models from 2D image sequences using the Structure from Motion (SfM) photogrammetric range imaging technique (Ullman, 1979, Westoby et al., 2012). Digital Surface Model (DSM) and Digital Elevation Model (DEM) are the final products of the photogrammetric processing. The DEM was imported as an input parameter into ArcGIS 10.3.1 for further processing, which requires the imposition of topographic constraints on the DEM to determine suitable locations for constructing dam-axes within the study area.

Twenty GCPs were coordinated on the ground with the aid of Hi-Target GNSS receivers for the DEM accuracy assessment. Before the flight mission, each point was marked with a reflective object visible in the acquired images. Later, the coordinates of these points were extracted directly from the generated orthophoto and DEM. Finally, they compared the extracted coordinates to the GNSS-acquired coordinates. The difference between the measured and extracted data (from UAV-produced DEM) was estimated and utilised in the calculation of Root Mean Square Error (RMSE), the horizontal and vertical precision.

2.17.2 Results and analysis

Following photogrammetric processing of the acquired image data, the following three-dimensional models were produced: Figure 2.12: Sparse point clouds; Figure 2.13: Dense point clouds; Figure 2.14: Orthophoto; Figure 2.15: Digital Surface Model (Fig. 2.15). Others include the DEM contour map, flow magnitude, and direction vector map. The sparse point cloud (Fig. 2.12) that was generated by triangulation (Snavely et al., 2006) could be described as a representation of a rendered set of data points; however, these have limited use in 3D applications; therefore, a dense point cloud (Fig. 2.13) must be generated from it by surface and depth reconstruction (Furukawa and Ponce 2007, Ajayi et al., 2017a). The orthophoto was created using aerial triangulation based on the measurement of tie points. It is the image of the scene obtained by successfully registering each overlapping image pair of the study area acquired by the UAV and ensuring that both the height and tilt distortions are removed (orthorectification) to ensure geometric correctness, which is crucial for the accurate extraction of spatial information from the orthophoto of the imaged area. The DSM and DEM are occasionally used interchangeably despite their distinct distinctions. The DEM depicts the digital representation of the earth's surface, whereas the DSM is the surface model that includes the terrain model and surface features visible in the study area.

Therefore, the DSM is more advantageous for urban planning (landscape modelling) than the DEM, which makes the DSM an appropriate input parameter or base map for identifying suitable dam-axes.

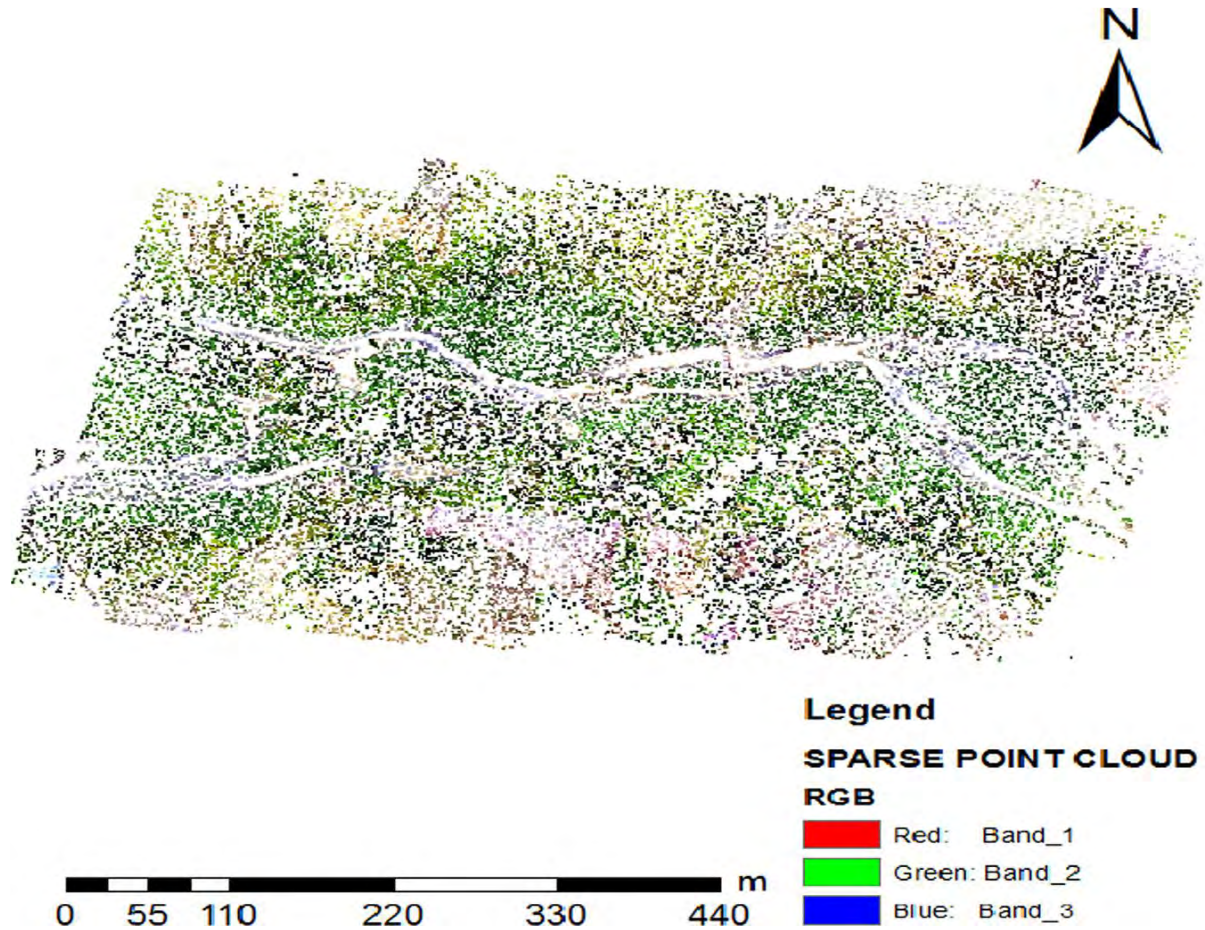


FIGURE 2.12: SPARSE POINT CLOUD

Source: Ajayi et al., 2018

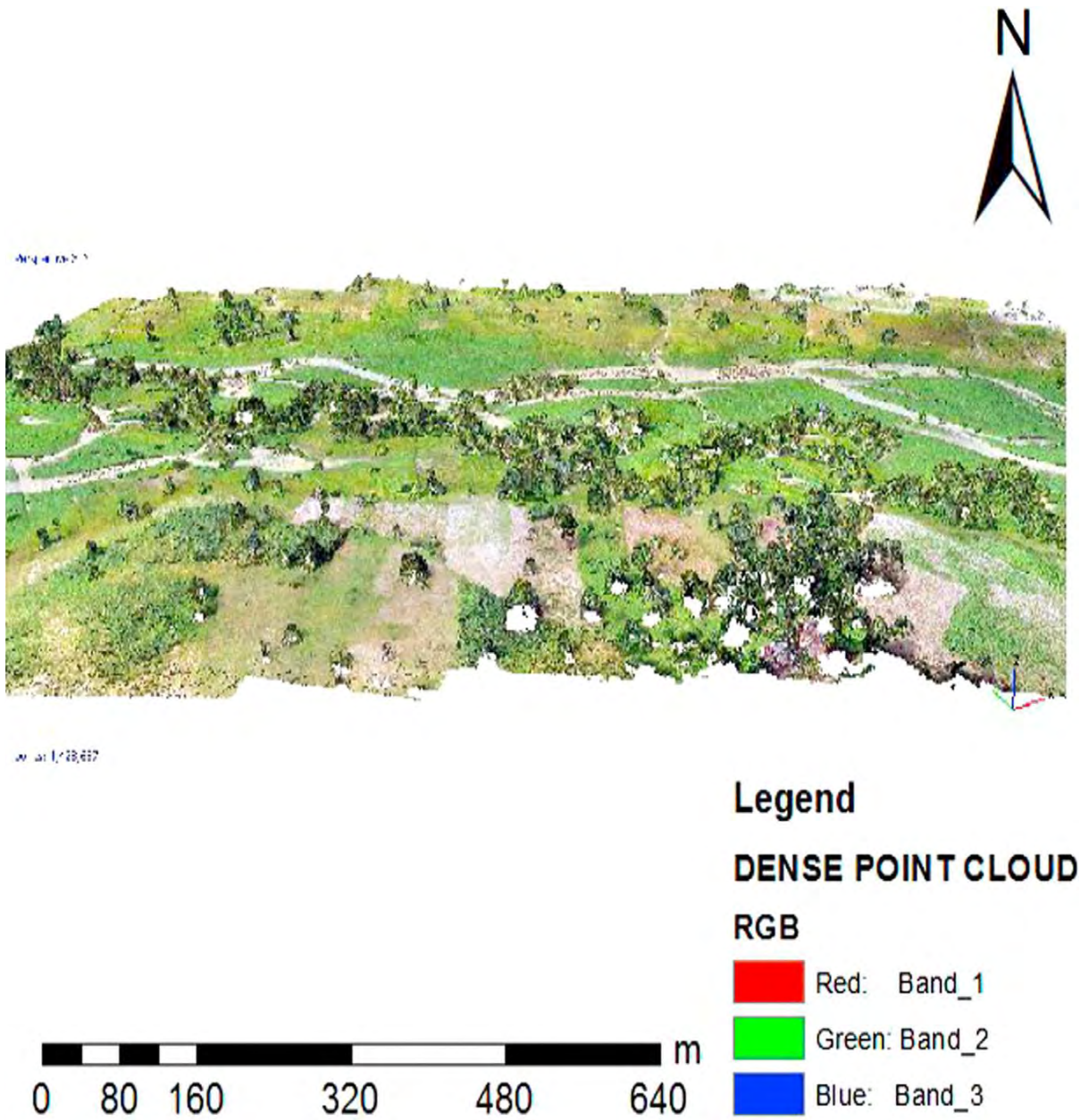


FIGURE 2.13: DENSE POINT CLOUD


Source: Ajayi et al., 2018



Legend

ORTHOMOSAIC

RGB

-  Red: Band_1
-  Green: Band_2
-  Blue: Band_3

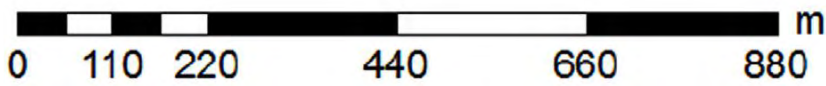


FIGURE 2.14: DIGITAL ORTHOPHOTO

Source: Ajayi et al., 2018

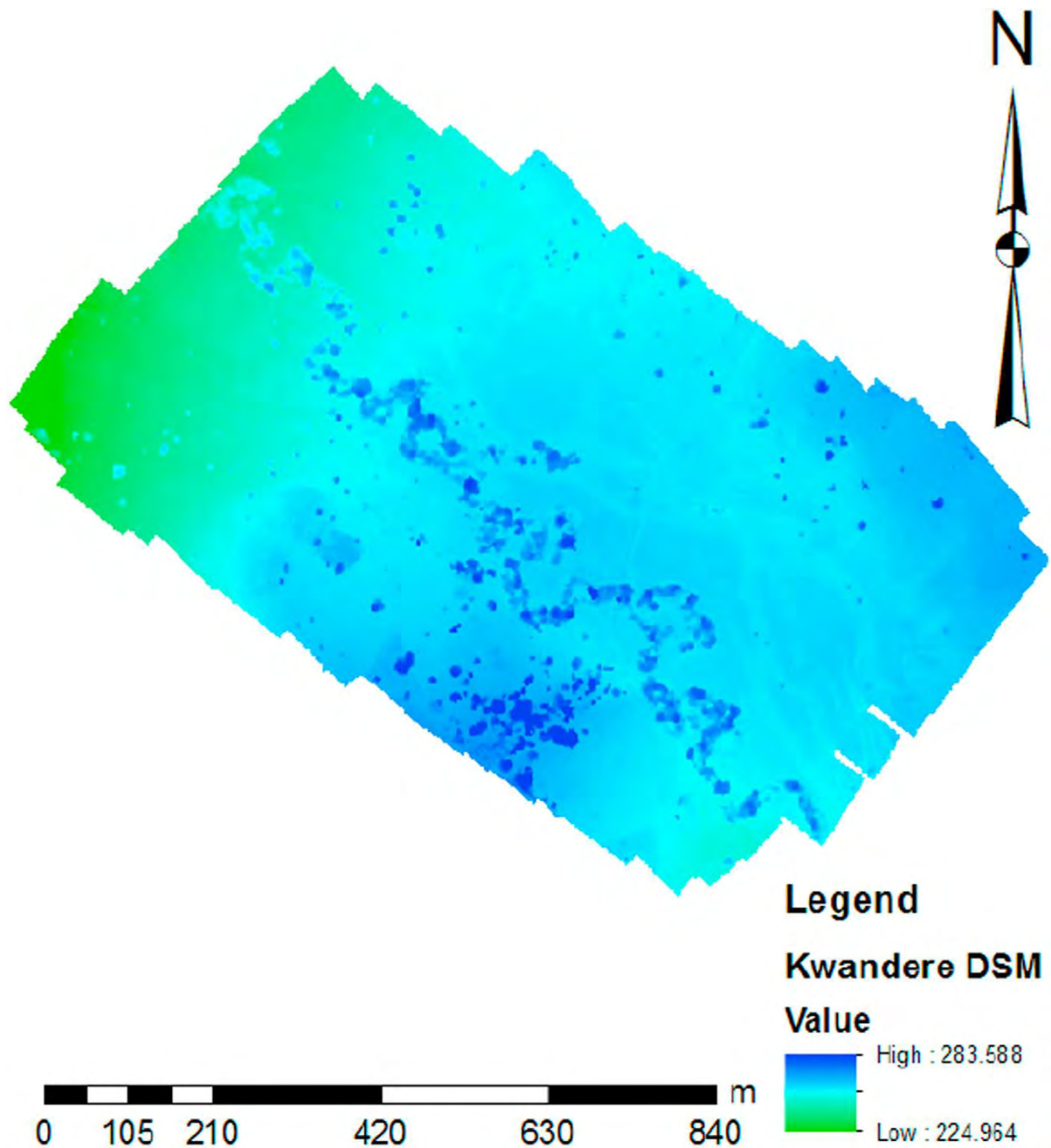


FIGURE 2.15: GENERATED DIGITAL SURFACE MODEL

Source: Ajayi et al., 2018

From the DEM, the elevation ranges between 224.964m and 268.445m. The variation observed in the elevation value of the highest point results from the disparity in model features (DSM). The DSM's maximum height value reflects the height of vegetation and natural features visible on the surface of the study area, such as trees.

2.18 DTM creation

The rapid development of digital technology has brought photogrammetry into the digital age. Consequently, automating interior and relative orientation, digital terrain models, and orthophoto generation has become one of the most crucial responsibilities in digital photogrammetry. Digital Elevation Model is a 3D model of a portion of the planet's surface (DEM). DEMs are used for various applications, including topographic mapping, engineering and environmental applications, spatial data visualisation, orthophoto production and integration into Geographic Information Systems, and analysis in conjunction with other data sets.

Typical DEM data sources include aerial photographs, satellite images, cartographic maps, and terrestrial point measurements. Deriving DEM points from digital images or photographs is one of the primary tasks of photogrammetry. Using photogrammetric techniques, it is simple to obtain DEM from stereo images of a large area. Typically, a process of automated correlation is used to generate digital elevation models from digital aerial photographs. The correlation between a pair of stereo images is calculated in digital photogrammetry. The points are identified based on where the best repairs can be made. Root Mean Square Errors characterise the accuracy of the produced DEMs for the elevations (RMS). Image matching is an essential research topic in digital photogrammetry. Matching methods can be categorised as either area-based or feature-based. For identifying image correspondence, area-based matching, correlation, or least squares methods may be employed (Karabork et al., 2004). Most digital photogrammetric software includes an automated DEM correlation procedure.

2.19 Traditional Surveying Methods

2.19.1 The theodolite and the evolution of the contemporary 'total station'

In the late 18th and early 19th centuries, Gunter's and optical circumferentors were the only instruments used for early South African surveys (Smith, 2013). The theodolite, an optical angular measurement instrument, was invented in the 18th century due to advancements in lens manufacturing technology. Throughout the 19th century, additional advances in the mass production of lenses made the theodolite more accessible to surveyors. By the turn of the twentieth century, the theodolite had become the industry standard for Surveyors' angular measurement in conjunction with riband or invar steel bands (survey chains) for distance measurement. With the ability to accurately measure angles and distances, surveyors developed a variety of trigonometric methods for conducting measurements. This combination of theodolite and steel bands was commonly regarded as having moderate to high accuracy for cadastral land surveying (Smith, 2013). Since the 1990s, the modern total station, which

combines a data recorder, an electronic distance measurement device, and an optical theodolite, has become the industry standard for field measurement in many modern surveying applications. The contemporary total station utilises the same trigonometric calculations as older surveying instruments. However, many of the calculations that Surveyors using theodolites would have manually performed are performed internally by the total station, and stored points are recorded by the total station.

2.19.2 GPS techniques for DEM generation

Static and kinematic data collection are the two primary methods utilised by GPS technology. The most effective technique for generating DEMs is the GPS kinematic method of data collection. Kinematic data collection requires at least two receivers to collect data simultaneously. One receiver, referred to as the base, must remain stationary during data collection. Typically, the base receiver will occupy a survey point whose exact location is known. Once operational, the base system collects and stores raw data from all satellites with a direct line of sight to the GPS antenna.

The kinematic base is essentially identical to a static occupation, except that the recording interval must be synchronised with the kinematic rover. The other GPS receiver(s) operating concurrently during a kinematic survey is referred to as the rover(s). During the survey, the rover unit(s) can move and are used to position new points relative to the base. The majority of receiver types support two types of kinematic survey:

- Stop-and-go (which can also refer to rapid static)
- Continuous kinematic (simply kinematic)

Stop-and-go surveying is optimal for point collection. During Stop-and-go, the system is centred over a specific point and collects data for a specified time. Stop-and-go occupation times typically range from 15 to 60 seconds. Continuous kinematic data collection is ideal for collecting bulk points with minimal attributing (terrain modelling) or linear features like a road centreline. Throughout the collection of continuous kinematic data, the user is never required to stop moving. Every time the receiver records a data record, a point is accrued. The recording interval for this application would typically be 1-5 seconds, and the accuracy is typically 0.03 to 0.05 metres. The rover system is designed to be carried easily and is mounted entirely to a range pole. The system software interface is provided by the onboard data collector of the receiver unit. Essential system functionality such as data recording and data attributing is operated with the control buttons. Kinematic data collection has the advantage of high productivity.

RTK GPS can deliver centimetre-level point coordinates almost instantaneously. Numerous applications, including topographic surveying, engineering construction, geodetic control, vehicle guidance and automation, can benefit from RTK technology. RTK positioning employs a stationary GPS receiver as a reference station at a known location. A second receiver serves as the rover, which can move and survey points of interest. Both receivers make simultaneous observations of the GPS signals, and a radio data link between the two receivers allows data to be transmitted from the reference receiver to the rover, where the coordinates are calculated.

2.20 Accuracy assessment of a DEM

Precision is a factor that influences the overall quality of a data set. Foote and Hutchinson (1997) define the similarity between a data set and the real world or true values. Error is a precise measurement of the disparity between a data set's values and their corresponding true values. Accuracy is defined by (Goodchild et al., 1994) as the difference between values recorded in a spatial data set and modelled or assumed values. The difference between the data set and the actual values is an error. Regarding continuous phenomena and their representation as surfaces in GIS, it is impossible to measure and calculate all true values. Therefore, the true values must be estimated or modelled. In the case of continuous phenomena, accuracy indices derived from a limited number of error measurements are utilised.

Due to time and accessibility constraints, measuring true elevation from the ground will be impossible. Instead of determining the DEM's absolute accuracy, the accuracy of the DEM is determined relative to the surrounding terrain. It is more common to measure the relative accuracy in comparison to sample point measurements that are known to be of a higher order of accuracy (Hirano et al., 2003). There are two factors to consider when evaluating DEM accuracy using sample points. Initially, how should the sample points be selected? How can measurements of a higher degree of precision be obtained? These issues are discussed further below.

2.20.1 Deciding on sample points

Comparing each grid point of the DEM to those of a more accurate DEM yields a highly reliable assessment of accuracy. This scenario is uncommon, as DEMs are typically generated using the most precise methods available. For example, (Day and Muller, 1988) created residual surfaces by subtracting the elevation values of a SPOT-derived DEM from the elevation values of an aerial photography-derived DEM, and (Sasowsky, 1992) compared a SPOT-derived DEM to one derived from a topographic map. Typically, more precise measurements are only

possible for a subset of the grid points. In terms of time and money, the quality assessment process will be more efficient with fewer samples. However, fewer samples result in a less reliable quality assessment, particularly in mountain environments with highly variable terrain. Therefore, the selection of sample size is crucial. According to (Li, 1991), the optimal sample size depends in part on the heterogeneity of the terrain and in part on how reliable the estimate of the mean elevation error or the standard deviation of the elevation error must be.

2.20.2 Accuracy measures

Calculating the difference between the DEM and the elevation of a control point requires obtaining a sample of control points from a more precise data source and assuming this sample is sufficiently large and representatively distributed. Next, it must be determined how to convert this collection of individual elevation errors into an estimate of the DEM's precision (Ravibabu and Jain, 2008).

2.21 Data Interpolation

2.21.1 Residual analysis and DEM accuracy

Error is the difference between a measured or estimated value and the actual value. DEMs contain a level of inherent error because they are models that estimate elevation (Fisher and Tate, 2006). Calculating the Z between a derived DEM and data acquired using a more accurate surveying technique or using frequent check data (e.g., re-sampling a set of control points) to derive statistical error measurements over the survey duration are common methods for assessing DEM accuracy (Brasington et al., 2003, Januchowski et al., 2010). If the residuals (ZDEM - ZTS) were small, it was inferred that the DEM accurately estimated elevation; if the residuals were significant, it was concluded that the DEM did not accurately estimate elevation. The residuals are utilised to estimate the mean error, root mean square error, and standard deviation (SD). ME eq 2.1 is a measure of DEM accuracy used to determine if there is a systematic under- or over-estimation of elevations (Fisher and Tate, 2006, Schwendel et al., 2010):

$$ME = \frac{\sum Z_{DEM-ZTS}}{n} \quad \text{Equation 2.1}$$

where ME is the mean error, ZDEM is the Forecast, ZTS is the actual, and n is the number of entries.

RMSE on eq. 2.2 is a measure of DEM precision and incorporates both random error (i.e., variance) and systematic error (i.e., bias):

$$RMSE = \sqrt{\frac{\sum (Z_{DEM-ZTS})^2}{n}} \quad \text{Equation 2.2}$$

Error-values (i.e., the deviation of the DEM Z from the measured TS Z) are squared in the RMSE calculation so that more significant errors are given more weight than more minor errors.

The RMSE formula assumes that errors are independent, normally distributed, and have a mean of zero. If bias in the DEM (i.e., the ME estimate) is significant, then the RMSE estimation is confounded by the ME and is no longer a valid measure of precision.

As a result, other researchers (e.g., Fisher and Tate, 2006, Li, 1988) have suggested calculating the SD eq. 2.3 to produce more accurate precision estimates:

$$SD = \sqrt{\frac{\sum((Z_{DEM} - Z_{TS}) - ME)^2}{n-1}} \quad \text{Equation 2.3}$$

2.22 Summary

The preceding sections provide background information on UAVs, the history and applications of UAVs, the development of UAVs as a photogrammetric instrument, the development of the theodolite and total station as the standard survey instruments, and the expected accuracy of the total station and UAV used in the fieldwork for this report. This background research has enhanced our knowledge of the survey and photogrammetric developments in the fields of total stations and unmanned aerial vehicles, respectively, for the development of the methodology and analysis presented in this report. Based on the specifications of the conventional surveying instrument, the Trimble M3 total station will provide an accuracy of approximately 5 to 10 mm at each measured point. Horizontally and vertically, the DJI Phantom 3 drone has an absolute positioning specification of 45 mm. Due to the specification's claim that the M3 total station is significantly more accurate, the measured points from the total station will be considered the control data for comparison with the photogrammetric three-dimensional model created from the images captured by the UAV.

Prior to conducting any photogrammetric survey, flight planning must be performed. This is performed in a laboratory. By performing flight planning, it is possible to determine the best flight lines to cover the area to be surveyed, the number of images to be captured, and the amount of forward and side lap for each mode. After determining this, the number of ground control points can be determined. Examining the various UAV platforms, data collection methods, and test results make it possible to draw some conclusions from the previous tests. To yield accurate results, certain system features must be correctly configured for a micro-UAV system. First, the camera used to capture the images must be of the highest quality and regularly calibrated. The camera calibration certificate will be utilised when obtained images are used to reference inner orientation. Before obtaining images, it will be necessary to establish and level ground control points (GCP) with a high degree of precision using RTK GPS and to mark them with a visible marker. High-precision GCP will ensure that your model is accurate.

In contrast to the cameras used in the tests conducted by (Grenzdorffer et al., 2008) and (Engel and Teichert, 2001), the UAV Literature review and theory system must be able to carry a high-quality camera as payload. Ideally, a camera system like the 24MP Sony next-7 utilised by (Barry and Coakley, 2013) during their research with the C-ASTRAL Bramor UAV should be employed. The UAV system should have a reliable GPS logging system so that each image's image information, such as exposure position, plains orientation, and pitch and roll, can be obtained. These types of information are essential for image orientation. If there is a delay between the camera's shutter release and the exposure, it must be calculated beforehand,

(Grenzdorffer et al., 2008). Additionally, the UAV system must be stable and adhere to the predetermined flight paths. This will guarantee the proper side and forward lap. Although most UAV helicopters appear to be the preferred option because most fixed-wing UAVs can take off vertically, take-off is not a problem. Fixed-wing UAVs are launched either manually or with a catapult system. Notably, the autopilot functionality of the UAV must also be of the highest standard. This will ensure that the UAV can adhere to the predetermined flight paths and account for any sudden changes, such as a change in wind direction. If the site is remote, a generator as part of the UAV platform could be useful (Haarbrink and Eisenbeiss, 2008). Important is the use of software capable of performing high-quality Bundle adjustments for aero triangulation, image matching to extract a digital Surface model (DSM), softcopy stereo models for 3D vector mapping, orthophoto generation, and texture mapping (Haarbrink and Eisenbeiss, 2008).

CHAPTER 3

RESEARCH METHODOLOGY

3.1 Introduction

This chapter of the thesis describes the planning and procedures implemented as part of the methodology for the field testing included in this thesis. This provides a better understanding of how the results were generated and allows for a more thorough analysis of the field testing results. This thesis also describes how to compare the horizontal and vertical precision and accuracy of traditional ground surveys with UAV drone surveys, as depicted in Figure 3.1.

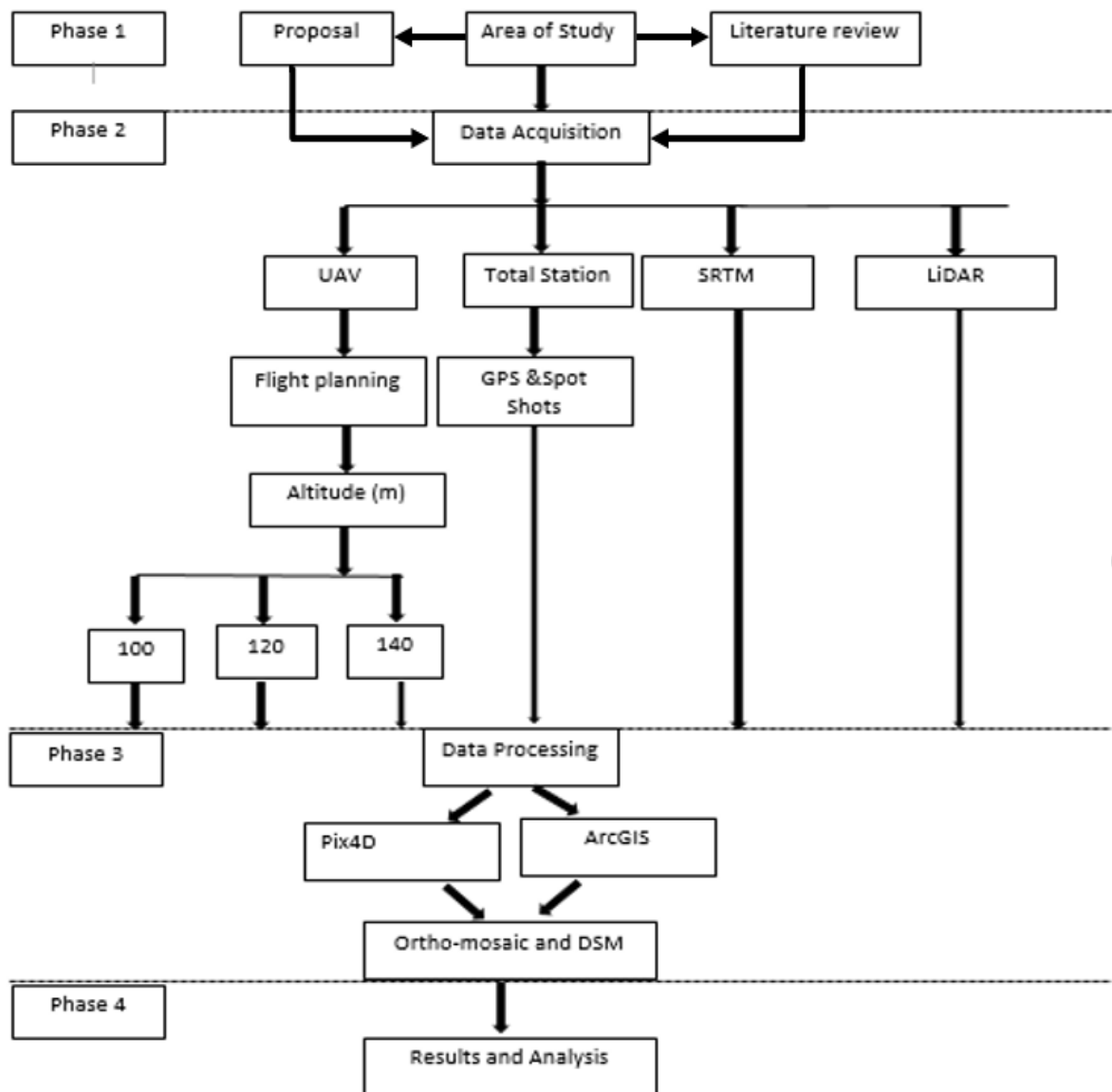


FIGURE 3.1: PROJECT WORKFLOW: PREPARATION, DATA COLLECTION, POST-FLIGHT DATA PROCESSING, AND INFORMATION GENERATION

3.2 Instruments and software used for research

The photogrammetric capabilities of UAVs are evaluated for this thesis. Access to field equipment for data collection and analysis is the critical factor influencing the feasibility of the research project. The traditional surveying equipment (total station, prism, prism pole, tripod, and tape measure) was provided by the researcher's workplace, Cape Peninsula University of Technology, along with office equipment and software. Pix4d software was used to calibrate the point cloud and the remaining images, while ArcGIS was used to classify and colourize the total station points. UAV DJI Phantom 4 Professional Drone was the Unmanned Aerial System (UAS) utilised. One camera was mounted on the multirotor aircraft that was manually piloted. The sensor was configured to take a photograph every second. Mission Planner software was utilised for flight planning. The photos were processed with Pix4D and exported as a LAS file, the ArcGIS drawing file format used for total station processing. ArcGIS analysed Pix4d to generate plans for contour lines, ortho-mosaic, and Digital surface models, which were then exported as shapefiles, JPEG, and PDF files.

3.3 Field Testing Site Description

3.3.1 Site Location

District Six (a former inner-city residential neighbourhood) served as the location for field testing. The site is between Nelson Mandela Boulevard, Christiaan Street, Zonnebloem, Cape Town, South Africa. The size of the site is approximately 33.16 ha. The site's elevation difference is approximately 107 metres above ground level. The takeoff point was located in the middle of the site, between the lower and upper portions. Open space was required for the landing site, so it was decided that the open area in the middle (same location) of the study area was the optimal landing site. The flown area is in Figure 3.2. In Google Earth, a polygon was created from the flying area. The polygon was given an absolute height to aid in analysing the site's overall elevation. This area's designated height was 107 metres, the highest in the study area. The terrain's maximum and minimum elevations were recorded to aid in determining the flying heights. The open field in the District 6 area was chosen as the test site. This open space field, with its morphologically dissected surface and undulating terrain, is thus suitable for testing the use of UAV photogrammetry to capture high-resolution surface features.



FIGURE 3.2: AREA OF STUDY

3.4 Planning Field Testing

3.4.1 Control Planning

Using georeferenced imagery, a rough layout of where the control points were located was created, considering the required accuracy for this study. The more the number of control points, the better the accuracy, Oniga et al., (2018). Several control points were established for this site; this excludes the outer control used for orientation and check purposes. This site features multiple control points, excluding the outer control used for orientation and checks. A portion of the control points was to be utilised to secure the model from the UAV (see Figure 3.3).

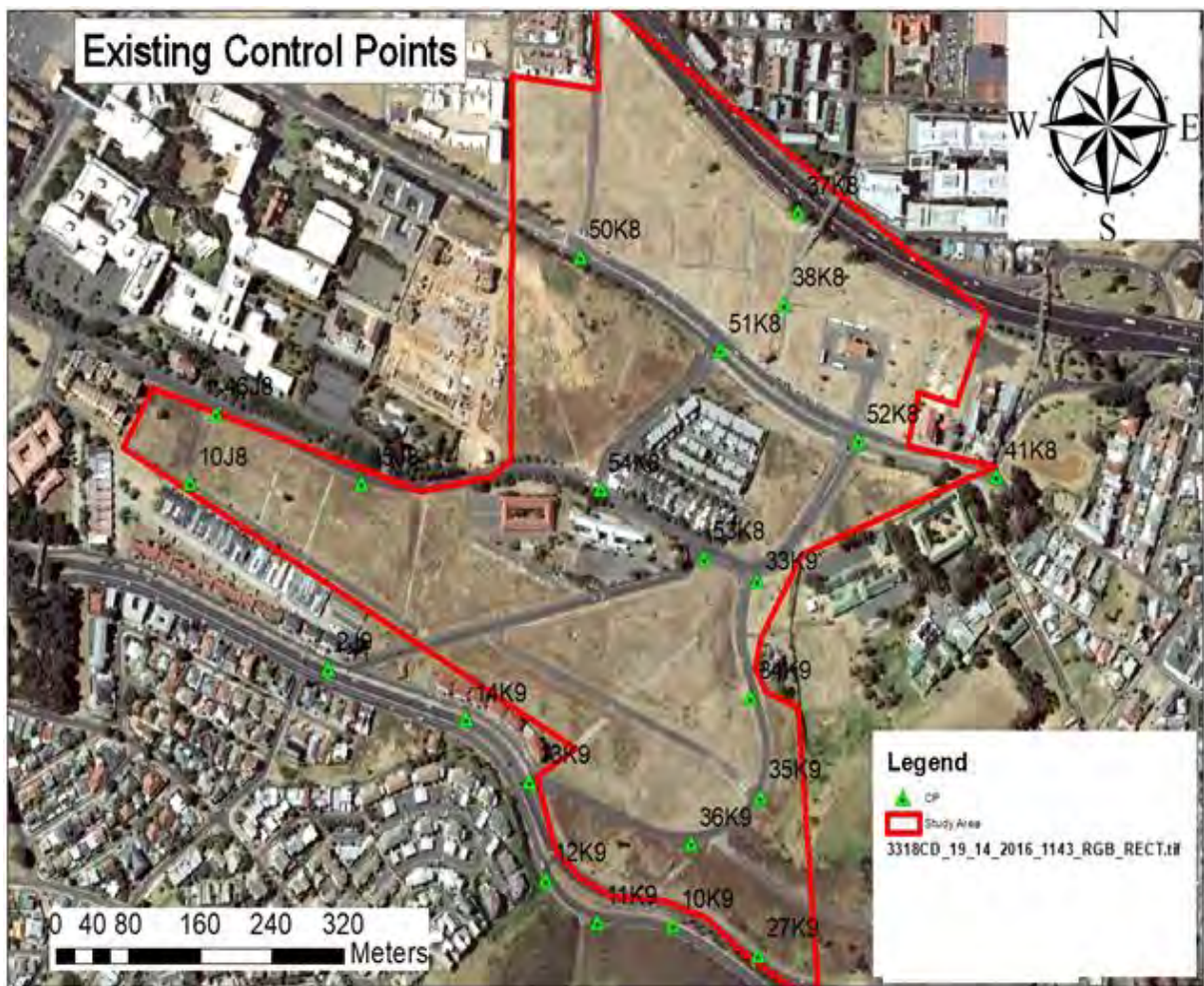


FIGURE 3.3: EXISTING CONTROL POINTS OF THE STUDY AREA

3.4.2 Establishment of RTK GPS Control at the Site

The test field contains eighteen (18) distributed Ground Control Points (GCPs), which were marked just prior to the flight using black and white target pre-marks (reflectors) as 29.7X42 cm squares, distinguishing them from the ground, see figure 3.5. As RTK observations, the points were measured using the Trimble GPS base and rover 5700 & 5800 series. Each GCP was measured with a 10-second data logging rate. To obtain reliable results, measurements were conducted with a time interval during various satellite configurations. This area of Cape Town, South Africa, uses WGS 84 (Hartebeeshoek 94) as the official coordinate system. These GCPs were surveyed with a Trimble M3 Total Station, which is considered more accurate than the GPS. The purpose of this was primarily to determine whether the GCPs correlate with the GPS survey and the other control in the area. Comparing the two datasets, the horizontal (y, x) and vertical (z) positions of measured points were satisfactory and were acceptable for this study. Table 3.1 illustrates the GCPs' measured coordinates. Figure 3.4 presents a map illustrating their distribution.

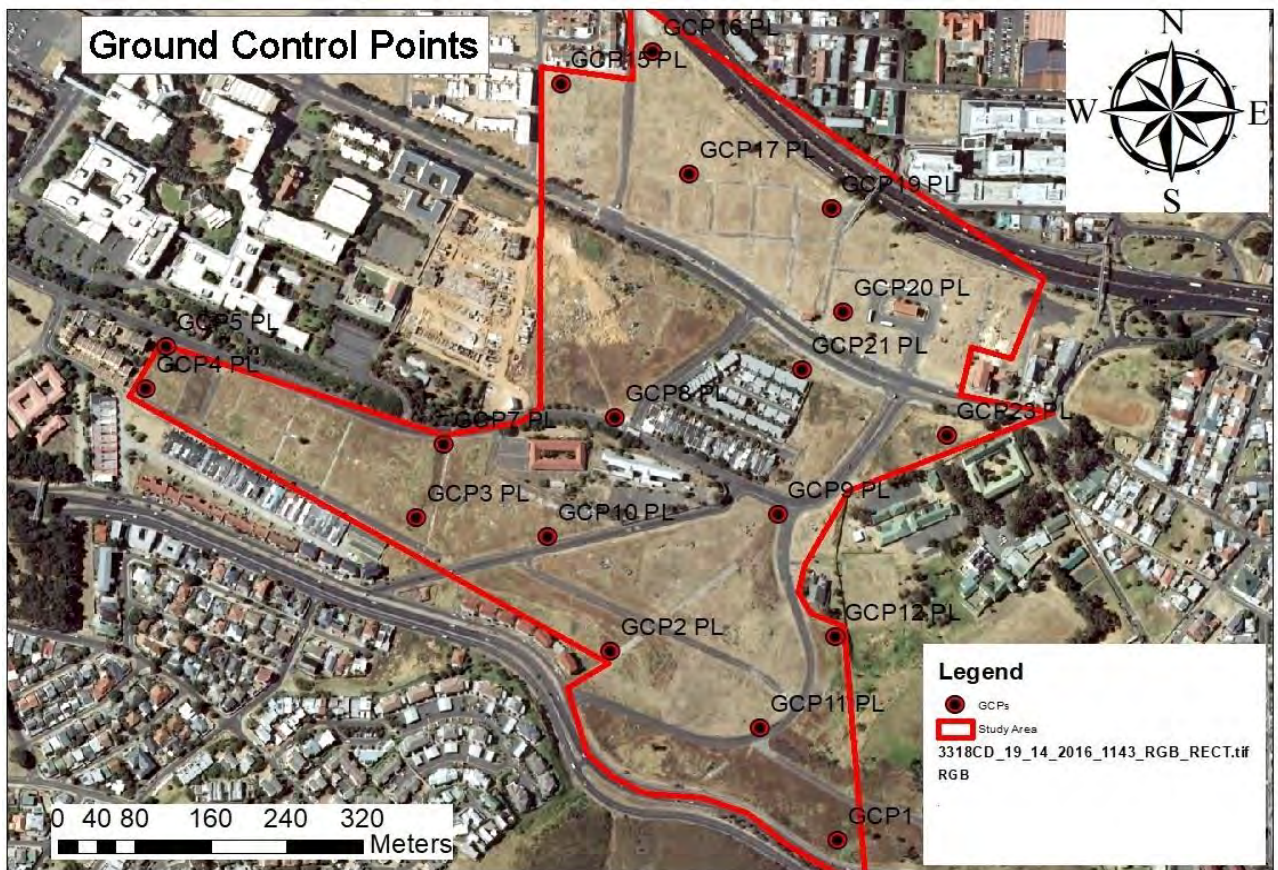


FIGURE 3.4: STUDY AREA WITH GROUND CONTROL POINTS (GCP)



FIGURE 3.5: TARGET PRE-MARKS

TABLE 3.1 MEASURED GROUND CONTROL POINTS

Measured with a GPS					Measured with a Total Station							
Name	y (m)	x (m)	Z (m)	Code	Δy (m)	Δx (m)	ΔZ (m)	Name	y (m)	x (m)	Z (m)	Code
GCP1 PL	52013,3	3756863	96,403	GCP	-0,051	0,033	-0,077	GCP1	52013,3	3756863	96,326	GCP
GCP2 PL	52252,6	3756658	87,394	GCP	-0,011	-0,032	-0,105	GCP2	52252,6	3756658	87,289	GCP
GCP3 PL	52456,8	3756514	66,299	GCP	0,041	0,057	-0,074	GCP3	52456,8	3756514	66,225	GCP
GCP4 PL	52741,8	3756375	53,885	GCP	-0,034	-0,009	-0,047	GCP4	52741,8	3756375	53,838	GCP
GCP5 PL	52720,1	3756330	49,056	GCP	-0,035	0,01	-0,039	GCP5	52720	3756330	49,017	GCP
GCP7 PL	52428	3756435	53,417	GCP	-0,023	0,063	-0,064	GCP7	52428	3756436	53,353	GCP
GCP8 PL	52248,1	3756406	50,123	GCP	-0,027	-0,024	-0,05	GCP8	52248,1	3756406	50,073	GCP
GCP9 PL	52076,6	3756511	54,106	GCP	-0,015	0,006	-0,048	GCP9	52076,6	3756511	54,058	GCP
GCP10 PL	52318,9	3756535	69,144	GCP	0,061	0,162	-0,074	GCP10	52319	3756535	69,07	GCP
GCP11 PL	52095	3756742	73,49	GCP	-0,031	-0,008	-0,059	GCP11	52095	3756742	73,431	GCP
GCP12 PL	52016,6	3756643	61,204	GCP	-0,019	0	-0,086	GCP12	52016,6	3756643	61,118	GCP
GCP15 PL	52304,6	3756046	18,551	GCP	-0,018	-0,012	0,017	GCP15	52304,6	3756046	18,568	GCP
GCP16 PL	52208,3	3756011	18,574	GCP	-0,033	-0,002	-0,017	GCP16	52208,2	3756011	18,557	GCP
GCP17 PL	52169,9	3756143	24,277	GCP	-0,034	0,005	-0,019	GCP17	52169,9	3756143	24,258	GCP
GCP19 PL	52020,2	3756181	29,002	GCP	-0,033	-0,049	-0,035	GCP19	52020,2	3756181	28,967	GCP
GCP20 PL	52007,5	3756292	35,989	GCP	-0,05	-0,003	-0,056	GCP20	52007,5	3756292	35,933	GCP
GCP21 PL	52051,4	3756355	40,578	GCP	-0,038	0,021	-0,044	GCP21	52051,4	3756355	40,534	GCP
GCP23 PL	51899,1	3756425	49,279	GCP	-0,047	-0,007	-0,041	GCP23	51899	3756425	49,238	GCP
				n	18	18	18					
				Minimum	-0,051	-0,049	-0,105					
				Maximum	0,061	0,162	0,017					
				Mean	-0,022	0,012	-0,051					
				SD	0,029	0,047	0,028					

3.4.3 Test points

The test points were positioned with the RTK GPS and verified with the total station. An approximately 50m x 50m grid was utilised as test points. The researcher was not permitted to enter certain areas containing wooden, and iron fencing surrounding a school, a construction site and private residences. Consequently, 159 test points were located throughout the 33-ha test area. Most of the test points were evenly distributed across the entire test area. The image below, extracted from ArcGIS software, illustrates the distribution of check points across the site (Figure 3.6).



FIGURE 3.6: CHECK POINTS DISTRIBUTION, DIGITISED CONTOUR LINES

3.4.4 Preparation for the Total Station Survey

During field testing, the National Geospatial Information (NGI) was used to acquire the coordinates of required points, which were then formatted so that the total station could import the coordinate and point information automatically. In this instance, the output file type is 'CSV'. Town Survey Marks and Trigonometrical Beacons were two of the data layers uploaded to the total station. A physical printout of all uploaded data in X, Y, and Z format was created. This backup is created in the improbable event that the automatically imported CSV file becomes corrupted and cannot be used during field testing. Reconnaissance was conducted in the field to plan how the survey would be conducted to cover the area of interest, including the order in which control points and external orientation points would be used. To facilitate accurate data collection, a check was conducted for intervisibility between control points in the study area and external points (orientation

3.4.5 Flight Planning

Previous research has demonstrated that numerous applications and programmes are devoted to flight mission planning (Zietara, 2014). Most photogrammetric flight planning software are free, but some are commercial software and therefore insufficient for fully autonomous, suitable photogrammetric flights (Zietara, 2014). The Pix4D team has released the most recent version of Pix4D Capture. In the previous version, it was impossible to define two distinct overlaps because the side and front had to be identical, limiting its applications (Pix4D, 2016). However, the most recent update was used to plan flight missions. After connecting the remote control to the drone, the application was automatically loaded with Phantom 4 professional camera characteristics such as camera constant and image pixel size ((3.43 [cm/pixel]) 1 x GSD. The study area was indicated on the map with a polygon. Next, the flight height and front and side overlaps were calculated. Factors such as low regulations, maximum flight time, and ground pixel size were considered to determine the desired flight height. The flight altitudes of 100m, 120m, and 140m above the ground are compatible with all aspects mentioned. It does not exceed the maximum acceptable flight height in South Africa; the mission can be completed with one battery per flight, which provides approximately 20 minutes of flight time; and GSD measurements smaller than 5 centimetres can be obtained from this flight height. Front and side overlaps of 75% and 70%, respectively, were used to maximise stereoscopy and prevent holes. It yielded 385 photos (100m), 290 photos (120m), and 213 photos (140m) in each of the required strips to cover the entire study area.

Another decisive factor was the picture trigger mode; the safe trigger mode was selected. It was determined that the drone's speed was normal, as there was no need to fly slowly or quickly between corresponding waypoints. The location of the mission's launch was a further consideration. As the flight height above the ground depends on the take-off point's height, it

was determined to be in the middle of the study area (65m contour). Consequently, the minimum flight height above the ground was 165 m (65 m height + 100 m flying height) and greater in the test field's upper portions.

Furthermore, it ensured that the minimum stereoscopy has front overlaps of 75% and side overlaps of 70%. Choosing a start point in lower areas would result in an insufficient number of overlaps, which could result in image matching gaps, whereas flying the drone too low in higher areas would place it closer to roads and vehicles. The mission was planned in the office before fieldwork commenced to avoid haste and confusion. However, after connecting the remote controller to the drone in the field, the list of coordinates that determined the flight path and photo capture locations was uploaded to the drone.

The UAV can only fly the programmed flight path precisely and capture images of stable quality in the absence of or with very light winds. When there are strong winds, the UAV will be less able to fly the flight path precisely and will capture blurry images due to its instability at the time of image capture. The amount of sunlight is another weather element that can affect image quality. The images will be affected by shadowing anomalies on sunny days (Zietara, 2014). In this regard, the field testing was scheduled for a day with cloudy weather forecasts, very light winds, and a low or non-existent chance of precipitation. The flight day's weather forecast is depicted in Figure 3.7.



FIGURE 3.7: UAV FORECAST (FLIGHT PLANNER)

Several steps were taken in the flight planning process:

- Launched the Pix4D;
- Imported the site's KML file into pix4D;
- Generated area points along the perimeter of the site KML area, which the software used to generate waypoints.

At this stage, it was beneficial to understand the site's prevailing climatic conditions. It was advised to fly against the wind for a more consistent flight path. When flying into the wind, the UAV would use more throttle power and consequently more battery power, thereby reducing its flight duration. Flying with the wind would expose the UAV to the risk of flying too quickly and being unable to capture images quickly enough to ensure adequate imagery overlap. For the creation of the flight plan, the following parameters were required:

- Launch Altitude: 65 metres above mean sea level
- Flying height: Initially set at 100m above the launch point, then changed to 120m and 140m
- Flying direction or Line Angle: Refer to Figure 3.8.1 for the second flight (100m). Figures 3.8.2 and 3.8.3 depict flight line angles at 120m and 140m, respectively
- Imagery Overlap and Sidelap percentages: 75% Overlap and 70% Sidelap
- Trigger speed for the camera: 2.5 seconds

Based on the above parameters, the Pix4d software calculated a series of waypoints by calculating the distance between flight lines and the required overshoot factor at the end of each flight line. This was the amount of space the UAV required to turn. The flights were conducted at the following altitudes above ground level:

- 165 metres (65 metres plus 100 metres);
- 185 metres (65 metres plus 120 metres);
- 205 metres (65 metres plus 140 metres).

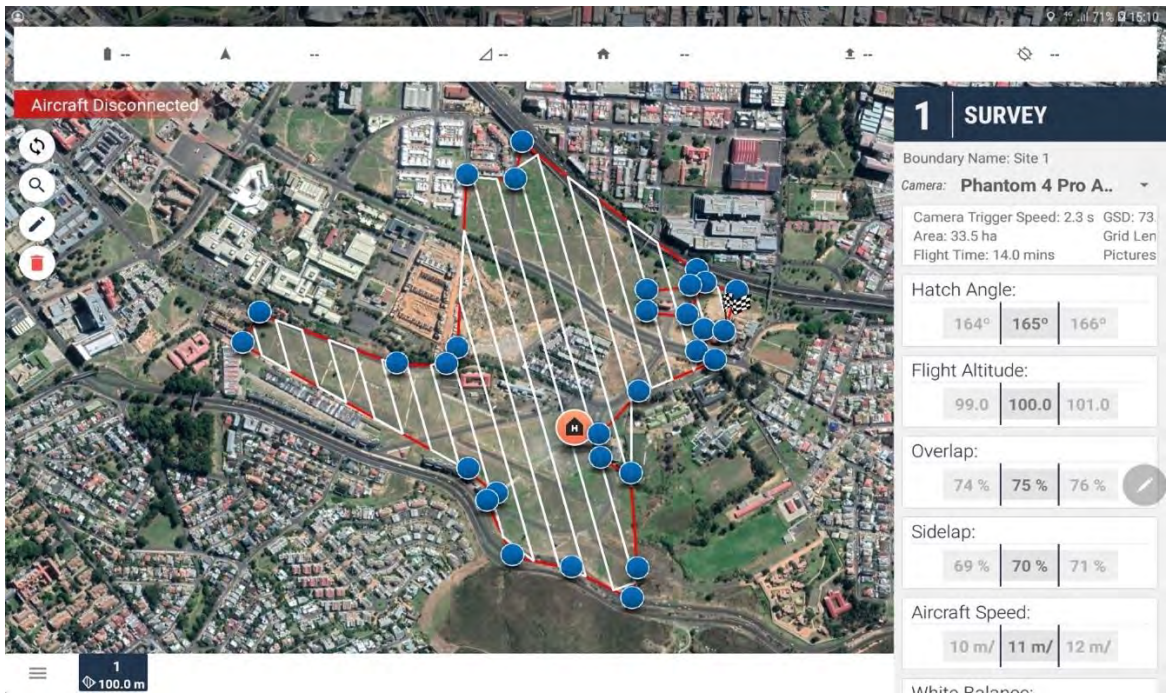


FIGURE 3.8: FLIGHT PLANNER - FLIGHT LINES, ANGLES, OVERLAPS (100M)

The following flight plan was for the 120m flight, which immediately followed the 100m flight.

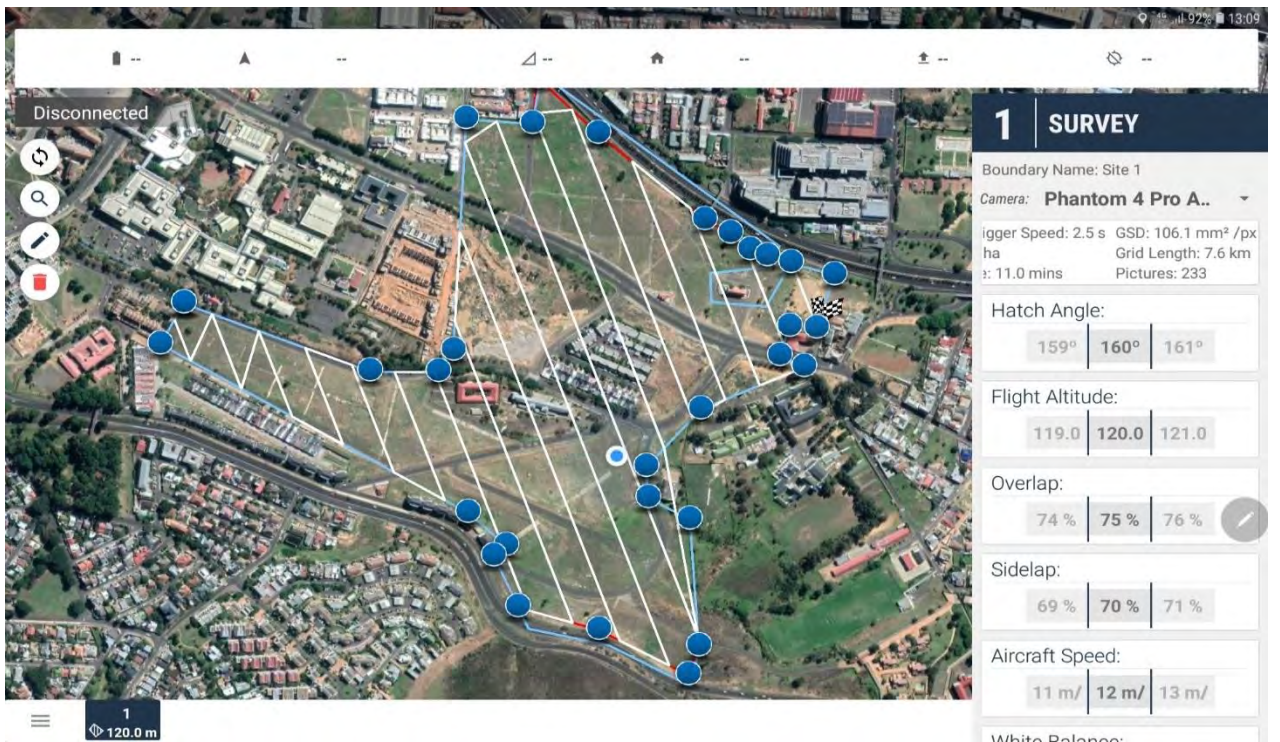


FIGURE 3.9: FLIGHT PLANNER - FLIGHT LINES, ANGLES, OVERLAPS (120M)

The flight plan below was for the 140m flight, which was flown directly after the 120m one.

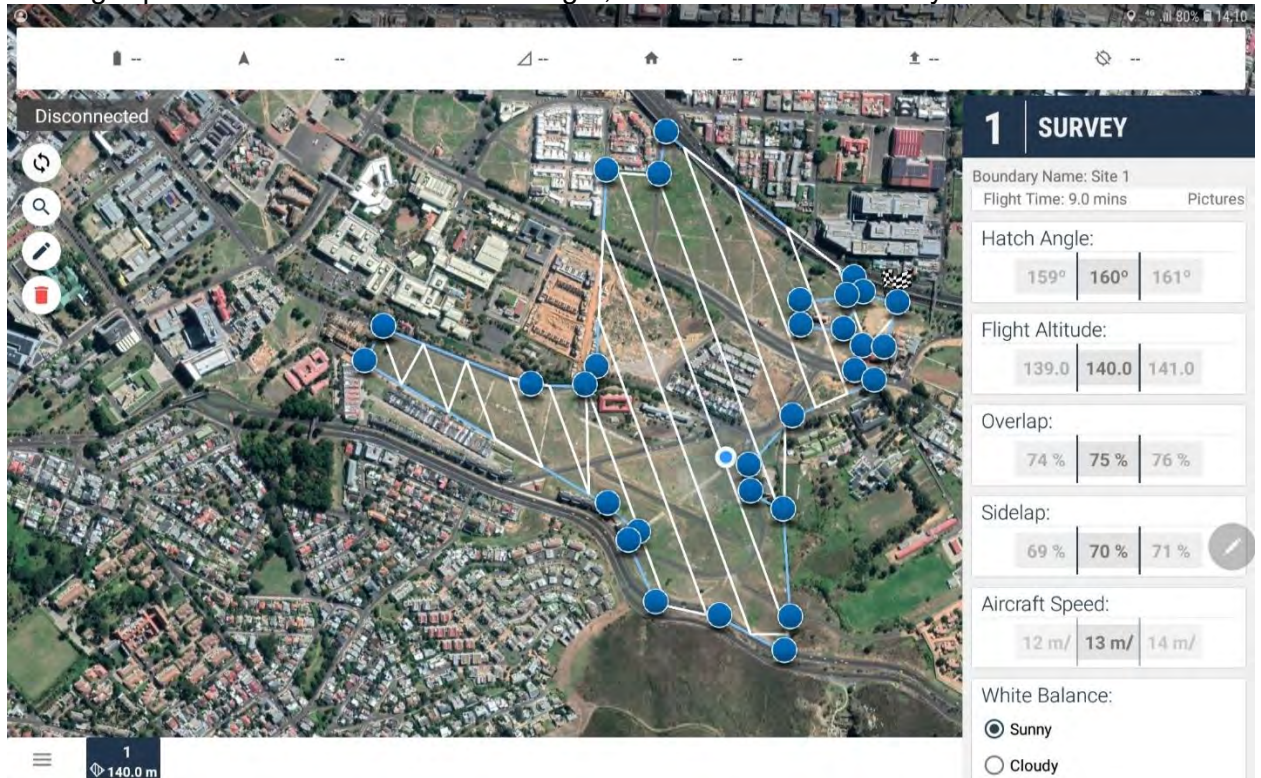


FIGURE 3.10: FLIGHT PLANNER - FLIGHT LINES, ANGLES, OVERLAPS (140M)

3.5 Field Methodology (Data)

3.5.1 Traditional Survey

Before collecting data using ground surveying techniques, the image of the polygon surrounding the study area was loaded into the GQIS software and associated with the correct coordinates. As shown in Figure 3.6, a shapefile containing 100 evenly spaced, evenly-distributed points approximately 50m apart were created. This shapefile has been saved for future use. Next, a point extraction was performed. These points were extracted as y,x (csv file) coordinates and loaded onto a GPS. Next, an RTK survey with a base station and a receiver was conducted. The RTK-GPS survey was calibrated to two TSMs, and 100 checkpoints were established in accordance with their locations. Finally, it was necessary to verify the location of these points using another traditional ground surveying technique.

Using a Trimble M3 total station, the other traditional field survey was conducted. A topographical survey (spot shots) was used to determine the horizontal and vertical positions by selecting points throughout the study area. Several Town Survey Marks were used to observe spot shots that covered the survey's area of interest. All field observations were made utilising trigonometric techniques from a total station to a 2-meter-long prism pole with a reflector attached. The trigonometric positioning data was then recorded along with detailed

feature coding information for each observation in the total station's internal data recorder. This precise feature coding allowed the survey software to draw lines between data, place different feature types on different data layers, and generate contour and break-line data. The contour and break-line information were used to generate the triangle file necessary for creating a DTM.

3.5.2 Flight

Prior to launching the UAV into flight, ground control points (GPCs) were established in a location with a clear view from above. These GPCs consisted of basic 30cm x 30cm (on upper and middle areas) and 1m x 1m (on lower areas) carpet squares with black painted triangles on opposite corners. The GPCs were located using the Trimble GPS base and rover 5700 & 5800 series (figure 3.9) and confirmed with an M3 Trimble total station (more accurate) in order to geo-reference coordinates and generate the photogrammetric model. This would also guarantee that the photogrammetric model is created using the same coordinate system as the traditional survey field testing. After positioning and locating the GPCs, the DJI Phantom 4 Pro UAV took off from an open, grassy area on the site. The UAV followed the predetermined flight path while real-time flight data was displayed on the controller tablet. The weather conditions at the time of the flight were cloudy, with extremely light winds and no precipitation. This weather allowed the UAV to fly the flight path to the best of its abilities with minimal interference from prevailing weather conditions such as winds and precipitation.



FIGURE 3.11: LOCATION OF GROUND CONTROL POINTS USING GPS

The Phantom 4 UAV landed in the same grassy area as the launch area, with the weather conditions remaining as programmed by the pre-flight planning software. The recovered GCPs will be used for future UAV missions. Using the tablet used to control the UAV, the UAV operator uploaded the images captured by the UAV and the flight data file to a hard drive. The images were then saved to a removable disc in preparation for photogrammetric model post-processing. After uploading the previously planned mission, the manual flight mode was replaced with the automated flight mode. The aircraft ascended to a height of 165 m (65m + 100m - flying height) and moved in the location of the first image. The mission duration for each flight was less than 30 minutes, and the drone flew at a speed of +/- 12 metres per second. In the image EXIF files, the approximate GPS location expressed in the geographic coordinate system WGS84 and elevation is recorded and saved. As the drone camera can only record three bands, the spectral resolution of acquired images is minimal (red, green blue). The computer on the board also generates a log file that stores information about the drone's position during flight.

3.5.3 Processing and analysis of the data

3.5.3.1 Trimble M3 Total Station and 5700 & 5800 series Trimble GPS base and rover data

The M3 Total Station's digital data was exported to USB in a .csv file format. This is the default file format for the majority of survey software programmes. The csv file was transferred from the USB to the computer and then imported into the QGIS programme. The import procedure involves converting the observation data's raw angles and distances into points in coordinate format. Additional 'string' information is stored in conjunction with point coding, such as spot shots (SS), to create lines between common points. This coding and string system also permits software to automatically label contour points and break lines for the purpose of creating a 3-dimensional triangle file, which is used to generate contour data within the software. Then, a model depicting contour lines and DTM.

3.5.3.2 UAV drone data (Image processing)

Using the Pix4D software, the image processing was completed. During the field survey, 18 Ground Control Points (GCPs) were used to geo-reference the ortho-rectified images captured by the UAV drone. In addition, the specific accuracy of individual points (checkpoints) within the UAV survey model is compared to confirm their accuracy (see chapter 4).

3.6 Data Reduction and Calculations for Total Station and GPS Field data

The digital data from the M3 Trimble Total Station and Trimble GPS were exported to an SD card as a .csv file. This is the standard file format for QGIS and other survey software applications. The .csv file was imported into QGIS after being copied from the SD card to the computer. The import procedure involves converting the observation data's raw bearings and distances into points in coordinate format. Next, a unique point identifier that the QGIS software can understand is encoded into the observation data in the field using an alphabetic coding system. Finally, additional string information is stored in conjunction with point coding to create lines between common points. This coding and string system also permits QGIS to automatically label contour-able points and break-lines for the purpose of creating a 3-dimensional triangle file, which is used to generate contour data, DSM and DEM within the software. Following the completion of the reduction process, the reduction report and data were manually inspected for errors.

3.7 Photo Ortho-Rectification, Mosaic, DSM and DEM of UAV Data

The Pix4D software package was chosen after additional research into alternative image processing applications. This package is provided for DJI Phantom UAV owners and operators in a specialised software format.

Thankfully, the standard version of the software has the same features as the specialised format; therefore, the traditional version was used for this thesis. The software Pix4D's image import and tiling procedure was more focused on the UAV image, allowing the post-processing of the UAV images to be completed in a comparable amount of time to that of traditional survey data. After evaluating several software packages, it was determined that Pix4D was the most suitable for creating photogrammetric and digital elevation models (DEM). After determining that Pix4D was the most suitable software for processing the field data within this thesis, the images were imported into the Pix4D programme. The Pix4D software contains a three-stage automatic image processing capability, with each automatic processing being performed in response to the user's instructions.

The first section of processing is image tiling, which combines unprocessed raw images into an orthophoto and generates an approximate DEM using automatic tie points within the photos. An additional section of the programme allows the software user to manually select tie points and enter the three-dimensional coordinates of the ground control points (GCPs). The GCP is associated with each image by selecting the control point, zooming in on the portion of the image containing the GCP, and clicking on the GCP's centre. Figure 3.9 depicts the preliminary processing. After selecting GCP points, the programme's first section was reprocessed to generate a georeferenced orthophoto.

Figure 3.12 is a screenshot of the initial processing options within Pix4D

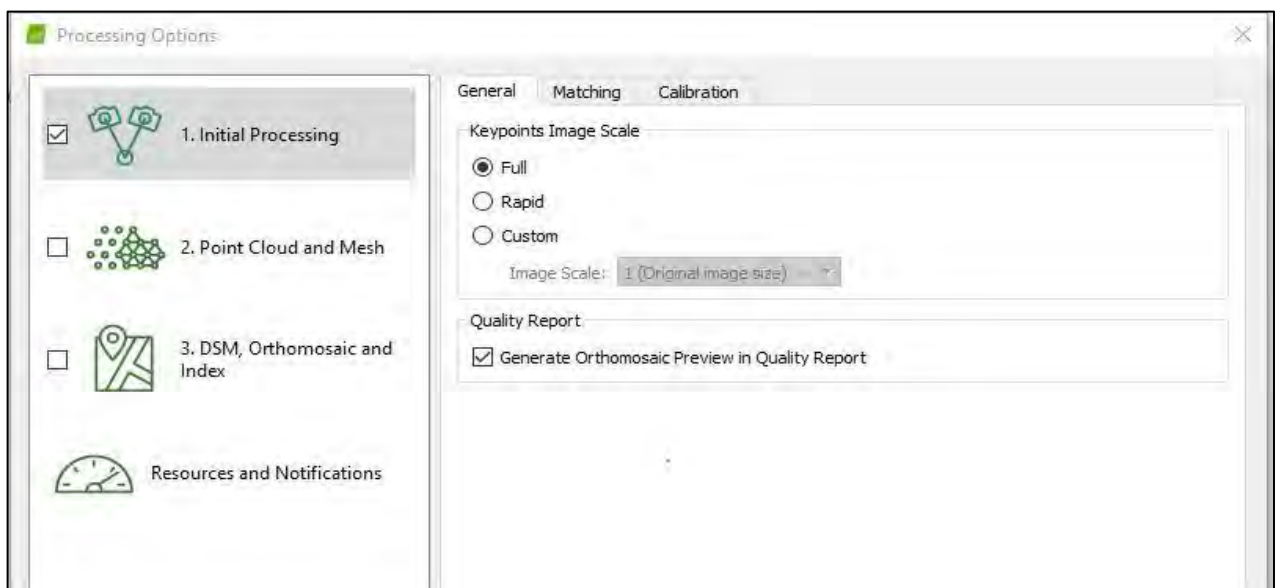


Figure 3.12: Screenshot of the processing options for initial processing within Pix4D

In the beginning, a new project was created in Pix4d mapper. After the clean project was opened and saved, the images from the initial 100-meter-high flight were imported.

After choosing GCP points, the program's first section was re-processed to create a geo-referenced orthophoto.

Firstly, a new project was opened in Pix4d mapper. After the clean project was opened and saved, the images were imported from the first flight at 100m above ground level.

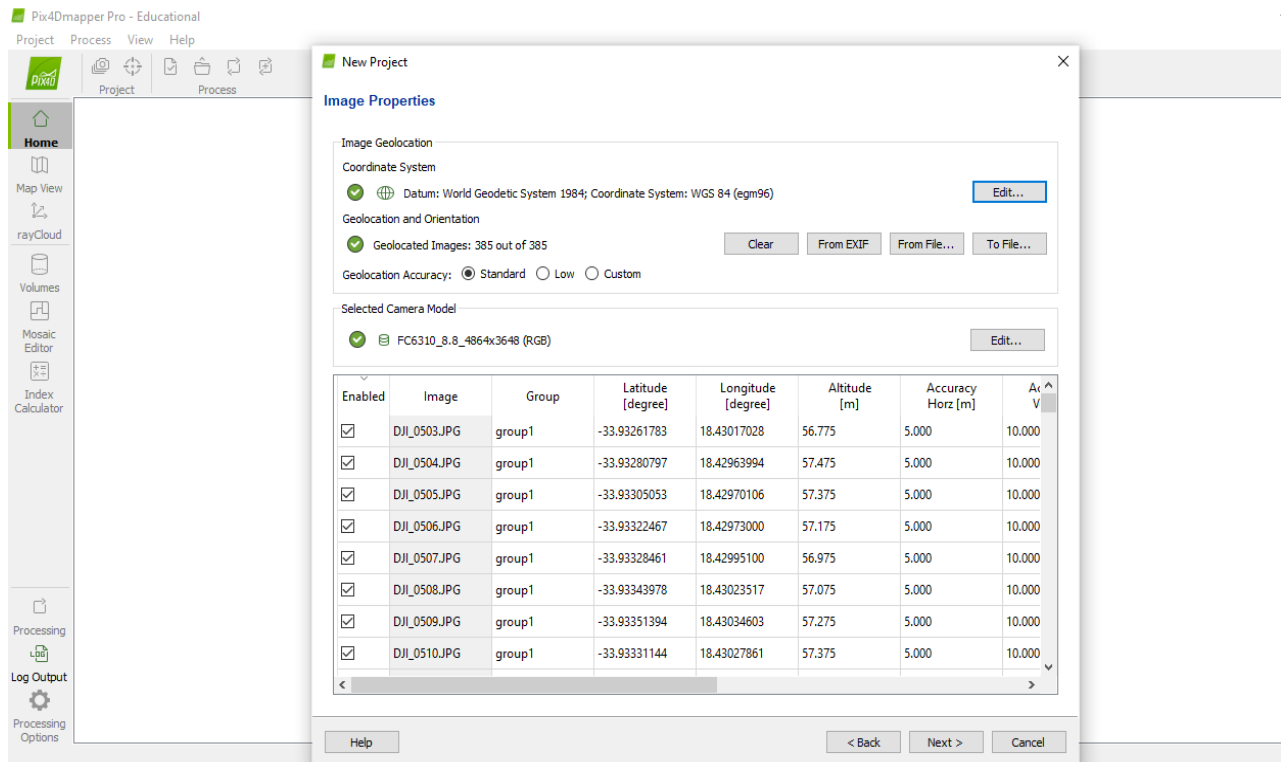


FIGURE 3.13: THE IMAGES IMPORTED IN PIX4D SOFTWARE (NB, THESE ARE APPROXIMATE COORDINATES)

Figure 3.14 demonstrates that the second phase of Pix4D's automatic processing creates a densified point cloud, which generates, a dense three-dimensional point cloud model based on the user-specified point resolution. In this thesis, the point cloud density was optimised, and the image scale was set to 1:1 for field data processing.

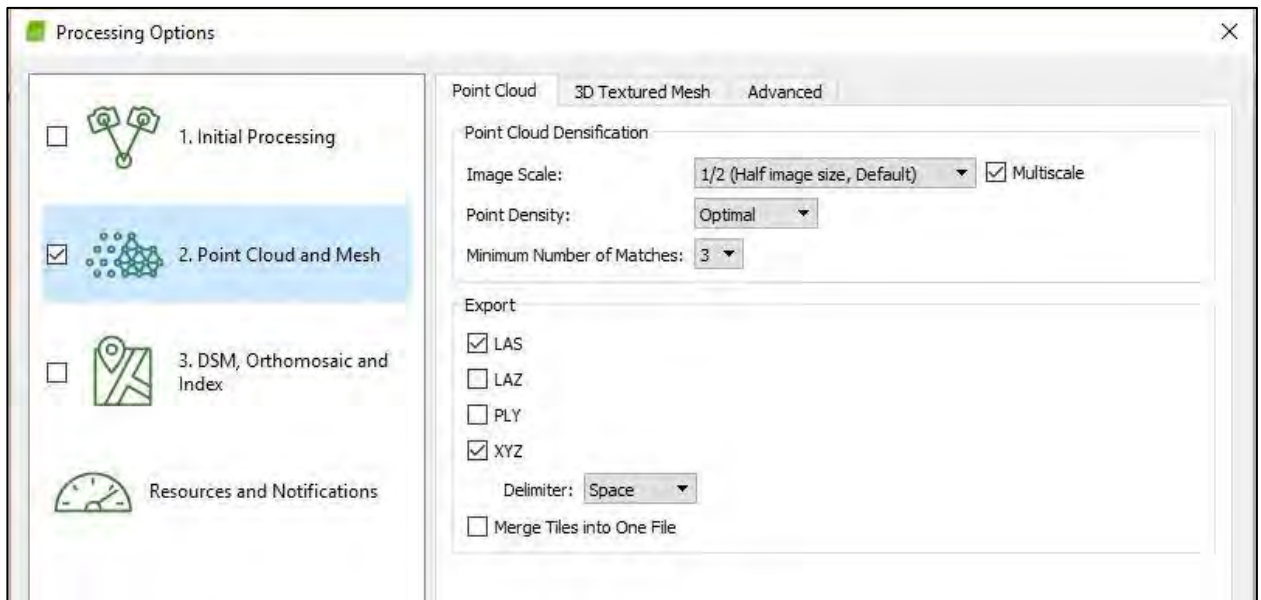


FIGURE 3.14: SCREENSHOT OF THE PROCESSING OPTIONS FOR THE POINT CLOUD AND MESH CREATION

The third phase of Pix4D's automatic processing generates a DSM model from the densified point cloud created in the second phase is illustrated in Figure 3.15. The DEM model created in this section may be the most useful spatial data provided by the software, as the large size of the densified point cloud makes it challenging to import into alternative CAD programmes. The DEM is generated based on the user-specified resolution, which is determined in relation to the ground sampling distance derived in sections one and two of Pix4D processing. Before processing, the additional output of an AutoCAD DXF file was designated for use. The third section also generates a high-resolution ortho-rectified image, which is extremely useful for the output of the final product. The resolution of this ortho-rectified image was set to 1 x ground sampling distance (GSD), with the GSD value determined as 1 x GSD (2.91 [cm/pixel])-[100m], 1 x GSD (3.43 [cm/pixel]) [120m], and 1 x GSD (3.88 [cm/pixel]). For more information, refer to the Pix4D processing reports in Appendix D, E and F

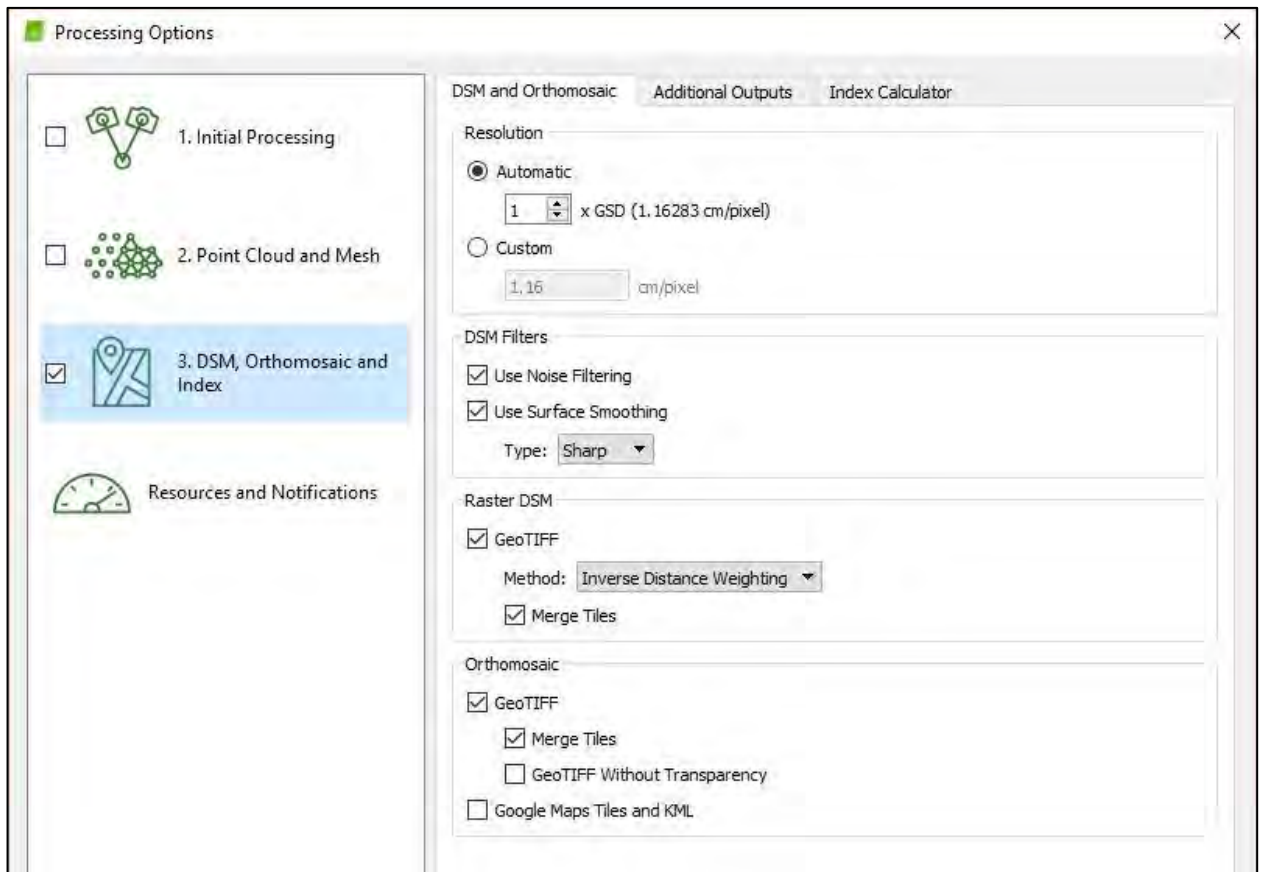


FIGURE 3.15: SCREENSHOT OF THE PROCESSING OPTIONS FOR THE DSM & ORTHO-MOSAIC CREATION

Using the Pix4D point cloud editor, any unwanted data within the photogrammetric point cloud model can be removed, allowing unwanted objects such as vegetation, and other structures to be removed from the point cloud (see Figure 3.16). This enables the point cloud model to provide a more accurate measurement of the site; see the section on analysis for more information on the point cloud editing performed during the field testing for this thesis.



FIGURE 3.16: POINT CLOUD GENERATION FROM THE PIX4D SOFTWARE INITIAL ANALYSIS

3.8 Shuttle Radar Topography Mission data

The National Aeronautics and Space Administration (NASA) Shuttle Radar Topographic Mission (SRTM) has provided digital elevation data (DEMs) for over 80% of the globe, (Rodriguez et al.,2005). This data is currently distributed by USGS and is available for download from the National Map Seamless Data Distribution System or the USGS ftp site (<https://earthexplorer.usgs.gov/>). The SRTM 1 Arc-Second Global elevation data offer worldwide coverage of void-filled data at a resolution of 1 arc-second (30 meters) and provide open distribution of this high-resolution global data set. To extract height information from SRTM imagery for the study area, the downloaded file (GeoTiff) was plotted on ArcGIS with a defined WGS84 Hartebeeshoek 94 coordinate system. The extracted elevations corresponded with elevations obtained from the ground survey and the two datasets were compared. The horizontal datum is the World Geodetic System of 1984 (WGS84), and the vertical datum is the Earth Gravitational Model of 1996 (EGM96).

3.9 LiDAR data

Light Detection and Ranging (LiDAR) data was provided by the City of Cape Town. It was captured in the years 2011 to 2015. The point cloud has a density of 2 to 3 points/m². The LiDAR data was processed and referenced onto the current South African geodetic datum (Hart94 datum) and land levelling datum, for horizontal and vertical positioning, respectively. Hart94 datum is based on WGS84 reference system (Wonnacott, 1999), hence all datasets (LiDAR, TS, UAV and SRTM) are based on the same horizontal geodetic datum. The heights obtained from TS survey, LiDAR, UAV and SRTM are also compatible because spheroidal orthometric height system used in South Africa is close to normal height system as applied in practice. Assessment of the vertical accuracy of DEMs is achieved by comparing SRTM, UAV and LiDAR DEMs heights with the ground total station data in western part of South Africa and the City of Cape Town (District 6 area). The LiDAR DEM used for this research has a resolution of 1m. This enabled the research to compare with the total station survey and UAV and SRTM DEMs.

3.10 Product Specification and Expected Accuracies

3.10.1 DJI Phantom 4 Pro drone

Table 3.2 summarises the instrument setting and related specifications of the UAV drone that are relevant to the fieldwork requirements within this thesis.

TABLE 3.2 PHANTOM 4 PRO SPECIFICATIONS

Source: (DJI, 2015)

Aircraft	
Weight (with battery)	1280 g
Max speed	16 m/s
Max flight altitude	6000 m
Max flight time	App. 23 min
Operating Temperature range	0°C to 40°C
Remote Controller	
Operating Frequency	2.400 GHz – 2.483 GHz
Video Output Port	USB
Intelligent flight battery	
Capacity	4480 mAh
Voltage	15.2V
Battery Type	LiPo 4S
Energy	68 Wh
Operating Temperature	-10°C to 40°C
Max charging power	100W
Camera	
Sensor	Sony EXMOR 1/2.3" Effective pixels: 12.4
Lens	FOV 94° 20mm f/2.8
ISO range	100-3200 (video) 100-1600 (photo)
Electronic Shutter speed	8s – 1/8000s
Image size	4000x3000
Photo	JPEG, DNG
Video	MP4/MOV
Supported SD cards	MicroSD

DJI has also released DJI GO, a mobile application specifically designed for its products. It permits manual control over all flight parameters, such as gimbal position, camera parameters, and flight modes. Unfortunately, the mission planning module is underdeveloped, limiting the user's ability to plan an autonomous flight that meets photogrammetric requirements. Therefore, the Pix4D Capture application was utilised for flight plan design.

3.10.2 Trimble M3 total station specifications

Table 3.3 shows a summary of the instrument setting to be used and related specifications of the total station relevant to the fieldwork requirements within this thesis.

TABLE 3.3 TRIMBLE M3 DATASHEET

Source: <http://www.kbse.com.pk/pdf/trimble-m3.pdf>

DISTANCE MEASUREMENT		POWER	
Reflectorless mode (white target) ¹	1.5 m to 300 m (4.9 ft to 984 ft)	Internal Li-ion battery (x2)	
Range with specified prisms		Output voltage	3.8 V DC
Good conditions (No haze, visibility over 40 km (25 miles))		Operating time ⁴	
With reflector sheet 5 cm x 5 cm (2 in x 2 in)		2"	approx. 12 hours (continuous distance/angle measurement)
2"	1.5 m to 270 m (4.9 ft to 886 ft)		approx. 26 hours (distance/angle measurement every 30 seconds)
3", 5"	1.5 m to 300 m (4.9 ft to 984 ft)		approx. 28 hours (continuous angle measurement)
With single prism 6.25 cm (2.5 in)		3", 5"	approx. 7.5 hours (continuous distance/angle measurement)
2"	1.5 m to 3,000 m (4.9 ft to 9,843 ft)		approx. 16 hours (distance/angle measurement every 30 seconds)
3", 5"	1.5 m to 5,000 m (4.9 ft to 16,404 ft)		approx. 20 hours (continuous angle measurement)
Accuracy ²		Charging time	
2" Prism	±(2+2 ppm x D) mm	Full charge	4 hours
2" Reflectorless	±(3+2 ppm x D) mm		
3", 5" Prism	±(3+2 ppm x D) mm	GENERAL SPECIFICATIONS	
3", 5" Reflectorless	±(3+2 ppm x D) mm	Level vials	
Winterized version		Sensitivity of Circular level vial	10/2 mm
Prism	±(3 + 2 ppm x D) mm (-10 °C to +40 °C)	Tangent/Clamps	Endless
	±(3 + 3 ppm x D) mm (-20 °C to -10 °C, +40 °C to +50 °C)	Display face 1	QVGA, 16 bit color, TFT LCD, backlit (320x240 pixel)
Reflectorless	±(3 + 2 ppm x D) mm (-10 °C to +40 °C)	Display face 2	Backlit, graphic LCD (128x64 pixel)
	±(3 + 3 ppm x D) mm (-20 °C to -10 °C, +40 °C to +50 °C)	Point memory	128 MB RAM, 128 MB Flash memory
Measuring interval ¹		Dimensions (W x D x H)	149 mm x 145 mm x 306 mm
Prism mode			(5.8 in x 5.7 in x 12.0 in)
2"	1.6 sec.	Weight (approx.)	
3", 5"	1.5 sec.	2" Main unit (without battery)	3.9 kg (8.6 lb)
Reflectorless mode		3", 5" Main unit (without battery)	3.8 kg (8.4 lb)
2"	2.1 sec.	Battery	0.1 kg (0.2 lb)
3", 5"	1.8 sec.	Carrying case	2.3 kg (5.1 lb)
Least count	1 mm (0.002 ft)	ENVIRONMENTAL	
ANGLE MEASUREMENT		Operating temperature range	-20 °C to +50 °C (-4 °F to +122 °F)
DIN 18723 accuracy (horizontal and vertical)	2"/0.5 mgon	Winterized	-30 °C to +50 °C (-22 °F to +122 °F)
	3"/1.0 mgon, 5"/1.5 mgon	Storage temperature range	-25 °C to +60 °C (-13 °F to +140 °F)
Reading system	Absolute encoder	Winterized	-30 °C to +60 °C (-22 °F to +140 °F)
Circle diameter	62 mm (2.4 in)	Atmospheric correction	
Horizontal/Vertical angle	Diametrical	Temperature range	-40 °C to +60 °C (-40 °F to +140 °F)
Minimum increment (Degree, Gon, MIL6400)	Degree: 1/5/10"	Barometric pressure	400 mmHg to 999 mmHg/533 hPa to
	Gon: 0.2/1/2 mgon		1,332 hPa/15.8 inHg to 39.3 inHg
	MIL6400: 0.005/0.02/0.05 mil	Dust and water protection	IP66
TELESCOPE		CERTIFICATION	
Tube length	125 mm (4.9 in)	Class B Part 15 FCC certification, CE Mark approval. C-Tick.	
Image	Erect	Laser safety IEC 60825-1 am2:2007	
Magnification	30x (18x/36x with optional eyepieces)	2" Prism mode	
2" Effective diameter of objective	40 mm (1.6 in)	2" Prism mode: Class 1 laser	
2" EDM diameter	45 mm (1.8 in)	2" Reflectorless/Laser Pointer: Class 3R laser	
3", 5" Effective diameter of objective	45 mm (1.8 in)	3", 5" Reflectorless / Prism mode: Class 1 laser	
3", 5" EDM diameter	50 mm (2.0 in)	3", 5" Laser Pointer: Class 2 laser	
Field of view	1°20'	Laser Plummet: Class 2 laser	
Resolving power	3", 5"		
Minimum focusing distance	1.5 m (4.9 ft)	Bluetooth type approvals are country specific.	
Laser Pointer	Coaxial Red Light		

3.10.3 Trimble R8 GNSS Receiver

Table 3.4 summarises the instrument setting to be used and related specifications of the GPS relevant to the fieldwork requirements within this thesis.

TABLE 3.4 TRIMBLE R8 GNSS RECEIVER

<http://www.inlandgps.com/Products/R8M3%20Datasheet%20200911.pdf>

<p>PERFORMANCE SPECIFICATIONS</p> <p>Measurements</p> <ul style="list-style-type: none"> • Trimble R-Track technology • Advanced Trimble Maxwell 6 Custom Survey GNSS chip with 220 channels • High precision multiple correlator for GNSS pseudorange measurements • Unfiltered, unsmoothed pseudorange measurements data for low noise, low multipath error, low time domain correlation and high dynamic response • Very low noise GNSS carrier phase measurements with <1 mm precision in a 1 Hz bandwidth • Signal-to-Noise ratios reported in dB-Hz • Proven Trimble low elevation tracking technology • Satellite signals tracked simultaneously: <ul style="list-style-type: none"> - GPS: L1C/A, L2C, L2E (Trimble method for tracking L2P), L5 - GLONASS: L1C/A, L1P, L2C/A (GLONASS M only), L2P - SBAS: L1C/A, L5 - Galileo GIOVE-A and GIOVE-B <p>Code differential GNSS positioning¹</p> <p>Horizontal 0.25 m + 1 ppm RMS</p> <p>Vertical 0.50 m + 1 ppm RMS</p> <p>WAAS differential positioning accuracy² typically <5 m 3DRMS</p> <p>Static and FastStatic GNSS surveying¹</p> <p>Horizontal 3 mm + 0.1 ppm RMS</p> <p>Vertical 3.5 mm + 0.4 ppm RMS</p> <p>Kinematic surveying¹</p> <p>Horizontal 10 mm + 1 ppm RMS</p> <p>Vertical 20 mm + 1 ppm RMS</p> <p>Initialization time³ typically <10 seconds</p> <p>Initialization reliability⁴ typically >99.9%</p> <p>HARDWARE</p> <p>Physical</p> <p>Dimensions (WxH) 19 cm x 11.2 cm (7.5 in x 4.4 in), including connectors</p> <p>Weight 1.34 kg (2.95 lb) with internal battery, internal radio, standard UHF antenna.</p> <p style="padding-left: 100px;">3.70 kg (8.16 lb) entire RTK rover including batteries, range pole, controller and bracket</p>	<p>Shock and vibration Tested and meets the following environmental standards:</p> <p>Shock Non-operating: Designed to survive a 2 m (6.6 ft) pole drop onto concrete. Operating: to 40 G, 10 msec, sawtooth</p> <p>Vibration MIL-STD-810F, FIG.514.5C-1</p> <p>Electrical</p> <ul style="list-style-type: none"> • Power 11 to 28 V DC external power input with over-voltage protection on Port 1 (7-pin Lemo) • Rechargeable, removable 7.4 V, 2.4 Ah Lithium-Ion battery in internal battery compartment. Power consumption is 3.2 W, in RTK rover mode with internal radio. Operating times on internal battery: <ul style="list-style-type: none"> - 450 MHz receive only option 5.8 hours⁷ - 450 MHz receive/transmit option 3.7 hours⁸ - GSM/GPRS 4.1 hours⁷ • Certification Class B Part 15, 22, 24 FCC certification, 850/1900 MHz. Class 10 GSM/GPRS module. CE Mark approval, and C-tick approval <p>Communications and Data Storage</p> <ul style="list-style-type: none"> • 3-wire serial (7-pin Lemo) on Port 1. Full RS-232 serial on Port 2 (Dsub 9 pin) • Fully integrated, fully sealed internal 450 MHz receiver/transmitter option: <ul style="list-style-type: none"> - Transmit power: 0.5 W - Range⁶: 3-5 km typical / 10 km optimal • Fully integrated, fully sealed internal GSM/GPRS option⁷ • Fully integrated, fully sealed 2.4 GHz communications port (Bluetooth[®])⁹ • External cellphone support for GSM/GPRS/CDPD modems for RTK and VRS operations • Data storage on 57 MB internal memory: 40.7 days of raw observables (approx. 1.4 MB /Day), based on recording every 15 seconds from an average of 14 satellites • 1 Hz, 2 Hz, 5 Hz, 10 Hz, and 20 Hz positioning • CMR+, CMRx, RTCM 2.1, RTCM 2.3, RTCM 3.0, RTCM 3.1 Input and Output • 16 NMEA outputs, GSO, RT17 and RT27 outputs. Supports BINEX and smoothed carrier
---	---

3.11 Software

With the introduction of UAV photogrammetry, drone-specific software has begun to be developed and distributed. At least two of them became extremely popular and widespread. Agisoft PhotoScan and Pix4D are commercial programmes with annual costs of \$3499 and €2600 for Agisoft PhotoScan and Pix4D, respectively. Both are presented as advanced and comprehensive mapping and modelling solutions for transforming images into geo-referenced mosaics and 3D models. Both use similar step-by-step processes to process data and generate final products. While setting up the project and loading images, programs automatically read image metadata, including approximate image centre coordinates, flight altitude, and camera parameters. When common points on images are located, and photos are matched, image alignment is the first step of processing.

In addition, an approximate position is determined for each image, and interior orientation parameters are refined due to self-calibration. As a result, a sparse point cloud and a set of camera positions are generated. The next step is to generate a dense point cloud using a dense stereo matching algorithm. Depending on the RAM of the computer and the number of images, the process could take anywhere from a few minutes to several hours. The point cloud may contain gaps and holes in those locations where the image matching failed (Bhandari et al., 2015). However, the output can be modified or categorised prior to the next step, which is mesh construction. Mesh represents the editable, smoothable surface of the object. The final step depends on the user's specific project goals, such as whether they wish to texture a 3D model or create an orthomosaic and Digital Elevation Model.

3.12 Pix4D Mapper

In addition, Pix4D mapper software enables the classification of point clouds and DEM generation. However, the process is more straight forward than in Agisoft PhotoScan. This program's algorithm accepts the merged Raster DSM (Digital Surface Model) as input, computes a classification mask representing the terrain/objects, and generates the Raster DTM automatically (Digital Terrain Model). The primary drawback is that users can only view DTM due to the process, without the option to display a classified point cloud and visually evaluate its accuracy. In the previous software version, the point cloud classification option was available, and more user input was possible when extracting ground points. The Pix4D technical support team guarantees that the module is currently under development and will be reintroduced in future versions (Pix4D, 2016).

3.13 ArcGIS Pro

Unlike Agisoft PhotoScan and Pix4D Mapper, ArcGIS Pro is not drone-specific software but one of the most powerful GIS packages; it will be utilised for image classification. The ESRI Company developed software from which numerous GIS programmes, including ArcMap, ArcCatalog, ArcScene, and ArcGIS Online, are derived. ArcGIS Pro offers 2D and 3D mapping tools, performs advanced geospatial analyses, creates and manages datasets, works with imagery, and generates complex visualisations and other GIS-related applications. The functionality of the image processing module enables the manipulation of rasters in various formats and can be utilised for various purposes. Because image classification can be a lengthy workflow with many processing steps, ArcGIS Pro supports two methods. One of these is the Classification Wizard Module, which guides the user step-by-step through the entire process and provides necessary guidance. In addition, separate tools such as segmentation, training sample manager, classify, merge classes, assign classes, accuracy assessment, and re-classifier are available for advanced users to perform desirable classification. To guarantee the impartiality of the classification procedure, the author adopted the second method.

3.14 Summary

In conclusion, the above sections describe in detail the methodology utilised in this thesis' field testing. In addition, it details the pre-field test planning and field methodology for both types of surveys.

The test field contained eighteen (18) evenly dispersed GCPs marked and distinguishable just before the flight. These GCPs were surveyed using the GPS and Trimble M3 Total Station. The total station measurements were selected because they were deemed more precise than the GPS survey. Total station-based systems offer the highest degree of accuracy for site positioning, stakeout, grade verification, and measurement. A Total Station-based system has a shorter range than a GNSS-based system and is better suited for projects where precision is of the utmost importance. Over the 33-ha test site, a total of 159 test points were placed. The test points were evenly spaced across the entire test area. These points were then compared for accuracy. Total Station survey field data files imported into and edited in ArcGIS were exported as a shapefile (.shp). This export function permits point, line, arc, text, and DTM data output in three dimensions. Using the Pix4D software, the image processing was completed. During the field survey, the Ground Control Points (GCPs) were used to georeference the ortho-rectified images captured by the UAV drone. The Pix4D software package exported UAV data in DSM and orthomosaic formats. Throughout the total station and UAV survey, the specific accuracy of individual points (check points) is compared to confirm survey accuracy (see chapter 4).

CHAPTER 4

RESULTS

4.1 Introduction

The subsequent chapter describes the outcomes of the field testing conducted for this thesis. These results represent the typical output for the various survey types evaluated.

4.2 Traditional survey

4.2.1 Total station field data

As depicted in figure 4.1, the total station (TS) survey point data was imported into the ArcGIS software using the neutral file format (.csv) as prescribed by the software. Manual comparisons were conducted between the data observed during the automatic reduction of the neutral file and the other randomly selected manual field observations. The automatic reduction procedure was completed with no datasheet errors. Appendix D contains the field observation notes

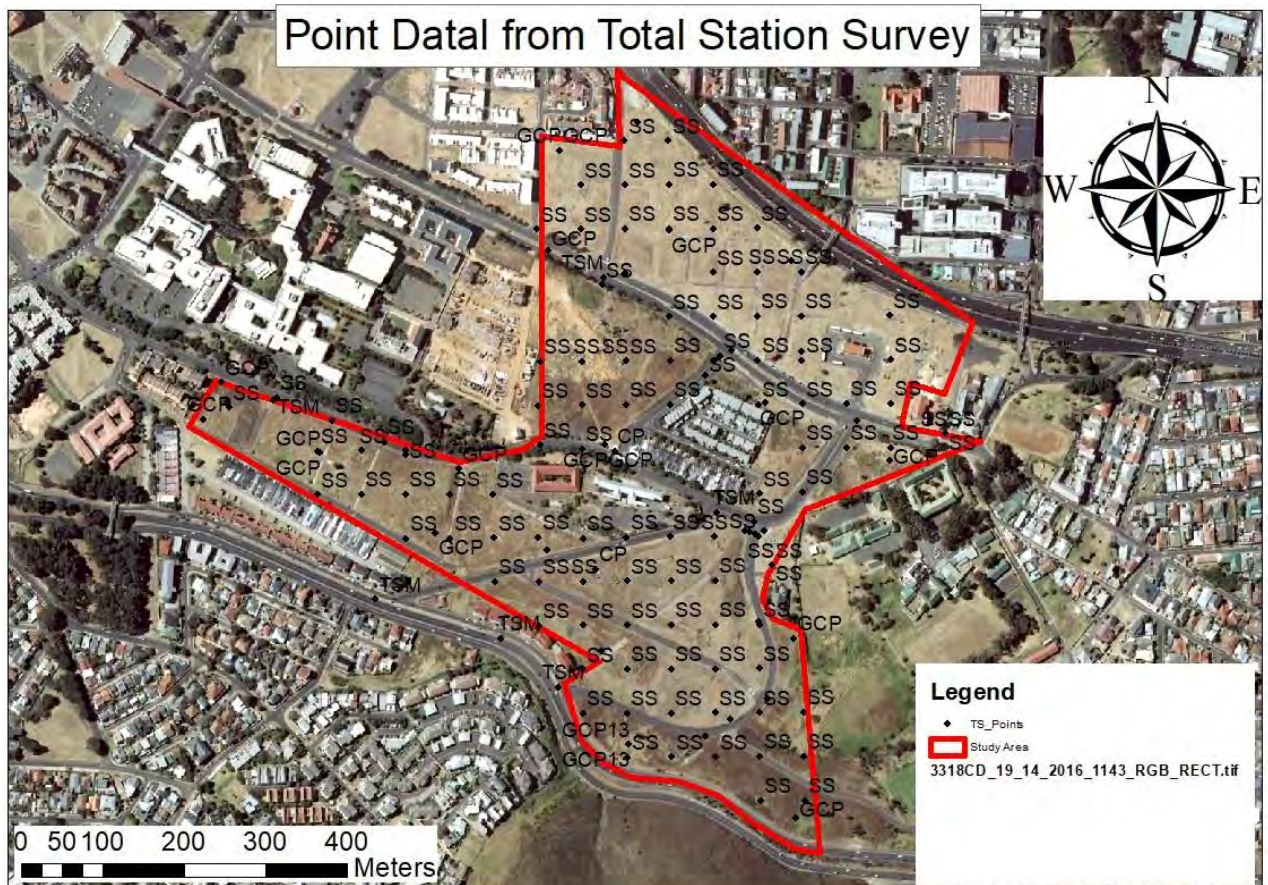


FIGURE 4.1: SCREENSHOT OF THE POINT DATA FROM THE TOTAL STATION SURVEY AFTER BEING REDUCED INTO ARCGIS

Once the point and line data have been verified, and any necessary corrections to point codes and string errors have been made, it is possible to create a three-dimensional triangle model from the point and line data. As depicted in figure 4.2, the ArcGIS software uses contour point and break-line information to generate a digital triangle mesh (DTM). This DTM can generate contours at various user-defined intervals, as shown in figure 4.3.

This contour data was output with contour intervals of 5 metres for analysis and comparison with UAV data. In addition, the DTM was exported for comparison with the UAV data. The output files were then analysed using the ArcGIS software package.

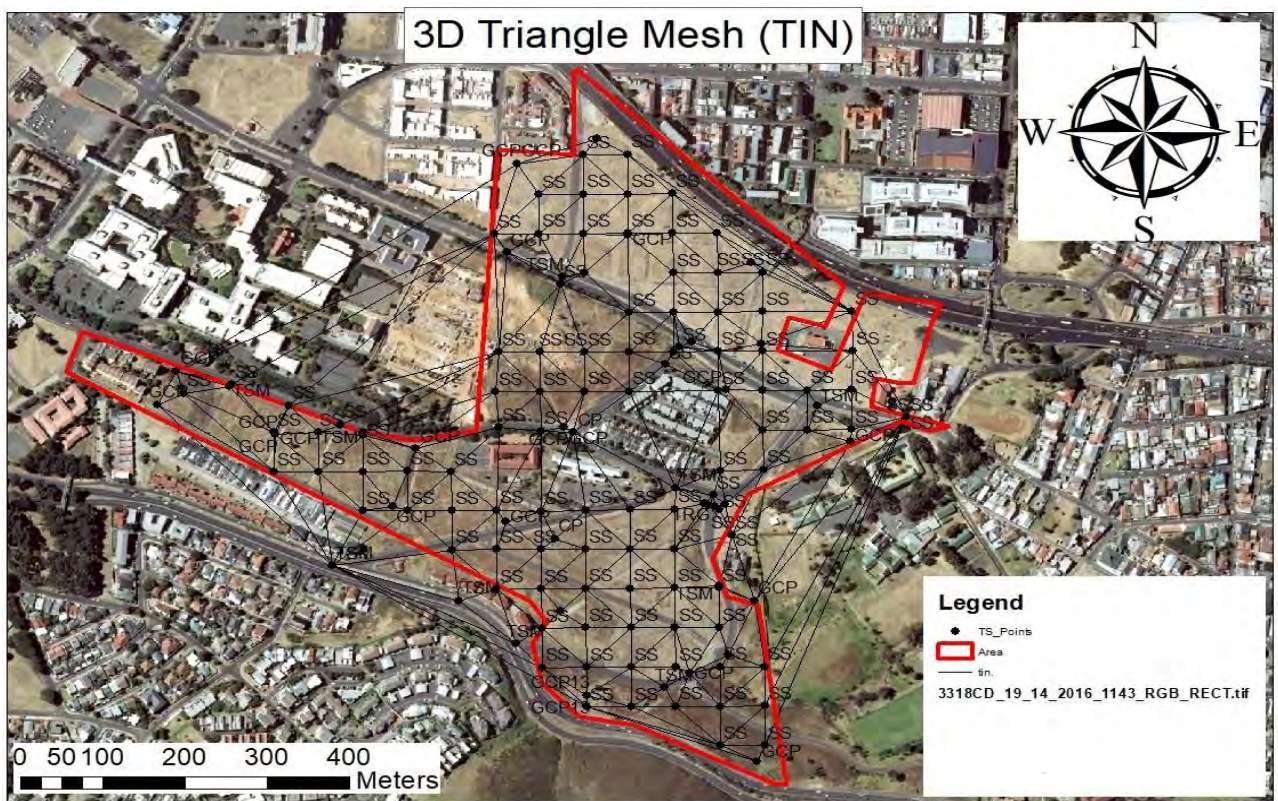


FIGURE 4.2: SCREENSHOTS OF THE 3D TRIANGLE TIN AND CONTOUR DATA FROM THE TOTAL STATION SURVEY AFTER BEING COMPUTED INTO ARCGIS

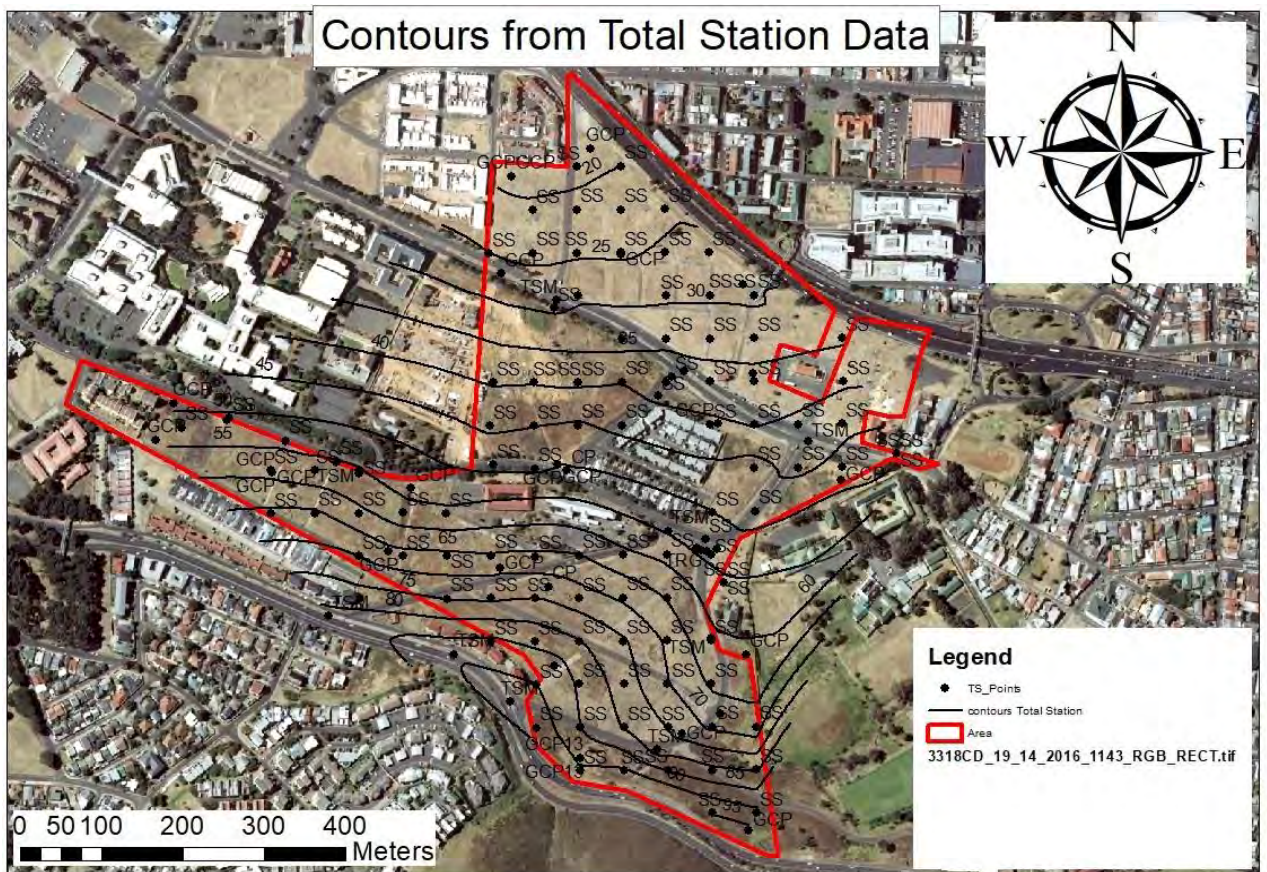


FIGURE 4.3: SCREENSHOTS OF THE 3D TRIANGLE TIN AND CONTOUR DATA FROM THE TOTAL STATION SURVEY AFTER BEING COMPUTED INTO ARCGIS

The first output of the traditional total station survey was a detailed feature survey plan. This plan illustrates the site's infrastructure and topography. As depicted in the plan legend, the detailed feature survey plan displays symbols for specific point features such as points (total stations). The contour lines depicted on the plan as indicated in the plan legend. The plan depicts the contours, origin of levels and additional survey data; see Figure 4.3. This plan is a detailed standard survey plan for the size of the field-testing site's features. The traditional total station survey detailed feature plan is depicted at a reduced scale in Figure 4.1 and appended as Appendix D.

4.2.2 Results of Total Station Surveys

As depicted in the plans, the results presented above represent the typical output of a surveyor for the types of surveys relevant to this thesis. The first plan is a point data feature, while the TIN + Contour plan is a typical output for both the detailed feature survey and the topographical survey. Together with the DTM (See Figure 4.4) plan, these plans served as a standard against which the UAV survey results and plans could be compared. The following plan depicts the DTM of the total station as measured in the field and processed in ArcMap.

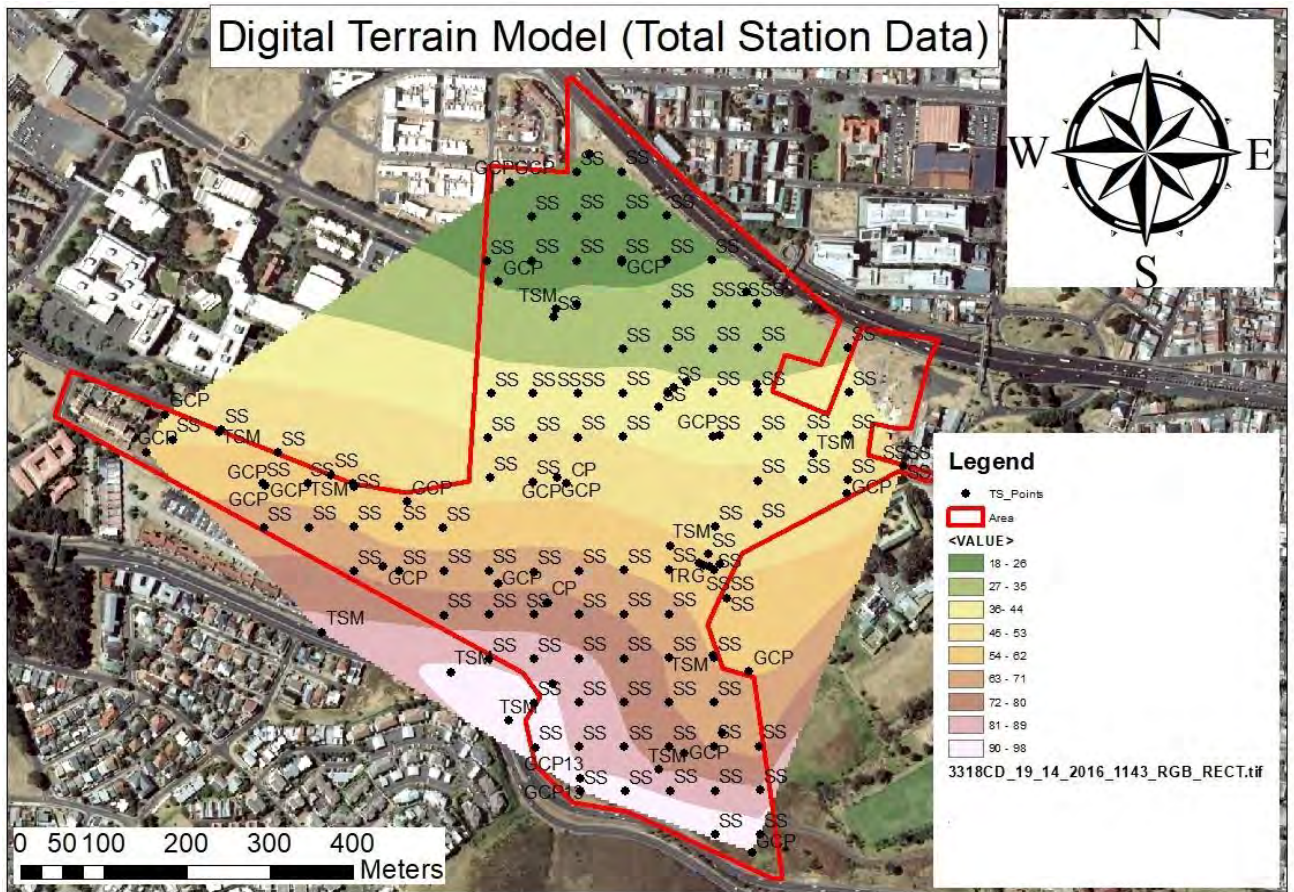


FIGURE 4.4: DIGITAL TERRAIN MODEL OF THE TOTAL STATION

4.3 Photogrammetric Data from UAV Surveys

The subsequent section summarises the outcomes of image processing, ortho rectification, and georeferencing. Again, version 4.6.4 of the software package Pix4Dmapper was used to process images. Refer to Appendices E, F, and G for additional technical information regarding the Pix4D software processing report for the three flights.

4.3.1 Image Processing

After each of the three described steps - Initial Processing, Point Cloud and Mesh - DSM and Ortho-mosaic software automatically generated statistical and quality parameter reports. It enabled the author to manage the entire process and interpret results regarding the data's nature and the project's purpose. Using the Pix4D point cloud editor, any unwanted data within the photogrammetric point cloud model can be edited out, allowing unwanted objects such as vegetation, and other structures to be edited out of the point cloud, see figure 4.5.

This enables the point cloud model to provide a more accurate measurement of the site; see the section on analysis for more information on the point cloud editing performed during the field testing for this dissertation.



FIGURE 4.5: COMPARISON SECTION SCREENSHOT OF THE POINT CLOUD EDITOR SECTION OF THE PIX4D SOFTWARE PACKAGE

The image processing was completed in less than 5 hours through the Pix4D software per flight. A total of 385 images with a ground sampling resolution (GSR) of 29.1mm/ pixel for flight (100m), 290 images with a GSR of 34.30mm/pixel for flight (120m), and 212 images with a GSR of 38.80mm/pixel for flight (150m) were processed (140m). The Pix4D software calculated that the total site area within the ortho-rectified georeferenced image was 0.583km² for all three flights. During field testing, 18 Ground Control Points (GCPs) were used to georeference the ortho-rectified or 'tiled' images captured by the DJI Phantom UAV. The Pix4D software computed the Root Mean Square Error (RMSE) for the GCPs to be 0.005m (100m), 0.006m (120m), and 0.005m (140m) during the geo-rectification process. The low RMSE for the GCPs indicates that the georeferenced UAV survey model has a high degree of three-dimensional accuracy. In the analysis section of this dissertation, the specific accuracy of individual points throughout the UAV survey model will be compared to confirm accuracy.

4.3.2 Point Cloud, Ortho-mosaic, and Digital Surface Model

As computed from the ortho-rectified geo-referenced image, the point cloud data processed by the Pix4D software contained 47 573 891, 36 348 581, and 26 554 472 points for flights 100, 120, and 140m million points, respectively. In addition, figures 4.6 (100m), 4.7 (120m), and 4.8 (200m) illustrate that the software also produced DSM and ortho-mosaic products (140m). The two items were subsequently imported into ArcGIS. Finally, the elevation model was calculated using the surface model for comparison with the ground survey.

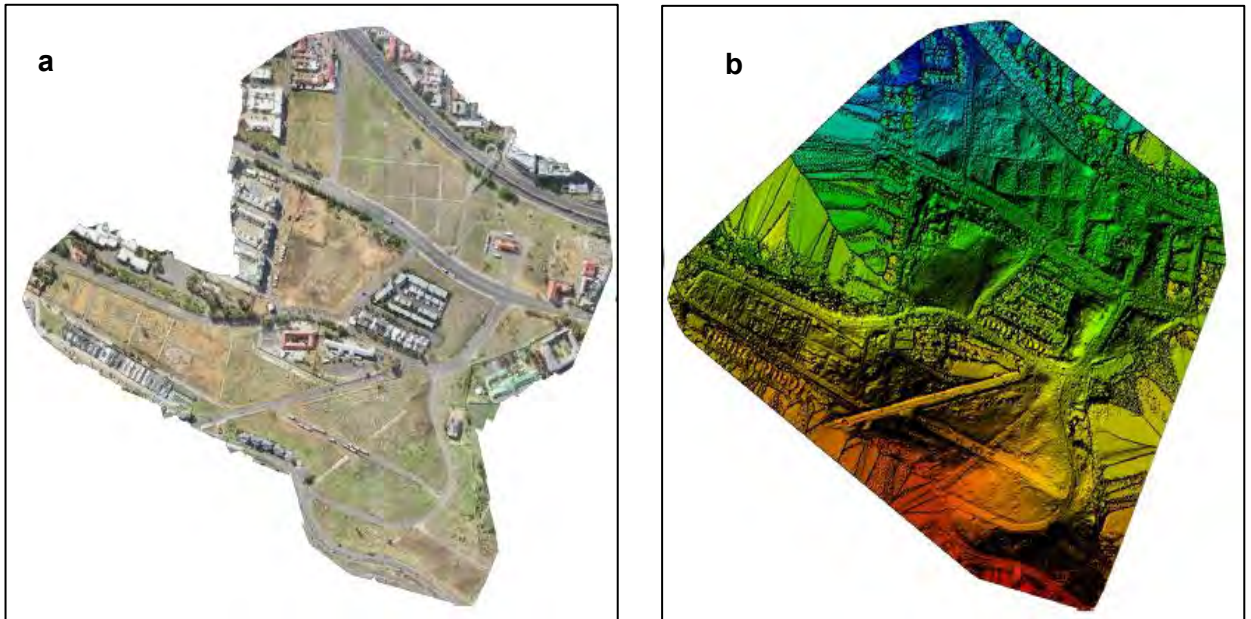


FIGURE 4.6: (A) ORTHO-MOSAIC OF THE COMPARISON AREA AT FLIGHT HEIGHT 100 M AND (B) DIGITAL SURFACE MODEL OF THE COMPARISON AREA AT FLIGHT HEIGHT 100M

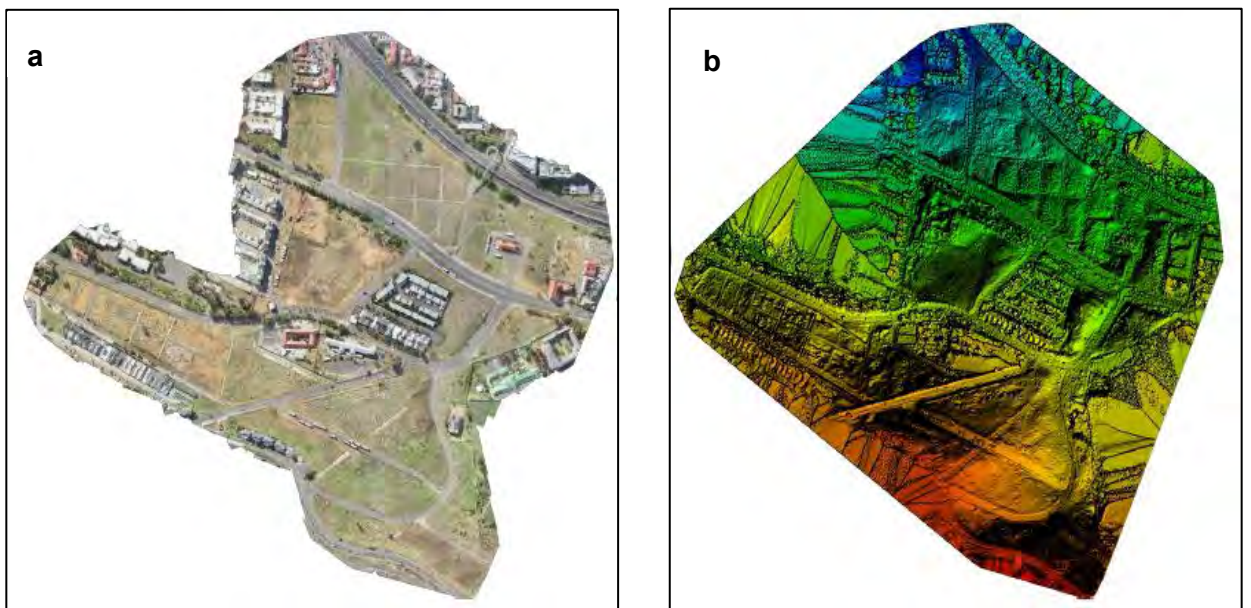


FIGURE 4.7: (A) ORTHO-MOSAIC OF THE COMPARISON AREA AT FLIGHT HEIGHT 120 M AND (B) DIGITAL SURFACE MODEL OF THE COMPARISON AREA AT FLIGHT HEIGHT 120M

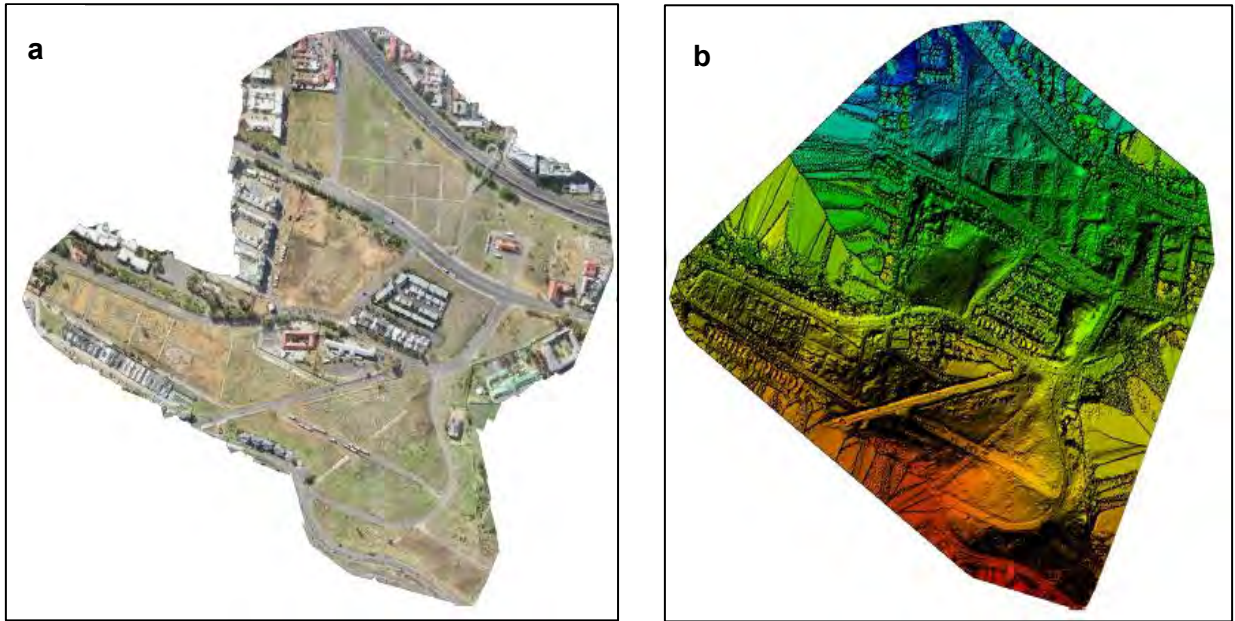


FIGURE 4.8: (A) ORTHO-MOSAIC OF THE COMPARISON AREA AT FLIGHT HEIGHT 140 M AND (B) DIGITAL SURFACE MODEL OF THE COMPARISON AREA AT FLIGHT HEIGHT 140M

4.3.3 Surface Model Points Extraction

The Pix4D Mapper-exported surface models for all three flights were imported into a new ArcGIS project. The coordinate system for the project workspace was set to WGS 84 Hartebeeshoek 94. The DSM was generated using the medium resolution mode. Independent verification of the horizontal and vertical accuracy of the DSM is the most crucial evaluation of all of these procedures. For this purpose, the checkpoints were surveyed during image acquisition. The UAV DSM was compared to the measured points using a total station for these points. These differences' statistics were calculated. The orthophoto was created using aerial triangulation based on the measurement of tie points. It is the image of the scene obtained by successfully registering each overlapping image pair of the study area acquired by the UAV and ensuring that both the height and tilt distortions are removed (orthorectification) to ensure geometric correctness, which is crucial for the accurate extraction of spatial information from the orthophoto of the imaged area. Before flying the drone, the reason for pre-marking the points was to ensure that the points were visible on the image after the flight. As depicted in figure 4.9, the points were then digitised, and their horizontal coordinates (x, y) and height (z) were derived from the orthomosaic georeferenced image and DSM. The "Extract Values To Points" tool under spatial analysis tools in ArcGIS creates a new feature class of points containing the values of a single raster at a set of input point features after digitising the points. Using the total station survey points, values were extracted from the UAV DSM, and the two data sets (TS and UAV) were compared for all three flights.

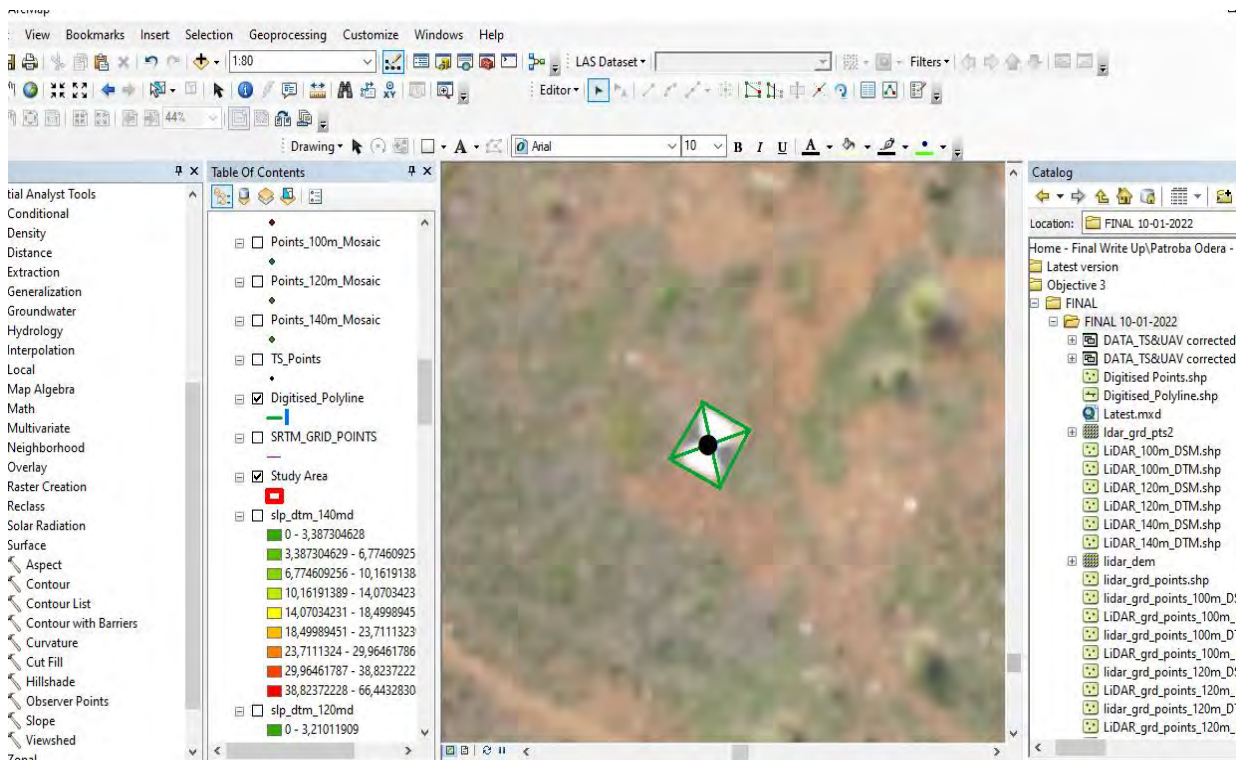


FIGURE 4.9: SCREENSHOT OF DIGITISING OF POINTS PROCESS FROM ORTHOMOSAICS

Both horizontal and vertical positions—the elevation range of the DSMs as depicted in figures 4.10, 4.11, and 4.12—were compared.

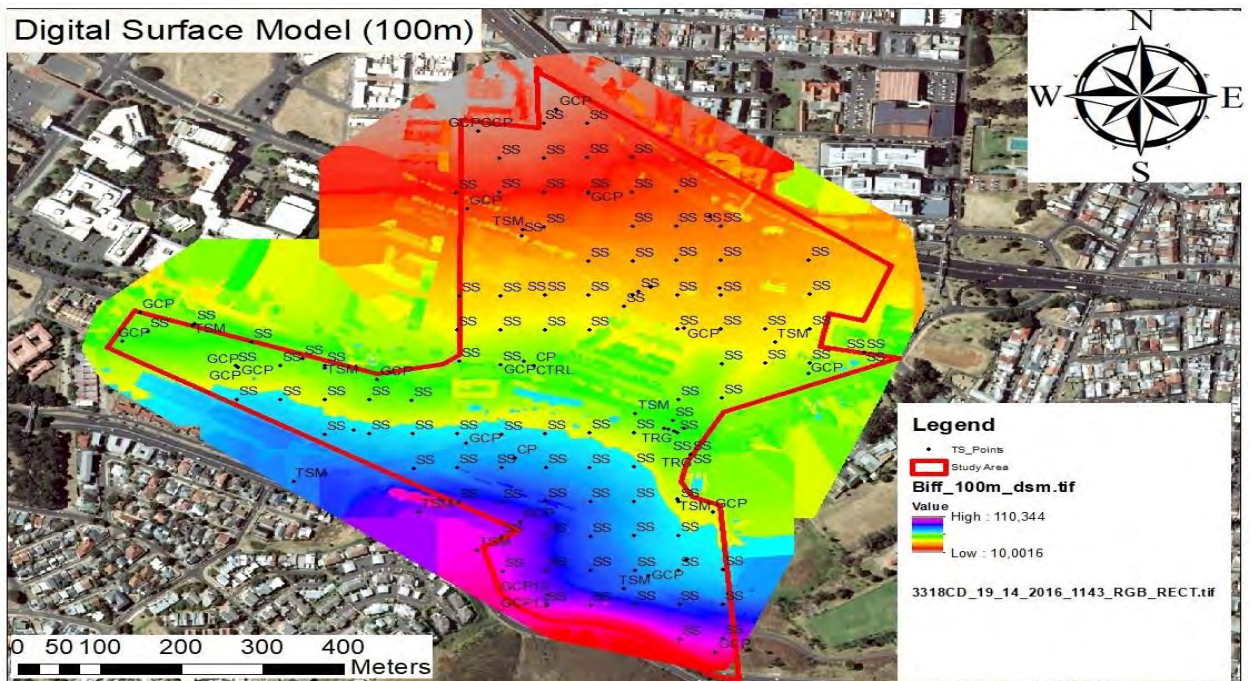


FIGURE 4.10: DSM ELEVATION RANGES FOR FLIGHT 100M (10.0016M – 110.344M)

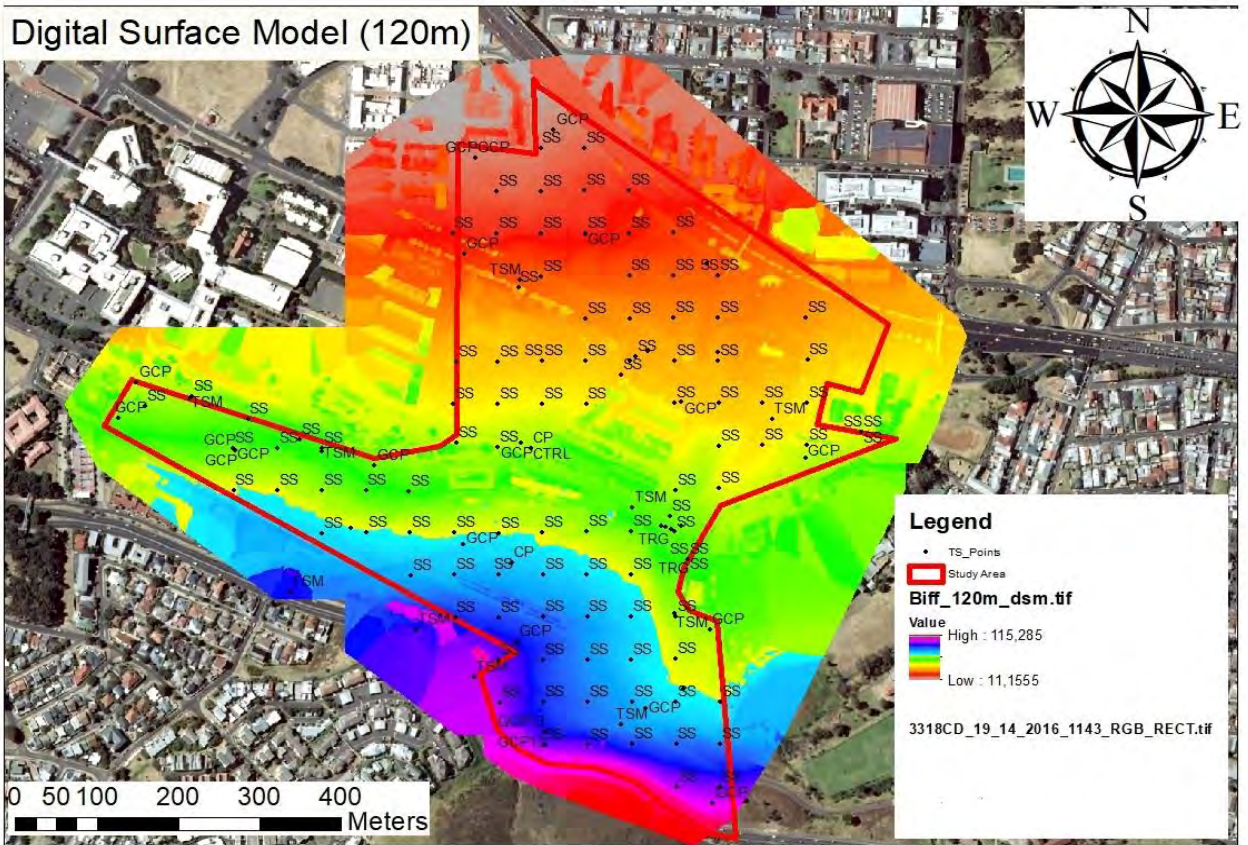


FIGURE 4.11: DSM ELEVATION RANGES FOR FLIGHT 120M (11.1555M – 115.285M)

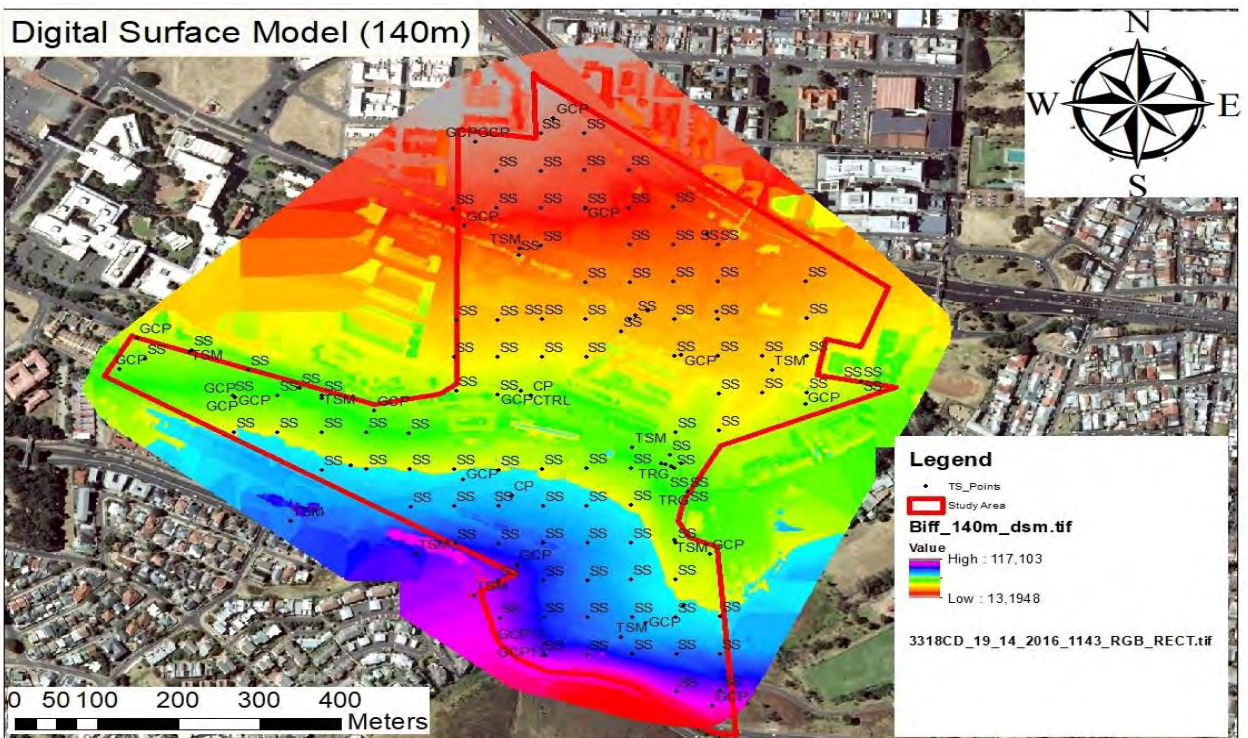


FIGURE 4.12: DSM ELEVATION RANGE FOR FLIGHT 140M (13.1948M – 117.103M)

Using pix4d software, the above DSMs were efficiently generated through automated image matching of high-resolution optical stereo images or stereo photogrammetry. Since both the exterior and interior orientations are known, stereo matching is utilised to locate corresponding pixels in pairs of images, thereby enabling 3D reconstruction via triangulation. The three DSMs generated from different UAV flight heights (100, 120, and 140m) are integral to this study. This study examines the spatial scale in relation to UAV flight altitudes. The flight datum was derived from the same take-off point for each of the three drone flights. The three models presented above illustrate the height ranges for each flight.

4.3.4 Results of the model accuracy assessment for the generated DEM

The method used to assess the accuracy of the derived models compared to the total station survey is to report the discrepancies between the precisely surveyed check points and their location in the derived point cloud and surface models. For each scenario, a set of metrics for evaluating X, Y, and Z accuracy were derived (RMSE, SD, mean, minimum and maximum). The statistical results between the DSM extracted coordinates and the total station acquired coordinates at 100, 120, and 140m flight height is presented in Table 4.1. Nonetheless, the most important statistic in the table is the root-mean-squared error (RMSE), which represents the measure of the differences between sample or population values predicted by a model or estimator and the observed values obtained from the DGPS acquired and orthophoto/DSM extracted coordinates of the test points. The horizontal RMSE computed using Eq. (3) and the discrepancy values listed in Table 4.1 is 0.050m & 0.040m (100m), 0.046m & 0.038m (120m), and 0.052m & 0.052m (140m) for the X and Y, respectively, while the computed vertical RMSE is 0.338m (100m), 0.079m (120m), and 0.264m(140m) (140m).

TABLE 4.1 DIFFERENCES IN X, Y AND Z BETWEEN TOTAL STATION AND UAV DEM DATA AT 100, 120 AND 140 FLIGHT HEIGHTS (ABSOLUTE)

Flight height (m)	Number of points	Differences (m)	Minimum (m)	Maximum (m)	Mean (m)	Standard deviation (m)	RMSE (m)
100	150	x	-0.247	0.156	0.005	0.049	0.050
		y	-0.152	0.141	0.003	0.040	0.040
		z	-0.319	1.377	0.136	0.310	0.338
120	157	x	-0.164	0.178	0.003	0.046	0.046
		y	-0.136	0.097	-0.001	0.038	0.038
		z	-0.270	0.369	-0.042	0.067	0.079
140	156	x	-0.131	0.209	0.013	0.050	0.052
		y	-0.224	0.107	-0.020	0.048	0.052
		z	-0.863	0.441	0.053	0.259	0.264

Table 4.1 shows some variations in the accuracy across flight heights. For example, better accuracy for x and y at 120 m flight height followed by 100 and 140 m in that order, while better accuracy for z is achieved at 120 followed by 140 and 100 in that order. The smaller the standard deviation or RMSE, the better the accuracy.

4.3.5 Results of the slope variation accuracy assessment

Slope quantifies the rate of elevation change at a surface location. Slope can be expressed as a percentage or a degree. The slope and aspect of an area unit (e.g., a cell or triangle) are determined by the unit's normal vector's magnitude and direction of tilt, which is a perpendicularly directed line. Diverse approximation (finite difference) methods for calculating slope from an elevation raster have been proposed. With the aid of established software, it is simple to determine the dimensions of the selected study area, which can be considered the primary focus of this investigation. In addition, it is possible to obtain the cross-section of a selected area, which aids in determining the highest and lowest points of each area and the terrain profiles. These slope profiles are determined based on their respective axes (vertical

and horizontal), as both axes produce distinct terrain profiles for each slope. See Figures 4.13, 4.14, and 4.15 below for the slope map, which was created and expressed in degrees. Table 4.2 illustrates the differences between total station and UAV DEM data at 100 m flight altitude and varying slopes. The range of slope degrees was 0 to 15.

Table 4.2 for 100m flying height, Table 4.3 for 120m flying height and Table 4.4 for 140m flying height display the RMSE for all slope ranges for x, y, and z. Chapter 5 of this thesis provides a concise analysis of these findings.

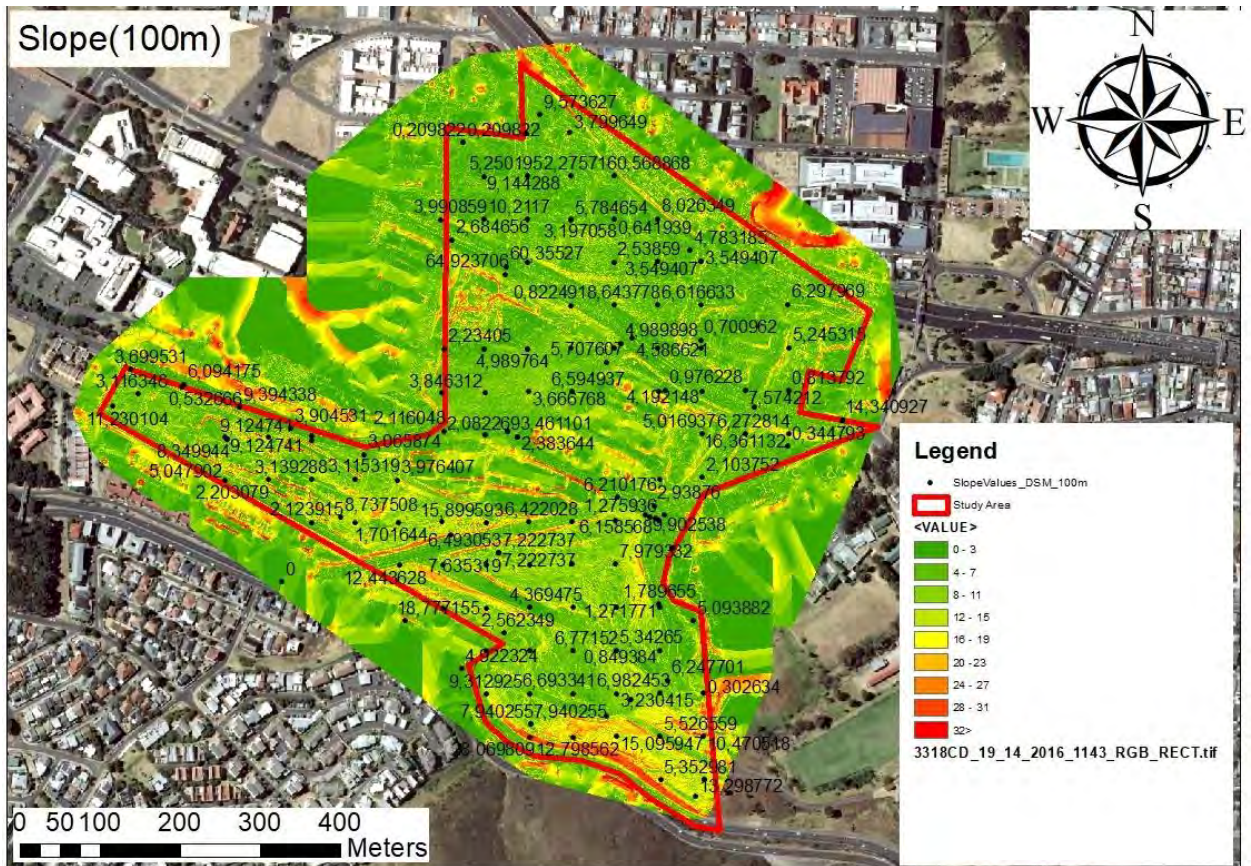


FIGURE 4.13: SLOPE MAP SHOWING 100M FLYING HEIGHT POINT VALUES.

TABLE 4.2 VARIATION OF DIFFERENCES BETWEEN TOTAL STATION AND UAV DEM DATA AT VARYING SLOPES
AT 100 M FLIGHT HEIGHT

Slope range (degrees)	Number of points	Differences (m)	Minimum (m)	Maximum (m)	Mean (m)	Standard deviation (m)	RMSE (m)
0 - 5	58	x	-0.143	0.156	0.003	0.050	0.050
		y	-0.118	0.119	0.009	0.041	0.041
		z	-0.319	1.377	0.206	0.357	0.410
5 - 10	48	x	-0.089	0.141	0.009	0.043	0.044
		y	-0.152	0.141	0.005	0.044	0.044
		z	-0.187	1.137	0.098	0.246	0.262
10 - 15	31	X	-0.247	0.093	-0.003	0.055	-0.055
		Y	-0.092	0.061	-0.001	0.031	0.030
		z	-0.177	1.191	0.131	0.335	0.355
>15	13	x	-0.110	0.111	0.018	0.054	0.055
		y	-0.070	0.043	-0.019	0.033	0.037
		z	-0.228	0.160	-0.024	0.124	0.121

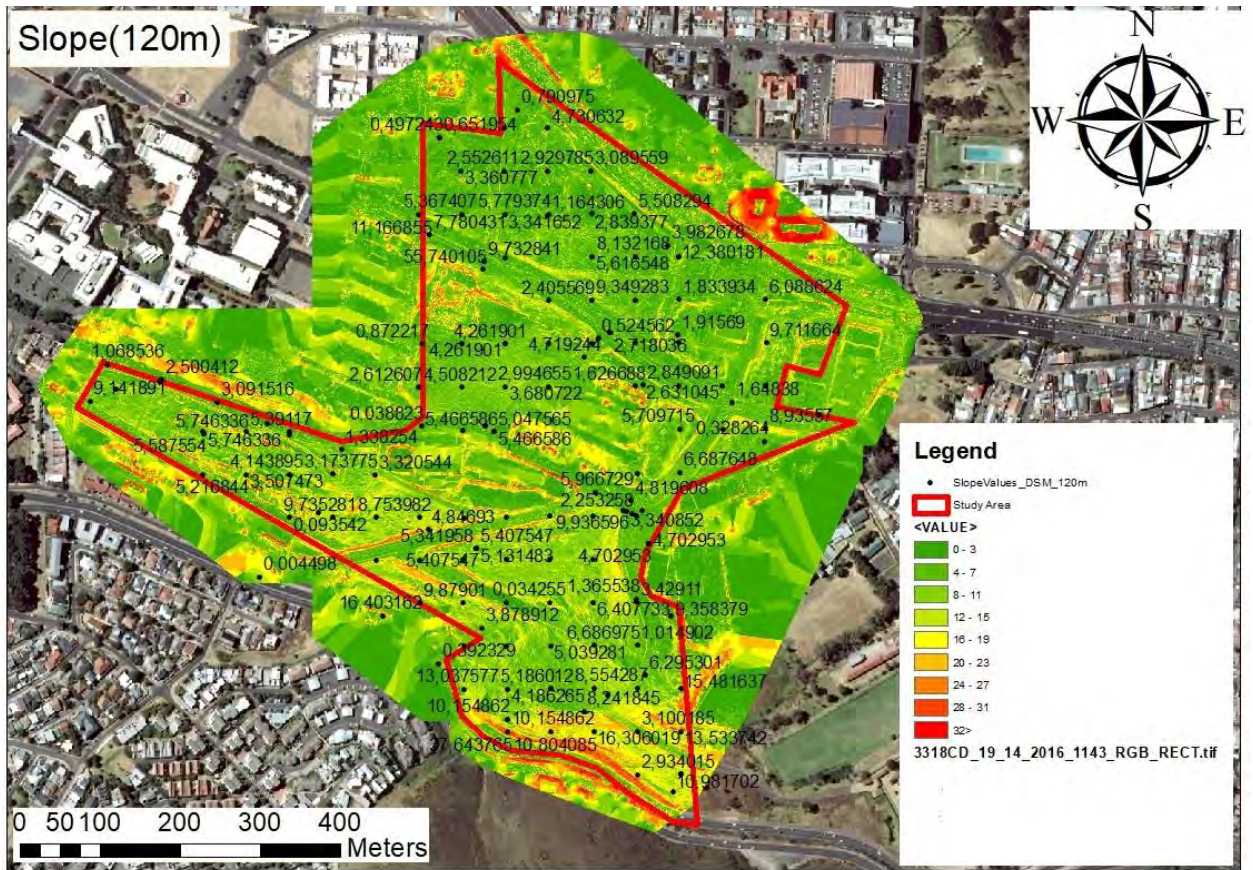


FIGURE 4.14: SLOPE MAP SHOWING POINT VALUES, 120M FLYING HEIGHT

TABLE 4.3 VARIATION OF DIFFERENCES BETWEEN TOTAL STATION AND UAV DEM DATA AT VARYING SLOPES
AT 120 M FLIGHT HEIGHT

Slope range (degrees)	Number of points	Differences (m)	Minimum (m)	Maximum (m)	Mean (m)	Standard deviation (m)	RMSE (m)
0 - 5	74	x	-0.164	0.178	0.005	0.055	0.055
		y	-0.112	0.097	0.007	0.038	0.038
		z	-0.233	0.369	-0.039	0.074	0.083
5 – 10	50	x	-0.088	0.107	0.007	0.034	0.035
		y	-0.092	0.074	-0.002	0.029	0.029
		z	-0.270	0.120	-0.039	0.063	0.073
10 - 15	26	x	-0.044	0.051	-0.002	0.025	0.025
		y	-0.078	0.070	-0.010	0.040	0.040
		z	-0.215	0.006	-0.057	0.052	0.077
>15	6	x	-0.164	0.021	-0.032	0.068	0.070
		y	-0.136	0.015	-0.057	0.052	0.074
		z	-0.156	0.050	-0.041	0.087	0.090

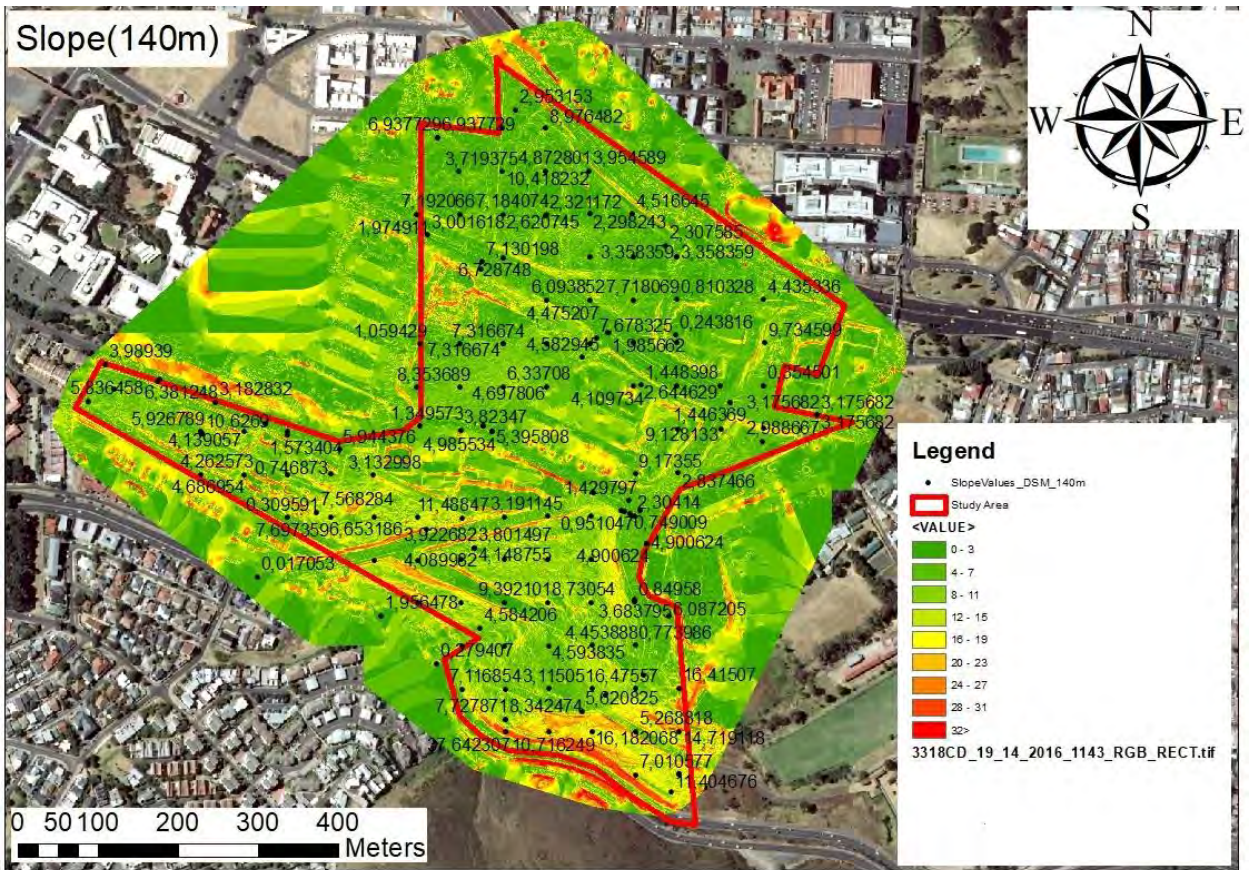


FIGURE 4.15: SLOPE MAP SHOWING POINT VALUES, 140M FLYING HEIGHT

TABLE 4.4 VARIATION OF DIFFERENCES BETWEEN TOTAL STATION AND UAV DEM DATA AT VARYING SLOPES
AT 140 M FLIGHT HEIGHT

Slope range (degrees)	Number of points	Differences (m)	Minimum (m)	Maximum (m)	Mean (m)	Standard deviation (m)	RMSE (m)
0 - 5	80	x	-0.131	0.177	0.007	0.052	0.052
		y	-0.224	0.107	-0.020	0.053	0.056
		z	-0.863	0.441	-0.093	0.264	0.278
5 - 10	49	x	-0.063	0.128	0.021	0.047	0.051
		y	-0.133	0.089	-0.016	0.047	0.049
		z	-0.726	0.393	-0.034	0.276	0.275
10 - 15	17	x	-0.113	0.058	0.008	0.038	0.038
		y	-0.115	0.026	-0.027	0.038	0.046
		z	-0.524	0.280	0.040	0.185	0.184
>15	10	x	-0.007	0.209	0.045	0.068	0.079
		y	-0.107	0.009	-0.028	0.038	0.046
		z	-0.375	0.292	-0.022	0.226	0.216

4.3.6 Results of the elevation variation accuracy assessment

The surface model comparison plans shown in Tables 4.5, 4.6 and 4.7 permits a comparison of the test area's elevation variation. The elevation comparisons indicate range differences from 0 to 20 metres, 20 to 40 metres, 40 to 60 metres, 60 to 80 metres, and 80 to 100 metres. However, specific point accuracy comparisons are made based on the number of points that fall within a particular range. The tables depict the RMSE for x, y, and z for each of the three flights. The discussion chapter of this thesis contains a concise analysis of these results.

TABLE 4.5 VARIATION OF DIFFERENCES BETWEEN TOTAL STATION AND UAV DEM DATA AT VARYING ELEVATIONS AT 100 M FLIGHT HEIGHT

Height range (m)	Number of points	Differences (m)	Minimum (m)	Maximum (m)	Mean (m)	Standard deviation (m)	RMSE (m)
0 – 20	6	x	-0.085	-0.006	-0.045	0.028	0.051
		y	0.018	0.061	0.039	0.014	0.041
		z	0.995	1.377	1.188	0.154	1.196
20 – 40	37	x	-0.247	0.141	-0.006	0.063	0.062
		y	-0.152	0.119	0.016	0.050	0.052
		z	-0.107	0.986	0.313	0.320	0.445
40 – 60	51	x	-0.055	0.156	0.017	0.044	0.047
		y	-0.064	0.141	0.011	0.032	0.034
		z	-0.187	0.329	0.016	0.127	0.126
60 – 80	36	x	-0.110	0.057	0.004	0.039	0.038
		y	-0.064	0.065	-0.009	0.027	0.028
		z	-0.218	0.125	0.016	0.070	0.071
80 – 100	20	x	-0.143	0.111	0.009	0.048	0.047
		y	-0.118	0.020	-0.029	0.038	0.047
		z	-0.319	0.160	0.017	0.113	0.112

TABLE 4.6 VARIATION OF DIFFERENCES BETWEEN TOTAL STATION AND UAV DEM DATA AT VARYING ELEVATIONS AT 120 M FLIGHT HEIGHT

Height range (m)	Number of points	Differences (m)	Minimum (m)	Maximum (m)	Mean (m)	Standard deviation (m)	RMSE (m)
0 – 20	4	x	-0.052	-0.029	-0.042	0.010	0.043
		y	0.036	0.070	0.060	0.016	0.061
		z	-0.123	-0.052	-0.082	0.030	0.086
20 – 40	38	x	-0.114	0.115	-0.001	0.042	0.042
		y	-0.090	0.097	0.012	0.039	0.040
		z	-0.162	0.369	-0.029	0.085	0.088
40 – 60	55	x	-0.074	0.178	0.029	0.048	0.051
		y	-0.028	0.072	0.011	0.021	0.025
		z	-0.163	0.048	-0.041	0.043	0.052
60 – 80	39	x	-0.164	0.056	-0.003	0.040	0.046
		y	-0.090	0.031	-0.014	0.024	0.033
		z	-0.270	-0.011	-0.087	0.064	0.098
80 – 100	22	x	-0.139	0.006	-0.017	0.040	0.040
		y	-0.136	0.052	-0.029	0.055	0.057
		z	-0.065	0.049	-0.030	0.030	0.077

TABLE 4.7 VARIATION OF DIFFERENCES BETWEEN TOTAL STATION AND UAV DEM DATA AT VARYING ELEVATIONS AT 140 M FLIGHT HEIGHT

Height range (m)	Number of points	Differences (m)	Minimum (m)	Maximum (m)	Mean (m)	Standard deviation (m)	RMSE (m)
0 – 20	4	x	-0.067	0.003	-0.016	0.034	0.034
		y	-0.001	0.049	0.024	0.029	0.035
		z	-0.726	-0.690	-0.710	0.015	0.710
20 – 40	39	x	-0.080	0.124	0.011	0.046	0.047
		y	-0.224	0.068	-0.016	0.053	0.054
		z	-0.863	0.316	-0.209	0.236	0.313
40 – 60	54	x	-0.090	0.209	0.021	0.055	0.058
		y	-0.071	0.107	-0.002	0.030	0.030
		z	-0.818	0.304	-0.018	0.249	0.247
60 - 80	39	x	-0.113	0.125	0.013	0.048	0.049
		y	-0.129	0.067	-0.039	0.047	0.061
		z	-0.273	0.441	0.063	0.186	0.194
80 - 100	20	x	-0.131	0.090	0.003	0.051	0.050
		y	-0.205	0.006	-0.045	0.061	0.075
		z	-0.079	0.292	0.066	0.082	0.103

4.4 Accuracy assessment of UAV DEM and Other Satellite-Based DEMs

The global 1-arcsecond (30-m) SRTM DEM is now accessible to the public via sites such as Earth Explorer on the United States Geological Survey website. Figure 4.16 depicts the downloaded SRTM elevation data for the study area from the (<http://earthexplorer.usgs.gov>) website. The downloaded data were then projected to the Hart 94 coordinate system using ArcMap based on the WGS84 reference system

In two ways, comparisons were made:

4.4.1 Absolute differences in height:

- Extracting height values from SRTM using the coordinates of points surveyed with TS, then comparing extracted height with UAV and TS heights for the same points (SRTM and UAV, SRTM and TS).
- Extraction of height values from LiDAR using coordinates of the points surveyed with TS, followed by comparison of extracted height with UAV and TS heights for the same points (LiDAR and UAV, LiDAR and TS).

Comparing the heights of the LiDAR and SRTM grids.

Name	Status	Date modified
s34_e018_1arc_v3 (1)		2021-10-11 02:42 PM
s34_e018_1arc_v3 (1).tif.aux		2021-10-11 02:46 PM
s34_e018_1arc_v3 (1).tif.ovr		2021-10-11 02:46 PM
s34_e018_1arc_v3.dt2		2021-10-11 02:42 PM
s34_e018_1arc_v3.dt2.aux		2021-10-11 02:46 PM
s34_e018_1arc_v3.dt2.ovr		2021-10-11 02:46 PM
s34_e018_1arc_v3_bil		2021-10-11 02:42 PM

FIGURE 4.16: SCREENSHOT OF SRTM DATA DOWNLOAD

The SRTM and LIDAR elevation data for the study area were loaded into ArcMap to facilitate comparison with the UAV and TS survey, see figures 4.17 and 4.18:

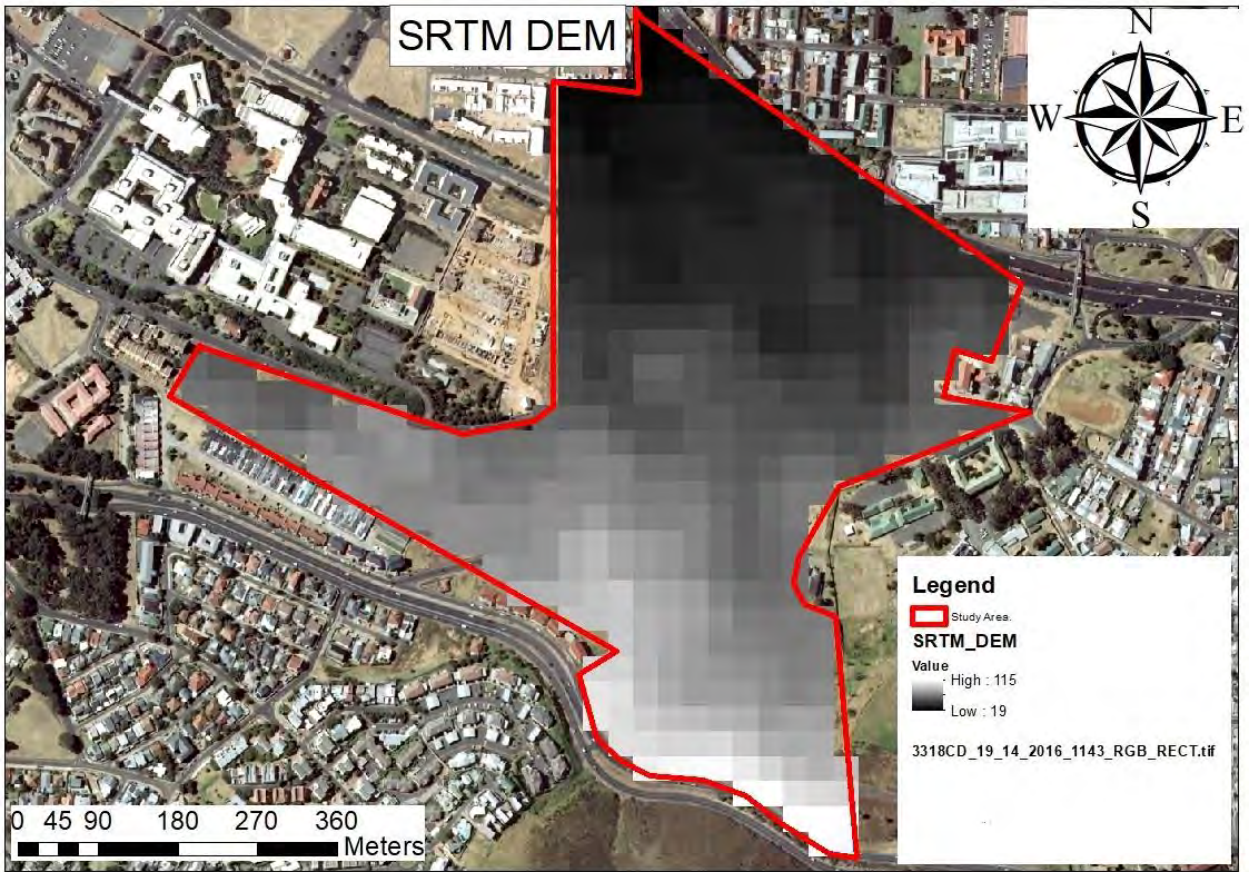


FIGURE 4.17: SRTM ELEVATION DATA



FIGURE 4.18: LIDAR ELEVATION DATA

TABLE 4.8 ABSOLUTE DIFFERENCES IN HEIGHT BETWEEN TOTAL STATION, UAV DEM, LiDAR DEM AND SRTM DEM DATA AT 100, 120 AND 140M FLIGHT HEIGHTS AT GROUND SURVEYED POINTS

Flight height (m)	Number of points	Differences in height (m)	Minimum (m)	Maximum (m)	Mean (m)	Standard deviation (m)	RMSE (m)
100	150	TS and UAV	-0.319	1.377	0.136	0.310	0.338
		TS and LiDAR	-2.867	0.751	-0.204	0.407	0.454
		TS and SRTM	-14.170	11.676	-1.157	4.053	4.202
		UAV and LiDAR	-2.973	0.396	-0.340	0.505	0.608
		UAV and SRTM	-14.244	11.660	-1.293	4.133	4.318
		LiDAR and SRTM	-14.040	11.785	-0.953	4.007	4.105
120	157	TS and UAV	-0.270	0.369	-0.042	0.067	0.079
		TS and LiDAR	-2.867	0.751	-0.198	0.400	0.445
		TS and SRTM	-14.170	11.676	-1.053	4.054	4.176
		UAV and LiDAR	-2.868	0.718	-0.156	0.401	0.429
		UAV and SRTM	-14.074	11.725	-1.011	4.054	4.166
		LiDAR and SRTM	-14.040	11.785	-0.855	4.003	4.081
140	156	TS and UAV	-0.863	0.441	0.053	0.259	0.264
		TS and LiDAR	-2.867	0.751	-0.195	0.402	0.445
		TS and SRTM	-14.170	11.676	-1.079	4.053	4.181
		UAV and LiDAR	-3.171	0.810	-0.142	0.510	0.528
		UAV and SRTM	-14.185	11.741	-1.026	4.033	4.149
		LiDAR and SRTM	-14.040	11.785	-0.884	3.999	4.083

4.4.2 Relative differences in height:

A total of 388 Grid points were generated in the study area using the fishnet function of the ArcGIS software (see figure 4.19). Table 4.9 displays the relative height differences between UAV DEM, LiDAR DEM and SRTM DEM at each of the three heights.

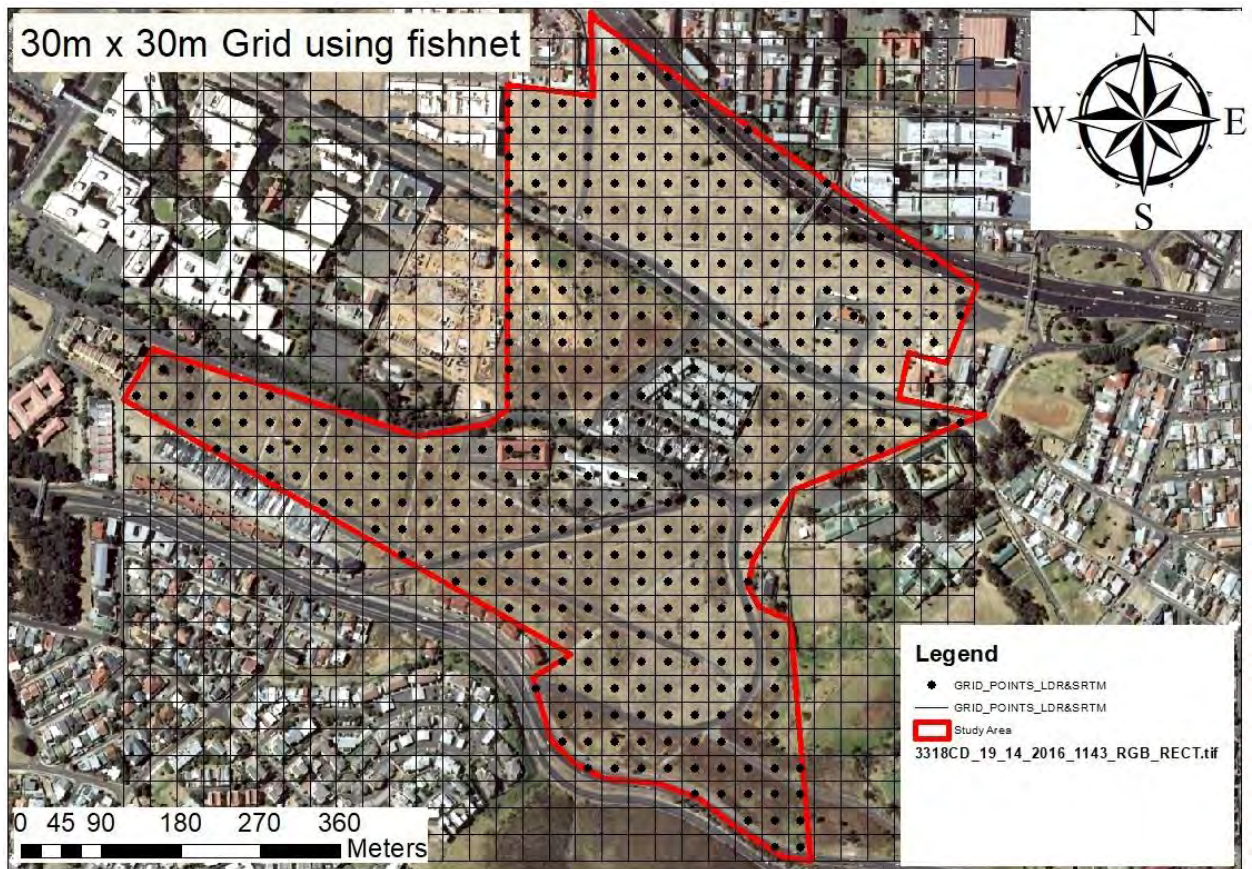


FIGURE 4.19: 30MX 30M GRID POINTS (FISHNET)

TABLE 4.9 RELATIVE DIFFERENCES IN HEIGHT BETWEEN UAV, LIDAR AND SRTM DEMS AT GRID POINTS AT 100, 120 AND 140M FLIGHT HEIGHTS

Flight height (m)	Number of points	Differences in height (m)	Minimum (m)	Maximum (m)	Mean (m)	Standard deviation (m)	RMSE (m)
100	388	UAV and LiDAR	-5.594	5.860	-0.278	0.977	1.014
		UAV and SRTM	-12.166	15.502	-0.607	4.647	4.681
		LiDAR and SRTM	-11.583	14.543	-0.330	4.381	4.388
120	388	UAV and LiDAR	-16.392	6.149	-0.095	1.216	1.218
		UAV and SRTM	-12.079	14.124	-0.424	4.511	4.525
		LiDAR and SRTM	-11.583	14.543	-0.330	4.381	4.388
140	388	UAV and LiDAR	-16.667	6.645	-0.039	1.301	1.300
		UAV and SRTM	-12.320	14.117	-0.369	4.462	4.472
		LiDAR and SRTM	-11.583	14.543	-0.330	4.381	4.388

Tables 4.10 and 4.11 display the relative differences between UAV, LiDAR and SRTM DEMs at varying slopes and elevations using grid points at a flying height of 120m.

TABLE 4.10 VARIATION OF RELATIVE DIFFERENCES BETWEEN UAV, LiDAR AND SRTM DEMs AT VARYING SLOPES USING GRID POINTS 120M FLYING HEIGHT

Slope range (degrees)	Number of points	Differences (m)	Minimum (m)	Maximum (m)	Mean (m)	Standard deviation (m)	RMSE (m)
0 – 5	126	UAV and LiDAR	-16.392	3.333	-0.224	1.638	1.646
		UAV and SRTM	-12.079	8.181	-1.460	3.972	4.217
		LiDAR and SRTM	-11.560	14.543	-1.235	4.057	4.226
5 – 10	128	UAV and LiDAR	-2.602	1.957	-0.137	0.437	0.456
		UAV and SRTM	-11.048	11.704	-0.206	4.053	4.042
		LiDAR and SRTM	-10.314	11.660	-0.069	3.981	3.966
10 – 15	67	UAV and LiDAR	-3.609	1.493	-0.189	0.642	0.664
		UAV and SRTM	-11.594	14.124	-0.248	5.365	5.330
		LiDAR and SRTM	-11.583	14.120	-0.059	5.295	5.256
>15	67	UAV and LiDAR	-2.347	6.149	0.323	1.607	1.627
		UAV and SRTM	-11.320	10.701	0.929	5.002	5.050
		LiDAR and SRTM	-11.103	10.223	0.606	4.489	4.496

TABLE 4.11: VARIATION OF RELATIVE HEIGHT DIFFERENCES BETWEEN UAV, LiDAR AND SRTM DEMs AT VARYING ELEVATIONS USING GRID POINTS 120M FLYING HEIGHT

Elevation range (m)	Number of points	Differences (m)	Minimum (m)	Maximum (m)	Mean (m)	Standard deviation (m)	RMS E (m)
0 – 20	7	UAV and LiDAR	-0.421	0.014	-0.192	0.160	0.243
		UAV and SRTM	-3.854	-0.902	-2.833	0.950	2.996
		LiDAR and SRTM	-3.868	-0.663	-2.750	1.025	2.909
20 – 40	127	UAV and LiDAR	-2.904	5.607	-0.052	0.767	0.766
		UAV and SRTM	-7.151	7.217	-1.290	3.113	3.359
		LiDAR and SRTM	-6.722	7.055	-1.239	2.885	3.129
40 – 60	116	UAV and LiDAR	-16.392	6.149	-0.165	2.009	2.007
		UAV and SRTM	-12.079	10.701	-1.035	4.461	4.561
		LiDAR and SRTM	-11.583	14.543	-0.869	4.389	4.455
60 – 80	96	UAV and LiDAR	-1.943	2.134	-0.085	0.455	0.460
		UAV and SRTM	-7.958	14.124	2.461	4.628	5.221
		LiDAR and SRTM	-7.787	14.120	2.546	4.469	5.124
80 – 100	39	UAV and LiDAR	-0.628	3.333	-0.033	0.578	0.572
		UAV and SRTM	-11.320	7.246	-1.878	5.262	5.523
		LiDAR and SRTM	-11.103	7.130	-1.844	5.104	5.365
>100	3	UAV and LiDAR	-0.130	-0.048	-0.099	0.045	0.105
		UAV and SRTM	-11.403	-2.882	-7.965	4.493	8.769
		LiDAR and SRTM	-11.285	-2.834	-7.866	4.451	8.665

4.5 Potential errors in the collected data

The UAV collected point cloud data that contained outliers. The data are impacted by systematic and random noise from various sources, such as capturing reflections on unwanted or multiple objects, such as the tops of trees and buildings. Figure 4.20 depicts examples of experimental measurement error. Outliers are values that are statistically inconsistent with the rest of the data in the set. Detecting outliers in data is frequently required prior to and after analysis. Outliers are measurement errors that the characteristics of the acquisition system They are statistically inconsistent values with the rest of the dataset's elements. It is crucial to eliminate outliers, as they frequently cause issues for point cloud analysis tools. They may result in erroneous object reconstruction and shape measurement bias. It causes numerous problems during statistical analysis and substantially affects the mean, standard deviation and root mean square error.



FIGURE 4.20: EXAMPLE OF OUTLIERS FROM THE 30X30M GRID FOR RELATIVE ACCURACY

After identifying the data set's outliers, tables 4.9, 4.10, and 4.11 were recalculated, and new statistical values were obtained (see tables 4.12, 4.13, and 4.14).

Comparing the two surveys using relative point values revealed 19 outliers. This is because the drone survey was conducted over trees and structures. Compared to the ground survey, these points were subsequently off by metres. This resulted in significant differences between compared points. These points consequently affected the standard deviation, and root mean square error, so they were eliminated. After removing the outliers, the accuracy of the model derived from the datasets increased. After identifying the data set's outliers, tables 4.9, 4.10, and 4.11 were re-calculated, and new statistical values were obtained (see tables 4.12, 4.13, and 4.14).

TABLE 4.12: RELATIVE DIFFERENCES IN HEIGHT BETWEEN UAV, LIDAR AND SRTM DEMs AT GRID POINTS AT 100, 120 AND 140M FLIGHT HEIGHTS (RE-CALCULATED)

Flight height (m)	Number of points	Differences in height (m)	Minimum (m)	Maximum (m)	Mean (m)	Standard deviation (m)	RMSE (m)
100	369	UAV and LiDAR	-5.594	5.860	-0.284	0.998	1.036
		UAV and SRTM	-12.166	14.074	-0.843	4.551	4.622
		LiDAR and SRTM	-11.583	14.120	-0.465	4.363	4.382
120	369	UAV and LiDAR	-3.712	1.957	-0.170	0.500	0.528
		UAV and SRTM	-12.079	14.124	-0.635	4.440	4.479
		LiDAR and SRTM	-11.583	14.120	-0.465	4.363	4.382
140	369	UAV and LiDAR	-4.020	4.895	-0.097	0.657	0.663
		UAV and SRTM	-12.320	14.117	-0.562	4.416	4.446
		LiDAR and SRTM	-11.583	14.120	-0.465	4.363	4.382

TABLE 4.13: VARIATION OF RELATIVE DIFFERENCES BETWEEN UAV, LIDAR AND SRTM DEMS AT VARYING SLOPES USING GRID POINTS 120M FLYING HEIGHT (RE-CALCULATED)

Elevation range (m)	Number of points	Differences (m)	Minimum (m)	Maximum (m)	Mean (m)	Standard deviation (m)	RMSE (m)
0 – 20	7	UAV and LiDAR	-0.421	0.014	-0.192	0.160	0.243
		UAV and SRTM	-3.854	-0.902	-2.833	0.950	2.996
		LiDAR and SRTM	-3.868	-0.663	-2.750	1.025	2.910
20 – 40	127	UAV and LiDAR	-2.904	5.607	-0.052	0.767	0.766
		UAV and SRTM	-7.151	7.217	-1.290	3.113	3.359
		LiDAR and SRTM	-6.722	7.055	-1.239	2.885	3.129
40 – 60	104	UAV and LiDAR	-3.712	1.957	-0.248	0.747	0.784
		UAV and SRTM	-12.079	10.105	-1.448	4.307	4.524
		LiDAR and SRTM	-11.583	8.148	-1.198	4.245	4.392
60 – 80	96	UAV and LiDAR	-1.943	2.134	-0.085	0.455	0.460
		UAV and SRTM	-7.958	14.124	2.461	4.628	5.221
		LiDAR and SRTM	-7.787	14.120	2.546	4.469	5.124
80 – 100	39	UAV and LiDAR	-0.628	3.333	-0.033	0.578	0.572
		UAV and SRTM	-11.320	7.246	-1.878	5.262	5.523
		LiDAR and SRTM	-11.103	7.130	-1.844	5.104	5.365
>100	3	UAV and LiDAR	-0.130	-0.048	-0.099	0.045	0.105
		UAV and SRTM	-11.403	-2.882	-7.965	4.493	8.769
		LiDAR and SRTM	-11.285	-2.834	-7.866	4.451	8.665

TABLE 4.14 VARIATION OF RELATIVE HEIGHT DIFFERENCES BETWEEN UAV, LIDAR AND SRTM DEMs AT VARYING ELEVATIONS USING GRID POINTS 120M FLYING HEIGHT (RE-CALCULATED)

Slope range (degrees)	Number of points	Differences (m)	Minimum (m)	Maximum (m)	Mean (m)	Standard deviation (m)	RMSE (m)
0 – 5	119	UAV and LiDAR	-3.712	0.674	-0.210	0.536	0.574
		UAV and SRTM	-12.079	8.181	-1.678	3.910	4.240
		LiDAR and SRTM	-11.560	8.162	-1.468	3.832	4.089
5 – 10	128	UAV and LiDAR	-2.602	1.957	-0.137	0.437	0.456
		UAV and SRTM	-11.048	11.704	-0.206	4.053	4.042
		LiDAR and SRTM	-10.314	11.660	-0.069	3.981	3.966
10 – 15	67	UAV and LiDAR	-3.609	1.493	-0.189	0.642	0.664
		UAV and SRTM	-11.594	14.124	-0.248	5.365	5.330
		LiDAR and SRTM	-11.583	14.120	-0.059	5.295	5.256
>15	55	UAV and LiDAR	-1.943	0.557	-0.139	0.344	0.368
		UAV and SRTM	-11.320	10.449	0.152	4.846	4.804
		LiDAR and SRTM	-11.103	10.223	0.291	4.768	4.734

4.6 Summary

In conclusion, the preceding results, the above sections described typical UAV accuracy for the types of surveys evaluated in this thesis. The tables above depict the achievable precision with the UAV tested for this project. The UAV survey models depict the Digital Surface Model and Ortho-mosaic, representing the typical client output.. However, the DSM may contain less detail than the orthomosaic; the model can be compared to TS data. The results mentioned above are further examined in the discussion section of this thesis (Chapter 5). This evaluation is conducted in the form of the three dimensions (x, y and z- height) point accuracy at each of the three flight heights, as well as concise discussions and recommendations regarding the professional utility of this type of data/output (DEM). In conclusion, comparing the two surveys provided qualitative and quantitative analysis for the purpose, objectives and outcomes stated in the introduction to this thesis. To reiterate the context of this study, the ultimate goal of this thesis is to determine the accuracy of UAV-generated DEMs generated using ground survey techniques and how they compare to other freely available satellite-based DEMs.

CHAPTER 5

DISCUSSION

5.1 Introduction

The subsequent section compares the field testing results by analysis and discussion method. This analysis and discussion focus on the precision of the DEM generated by UAVs. This section also discusses the effect of slope, terrain, and flying height variation on UAV DEM accuracy. Lastly, a comparison of the UAV DEM to other satellite-based and airborne-based DEMs, such as SRTM and LiDAR, and a discussion of the UAV DEM's potential applications.

5.2 Accuracy of UAV-generated DEM

Table 4.1 provides a comparison of the point accuracy of the UAV data and the Total Station data during field testing. We collected both datasets at the same location, an open field area with undulating terrain in District 6, and then compared the results. The drone-based elevations were derived using computer vision techniques for UAV drones. The reconstructed camera positions and terrain features were utilised to derive ultra-high-resolution point clouds, ortho-photos, and surface models from the multi-view UAV camera photos using the UAV drone. Root Mean Square Error (RMSE) values of 0.338m (for 100m flight height), 0.078m (for 120m flight height), and 0.265m (for 140m flight height) were determined for the vertical differences between the co-ordinates measured with a total station and the co-ordinates measured with a UAV drone. These residuals varied depending on flight altitude. On the X position, the same points gave RMSE values of 0.050m (100m), 0.046m (120m), and 0.051m (140m), and on the Y position, RMSE values of 0.040m (100m), 0.038m (120m), and 0.052m (140m) (horizontal differences).

The study demonstrates that UAV data can be used to generate DEMs using photogrammetric techniques with x, y, and z precisions of 0.040, 0.046 and 0.078 m, respectively. Therefore, it can be stated that the UAV Photogrammetry can be used for DEM generation, general topographical surveys, and other engineering applications with low cost, time conservation, minimal fieldwork, and competent accuracy. Consequently, we could accurately compare the UAV photogrammetry XYZ data with the Total Station XYZ data at highly dependable common points. For example, having compared 150 of 159 points for flight height 100m, 157 of 159 points for flight height 120m and 156 of 159 points for flight height 140m; all three flights with a less than 3cm ground sample distance; the overall accuracy of the 159 checkpoints was 95 per cent. However, comparing the two models revealed a small number of errors within the datasets.. These errors involve unwanted objects, such as trees and buildings, causing the UAV's contours to spike upward. Infrequently present within the actual testing area, these object errors consisted of trees located in various sections of the field-testing area (as depicted in Figure 4.17) and minor contour errors to the building at the field-testing area's perimeter.

This finding demonstrates that the practical accuracy of XYZ data derived from UAV photogrammetry is comparable to that of Total Station, which is commonly used for cadastral, topographic and engineering surveying. This indicates that UAV photogrammetry can be utilised as a surveying technique to collect data for topographical surveying and the generation of DEMs.

5.3 The effect of flying height, slope, and terrain variations on the accuracy of UAV DEM

5.3.1 Variation of flying height

The accuracy of DEMs generated from UAV datasets was determined through an experiment. The data was collected with UAV at three different flying heights, i.e., 100 m, 120 m, and 140 m above ground level of the terrain's surface. Therefore, a lightweight 1" CMOS camera mounted on an inexpensive DJI Phantom 4 Professional UAV was utilised. The number of images captured decreased from 385 to 290 to 212 as the flight altitude increased from 100 to 120 to 140 metres. The processing was conducted using 18 GCPs, while the assessment of accuracy was conducted using 159 highly precise checkpoints. DSMs and orthophoto images constitute the study's output products (ortho-mosaic). See table 4.1 for horizontal position RMSE of 0.050m (x) and 0.040m (y) at 100m altitude, and vertical position RMSE of 0.3381m (z). For the flight at a height of 120 metres, the horizontal position RMSE was 0.046m (x) and 0.038m (y), and the vertical position RMSE was 0.079m (z). For the flight at 140m height, horizontal position RMSE was 0.052m (x) and 0.052m (y), and the vertical position RMSE was 0.264m (z). It has been determined that flight height directly affects the output products' precision and resolution.

The results demonstrated that the vertical accuracy of DEM is reliable, with flight heights of 120 m, 140 m, and 100 m, in that order. The horizontal accuracy of DEM is reliable, with a flight height of 120m, followed by 100m and 140m for x and y, respectively. These indicate that image capture, GCP establishment, and photogrammetric processing were successfully completed. In addition, it is concluded that the drone's altitude affects DEM's horizontal and vertical accuracy. This study examined the effect of UAV flight altitude on the DEM accuracy generated by UAVs. The research demonstrated the effectiveness of UAV imagery. Lower flight heights such as 100 metres above the ground, are associated with the least accurate ground height measurements. Higher altitudes led to greater precision. The correlation between ground measurement and height derived from UAV imagery was greatest at 120 m flight height with an RMSE of 0.08 m in vertical position (z). Generally, the higher flight altitude (120-140) resulted in more accurate height measurements. Sadeghi and Sohrabi (2019) found comparable outcomes when they evaluated the precision of individual tree height estimations.

The results also indicate that horizontal position estimations are more accurate at lower flying altitudes.. However, an intriguing observation can be made regarding the horizontal position accuracy values, which appear to be relatively similar at 0.050m on average (see table 4.1). RMSE for X and Y positions was not affected by flight altitude or terrain morphology, as demonstrated by the results. Aguera-Vega et al. (2017) found comparable outcomes when they evaluated the accuracy of DSM and Ortho-photos from UAV Photogrammetry.

5.3.2 Slope variations

Unmanned aerial vehicle (UAV) mapping of slopes has recently been demonstrated. It is possible to create a slope map by collecting spatial data, including elevations and surface features of the surrounding terrain. It is essential to have spatial information about a slope in order to improve the efficacy of slope modelling. Therefore, the spatial information must be accurate and trustworthy. This research aimed to determine the effect of a slope on both the horizontal and vertical accuracy of UAV Phantom 4 Pro spatial data collection. Both the DSM and Slope Map were created for analytical purposes. Figures 4.13, 4.14 and 4.15 illustrate the Slope Maps derived from the DSM via photogrammetric processing. The map categorises the area of study according to the slope steepness. In degrees, the slope gradient has been divided into four distinct categories: 0 to 5, 5 to 10, 10 to 15 and greater than 15 degrees. On the map, the locations of the 159 CP are positioned according to their respective classes. Based on the classification, it was determined that 58 CPs fell within the 0° – 5° class, 48 CPs fell within the 5° – 10° class, 31 CPs fell within the 10° – 15° class, and 13 CPs fell within the >15° class for 100m flight height. 74 CP fell within the 0° – 5° class, 50 CP fell within the 5°- 10° class, 26 CP fell within the 10°-15° class, and 6 CP fell within the >15° class. At 140m flight height, 80 CP fell within the 0° – 5° class, 49 CP fell within the 5° – 10° class, 17 CP fell within the 10° – 15° class, and 10 CP fell within the >15° class.

As shown above, the CP are differentiated according to their steepness classes based on the Slope Maps. The RMSE is calculated for each class to analyse the effect of slope steepness on the horizontal and vertical precision of UAV-collected spatial data. The RMSE calculations for each class are displayed in Tables 4.2, 4.3 and 4.4 for each of the three flying heights. The results of these tables indicate that the most significant vertical error (0.441m) occurs at slope steepness between 0° and 5°, while the most negligible error (0.121m) occurs at slope steepness greater than 15° at 100m flight height. For a 120m flight height, the most significant vertical error (0.090m) occurs at slopes steeper than 15°, while the most minor error (0.073m) occurs at slopes steeper than 5°- 10 The 140m flight height indicates that the most significant vertical error (0.278m) occurs at slope steepness between 0° and 5°, while the slightest error (0.216m) occurs at slope steepness greater than 15°. The tables reveal that the most significant error for x and y is 0.055m and 0.044m at slope steepness >15° and 5°- 10°,

respectively, while a minor error is 0.044m and 0.030m at slope steepness 5°- 10° and 10°- 15° at 100m flight height. For a 120m flight height, the greatest error of 0.070m and 0.074m for x and y occurs at slope steepness >15° for both x and y, while the smallest error of 0.035m, and 0.029m for x and y occurs at slope steepness between 5° and 10° for both x and y. The 140m flight height reveals that the greatest error for x and y is 0.079m and 0.056m at slope steepnesses of >15 and 0° – 5°, respectively, while the most negligible error is 0.038m and 0.046m at slope steepnesses of 10° - 15° and >15°.

The results from flight 120m are more reliable and consistent with those of Talib et al. (2020) and were thus used to draw some conclusions. Various comparison results were obtained to investigate the effects of slope on UAV DEMs. It is generally accepted that as land slope increases, DEM elevation accuracy will decrease. The slope affects the DEM elevation accuracy, but the increase or decrease is not uniform; see the RMSE (Z) in table 4.3. The error pattern reveals that errors are greatest on slopes steeper than 15 degrees and lowest on slopes less than 15. The slope is between 5° and 10°. On the upper slope of the study area, it has been observed that height differences between reference point data (TS) and point data generated from DEMs acquired are greater near trees and buildings (flats). It was discovered that the vertical accuracy of spatial data improves as the slope's elevation and gradient decrease. In conclusion, slope elevation and steepness influence the vertical accuracy of UAV-collected spatial data.

5.3.3 Elevation variations

This is included in the discussion of the results for the second objective, which was to determine the effect of slope elevation on the horizontal and vertical accuracy of DEMs generated using UAV technology. The statistical analysis of elevation variation for the three different flying heights is presented in Tables 4.5, 4.6, and 4.7. Figures 4.10, 4.11 and 4.12 depict the elevation ranges of the study area derived from the DSM using photogrammetry-collected spatial data. From 0 metres to 100 metres, the elevations have been divided into five classes at 20-meter intervals. In addition, the variation in altitude has been divided into five distinct classes: 0 to 20, 20 to 40, 40 to 60, 60 to 80, and 80 to 100 m.

The DSM map that has been created demonstrates that the CP vary based on their elevation classes. Therefore, the RMSE is computed for each class in order to analyse the effect of various elevation ranges on the horizontal and vertical accuracy of the DSM. At 100m flight height, the results indicate that the vertical error is greatest (0–20m, 1.196m) in the elevation range 0–20m and smallest (0–100m, 0.071m) in the elevation range 80–100m. For a 120m flight height, the vertical error is greatest (0.098m) between 60 and 100 metres in elevation and smallest (0.052m) between 40 and 60 metres in elevation. The 140m flight height reveals

that the vertical error is greatest (0.720m) between 0 and 20 metres in elevation and smallest (0.103m) between 80 and 100 metres in elevation. According to the tables, the highest error of 0.062m and 0.052m for x and y is at an elevation range of 20 – 40m for both x and y, while the lowest error of 0.038m and 0.028m for x and y is at an elevation range of 60 – 80m at a flight altitude of 100m. For a 120m flight height, the greatest error for x and y is 0.051m and 0.061m at an elevation range of 0 – 20m and 40 – 60m respectively, while the least error is 0.040m and 0.025m at an elevation range of 80 – 100m and 40 – 60m respectively. The 140m flight height reveals that the greatest error of 0.058m and 0.075m for x and y occurs between the elevation ranges of 40 – 60m and 80 – 100m, while the smallest error of 0.034m and 0.030m for x and y occurs between the elevation ranges of 0 – 20m and 40 – 60m

The results from flight 120m are more reliable and consistent with those obtained by Talib et al. (2020) and were used to conclude elevation variations. Table 4.6 depicts an increase in error between the 0-20m class and the 20-40m class, followed by a decrease for the 40m-60m class. The error then increases between 60m and 100m. The error pattern indicates that errors are greatest between 60 and 100 metres in elevation and are lowest between 0 and 40 metres in elevation. The high elevation region exhibits greater error than the low elevation region. It was discovered that the vertical precision of spatial data improves as the elevation range decreases. The high elevation error for class 60m-100m may be caused by the trees and structures (the school) within this height range in the middle and towards the periphery of the study area. In conclusion, elevation variations influence the vertical accuracy of UAV-collected DEMs.

5.4 Outliers

A further investigation was conducted to determine why 120m flight height results differ from 100m and 140m flight height results. A few outliers were identified, which explained the varying number of checkpoints between the three flights after the data was rechecked. When removing outliers per flight, points 125 (100m), 157 (120m), and 122 remained (140m). These results indicate no outliers on flight 120m, whereas there were outliers on the other two flights. Large outliers observed in unwanted objects such as trees, rocks and buildings make the results from the 100m and 140m flights less reliable. The results from flight 120m are more reliable and consistent with those obtained by Talib et al. (2020). The UAV-collected point cloud data contained outliers. The data are impacted by systematic and random noise from various sources, such as the capturing of reflection on unwanted or multiple objects, such as the top of the trees and buildings; examples of this experimental measurement error are displayed in Figure 4.20.. It is crucial to eliminate outliers, as they frequently cause issues for point cloud analysis tools. They may result in erroneous object reconstruction and shape measurement bias. It causes numerous problems during statistical analysis and substantially affects the

mean, standard deviation and root mean square error. Compared to the ground survey, these points were incorrect. This resulted in substantial disparities in a few points that were compared and eliminated. After removing the outliers, the model derived from the datasets improved its accuracy. The results of the 120m flight were accepted and utilised, particularly when discussing the slope and elevation variations.

5.5 Comparative Analysis of UAV and other Satellite-Based DEMs

5.5.1 Absolute comparisons of UAV, LiDAR and SRTM based on total station data

This study examined free satellite and airborne (SRTM & LiDAR) DEM for elevation reference data at 159 CPs. The absolute differences between TS and UAV, TS and LiDAR, and TS and SRTM were presented in three ways. First, the map depicts the locations of the 159 CPs (Figure 3.6). Using total station elevations as reference data and excluding outliers, the statistical computation (RMSE) for the absolute vertical accuracy of SRTM elevation data for the study site yielded values of 4.202m, 4.176m, and 4.181m for flight heights of 100m, 120m, and 140m, respectively. When comparing TS and UAV for the study site, the RMSE for absolute vertical (z) accuracy was 0.338m, 0.079m and 0.264m for 100m, 120m, and 140m flight heights, respectively. When comparing TS and LiDAR for absolute vertical accuracy at the study site, the RMSE values for the three flight heights were 0.454m, 0.445m, and 0.445m, respectively. The absolute vertical accuracy of the UAV and SRTM elevation data is significantly lower than the value of 16m specified in the SRTM data specification. The analyses presented in this paper indicate that the absolute vertical accuracy of less than 5m for all three flights is less than the original SRTM requirement specification value of 16m.

5.5.2 Relative comparisons between UAV, LiDAR and SRTM DEMs

As depicted in Figure 4.19, 388 grid points (30x30m) were generated using the fishnet function in the ArcGIS software Table 4.9 displays the relative height differences between UAV DEM, LiDAR DEM and SRTM DEM at each of the 3 different heights. Three methods were used to determine the relative differences: UAV and SRTM, UAV and LiDAR and LiDAR and SRTM. After excluding outliers, there remained 369 grid points see table 4.12. For flight heights of 100m, 120m, and 140m, the relative vertical accuracy (RMSE) between UAV and SRTM elevation data for the study site was calculated to be 4.622m, 4.479m, and 4.446m, respectively. For the three flight heights, the RMSE for relative vertical accuracy between UAV and LiDAR at the study site was 1.036m, 0.528m and 0.663m, respectively. The RMSE for relative vertical accuracy between SRTM and LiDAR at the study site was 4,382 metres for all three flight heights. The relative vertical accuracy of the UAV and SRTM elevation data is less than 5m which is acceptable given the SRTM data relative accuracy specification of 6m. According to the analyses presented in this paper, the relative vertical accuracy of UAV data

for our datasets has proven to be comparable to that of SRTM. The UAV elevation data exhibits acceptable relative vertical accuracy compared to LiDAR elevation data. Compared to LiDAR data, the relative vertical accuracy of UAV data for our datasets has proven to be acceptable, according to the analyses presented in this paper. The relative vertical accuracy of the LiDAR and SRTM elevation data is less than 4.5 metres, which is acceptable given the SRTM data relative accuracy specification of 6 metres.

5.6 Conclusions

The results of this study indicate that UAV Photogrammetry data are sufficiently precise. Therefore, it is possible to use UAV Photogrammetry data for map-making, surveying, and topographical surveying applications with low-cost, time-saving, and minimal fieldwork benefits. SRTM data are frequently incorporated into global elevation models. Nonetheless, this data, with a resolution of 30m, is not favoured for sensitive geographical research. The error margin is significantly larger, even though the data is widely accepted and widely used, as demonstrated by the results of this study. The method's applicability is confirmed by the accuracy of the UAV DEM generated from SRTM DEM and LiDAR comparisons. It was observed that LiDAR and UAV-based data and products were in good agreement. UAV data provides more geometrical details than LiDAR, resulting in enhanced feature detection. The UAV-based data have a larger RMSE in heights than the LiDAR-based data. This observation can be explained by the higher point density in the UAV data, as discussed in the results. According to these results, UAV image data can be used as a substitute for LiDAR data in areas where it is unavailable or where frequent acquisitions are required. The results indicate that photogrammetry data products are a viable alternative to LiDAR in areas with limited vegetation and surface disturbances and may be preferred due to their lower cost and immediate access to data products, as observed by Vilbig et al. (2020).

CHAPTER 6

CONCLUSIONS AND RECOMMENDATIONS

6.1 Final Conclusions

In conclusion, this thesis evaluated has tested the capabilities of the photogrammetric measurement capabilities of a multirotor DJI Phantom UAV. Comparing the UAV survey data to the conventional TS survey over the same testing site was used to test the measurement capability. This comparison also included recommendations for the DJI Phantom 4 UAV's optimal flying height, slope, and elevations, as well as the use of UAVs as survey instruments to generate DEMs.

Results indicate that the DJI Phantom UAV can deliver precise data with a 1 x GSD resolution (34.3mm x 34.3mm). Root Mean Square Error (RMSE) values of 0.338m (100m), 0.078m (120m), and 0.265m (140m) were determined for the vertical (Z) differences between the co-ordinates measured with a total station and the co-ordinates measured with a UAV drone for a total of 159 common points. Based on the elevations of the selected test points, these residuals varied. The same points provided RMSE values of 0.050m (for 100m flight height), 0.046m (for 120m flight height), and 0.051m (for 140m flight height) on the X positions and RMSE values of 0.040m (for 100m flight height), 0.038m (for 120m flight height), and 0.052m (for 140m flight height) on the Y position for horizontal differences. The UAV field measurements were obtained in less than a third of the time required to conduct field measurements over the site of field testing using conventional total station techniques. This demonstrates that UAVs are significantly more efficient than conventional surveying techniques over expansive terrain. There was a sub-millimetre difference in horizontal accuracy across all three flights, indicating that the horizontal accuracy is not affected by flight altitude or terrain morphology

Regarding slope, results are more precise at slope degrees 10 to 15, with an RMSE of 0.090m for the z position at 120m altitude. This means that drone surveys can map gentle slopes and flat surfaces with high precision and efficiency. Regarding elevation, results are more accurate between 0 and 40 metres at a flight altitude of 120 metres, which is advantageous, mainly when dealing with gentle and flat terrains. Furthermore, the UAV elevation data exhibits acceptable relative vertical accuracy compared to LiDAR elevation data. Compared to LiDAR, Total Station, and SRTM data, the relative vertical accuracy of UAV data for our datasets has proven to be acceptable, according to the analyses presented in this paper. Our findings corroborate those of comparable studies and further validate the use of UAVs for DEM generation and other general applications such as topographical mapping, which offer cost and time savings.

In addition, the data processing times for the UAV Survey were more than double those of the TS Survey; consequently, the two projects took roughly the same amount of time. Using a DJI Phantom 4 Pro UAV, it was determined that the type of survey evaluated in this thesis is the most suitable type. The UAV was determined to be suitable for DEM generation and Topographic Surveys. Due to the required specific point accuracy and information, it was also determined that UAVs were not suitable for precise surveys at this time. In the coming years, the use of UAV photogrammetry to generate 3D visualisations is likely to increase due to its low cost and relative simplicity. Inputting 290 images into Pix4D produced a dense point cloud consisting of an average of 64.95 points per m³ and a total of 36348581 3D points for visualisation and analysis. Increased image overlap tends to result in greater point densities. A total station survey's spatial resolution is limited to the points surveyed whereas the UAV-derived topography is a by-product of the resulting three-dimensional point cloud, which is used to generate a high-resolution orthophoto.

6.2 Recommendations

The combination of field testing, results, and analysis in the preceding sections of this thesis provides clear indications of the accuracy of UAVs in DEM generation and the suitability of using photogrammetric unmanned aerial vehicles for survey applications. However, this thesis has several limitations, including using only one commercially available UAV for mapping and the relatively small site area. Consequently, the researcher believes that the suitability of UAV's in surveying applications could be more accurately determined by testing it in various terrains and under varying site conditions. In addition, several additional potential research areas have been identified in this thesis. These possible research areas and outcomes are listed in the following paragraph.

6.2.1 Possible areas and outcomes for future research

This thesis did not test the ability of the UAV photogrammetric model to remove unwanted data from the point cloud generated by the UAV ortho-rectified georeferenced 3D image. This would enable the creation of an accurate digital surface model unaffected by unwanted objects such as top of the trees. To determine the validity of the data, additional testing could be conducted on the accuracy of the points underneath the removed objects. Another testable aspect is using additional DJI Phantom UAVs over a similar field-testing comparison to determine the accuracy of all different makes and models of DJI Phantom UAVs. In addition to, testing a different model of UAV, the use of fixed-wing UAVs for surveying applications should be evaluated under similar field conditions. This would indicate which UAV type is most suitable for photogrammetric surveying applications. This should also be tested on various fixed-wing UAV models to provide insight into the accuracies of all different fixed-wing UAV makes and models.

Another aspect that could be evaluated with fixed-wing UAVs is capturing terrestrial or non-aerial images. These images can be utilised to generate more accurate three-dimensional photogrammetric models for a variety of objects, including buildings, bridges, towers, and other civil structures.

In contrast, parameters such as weather, vibrations, lens distortions, and software directly impact the process and model accuracy, excluding GCP. In addition to these, the UAV system is not fully automated and requires user input. Future research may provide an automated UAV approach that minimises user attraction. Finally, additional experiments involving the modification of GSD and flight planning parameters are necessary for a more comprehensive analysis of DEM accuracy. Lastly, to conduct the same research investigation as was done in this research project, but to consider the impact of time of day and temperature on the digital terrain model's accuracy. Also, consider flying more than three times over the same region.

REFERENCES

- Agüera-Vega, F., Carvajal-Ramírez, F., & Martínez-Carricondo, P.J, (2016) 'Accuracy of Digital Surface Model and Orthophotos Derived from UAV photogrammetry', *Journal of Surveying Engineering*, vol. 143, no. 2, 04016025.
- Ajay, G.O, Palmer, P, Salubi, A.A, (2018). Modelling farmland topography for suitable site selection of dam construction using unmanned aerial vehicle (UAV) photogrammetry, *Remote Sensing Applications: Society and Environment*, Volume 11, 2018, Pages 220-230,
- Bamler, R (1999): "The SRTM Mission: A World-Wide 30m Resolution DEM from SAR Interferometry in 11 Days", *Photogrammetric Week*, Vol 99, pp. 145-154,
- Barry, P. & Coakley, R. (2013). Accuracy of UAV photogrammetry compared with network RTK GPS. [Online] Available at: <http://www.uav.ie/PDF/AccuracyUAVcompareRTKGPS.pdf>
- Berni, J.A.J., Zarco-Tejada, P.J., Suarez, L., Fereres, E. (2009). Thermal and Narrowband Multispectral Remote Sensing for Vegetation Monitoring from an Unmanned Aerial Vehicle. *Transactions on Geoscience and Remote Sensing*, Vol. 47, pp. 722-738.
- Brasington, J., Rumsby, B., McVey, R., (2000). Monitoring and modelling morphological change in a braided gravel-bed river using a high-resolution GPS-based survey. *Earth Surface Processes and Landforms* 25 (9), 973-990.
- Brown, D. C. (1971). 'Close-range camera calibration', *Photogrammetric Engineering*, 37(8): 855-866.
- Campbell, J.B. & Wynne, R. H. 2011. *Introduction to Remote Sensing*. New York: Guilford Press.
- Colomina, I., Blazquez, M., Molina, P., Pares, M.E., Wis, M. (2008). Towards a new paradigm for high-resolution, low-cost photogrammetry and remote sensing. In: *Int. Archives of Photogrammetry, Remote Sensing and Spatial Information Sciences*, Beijing, China, Vol. 37 (B1), pp. 1201-1206.
- Colomina, I., Molina, P. (2014) Unmanned aerial systems for photogrammetry and remote sensing: A review, *ISPRS Journal of Photogrammetry and Remote Sensing*, Volume 92, 2014, Pages 79-97, ISSN 0924-2716, <https://doi.org/10.1016/j.isprsjprs.2014.02.013>.
- Day, T. & Muller, J.P. (1988). Quality assessment of digital elevation models produced by automatic stereo-matchers from SPOT image pairs. *Photogrammetric Rec*, 12: 797 – 808
- Day, T., and J.P Muller, (1988). Quality assessment of digital elevation models produced by automatic stereo-matchers from SPOT image pairs. *Photogrammetric Rec*, 12: 797 – 808

- Eisenbein, H. 2009. 'UAV Photogrammetry', Dissertation for Doctor of Sciences, University of Technology Dresden, D. E. # 18515
- Eisenbeiss, H. & Zhang, I. 2006. A cultural heritage application compares DSMs generated from mini UAV imagery and terrestrial laser scanners. IAPRS Volume XXXVI, Part 5, Dresden, 25 - 27 September 2006, pp. 90-96
- Eisenbeiss, H. 2004. A mini unmanned aerial vehicle (UAV): system overview and image acquisition. In International Workshop on Processing and Visualization using High-Resolution Imagery, Pitsanulok, Thailand, Gruen, A., Murai, S.H., Fuse, T., Remondino, F. (eds). International Society for Photogrammetry and Remote Sensing.
- Ellis, N. 2013. '*Inspection of power transmission lines using UAVs*', Undergraduate Research Project, University of Southern Queensland, Toowoomba.
- El Meouche, R., Hijazi, I., Poncet, P.A., Abunemeh, M., Rezoug, M. (2016) UAV Photogrammetry Implementation to enhance land surveying, comparisons, and possibilities. In: International Archives of the spatial information sciences – ISPRS Archives. Vol: 42 (2W2). 10.5194/isprs-archives-XLII-2-W2-107
- eMotion Flight Planning Software Screenshot* 2013, eMotion2 Requirements, Aerios Media Inc., viewed 21 July 2015 <https://www.youtube.com/watch?v=7EZ5J1H1C5E>
- Everaerts, J. 2008. Using unmanned aerial vehicles (UAVs) for remote sensing and mapping. *The International Archives of the Photogrammetry, Remote Sensing and Spatial Information Sciences*, 37. Part B1. Beijing 2008, pp. 1187-1192
- Fisher, P., Tate, N., 2006. Causes and consequences of error in digital elevation models. *Progress in Physical Geography* 30 (4), 467-489.
- Fonstad M.A, Dietrich J.T, Courville B.C, Jensen J.L, Carbonneau P.E 2013, Topographic structure from motion: a new development in photogrammetric measurement
- Foot, K.E and D.J. Huebner. (1997). *The Geographers craft*, University of Texas, Austin. <http://www.utexas.edu/depts/grg/gcraft/notes/error/error.html>
- Gilani, H., Saeed, U., Ashraf, S., Daud, A. (2014) Extraction of Digital Elevation Model from Stereo Satellite Data
- Goodchild, M., B. Buttenfield and J. Wood, 1994. Introduction to visualizing data validity. In: *Visualisation in Geographical Information Systems*. Hearnshaw, H.M and D.J Unwin (Eds.), John Wiley and Sons, Chichester, pp: 141 – 149
- Goodchild, M., Buttenfield, B. & Wood, J. 1994. Introduction to visualizing data validity. In: *Visualisation in Geographical Information Systems*. Hearnshaw, H.M and D.J Unwin (Eds.), John Wiley and Sons, Chichester: 141 – 149

- Graeve, J. & Smith, J. 2013. *History of Surveying*, International Federation of Surveyors, Copenhagen, Denmark, viewed 21 April 2015,
- Grenzdoffer, G., Niemeyer, F., Schmidt, F. (2012) Development of four vision camera system for micro-UAV. In: *Int. Archives of Photogrammetry, Remote Sensing and Spatial Information Sciences*, Melbourne, Australia, Vol. 39(1).
- Grenzdörffer, G.J., Engel, A. & Teichert, B. 2008. The photogrammetric potential of low-cost UAVs in forestry and agriculture. *The International Archives of the Photogrammetry, Remote Sensing and Spatial Information Sciences*. 37. Part B1. Beijing 2008: 1207-1213
- Guth, P.L (2006) Geomorphometry from SRTM: Comparing to NED: *Photogrammetric Engineering & Remote Sensing*, vol.72, no.3, p.269 – 277.
- Haarbrink, R. B. & Eisenbeiss, H. 2008. Accurate DSM production from unmanned helicopter systems. *The International Archives of the Photogrammetry, Remote Sensing and Spatial Information Sciences*. 37. Part B1. Beijing 2008:1259-1264
- Haarbrink, RB 2011, 'UAS for geo-information: current status and perspectives', *International Archives of the Photogrammetry, Remote Sensing and Spatial Information Sciences*, Zurich, Switzerland, 14-16 September.
- Haarbrink, RB, and Eisenbeiss, H 2008, 'Accurate DSM production from unmanned helicopter systems',
- Haarbrink, R.B. (2011), 'UAS for geo-information: current status and perspectives, *International Archives of Photogrammetry, Remote Sensing and Spatial Information Sciences*, ISPRS Congress, Beijing, China
- Harbin, A. L. 2001. *Land Surveyor Reference Manual, Third Edition*, (Belmont: Professional Publications, Inc).
- Heipke, C. 1997. Automation of interior, relative, and absolute orientation. *ISPRS Journal of Photogrammetry & Remote Sensing* 52 (1997): 1-19
- Heritage, G.L., Milan, D.J., Large, A.R.G., Fuller, I.C., 2009. Influence of survey strategy and interpolation model on DEM quality. *Geomorphology* 112 (3-4), 334-344.
- Hirano, A., R. Welch, and H. Lang, 2003. Mapping from ASTER stereo image data: DEM validation and accuracy assessment. *J. P RS*, 57: 356 – 370
- Hudzietz, B.P and Saripalli, S (2011) An experimental Evaluation of 3D Terrain Mapping with an autonomous helicopter, *ISPRS International Archives of the Photogrammetry, Remote Sensing and Spatial Information Sciences*, Volume XXXVIII-1/C22,2011,pp.137 - 142

Jensen, A.M., Morgan, D., Chen, Y. Clemens, S & Hardy, T. 2009. Using multiple open-source low-cost unmanned aerial vehicles (UAVs) for 3D photogrammetry and distributed wind measurements. Proceedings of the ASME 2009 International Design Engineering Technical and Information in Engineering Conference, 30 August – 2 September 2009, San Diego, California, USA

Jet Propulsion Laboratory, 2019. ASTER GDEM Map Announcement. <https://asterweb.jpl.nasa.gov/gdem.asp>

Karabork H., Yildiz F., Coskun, E. Yilmaz, H.M & Yakar, M. 2004. Investigation of accuracy for digital elevation models generated with different methods in photogrammetry. International Archives of Photogrammetry, Remote Sensing and Spatial Information Sciences, 35, B3, 156-161.

Küng, O, Strecha, C., Beyeler, A, Zufferey, J.-C., Floreano, D, Fua, P, and Gervais, F (2011). The Accuracy of Automatic Photogrammetric Techniques on Ultra-Light UAV Imagery. International Archives of the Photogrammetry, Remote Sensing and Spatial Information Sciences 38 (1/C22 UAV-g), pp. 125–130.

Li, Z. 1991. Effects of checkpoints on the reliability of DTM accuracy estimates obtained from experimental tests. Photogrammetric Engineering and Remote Sensing, 57: 1333 – 1340

Liu, Z., Zhu, J., Fu, H., Zhou, C., Zuo, T. (2020) Evaluation of the Vertical Accuracy of Open Global DEMs over Steep Terrain Regions Using ICESat Data: A Case Study over Hunan Province, China. Sensors (Basel). Aug 28, 20 (17): 4865. doi: 10.3390/s20174865. PMID: 32872143; PMCID: PMC 7506671

Madawalagama S, Munasinghe N and Dampegama S. (2016). Low cost aerial mapping with consumer grade drones. In: *37th Asian Conference on Remote Sensing*. Colombo, Sri Lanka: ACRS, pp, 1 - 8

Manyoky, M., Theiler, P., Steudler, D. & Eisenbeiss, H. 2011. Unmanned Aerial Vehicle in Cadastral Application, International Archives of the Photogrammetry, Remote Sensing and Spatial Information Sciences,

Molina, P., Colomina, I., Vitoria, T., Silva, P. F., Skaloud, J., Kornus, W., Prades, R., Aguilera, C (2012). Searching lost people with UAVs: the system and results of the close-search project. In: Int. Archives of Photogrammetry, Remote Sensing and Spatial Information Sciences, Melbourne, Australia, Vol. 39(1).

Moore, R.J.D., Thurrowgood, S., Soccol, D., Bland, D., Srinivisan, M.V (2007): A bio-inspired stereo vision system for guidance of autonomous aircraft. Proc. Int. Symposium on Flying Insects and Robots, Ascona, Switzerland.

- Muhadi, N.A., Abdullah, A.F., Bejo, S.K., Mahadi, M.R., Mijic, A. (2020) The use of LiDAR-Derived DEM in Flood Applications: A Review
- Mukherjee, S., Joshi P.K., Ghosh, A., Mukhopadhyay, A. (2013). Evaluation of vertical accuracy of open source Digital Elevation Model (DEM)
- Oniga, V.E., Breabon, A.I., Statescue, F. (2018) Determining the Optimum Number of Ground Control Points for obtaining High Precision Results Based on UAS Images Proceedings, 2, 352. <https://doi.org/10.3390/ecrs-2-05/65>
- Ozturk, D., Batuk, F., Bektas, S. (2011) Determination of land use/cover and Topographical/Morphological Features of River Watershed for Water Resources Management Using Remote Sensing and Geographic information Systems. *Tarım Bilimleri Araştırma Dergisi*, 4 no. 2, pp. 35-42,
- Patel, A, Katiyar, S.K, Prasad, V (2016) Performances evaluation of different open source DEM using Differential Global Positioning System (DPGS). *Egyp.J.Remote Sens.Space Sci.* **19** 7-16
- Pix4D, (2016) *Pix4D Mapper 3.1 User Manual*.
- Polat, N., Uysal, M. (2015) Investigating performances of air-borne LiDAR data filtering algorithms for Digital Terrain Model generation. *Measurement* 63. pp. 61 – 68.
- Puri, A., Valavanis, P., Kontitsis, M (2007). Statistical profile generation for traffic monitoring using real-time UAV based video data. In: *Mediterranean Conference on Control & Automation*, Athens, Greece; on CD-ROM.
- Ravibabu, M.V. & Jain, K. (2008). *Digital Elevation Model Accuracy Aspects*
- Remondino, F., Barazzetti, L., Nex, F. & Sarazzi, D. 2011. UAV photogrammetry for mapping and 3D modelling – current status and future perspectives. *International Archives of the Photogrammetry*, Appendix A. A comparison from the point cloud that was generated from the 125m flight data
- Remondino, F., Gruen, A., Von Schwerin, J., Eisenbeiss, H., Rizzi, A., Sauerbier, M., Richards-Rissetto, H (2009). Multi-sensors 3D documentation of the Maya site of Copan. In: *Proc. of 22nd CIPA Symposium*, Kyoto, Japan; on CD-ROM.
- Rinaudo, F., Chiabrando, F., Lingua, A., Spano, A (2012). Archaeological site monitoring: UAV photogrammetry could be an answer. In: *Int. Archives of Photogrammetry, Remote Sensing and Spatial Information Sciences*, Melbourne, Australia, Vol. 39(5).
- Rock, G., Ries, J.B., Udelhoven, T., (2011). Sensitivity analysis of UAV-photogrammetry for creating digital elevation models (DEM). *International Archives of the Photogrammetry*,

Remote Sensing and Spatial Information Sciences, Vol. XXXVIII1/C22 UAV-g 2011, Conference on Unmanned Aerial Vehicle in Geomatics, Zurich, Switzerland.

Rodriguez, E., Morris, C.S., Belz, J.E., Chapin, E.C., Martin, J.M., Daffer, W., Hensley, S (2005) An assessment of the SRTM topographic products (Technical report JPL D-31639). Pasadena, California, Jet Propulsion Laboratory, 2005.p.143

Ruiz, J.J, Diaz-Mas, L., Perez, F. & Viguria, A. (2013). Evaluating the accuracy of DEM generation algorithms from UAV imagery.

Ruzgiene, B., Berteska, T., Gecycle, Jakubauskiene, E., Aksamitauskas, V.C. (2015) The surface modelling based on UAV Photogrammetry and qualitative estimation, Measurement 73., pp. 619 – 627

Sadeghi S., Sohrabi H., (2019) The effect of UAV flight altitude on the accuracy of individual tree height extraction in a broad-leaved forest. Remote Sens. Spat. Inf. Sci., 42 (4/W18), doi: 10.5194/isprs-archives-xlii-4-w18-1168-2019

Sanna, A., Pralio, B. Simulation (2005) Control of mini UAVs. Proc. 5th WSEAS Int. Conference on Simulation, Modelling and Optimization, pp. 135-141.

Sasowsky, K.C, Petersen, G.W & Evans, B.M. (1992). Accuracy of SPOT digital elevation model and derivatives: Utility for Alaska's North Slope. Photogrammetry. Eng. Remote Sens, 58: 815 – 824

Singh, V., Ray, P., Jayaseelan, A. (2010) 'Ortho-rectification and Digital Elevation Model (DEM) Generation Using Cartosat-1 Satellite Stereo Pair in Himalayan Terrain' Journal of Geographic Information Systems, Vol . 2 No. 2. pp. 85 – 92 . doi:10.4236/jgis.2010.22013

Schafroth, D., Bouabdallah, S., Bermes, C., Siegwart, R. (2009): From the test benches to the first prototype of the muFly micro helicopter. Journal of Intelligent and Robotic Systems, Vol. 54(1-3), pp. 245-260.

Siebert, S and Teizer, J. (2014). Mobile 3D mapping for surveying earthwork projects using an Unmanned Aerial Vehicle (UAV) system. *Automation in Construction*, 41 (Supplement C):1 – 14

Smeaton, C.H.(2015) Surveying 'Applications of Photogrammetric UAV's – a comparison with a conventional Surveying techniques', Undergraduate Research Project, University of Southern Queensland, Toowoomba.

Smith (2013), A Brief History of Surveying in NSW, Doherty Smith and Associates Consulting Surveyors, viewed 13 March 2015, <http://www.dohertysmith.com.au/blog/a-brief-history-of-surveying-in-NSW>

Standard Survey Methods TMH11 Draft Version 2.0, February 2013

- Stocks, AM, and DI Heywood, (1994). Terrain modelling for mountains. In: Mountain Environments and GIS
- Talib, N. Narashid, R.H. Pa'suya, M.F.B., (2020) *IOP Conf. Ser.: Earth Environment. Sci.* 540 012089
- Uysal, M., Toprak, A. S. & Polat, N., (2015). DEM generation with UAV Photogrammetry and accuracy analysis in Sahitler hill. Measurement, pp. 539-543.
- Vallet, J. Panissod F. Strecha, C, Tracol, M,(2011). Photogrammetric performance of an ultralightweight Swinglet UAV. In: *Int. Archives of Photogrammetry, Remote Sensing and Spatial Information Sciences*, Zurich, Switzerland
- Van Niekerk, A. (2014) ' Stellenbosch University Digital Elevation Model': www.innovus.co.za/media/documents/SUDEM_Product_Description_201410.pdf.
- Verhulp, J. (2015), 'Towards a National Digital Elevation Model'. Geomatics Indaba Proceedings – Stream 1
- Vilbig, J., Sagan, V., Bodine, C (2020) Archaeological surveying with airborne LiDAR and UAV photogrammetry: A comparative analysis at Cahokia Mounds.
- Von Blyenberg, P. (1999). UAVs-Current Situation and Considerations for the Way Forward. In: RTO-AVT Course on Development and Operation of UAVs for Military and Civil Applications.
- Watts, A.C., Ambrosia, V.G., Hinkley, E.A.(2012) Unmanned Aircraft Systems in Remote Sensing and Scientific Research: Classification and Considerations of Use. *Remote Sens.* 2012, 4, 1671-1692. <https://doi.org/10.3390/rs4061671>
- Wonnacott, R.T. (1990) The implementation of the Hartebeesthoek 94 coordinate system in South Africa. *Survey Review*, 35 (274), pp. 243 – 250. <https://doi.org/10.1179/sre.1999.35.274.243>
- Yusoff, A.R., Darwin, N., Majid, Z., Ariff, M.F.M., Idris, K.M (2018) Comprehensive analysis of flying altitude for high-resolution slope mapping using UAV Technology.
- Zhang, B., Song, Z., Zhao, F., Liu, C. (2022) Overview of Propulsion Systems for Unmanned Aerial Vehicles. *Energies*, 15, 455.
- Zietara, M.A. (2017). Creating Digital Elevation Model (DEM) based on ground points extracted from classified aerial images obtained from Unmanned Aerial Vehicle (UAV)
- Zongjian, L. (2008). UAV for mapping – low altitude photogrammetric survey. *The International Archives of the Photogrammetry, Remote Sensing and Spatial Information Sciences*, 37. Part B1. Beijing: 1183-1186

APPENDICES

Appendix A DJI Phantom 4 Drone UAV

A summary of the instrument setting used and related specifications of the UAV drone are relevant for the fieldwork requirements within this thesis.

Camera	
Sensor	Sony EXMOR 1/2.3" Effective pixels:12.4 M (total pixels: 12.76 M)
Lens	FOV 94° 20mm(35mm format equivalent) f/2.8
ISO Range	100-3200(video) 100-1600(photo)
Electronic Shutter Speed	8s - 1/8000s
Image Max. Size	4000 x 3000
Still Photography Modes	Single shot
	Burst shooting: 3/5/7 frames
	Auto Exposure Bracketing (AEB): 3/5
	Bracketed frames at 0.7EV Bias
Supported SD Card Types	Time-lapse
	Micro SD
Video Recording Modes	Max. capacity: 64 GB. Class 10 or UHS-1 rating required
	UHD : 4096x2160p 24/25, 3840x2160p24/25/30
	FHD:1920x1080p 24/25/30/48/50/60
Max. Bitrate Of Video Storage	HD:1280x720p 24/25/30/48/50/60
	60 Mbps
Supported File Formats	FAT32/exFAT
	Photo: JPEG, DNG
Operating Temperature Range	Video: MP4/MOV (MPEG-4 AVC/H.264)
	0°C to 40°C

Specifications

Aircraft

Weight (Battery & Propellers Included)	1280 g
Max. Ascent Speed	5 m/s
Max. Descent Speed	3 m/s
Max. Speed	16 m/s (ATTI mode, no wind)
Max. Flight Altitude	6000 m
Max. Flight Time	Approximately 23 minutes
Operating Temperature	0°C to 40°C
GPS Mode	GPS/GLONASS

Gimbal

Controllable Range	Pitch: - 90° to + 30°
--------------------	-----------------------

Vision Positioning

Velocity Range	< 8 m/s (2 m above ground)
Altitude Range	30 cm-300 cm
Operating Range	30 cm-300 cm
Operating Environment	Brightly lit (lux > 15) patterned surfaces

Appendix B Total Station Datasheet

DISTANCE MEASUREMENT

Reflectorless mode (white target)¹ 1.5 m to 300 m (4.9 ft to 984 ft)

Range with specified prisms

Good conditions (No haze, visibility over 40 km (25 miles))

With reflector sheet 5 cm x 5 cm (2 in x 2 in)

2" 1.5 m to 270 m (4.9 ft to 886 ft)

3", 5" 1.5 m to 300 m (4.9 ft to 984 ft)

With single prism 6.25 cm (2.5 in)

2" 1.5 m to 3,000 m (4.9 ft to 9,843 ft)

3", 5" 1.5 m to 5,000 m (4.9 ft to 16,404 ft)

Accuracy²

2" Prism $\pm(2+2 \text{ ppm} \times D)$ mm

2" Reflectorless $\pm(3+2 \text{ ppm} \times D)$ mm

3", 5" Prism $\pm(3+2 \text{ ppm} \times D)$ mm

3", 5" Reflectorless $\pm(3+2 \text{ ppm} \times D)$ mm

Winterized version

Prism $\pm(3 + 2 \text{ ppm} \times D)$ mm (-10 °C to +40 °C)

$\pm(3 + 3 \text{ ppm} \times D)$ mm (-20 °C to -10 °C, +40 °C to +50 °C)

Reflectorless $\pm(3 + 2 \text{ ppm} \times D)$ mm (-10 °C to +40 °C)

$\pm(3 + 3 \text{ ppm} \times D)$ mm (-20 °C to -10 °C, +40 °C to +50 °C)

Measuring interval³

Prism mode

2" 1.6 sec.

3", 5" 1.5 sec.

Reflectorless mode

2" 2.1 sec.

3", 5" 1.8 sec.

Least count 1 mm (0.002 ft)

ANGLE MEASUREMENT

DIN 18723 accuracy (horizontal and vertical) 2"/0.5 mgon

3"/1.0 mgon, 5"/1.5 mgon

Reading system Absolute encoder

Circle diameter 62 mm (2.4 in)

Horizontal/Vertical angle Diametrical

Minimum increment (Degree, Gon, MIL6400) Degree: 1/5/10°

Gon: 0.2/1/2 mgon

MIL6400: 0.005/0.02/0.05 mil

TELESCOPE

Tube length 125 mm (4.9 in)

Image Erect

Magnification 30x (18x/36x with optional eyepieces)

2" Effective diameter of objective 40 mm (1.6 in)

2" EDM diameter 45 mm (1.8 in)

3", 5" Effective diameter of objective 45 mm (1.8 in)

3", 5" EDM diameter 50 mm (2.0 in)

Field of view 1°20'

Resolving power 3", 5"

Minimum focusing distance 1.5 m (4.9 ft)

Laser Pointer Coaxial Red Light

POWER

Internal Li-ion battery (x2)

Output voltage 3.8 V DC

Operating time⁴

2" approx. 12 hours (continuous distance/angle measurement)

approx. 26 hours (distance/angle measurement every 30 seconds)

approx. 28 hours (continuous angle measurement)

3", 5" approx. 7.5 hours (continuous distance/angle measurement)

approx. 16 hours (distance/angle measurement every 30 seconds)

approx. 20 hours (continuous angle measurement)

Charging time

Full charge 4 hours

GENERAL SPECIFICATIONS

Level vials

Sensitivity of Circular level vial 10/2 mm

Tangent/Clamps Endless

Display face 1 QVGA, 16 bit color, TFT LCD, backlit (320x240 pixel)

Display face 2 Backlit, graphic LCD (128x64 pixel)

Point memory 128 MB RAM, 128 MB Flash memory

Dimensions (W x D x H) 149 mm x 145 mm x 306 mm

(5.8 in x 5.7 in x 12.0 in)

Weight (approx.)

2" Main unit (without battery) 3.9 kg (8.6 lb)

3", 5" Main unit (without battery) 3.8 kg (8.4 lb)

Battery 0.1 kg (0.2 lb)

Carrying case 2.3 kg (5.1 lb)

ENVIRONMENTAL

Operating temperature range -20 °C to +50 °C (-4 °F to +122 °F)

Winterized -30 °C to +50 °C (-22 °F to +122 °F)

Storage temperature range -25 °C to +60 °C (-13 °F to +140 °F)

Winterized -30 °C to +60 °C (-22 °F to +140 °F)

Atmospheric correction

Temperature range -40 °C to +60 °C (-40 °F to +140 °F)

Barometric pressure 400 mmHg to 999 mmHg/533 hPa to

1,332 hPa/15.8 inHg to 39.3 inHg

Dust and water protection IP66

CERTIFICATION

Class B Part 15 FCC certification, CE Mark approval. C-Tick.

Laser safety IEC 60825-1 am2:2007

2" Prism mode

2" Prism mode: Class 1 laser

2" Reflectorless/Laser Pointer: Class 3R laser

3", 5" Reflectorless / Prism mode: Class 1 laser

3", 5" Laser Pointer: Class 2 laser

Laser Plummet: Class 2 laser

Bluetooth type approvals are country specific.



Appendix C Trimble GPS Base and Rover 5700 & 5800 Series Datasheet

PERFORMANCE SPECIFICATIONS

Measurements

- Trimble R-Track technology
- Advanced Trimble Maxwell 6 Custom Survey GNSS chip with 220 channels
- High precision multiple correlator for GNSS pseudorange measurements
- Unfiltered, unsmoothed pseudorange measurements data for low noise, low multipath error, low time domain correlation and high dynamic response
- Very low noise GNSS carrier phase measurements with <1 mm precision in a 1 Hz bandwidth
- Signal-to-Noise ratios reported in dB-Hz
- Proven Trimble low elevation tracking technology
- Satellite signals tracked simultaneously:
 - GPS: L1C/A, L2C, L2E (Trimble method for tracking L2P), L5
 - GLONASS: L1C/A, L1P, L2C/A (GLONASS M only), L2P
 - SBAS: L1C/A, L5
 - Galileo GIOVE-A and GIOVE-B

Code differential GNSS positioning¹

Horizontal 0.25 m + 1 ppm RMS
 Vertical 0.50 m + 1 ppm RMS
 WAAS differential positioning accuracy² typically <5 m 3DRMS

Static and FastStatic GNSS surveying¹

Horizontal 3 mm + 0.1 ppm RMS
 Vertical 3.5 mm + 0.4 ppm RMS

Kinematic surveying¹

Horizontal 10 mm + 1 ppm RMS
 Vertical 20 mm + 1 ppm RMS
 Initialization time³ typically <10 seconds
 Initialization reliability⁴ typically >99.9%

HARDWARE

Physical

Dimensions (WxH) 19 cm x 11.2 cm (7.5 in x 4.4 in), including connectors
 Weight 1.34 kg (2.95 lb) with internal battery, internal radio, standard UHF antenna.
 3.70 kg (8.16 lb) entire RTK rover including batteries, range pole, controller and bracket

Shock and vibration Tested and meets the following environmental standards:

Shock Non-operating: Designed to survive a 2 m (6.6 ft) pole drop onto concrete. Operating: to 40 G, 10 msec, sawtooth
 Vibration MIL-STD-810F, FIG.514.5C-1

Electrical

- Power 11 to 28 V DC external power input with over-voltage protection on Port 1 (7-pin Lemo)
- Rechargeable, removable 7.4 V, 2.4 Ah Lithium-Ion battery in internal battery compartment. Power consumption is 3.2 W, in RTK rover mode with internal radio. Operating times on internal battery:
 - 450 MHz receive only option 5.8 hours⁷
 - 450 MHz receive/transmit option 3.7 hours⁸
 - GSM/GPRS 4.1 hours⁷
- Certification Class B Part 15, 22, 24 FCC certification, 850/1900 MHz. Class 10 GSM/GPRS module. CE Mark approval, and C-tick approval

Communications and Data Storage

- 3-wire serial (7-pin Lemo) on Port 1. Full RS-232 serial on Port 2 (Dsub 9 pin)
- Fully Integrated, fully sealed internal 450 MHz receiver/transmitter option:
 - Transmit power: 0.5 W
 - Range⁶: 3-5 km typical / 10 km optimal
- Fully integrated, fully sealed internal GSM/GPRS option⁷
- Fully integrated, fully sealed 2.4 GHz communications port (Bluetooth[®])⁹
- External cellphone support for GSM/GPRS/CDPD modems for RTK and VRS operations
- Data storage on 57 MB internal memory: 40.7 days of raw observables (approx. 1.4 MB /Day), based on recording every 15 seconds from an average of 14 satellites
- 1 Hz, 2 Hz, 5 Hz, 10 Hz, and 20 Hz positioning
- CMR+, CMRx, RTCM 2.1, RTCM 2.3, RTCM 3.0, RTCM 3.1 Input and Output
- 16 NMEA outputs, GSOF, RT17 and RT27 outputs. Supports BINEX and smoothed carrier

Appendix D M3 Total Station Survey Report

Survey Report

Job name	D6 Research
Version	7.00
Distance Units	Meters
Angle units	Degrees
Pressure Units	mbar
Temperature Units	Celsius

Coordinate system (Job)

System	South Africa
Zone	WG 19
Datum	Hartebeesthoek 94

Projection

Projection	Transverse Mercator
Origin lat	0°00'00.00000"N
Origin long	19°00'00.00000"E
False easting	0.000
False northing	0.000
Scale	1.00000000
South azimuth (grid)	Yes

Grid coords	Increase South-West
Ellipsoid	Semi-major axis: 6378137.000 Flattening: 298.25722293

Local site

Type	Grid
-------------	------

Datum transformation

Type	Three parameters
Semi-major axis	6378137.000
Flattening	298.257223
Translation X	0.000
Translation Y	0.000
Translation Z	0.000

Collected Field Data

Corrections

South azimuth (grid)	Yes
Grid coords	Increase South-West
Magnetic declination	0°00'00"
Distances	Ground
Neighbourhood adjustment	Off

Projection

Projection	Transverse Mercator
Origin lat	0°00'00.00000"N
Origin long	19°00'00.00000"E
False easting	0.000
False northing	0.000
Scale	1.00000000
Ellipsoid	Semi-major axis: 6378137.000 Flattening: 298.25722293

Local site

Type	Grid
-------------	------

Datum transformation

Type	Three parameters
Semi-major axis	6378137.000
Flattening	298.257223
Translation X	0.000
Translation Y	0.000
Translation Z	0.000

Coordinate system

System	South Africa
Zone	WG 19

Datum		Hartebeesthoek 94							
Point	50K8	Y	52249.780	X	3756200.870	Z	28.637	Code	TSM
Point	51K8	Y	52092.620	X	3756290.070	Z	36.189	Code	TSM
Point	52K8	Y	51939.640	X	3756376.750	Z	42.039	Code	TSM
Point	TR124	Y	54807.360	X	3754515.220	Z	275.800	Code	TRG
Point	TR125	Y	54853.460	X	3754583.190	Z	289.000	Code	TRG

Instrument

Instrument type	Unknown								
EDM Refractive Index	275.0								
EDM Carrier Wavelength	79.5								
Horizontal Circle Mode	Set to azimuth								
Horizontal Angle Precision	0°00'03"								
Vertical Angle Precision	0°00'03"								
EDM precision	3000mm +2ppm								

Atmosphere

Pressure	1013.00mb	Temperature	20.0°C	ppm	0.3				
-----------------	-----------	--------------------	--------	------------	-----	--	--	--	--

Curvature correction	Yes	Refraction correction	Yes	Refraction const.	0.142				
-----------------------------	-----	------------------------------	-----	--------------------------	-------	--	--	--	--

Station setup

Station	50K8	Instrument height	1.740	Station type	Station setup	Scale factor	1.00000000	Std Error	?
----------------	------	--------------------------	-------	---------------------	---------------	---------------------	------------	------------------	---

Orientation

Station	50K8	Backsight point	TR124	Orientation correction	0°00'00"	Orientation Std Err	?		
Point (B.S.)	TR124	HA	123°23'17"	VA	85°28'41"	SD	?	Code	TRG
Std Errors		HA	0°00'03"	VA	0°00'03"	SD	?		
Target height	?	Prism constant	-30.0mm						
Point	TR544	Y	55123.370	X	3754615.780	Z	352.300	Code	TRG
Point	TR544	HA	118°52'43"	VA	84°25'49"	SD	?	Code	TRG
Std Errors		HA	0°00'03"	VA	0°00'03"	SD	?		
Target	2.000	Prism	-30.0mm						

height		constant							
Deltas	TR544	Azimuth	?	H.Dist	?	V.Dist	?		
Point	1	HA	188°38'00"	VA	93°17'54"	SD	169.087	Code	SS
Std Errors		HA	0°00'03"	VA	0°00'03"	SD	3.000		
Target height	2.000	Prism constant	-30.0mm						
Point	2	HA	205°25'21"	VA	92°35'18"	SD	185.262	Code	SS
Std Errors		HA	0°00'03"	VA	0°00'03"	SD	3.000		
Target height	2.000	Prism constant	-30.0mm						
Point	3	HA	165°47'42"	VA	93°46'54"	SD	116.524	Code	SS
Std Errors		HA	0°00'03"	VA	0°00'03"	SD	3.000		
Target height	2.000	Prism constant	-30.0mm						
Point	4	HA	192°47'46"	VA	93°31'32"	SD	116.081	Code	SS
Std Errors		HA	0°00'03"	VA	0°00'03"	SD	3.000		
Target height	2.000	Prism constant	-30.0mm						
Point	5	HA	215°07'49"	VA	92°19'21"	SD	138.696	Code	SS
Std		HA	0°00'03"	VA	0°00'03"	SD	3.000		

Errors									
Target height	2.000	Prism constant	-30.0mm						
Point	6	HA	229°42'10"	VA	91°25'23"	SD	175.666	Code	SS
Std Errors		HA	0°00'03"	VA	0°00'03"	SD	3.000		
Target height	2.000	Prism constant	-30.0mm						
Point	8	HA	154°20'51"	VA	94°19'53"	SD	65.420	Code	SS
Std Errors		HA	0°00'03"	VA	0°00'03"	SD	3.000		
Target height	2.000	Prism constant	-30.0mm						
Point	10	HA	233°27'12"	VA	92°20'26"	SD	99.777	Code	SS
Std Errors		HA	0°00'03"	VA	0°00'03"	SD	3.000		
Target height	2.000	Prism constant	-30.0mm						
Point	11	HA	246°02'44"	VA	91°04'00"	SD	146.923	Code	SS
Std Errors		HA	0°00'03"	VA	0°00'03"	SD	3.000		
Target height	2.000	Prism constant	-30.0mm						
Point	12	HA	252°20'48"	VA	90°19'51"	SD	197.719	Code	SS

Std Errors		HA	0°00'03"	VA	0°00'03"	SD	3.000		
Target height	2.000	Prism constant	-30.0mm						
Point	15	HA	258°52'02"	VA	87°32'17"	SD	26.792	Code	SS
Std Errors		HA	0°00'03"	VA	0°00'03"	SD	3.000		
Target height	2.000	Prism constant	-30.0mm						

Instrument

Instrument type	Unknown								
EDM Refractive Index	275.0								
EDM Carrier Wavelength	79.5								
Horizontal Circle Mode	Set to azimuth								
Horizontal Angle Precision	0°00'03"								
Vertical Angle Precision	0°00'03"								
EDM precision	3000mm +2ppm								

Atmosphere

Pressure	1013.00mb ar	Temperature	20.0°C	ppm	0.3				
-----------------	-----------------	--------------------	--------	------------	-----	--	--	--	--

Curvature correction	Yes	Refraction correction	Yes	Refraction const.	0.142				
-----------------------------	-----	------------------------------	-----	--------------------------	-------	--	--	--	--

Station setup

Station	51K8	Instrument height	1.729	Station type	Station setup	Scale factor	1.0000000 0	Std Error	?
----------------	------	--------------------------	-------	---------------------	---------------	---------------------	----------------	------------------	---

Orientation

Station	51K8	Backsight point	TR124	Orientation correction	0°00'00"	Orientation	?		
Point (B.S.)	TR124	HA	123°10'33"	VA	85°51'54"	SD	?	Cod e	TR G
Std Errors		HA	0°00'03"	VA	0°00'03"	SD	?		
Target height	?	Prism constant	-30.0mm						
Point	TR544	HA	118°55'07"	VA	84°50'39"	SD	?	Cod e	TR G
Std Errors		HA	0°00'03"	VA	0°00'03"	SD	?		
Target height	?	Prism constant	-30.0mm						
Deltas	TR544	Azimuth	?	H.Distance	?	V.Distance	?		

Point	16	HA	166°36'26"	VA	94°03'11"	SD	97.899	Cod e	SS
Std Errors		HA	0°00'03"	VA	0°00'03"	SD	3.000		
Target height	2.000	Prism constant	-30.0mm						
Point	17	HA	198°17'11"	VA	93°45'02"	SD	100.613	Cod e	SS
Std Errors		HA	0°00'03"	VA	0°00'03"	SD	3.000		
Target height	2.000	Prism constant	-30.0mm						
Point	18	HA	221°51'59"	VA	93°03'23"	SD	128.557	Cod e	SS
Std Errors		HA	0°00'03"	VA	0°00'03"	SD	3.000		
Target height	2.000	Prism constant	-30.0mm						
Point	19	HA	221°51'58"	VA	93°03'21"	SD	128.558	Cod e	SS
Std Errors		HA	0°00'03"	VA	0°00'03"	SD	3.000		
Target height	2.000	Prism constant	-30.0mm						
Point	23	HA	118°03'14"	VA	91°56'37"	SD	86.743	Cod e	SS

Std Errors		HA	0°00'03"	VA	0°00'03"	SD	3.000		
Target height	2.000	Prism constant	-30.0mm						
Point	24	HA	151°26'45"	VA	91°59'04"	SD	46.797	Cod e	SS
Std Errors		HA	0°00'03"	VA	0°00'03"	SD	3.000		
Target height	2.000	Prism constant	-30.0mm						
Point	25	HA	217°33'57"	VA	93°16'05"	SD	52.317	Cod e	SS
Std Errors		HA	0°00'03"	VA	0°00'03"	SD	3.000		
Target height	2.000	Prism constant	-30.0mm						
Point	26	HA	244°07'52"	VA	92°08'12"	SD	95.616	Cod e	SS
Std Errors		HA	0°00'03"	VA	0°00'03"	SD	3.000		
Target height	2.000	Prism constant	-30.0mm						
Point	28	HA	257°43'43"	VA	90°32'08"	SD	198.791	Cod e	SS
Std Errors		HA	0°00'03"	VA	0°00'03"	SD	3.000		

Target height	2.000	Prism constant	-30.0mm						
Point	33	HA	59°48'41"	VA	87°23'06"	SD	25.560	Cod e	SS
Std Errors		HA	0°00'03"	VA	0°00'03"	SD	3.000		
Target height	2.000	Prism constant	-30.0mm						
Point	34	HA	291°14'55"	VA	88°11'26"	SD	34.459	Cod e	SS
Std Errors		HA	0°00'03"	VA	0°00'03"	SD	3.000		
Target height	2.000	Prism constant	-30.0mm						

Instrument

Pressure	1013.00mbar	Temperature	20.0°C	ppm	0.3				
Curvature correction	Yes	Refraction correction	Yes	Refraction const.	0.142				

Station setup

Station	52K8	Instrument height	1.672	Station type	Station setup	Scale factor	1.00000000	Std Error	?
Instrument type	Unknown								
EDM Refractive Index	275.0								
EDM Carrier Wavelength	79.5								

Horizontal Circle Mode	Set to azimuth
Horizontal Angle Precision	0°00'03"
Vertical Angle Precision	0°00'03"
EDM precision	3000mm +2ppm

Atmosphere Orientation

Station	52K8	Backsight point	TR124	Orientation correction	0°00'00"	Orient. Std Err	?		
Point (B.S.)	TR124	HA	122°59'20"	VA	86°10'48"	SD	?	Code	TRG
Std Errors		HA	0°00'03"	VA	0°00'03"	SD	?		
Target height	?	Prism constant	-30.0mm						
Point	TR544	HA	118°56'48"	VA	85°12'39"	SD	?	Code	TRG
Std Errors		HA	0°00'03"	VA	0°00'03"	SD	?		
Target height	?	Prism constant	-30.0mm						
Deltas	TR544	Azimuth	?	H.Distance	?	V.Distance	?		
Point	36	HA	209°45'28"	VA	91°41'56"	SD	86.157	Code	SS
Std Errors		HA	0°00'03"	VA	0°00'03"	SD	3.000		

Target height	2.000	Prism constant	-30.0mm						
Point	44	HA	99°33'24"	VA	90°22'09"	SD	122.328	Code	SS
Std Errors		HA	0°00'03"	VA	0°00'03"	SD	3.000		
Target height	2.000	Prism constant	-30.0mm						
Point	45	HA	107°11'51"	VA	91°45'16"	SD	69.630	Code	SS
Std Errors		HA	0°00'03"	VA	0°00'03"	SD	3.000		
Target height	2.000	Prism constant	-30.0mm						
Point	46	HA	149°16'32"	VA	91°57'56"	SD	24.305	Code	SS
Std Errors		HA	0°00'03"	VA	0°00'03"	SD	3.000		
Target height	2.000	Prism constant	-30.0mm						
Point	47	HA	243°06'40"	VA	87°26'47"	SD	46.966	Code	SS
Std Errors		HA	0°00'03"	VA	0°00'03"	SD	3.000		
Target height	2.000	Prism constant	-30.0mm						
Point	56	HA	63°17'15"	VA	85°55'04"	SD	74.306	Code	SS
Std		HA	0°00'03"	VA	0°00'03"	SD	3.000		

Errors									
Target height	2.000	Prism constant	-30.0mm						
Point	57	HA	20°00'40"	VA	87°21'30"	SD	35.190	Code	SS
Std Errors		HA	0°00'03"	VA	0°00'03"	SD	3.000		
Target height	2.000	Prism constant	-30.0mm						
Point	58	HA	307°48'52"	VA	85°06'39"	SD	53.552	Code	SS
Std Errors		HA	0°00'03"	VA	0°00'03"	SD	3.000		
Target height	1.550	Prism constant	-30.0mm						
Point	66	HA	37°04'40"	VA	87°06'07"	SD	109.461	Code	SS
Std Errors		HA	0°00'03"	VA	0°00'03"	SD	3.000		
Target height	2.000	Prism constant	-30.0mm						

Instrument

Instrument type	Unknown
EDM Refractive Index	275.0
EDM Carrier Wavelength	79.5

Horizontal Circle Mode	Set to azimuth								
Horizontal Angle Precision	0°00'03"								
Vertical Angle Precision	0°00'03"								
EDM precision	3000mm +2ppm								
Point	36K9	Y	52125.170	X	3756762.460	Z	77.830	Code	TSM

Instrument

Instrument type	Unknown								
EDM Refractive Index	275.0								
EDM Carrier Wavelength	79.5								
Horizontal Circle Mode	Set to azimuth								
Horizontal Angle Precision	0°00'03"								
Vertical Angle Precision	0°00'03"								
EDM precision	3000mm +2ppm								

Atmosphere

Pressure	1013.00 mbar	Temperature	20.0°C	ppm	0.3			
Curvature correction	Yes	Refraction correction	Yes	Refraction const.	0.142			

Station setup

		Instrument height		Station type	Scale factor		
Station	36K9		1. 6 6 2			1.0000000 0	?

Orientation

		Backsight point		Orientation correction	Orient. Std Err				
Station	36K9		T R 1 2 4			?			
Point (B.S.)	TR124	HA	129°57'27"	VA	86°52'27"	SD	?	Code	TRG
Std Errors		HA	0°00'03"	VA	0°00'03"	SD	?		
Target height	?	Prism constant	-30.0mm						
Point	TR544	HA	125°35'56"	VA	85°50'12"	SD	?	Code	TRG
Std		HA	0°00'03"	VA	0°00'03"	SD	?		

Errors									
Target height	?	Prism constant	-30.0mm						
Deltas	TR544	Azimuth	?	H.Dist	?	V.Dist	?		
Point	93	HA	100°25'23"	VA	83°59'31"	SD	152.959	Code	SS
Std		HA	0°00'03"	VA	0°00'03"	SD	3.000		

Errors									
Target height	2.000	Prism constant	-30.0mm						
Point	94	HA	106°14'35"	VA	85°41'07"	SD	99.766	Code	SS
Std		HA	0°00'03"	VA	0°00'03"	SD	3.000		
Errors									
Target height	2.000	Prism constant	-30.0mm						
Point	95	HA	124°15'46"	VA	87°28'48"	SD	50.052	Code	SS
Std		HA	0°00'03"	VA	0°00'03"	SD	3.000		
Errors									
Target height	2.000	Prism constant	-30.0mm						
Point	96	HA	204°18'49"	VA	94°38'11"	SD	31.330	Code	SS
Std		HA	0°00'03"	VA	0°00'03"	SD	3.000		
Errors									

Target height	2.000	Prism constant	-30.0mm						
Point	97	HA	246°46'58"	VA	96°40'53"	SD	73.418	Code	SS
Std Errors		HA	0°00'03"	VA	0°00'03"	SD	3.000		
Target height	2.000	Prism constant	-30.0mm						
Point	98	HA	256°31'40"	VA	94°53'55"	SD	125.020	Code	SS
Std Errors		HA	0°00'03"	VA	0°00'03"	SD	3.000		
Target height	2.000	Prism constant	-30.0mm						
Point	100	HA	57°50'51"	VA	74°48'59"	SD	50.239	Code	SS
Std Errors		HA	0°00'03"	VA	0°00'03"	SD	3.000		
Target height	2.000	Prism constant	-30.0mm						
Point	101	HA	332°41'10"	VA	76°05'17"	SD	29.548	Code	SS
Std Errors		HA	0°00'03"	VA	0°00'03"	SD	3.000		
Target height	2.000	Prism constant	-30.0mm						
Point	102	HA	290°30'13"	VA	87°11'42"	SD	71.955	Code	SS

Std Errors		HA	0°00'03"	VA	0°00'03"	SD	3.000		
Target height	2.000	Prism constant	-30.0mm						
Point	104	HA	319°28'21"	VA	80°35'04"	SD	105.452	Code	SS
Std Errors		HA	0°00'03"	VA	0°00'03"	SD	3.000		
Target height	2.000	Prism constant	-30.0mm						
Point	105	HA	302°54'21"	VA	84°34'10"	SD	145.679	Code	SS
Std Errors		HA	0°00'03"	VA	0°00'03"	SD	3.000		
Target height	2.000	Prism constant	-30.0mm						
Point	88	HA	118°30'59"	VA	85°45'14"	SD	171.056	Code	SS
Std Errors		HA	0°00'03"	VA	0°00'03"	SD	3.000		
Target height	2.000	Prism constant	-30.0mm						
Point	89	HA	130°30'49"	VA	86°52'24"	SD	126.458	Code	SS
Std Errors		HA	0°00'03"	VA	0°00'03"	SD	3.000		
Target height	2.000	Prism constant	-30.0mm						

Point	90	HA	153°06'36"	VA	89°55'34"	SD	92.039	Code	SS
Std Errors		HA	0°00'03"	VA	0°00'03"	SD	3.000		
Target height	2.000	Prism constant	-30.0mm						
Point	91	HA	188°39'22"	VA	94°59'54"	SD	83.612	Code	SS
Std Errors		HA	0°00'03"	VA	0°00'03"	SD	3.000		
Target height	2.000	Prism constant	-30.0mm						
Point	92	HA	218°54'26"	VA	97°05'48"	SD	107.017	Code	SS
Std Errors		HA	0°00'03"	VA	0°00'03"	SD	3.000		
Target height	2.000	Prism constant	-30.0mm						

Instrument

Instrument type	Unknown
EDM Refractive Index	275.0
EDM Carrier	79.5
Wavelength	
Horizontal Circle Mode	Set to azimuth
Horizontal Angle	0°00'03"
Precision	

Vertical Angle Precision		0°00'03"							
EDM precision		3000mm +2ppm							
Point	46J8	Y	52655.070	X	3756350.990	Z	50.750	Code	TSM

Instrument

Instrument type	Unknown								
EDM Refractive Index	275.0								
EDM Carrier	79.5								
Wavelength									
Horizontal Circle Mode	Set to azimuth								
Horizontal Angle Precision	0°00'03"								
Vertical Angle Precision	0°00'03"								
EDM precision	3000mm +2ppm								

Atmosphere

Pressure	1013.00mbar	Temperature	20.0°C	ppm	0.3				
Curvature correction	Yes	Refraction correction	Yes	Refraction const.	0.142				

Station setup

Station	46J8	Instrument height	1.698	Station type	Station setup	Scale factor	1.00000000	Std Error	?
----------------	------	--------------------------	-------	---------------------	---------------	---------------------	------------	------------------	---

Orientation

Station	46J8	Backsight point	TR124	Orientation correction	0°00'00"	Orient. Std Err	?		
Point (B.S.)	TR124	HA	130°27'44"	VA	85°33'21"	SD	?	Code	TRG
Std Errors		HA	0°00'03"	VA	0°00'03"	SD	?		
Target height	?	Prism constant	-30.0mm						
Point	TR544	HA	125°06'25"	VA	84°22'36"	SD	?	Code	TRG
Std Errors		HA	0°00'03"	VA	0°00'03"	SD	?		
Target height	?	Prism constant	-30.0mm						
Deltas	TR544	Azimuth	?	H.Dist	?	V.Dist	?		
Point	38	HA	80°34'56"	VA	88°11'30"	SD	55.700	Code	SS
Std Errors		HA	0°00'03"	VA	0°00'03"	SD	3.000		
Target height	2.000	Prism constant	-30.0mm						
Point	50	HA	319°16'10"	VA	84°21'54"	SD	82.781	Code	SS
Std Errors		HA	0°00'03"	VA	0°00'03"	SD	3.000		

Target height	2.000	Prism constant	-30.0mm						
Point	59	HA	335°04'37"	VA	83°06'39"	SD	129.155	Code	SS
Std Errors		HA	0°00'03"	VA	0°00'03"	SD	3.000		
Target height	2.000	Prism constant	-30.0mm						
Point	51	HA	299°55'03"	VA	87°13'14"	SD	124.617	Code	SS
Std Errors		HA	0°00'03"	VA	0°00'03"	SD	3.000		
Target height	2.000	Prism constant	-30.0mm						
Point	52	HA	290°52'21"	VA	88°23'54"	SD	173.480	Code	SS
Std Errors		HA	0°00'03"	VA	0°00'03"	SD	3.000		
Target height	2.000	Prism constant	-30.0mm						

Instrument

Instrument type	Unknown
EDM Refractive Index	275.0
EDM Carrier Wavelength	79.5
Horizontal Circle Mode	Set to azimuth
Horizontal Angle	0°00'03"

Precision									
Vertical Angle Precision		0°00'03"							
EDM precision		3000mm +2ppm							
Point	45J8	Y	52492.830	X	3756417.850	Z	55.320	Code	TSM

Instrument

Instrument type Unknown

EDM Refractive Index 275.0

EDM Carrier	79.5
Wavelength	
Horizontal Circle Mode	Set to azimuth
Horizontal Angle Precision	0°00'03"
Vertical Angle Precision	0°00'03"
EDM precision	3000mm +2ppm

Atmosphere

Pressure	1013.00mbar	Temperature	20.0°C	ppm	0.3				
Curvature correction	Yes	Refraction correction	Yes	Refraction const.	0.142				

Station setup

Station	45J8	Instrument height	1.728	Station type	Station setup	Scale factor	1.00000000	Std Error	?
----------------	------	--------------------------	-------	---------------------	---------------	---------------------	------------	------------------	---

Orientation

Station	45J8	Backsight point	TR124	Orientation correction	0°00'00"	Orient. Std Err	?		
Point (B.S.)	TR124	HA	129°25'17"	VA	85°54'19"	SD	?	Code	TRG
Std Errors		HA	0°00'03"	VA	0°00'03"	SD	?		
Target height	?	Prism constant	-30.0mm						
Point	TR544	HA	124°24'51"	VA	84°45'36"	SD	?	Code	TRG
Std Errors		HA	0°00'03"	VA	0°00'03"	SD	?		
Target height	?	Prism constant	-30.0mm						
Deltas	TR544	Azimuth	?	H.Dist	?	V.Dist	?		
Point	60	HA	47°44'50"	VA	81°30'03"	SD	73.909	Code	SS
Std Errors		HA	0°00'03"	VA	0°00'03"	SD	3.000		
Target height	2.000	Prism constant	-30.0mm						
Point	61	HA	359°57'10"	VA	82°48'09"	SD	49.267	Code	SS
Std Errors		HA	0°00'03"	VA	0°00'03"	SD	3.000		

Target height	2.000	Prism constant	-30.0mm						
Point	62	HA	311°49'31"	VA	88°34'57"	SD	72.769	Code	SS
Std Errors		HA	0°00'03"	VA	0°00'03"	SD	3.000		
Target height	2.000	Prism constant	-30.0mm						
Point	63	HA	294°48'23"	VA	89°30'09"	SD	118.035	Code	SS
Std Errors		HA	0°00'03"	VA	0°00'03"	SD	3.000		
Target height	2.000	Prism constant	-30.0mm						
Point	67	HA	359°48'30"	VA	81°41'23"	SD	103.815	Code	SS
Std Errors		HA	0°00'03"	VA	0°00'03"	SD	3.000		
Target height	2.000	Prism constant	-30.0mm						
Point	68	HA	331°59'46"	VA	84°19'57"	SD	116.619	Code	SS
Std Errors		HA	0°00'03"	VA	0°00'03"	SD	3.000		
Target height	2.000	Prism constant	-30.0mm						
Point	69	HA	313°14'28"	VA	85°46'06"	SD	149.498	Code	SS
Std		HA	0°00'03"	VA	0°00'03"	SD	3.000		

Errors									
Target height	2.000	Prism constant	-30.0mm						
Point	70	HA	302°02'14"	VA	86°54'54"	SD	192.279	Code	SS
Std Errors		HA	0°00'03"	VA	0°00'03"	SD	3.000		
Target height	2.000	Prism constant	-30.0mm						
Point	71	HA	295°20'34"	VA	87°22'53"	SD	241.094	Code	SS
Std Errors		HA	0°00'03"	VA	0°00'03"	SD	3.000		
Target height	2.000	Prism constant	-30.0mm						

Instrument

Instrument type	Unknown
EDM Refractive Index	275.0
EDM Carrier Wavelength	79.5
Horizontal Circle Mode	Set to azimuth
Horizontal Angle Precision	0°00'03"
Vertical Angle Precision	0°00'03"

EDM precision	3000mm +2ppm
Note	Used last station setup

Instrument

Instrument type	Unknown								
EDM Refractive Index	275.0								
EDM Carrier Wavelength	79.5								
Horizontal Circle Mode	Set to azimuth								
Horizontal Angle Precision	0°00'03"								
Vertical Angle Precision	0°00'03"								
EDM precision	3000mm +2ppm								
Point	33K9	Y	52052.400	X	3756511.480	Z	53.240	Code	TSM
Point	53K8	Y	52111.260	X	3756489.060	Z	54.460	Code	TSM

Instrument

Instrument type	Unknown								
EDM Refractive Index	275.0								
EDM Carrier Wavelength	79.5								

Horizontal Circle Mode	Set to azimuth
Horizontal Angle Precision	0°00'03"

Vertical Angle Precision 0°00'03"

EDM precision 3000mm +2ppm

Atmosphere

Pressure	1013.00mbar	Temperature	20.0°C	ppm	0.3				
Curvature correction	Yes	Refraction correction	Yes	Refraction const.	0.142				

Station setup

Station	53K8	Instrument height	1.738	Station type	Station setup	Scale factor	1.00000000	Std Error	?
----------------	------	--------------------------	-------	---------------------	---------------	---------------------	------------	------------------	---

Orientation

Station	53K8	Backsight point	33K9	Orientation correction	0°00'00"	Orient. Std Err	?		
Point (B.S.)	33K9	HA	290°51'07"	VA	92°36'24"	SD	?	Code	TSM
Std Errors		HA	0°00'03"	VA	0°00'03"	SD	?		
Target height	?	Prism constant	-30.0mm						
Point	73	HA	62°13'17"	VA	83°47'34"	SD	64.130	Code	SS

Std Errors		HA	0°00'03"	VA	0°00'03"	SD	3.000		
Target height	2.000	Prism constant	-30.0mm						
Point	74	HA	4°20'34"	VA	81°26'36"	SD	29.861	Code	SS
Std Errors		HA	0°00'03"	VA	0°00'03"	SD	3.000		
Target height	2.000	Prism constant	-30.0mm						
Point	75	HA	299°17'04"	VA	90°39'56"	SD	59.558	Code	SS
Std Errors		HA	0°00'03"	VA	0°00'03"	SD	3.000		
Target height	2.000	Prism constant	-30.0mm						
Point	81	HA	1°19'52"	VA	82°49'57"	SD	84.008	Code	SS
Std Errors		HA	0°00'03"	VA	0°00'03"	SD	3.000		
Target height	2.000	Prism constant	-30.0mm						
Point	80	HA	33°51'32"	VA	81°28'31"	SD	101.824	Code	SS
Std Errors		HA	0°00'03"	VA	0°00'03"	SD	3.000		
Target height	2.000	Prism constant	-30.0mm						

Point	78	HA	62°52'39"	VA	83°24'33"	SD	185.930	Code	SS
Std Errors		HA	0°00'03"	VA	0°00'03"	SD	3.000		
Target height	2.500	Prism constant	-30.0mm						
Point	65	HA	246°37'20"	VA	93°34'54"	SD	58.175	Code	SS
Std Errors		HA	0°00'03"	VA	0°00'03"	SD	3.000		
Target height	2.500	Prism constant	-30.0mm						
Point	85	HA	22°05'56"	VA	81°46'14"	SD	149.944	Code	SS
Std Errors		HA	0°00'03"	VA	0°00'03"	SD	3.000		
Target height	2.000	Prism constant	-30.0mm						
Point	TT1	HA	121°06'36"	VA	91°26'08"	SD	146.241	Code	CTRL
Std Errors		HA	0°00'03"	VA	0°00'03"	SD	3.000		
Target height	2.000	Prism constant	-30.0mm						

Instrument

Instrument type	Unknown
EDM Refractive Index	275.0

EDM Carrier Wavelength	79.5
Horizontal Circle Mode	Set to azimuth
Horizontal Angle Precision	0°00'03"
Vertical Angle Precision	0°00'03"
EDM precision	3000mm +2ppm

Atmosphere

Pressure	1013.00mba r	Temperature	20.0°C	ppm	0.3				
Curvature correction	Yes	Refraction correction	Yes	Refraction const.	0.142				

Station setup

Station	51K8	Instrument height	1.723	Station type	Station setup	Scale factor	1.0000000 0	Std Error	?
----------------	------	--------------------------	-------	---------------------	---------------	---------------------	----------------	------------------	---

Orientation

Station	51K8	Backsight point	52K8	Orientation correction	0°00'00"	Orient	?		
Point (B.S.)	52K8	HA	299°32'11"	VA	88°37'59"	SD	?	Code	TSM

Std Errors		HA	0°00'03"	VA	0°00'03"	SD	?		
Target height	?	Prism constant	-30.0mm						
Point	TT1C	HA	49°20'41"	VA	85°35'34"	SD	190.115	Code	CTR L
Std Errors		HA	0°00'03"	VA	0°00'03"	SD	3.000		
Target height	2.000	Prism constant	-30.0mm						
Point	TTT1	Y	52236.40 6	X	3756413.43 0	Z	50.528	Code	CP

Instrument

Instrument type	Unknown
EDM Refractive Index	275.0
EDM Carrier Wavelength	79.5
Horizontal Circle Mode	Set to azimuth
Horizontal Angle Precision	0°00'03"
Vertical Angle Precision	0°00'03"

EDM precision 3000mm +2ppm

Atmosphere

Pressure	1013.00mba r	Temperature	20.0° C	ppm	0.3				
Curvature correction	Yes	Refraction correction	Yes	Refraction const.	0.142				

Station setup

Station	TTT1	Instrument height	1.632	Station type	Station setup	Scale factor	1.0000000 0	Std Error	?
----------------	------	--------------------------	-------	---------------------	---------------	---------------------	----------------	------------------	---

Orientation

Station	TTT1	Backsight point	53K8	Orientation correction	0°00'00"	Orient	?		
Point (B.S.)	53K8	HA	301°08'46"	VA	88°54'19"	SD	?	Code	TS M
Std Errors		HA	0°00'03"	VA	0°00'03"	SD	?		
Target height	?	Prism constant	-30.0mm						
Point	51K8	HA	229°22'17"	VA	94°48'57"	SD	?	Code	TS M
Std Errors		HA	0°00'03"	VA	0°00'03"	SD	?		
Target height	?	Prism constant	-30.0mm						
Deltas	51K8	Azimuth	?	H.Distance	?	V.Distance	?		

Point	40	HA	120°28'59" "	VA	93°13'13"	SD	109.878	Code	SS
Std Errors		HA	0°00'03"	VA	0°00'03"	SD	3.000		
Target height	2.000	Prism constant	-30.0mm						
Point	41	HA	144°04'56" "	VA	94°23'57"	SD	69.117	Code	SS
Std Errors		HA	0°00'03"	VA	0°00'03"	SD	3.000		
Target height	2.000	Prism constant	-30.0mm						
Point	42	HA	193°47'23" "	VA	94°28'59"	SD	58.036	Code	SS
Std Errors		HA	0°00'03"	VA	0°00'03"	SD	3.000		
Target height	2.000	Prism constant	-30.0mm						
Point	54	HA	92°51'08" "	VA	91°29'34"	SD	40.183	Code	SS
Std Errors		HA	0°00'03"	VA	0°00'03"	SD	3.000		
Target height	2.000	Prism constant	-30.0mm						
Point	29	HA	140°18'28" "	VA	94°14'52"	SD	142.963	Code	SS
Std Errors		HA	0°00'03"	VA	0°00'03"	SD	3.000		

Target height	2.000	Prism constant	-30.0mm						
Point	30	HA	159°40'34"	VA	95°05'08"	SD	117.575	Code	SS
Std Errors		HA	0°00'03"	VA	0°00'03"	SD	3.000		
Target height	2.000	Prism constant	-30.0mm						
Point	43	HA	230°15'37"	VA	94°09'33"	SD	88.576	Code	SS
Std Errors		HA	0°00'03"	VA	0°00'03"	SD	3.000		
Target height	2.000	Prism constant	-30.0mm						
Point	31	HA	186°59'34"	VA	95°36'52"	SD	111.438	Code	SS
Std Errors		HA	0°00'03"	VA	0°00'03"	SD	3.000		
Target height	2.000	Prism constant	-30.0mm						
Point	31a	HA	186°59'34"	VA	95°36'50"	SD	111.438	Code	SS
Std Errors		HA	0°00'03"	VA	0°00'03"	SD	3.000		
Target height	2.500	Prism constant	-30.0mm						

Point	32	HA	211°30'40 "	VA	94°18'30"	SD	129.824	Code	SS
Std Errors		HA	0°00'03"	VA	0°00'03"	SD	3.000		
Target height	2.533	Prism constant	-30.0mm						
Point	53	HA	94°31'59"	VA	91°26'46"	SD	91.565	Code	SS
Std Errors		HA	0°00'03"	VA	0°00'03"	SD	3.000		
Target height	1.111	Prism constant	-30.0mm						
Point	34K9	Y	52059.62 0	X	3756622.32 0	Z	60.790	Code	TS M
Point	35K9	Y	52048.51 0	X	3756717.25 0	Z	66.560	Code	TS M

Instrument

Instrument type	Unknown
EDM Refractive Index	275.0
EDM Carrier Wavelength	79.5
Horizontal Circle Mode	Set to azimuth
Horizontal Angle Precision	0°00'03"

Vertical Angle Precision	0°00'03"
EDM precision	3000mm +2ppm

Atmosphere

Pressure	1013.00mb	Temperature	20.0°C	ppm	0.3				
Curvature correction	Yes	Refraction correction	Yes	Refraction const.	0.142				

Station setup

Station	35K9	Instrument height	1.720	Station type	Station setup	Scale factor	1.00000000	Std Error	?
----------------	------	--------------------------	-------	---------------------	---------------	---------------------	------------	------------------	---

Orientation

Station	35K9	Backsight point	34K9	Orientation correction	0°00'00"	Orientation Std Error	?		
Point (B.S.)	34K9	HA	173°19'29"	VA	94°01'10"	SD	?	Code	TS M
Std Errors		HA	0°00'03"	VA	0°00'03"	SD	?		
Target height	?	Prism constant	-30.0mm						
Point	36K9	HA	59°28'10"	VA	83°26'09"	SD	?	Code	TS M

Std Errors		HA	0°00'03"	VA	0°00'03"	SD	?		
Target height	?	Prism constant	-30.0mm						
Deltas	36K9	Azimuth	?	H.Dist	?	V.Dist	?		
Point	103	HA	327°26'10"	VA	80°56'42"	SD	84.245	Cod e	SS
Std Errors		HA	0°00'03"	VA	0°00'03"	SD	3.000		
Target height	2.000	Prism constant	-30.0mm						
Point	86	HA	144°43'15"	VA	88°29'36"	SD	111.552	Cod e	SS
Std Errors		HA	0°00'03"	VA	0°00'03"	SD	3.000		
Target height	2.000	Prism constant	-30.0mm						
Point	87	HA	173°35'08"	VA	93°18'44"	SD	92.042	Cod e	SS
Std Errors		HA	0°00'03"	VA	0°00'03"	SD	3.000		
Target height	2.000	Prism constant	-30.0mm						
Point	99	HA	67°28'20"	VA	82°18'36"	SD	187.678	Cod e	SS
Std		HA	0°00'03"	VA	0°00'03"	SD	3.000		

Errors									
Target height	2.000	Prism constant	-30.0mm						
Point	2J9	Y	52530.41	X	3756594.93	Z	81.711	Cod	TS
			0		0			e	M
Point	13K9	Y	52306.18	X	3756702.70	Z	93.814	Cod	TS
			0		0			e	M
Point	14K9	Y	52376.18	X	3756643.25	Z	89.214	Cod	TS
			0		0			e	M

Instrument

Instrument type	Unknown
EDM Refractive Index	275.0
EDM Carrier Wavelength	79.5
Horizontal Circle Mode	Set to azimuth
Horizontal Angle Precision	0°00'03"
Vertical Angle Precision	0°00'03"
EDM precision	3000mm +2ppm

Atmosphere

Pressure	1013.00mbar	Temperature	20.0°C	ppm	0.3				
-----------------	-------------	--------------------	--------	------------	-----	--	--	--	--

Curvature correction	Yes	Refraction correction	Yes	Refraction const.	0.142				
-----------------------------	-----	------------------------------	-----	--------------------------	-------	--	--	--	--

Station setup

Station	2J9	Instrument height	1.875	Station type	Station setup	Scale factor	1.0000000 0	Std Error	?
----------------	-----	--------------------------	-------	---------------------	---------------	---------------------	----------------	------------------	---

Orientation

Station	2J9	Backsight point	TR544	Orientation correction	0°00'00"	Orient	?		
Point (B.S.)	TR544	HA	127°21'13"	VA	85°21'52"	SD	?	Code	TRG
Std Errors		HA	0°00'03"	VA	0°00'03"	SD	?		
Target height	?	Prism constant	-30.0mm						
Point	14K9	HA	287°23'46"	VA	87°19'04"	SD	?	Code	TSM
Std Errors		HA	0°00'03"	VA	0°00'03"	SD	?		
Target height	?	Prism constant	-30.0mm						
Deltas	14K9	Azimuth	?	H.Dist	?	V.Dist	?		
Point	TT2	HA	262°22'19"	VA	91°49'54"	SD	273.468	Code	CTRL
Std		HA	0°00'03"	VA	0°00'03"	SD	3.001		

Errors									
Target height	2.000	Prism constant	-30.0mm						
Point	TT3	HA	262°22'18"	VA	91°49'54"	SD	273.468	Code	CTR L
Std Errors		HA	0°00'03"	VA	0°00'03"	SD	3.001		
Target height	2.000	Prism constant	-30.0mm						
Point	76	HA	261°49'21"	VA	92°39'01"	SD	148.208	Code	SS
Std Errors		HA	0°00'03"	VA	0°00'03"	SD	3.000		
Target height	2.000	Prism constant	-30.0mm						

Instrument

Instrument type	Unknown
EDM Refractive Index	275.0
EDM Carrier Wavelength	79.5
Horizontal Circle Mode	Set to azimuth
Horizontal Angle Precision	0°00'03"
Vertical Angle Precision	0°00'03"

EDM precision	3000mm +2ppm
----------------------	--------------

Atmosphere

Pressure	1013.00mbar	Temperature	20.0°C	ppm	0.3				
Curvature correction	Yes	Refraction correction	Yes	Refraction const.	0.142				

Station setup

Station	45J8	Instrument height	1.716	Station type	Station setup	Scale factor	1.00000000	Std Error	?
----------------	------	--------------------------	-------	---------------------	---------------	---------------------	------------	------------------	---

Orientation

Station	45J8	Backsight point	TR124	Orientation correction	0°00'00"	Orientation Std Err	?		
Point (B.S.)	TR124	HA	129°25'17"	VA	85°58'10"	SD	?	Code	TRG
Std Errors		HA	0°00'03"	VA	0°00'03"	SD	?		
Target height	?	Prism constant	-30.0mm						
Point	TR544	HA	124°24'42"	VA	84°59'28"	SD	?	Code	TRG
Std Errors		HA	0°00'03"	VA	0°00'03"	SD	?		

Target height	?	Prism constant	-30.0mm						
Deltas	TR544	Azimuth	?	H.Dist	?	V.Dist	?		
Point	TT2C	HA	301°06'02" "	VA	86°15'30" "	SD	273.077	Code	CTR L
Std Errors		HA	0°00'03"	VA	0°00'03"	SD	3.001		
Target height	2.000	Prism constant	-30.0mm						
Point	TT2D	HA	301°06'11" "	VA	86°15'24" "	SD	273.087	Code	CTR L
Std Errors		HA	0°00'03"	VA	0°00'03"	SD	3.001		
Target height	2.000	Prism constant	-30.0mm						

Instrument

Instrument type	Unknown
EDM Refractive Index	275.0
EDM Carrier Wavelength	79.5
Horizontal Circle Mode	Set to azimuth
Horizontal Angle Precision	0°00'03"

Vertical Angle Precision	0°00'03"
EDM precision	3000mm +2ppm

Instrument

Instrument type	Unknown								
EDM Refractive Index	275.0								
EDM Carrier Wavelength	79.5								
Horizontal Circle Mode	Set to azimuth								
Horizontal Angle Precision	0°00'03"								
Vertical Angle Precision	0°00'03"								
EDM precision	3000mm +2ppm								
Point	TTT2	Y	52259.524	X	3756558.622	Z	72.855	Code	CP

Instrument

Instrument type	Unknown								
EDM Refractive Index	275.0								
EDM Carrier Wavelength	79.5								

Horizontal Circle Mode	Set to azimuth
Horizontal Angle Precision	0°00'03"
Vertical Angle Precision	0°00'03"
EDM precision	3000mm +2ppm

Atmosphere

Pressure	1013.00mbar	Temperature	20.0°C	ppm	0.3				
Curvature correction	Yes	Refraction correction	Yes	Refraction const.	0.142				

Station setup

Station	TTT2	Instrument height	1.555	Station type	Station setup	Scale factor	1.00000000	Std Error	?
----------------	------	--------------------------	-------	---------------------	---------------	---------------------	------------	------------------	---

Orientation

Station	TTT2	Backsight point	TR124	Orientation correction	0°00'00"	Orient. Std Err	?		
Point (B.S.)	TR124	HA	128°43'48"	VA	86°42'33"	SD	?	Code	TRG
Std Errors		HA	0°00'03"	VA	0°00'03"	SD	?		
Target height	?	Prism constant	-30.0mm						
Point	53K8	HA	244°51'50"	VA	96°57'02"	SD	?	Code	TSM

Std Errors		HA	0°00'03"	VA	0°00'03"	SD	?		
Target height	?	Prism constant	-30.0mm						
Deltas	53K8	Azimuth	?	H.Distance	?	V.Distance	?		
Point	77	HA	77°59'19"	VA	88°36'40"	SD	71.843	Code	SS
Std Errors		HA	0°00'03"	VA	0°00'03"	SD	3.000		
Target height	2.000	Prism constant	-30.0mm						
Point	83	HA	12°58'16"	VA	80°44'00"	SD	71.300	Code	SS
Std Errors		HA	0°00'03"	VA	0°00'03"	SD	3.000		
Target height	2.000	Prism constant	-30.0mm						
Point	84	HA	330°37'48"	VA	84°16'09"	SD	78.695	Code	SS
Std Errors		HA	0°00'03"	VA	0°00'03"	SD	3.000		
Target height	2.000	Prism constant	-30.0mm						
Point	79	HA	290°39'14"	VA	89°59'29"	SD	40.688	Code	SS
Std Errors		HA	0°00'03"	VA	0°00'03"	SD	3.000		

Target height	2.000	Prism constant	-30.0mm						
Point	72	HA	224°10'40"	VA	97°31'49"	SD	54.671	Code	SS
Std Errors		HA	0°00'03"	VA	0°00'03"	SD	3.000		
Target height	2.000	Prism constant	-30.0mm						
Point	82	HA	45°27'22"	VA	82°00'15"	SD	99.116	Code	SS
Std Errors		HA	0°00'03"	VA	0°00'03"	SD	3.000		
Target height	2.000	Prism constant	-30.0mm						

Instrument

Instrument type	Unknown
EDM Refractive Index	275.0
EDM Carrier Wavelength	79.5
Horizontal Circle Mode	Set to azimuth
Horizontal Angle Precision	0°00'03"
Vertical Angle Precision	0°00'03"
EDM precision	3000mm +2ppm

Atmosphere

Pressure	1013.00mbar	Temperature	20.0°C	ppm	0.3				
Curvature correction	Yes	Refraction correction	Yes	Refraction const.	0.142				

Station setup

Station	50K8	Instrument height	1.705	Station type	Station setup	Scale factor	1.00000000	Std Error	?
----------------	------	--------------------------	-------	---------------------	---------------	---------------------	------------	------------------	---

Orientation

Station	50K8	Backsight point	TR124	Orientation correction	0°00'00"	Orient. Std Err	?		
Point (B.S.)	TR124	HA	123°23'17"	VA	85°30'56"	SD	?	Code	TRG
Std Errors		HA	0°00'03"	VA	0°00'03"	SD	?		
Target height	?	Prism constant	-30.0mm						
Point	TR544	HA	118°52'49"	VA	84°28'10"	SD	?	Code	TRG
Std Errors		HA	0°00'03"	VA	0°00'03"	SD	?		
Target height	?	Prism constant	-30.0mm						
Deltas	TR544	Azimuth	?	H.Dist	?	V.Dist	?		
Point	7	HA	125°22'34"	VA	91°53'16"	SD	101.104	Code	SS

Std Errors		HA	0°00'03"	VA	0°00'03"	SD	3.000		
Target height	2.000	Prism constant	-30.0mm						
Point	9	HA	203°43'42"	VA	93°37'43"	SD	64.675	Code	SS
Std Errors		HA	0°00'03"	VA	0°00'03"	SD	3.000		
Target height	2.000	Prism constant	-30.0mm						
Point	35	HA	292°37'18"	VA	88°04'38"	SD	263.863	Code	SS
Std Errors		HA	0°00'03"	VA	0°00'03"	SD	3.001		
Target height	2.500	Prism constant	-30.0mm						

Instrument

Instrument type	Unknown
EDM Refractive Index	275.0
EDM Carrier Wavelength	79.5
Horizontal Circle Mode	Set to azimuth
Horizontal Angle Precision	0°00'03"

Vertical Angle Precision	0°00'03"
EDM precision	3000mm +2ppm

Atmosphere

Pressure	1013.00mbar	Temperature	20.0°C	ppm	0.3				
Curvature correction	Yes	Refraction correction	Yes	Refraction const.	0.142				

Station setup

Station	36K9	Instrument height	1.712	Station type	Station setup	Scale factor	1.00000000	Std Error	?
----------------	------	--------------------------	-------	---------------------	---------------	---------------------	------------	------------------	---

Orientation

Station	36K9	Backsight point	TR124	Orientation correction	0°00'00"	Orient. Std Err	?		
Point (B.S.)	TR124	HA	129°57'27"	VA	86°52'11"	SD	?	Code	TRG
Std Errors		HA	0°00'03"	VA	0°00'03"	SD	?		
Target height	?	Prism constant	-30.0mm						
Point	TR544	HA	125°36'03"	VA	85°49'48"	SD	?	Code	TRG
Std Errors		HA	0°00'03"	VA	0°00'03"	SD	?		

Target height	?	Prism constant	-30.0mm						
Deltas	TR544	Azimuth	?	H.Dist	?	V.Dist	?		
Point	105 CHECK	HA	302°54'28"	VA	84°35'01"	SD	145.659	Code	TRG
Std Errors		HA	0°00'03"	VA	0°00'03"	SD	3.000		
Target height	2.000	Prism constant	-30.0mm						
Point	105 CHECK2	HA	302°54'32"	VA	84°35'01"	SD	145.657	Code	TRG
Std Errors		HA	0°00'03"	VA	0°00'03"	SD	3.000		
Target height	2.000	Prism constant	-30.0mm						

Instrument

Instrument type	Unknown
EDM Refractive Index	275.0
EDM Carrier Wavelength	79.5
Horizontal Circle Mode	Set to azimuth
Horizontal Angle Precision	0°00'03"

Vertical Angle Precision	0°00'03"								
EDM precision	3000mm +2ppm								
Point	TR116	Y	51849.200	X	3758730.110	Z	985.900	Code	TRG

Instrument

Instrument type	Unknown								
EDM Refractive Index	275.0								
EDM Carrier Wavelength	79.5								
Horizontal Circle Mode	Set to azimuth								
Horizontal Angle Precision	0°00'03"								
Vertical Angle Precision	0°00'03"								
EDM precision	3000mm +2ppm								

Atmosphere

Pressure	1013.00mbar	Temperature	20.0°C	ppm	0.3				
Curvature correction	Yes	Refraction correction	Yes	Refraction const.	0.142				

Station setup

Station	33K9	Instrument height	1.700	Station type	Station setup	Scale factor	1.00000000	Std Error	?
----------------	------	--------------------------	-------	---------------------	---------------	---------------------	------------	------------------	---

Orientation

Station	33K9	Backsight point	TR544	Orientation correction	0°00'00"	Orient. Std Err	?		
Point (B.S.)	TR544	HA	121°41'13"	VA	85°23'18"	SD	?	Code	TRG
Std Errors		HA	0°00'03"	VA	0°00'03"	SD	?		
Target height	?	Prism constant	-30.0mm						
Point	TR116	HA	354°46'06"	VA	67°23'10"	SD	?	Code	TRG
Std Errors		HA	0°00'03"	VA	0°00'03"	SD	?		
Target height	?	Prism constant	-30.0mm						
Deltas	TR116	Azimuth	?	H.Dist	?	V.Dist	?		
Point	CG1	HA	348°14'56"	VA	86°10'11"	SD	42.791	Code	SS
Std Errors		HA	0°00'03"	VA	0°00'03"	SD	3.000		
Target height	2.000	Prism constant	-30.0mm						
Point	CG1 C	HA	348°15'01"	VA	86°09'24"	SD	42.788	Code	SS
Std Errors		HA	0°00'03"	VA	0°00'03"	SD	3.000		

Target height	2.000	Prism constant	-30.0mm						
----------------------	-------	-----------------------	---------	--	--	--	--	--	--

Instrument

Instrument type	Unknown								
EDM Refractive Index	275.0								
EDM Carrier Wavelength	79.5								
Horizontal Circle Mode	Set to azimuth								
Horizontal Angle Precision	0°00'03"								
Vertical Angle Precision	0°00'03"								
EDM precision	3000mm +2ppm								

Atmosphere

Pressure	1013.00mbar	Temperature	20.0°C	ppm	0.3				
Curvature correction	Yes	Refraction correction	Yes	Refraction const.	0.142				

Station setup

Station	52K8	Instrument	1.714	Station	Station setup	Scale	1.00000000	Std	
Error			?						
	height		type		factor				

Orientation

Station	52K8	Backsight point	TR124	Orientation correction	0°00'00"	Orient. Std Err	?		
Point (B.S.)	TR124	HA	122°59'20"	VA	86°11'36"	SD	?	Code	TRG
Std Errors		HA	0°00'03"	VA	0°00'03"	SD	?		
Target height	?	Prism constant	-30.0mm						
Point	TR544	HA	118°56'47"	VA	85°13'47"	SD	?	Code	TRG
Std Errors		HA	0°00'03"	VA	0°00'03"	SD	?		
Target height	?	Prism constant	-30.0mm						
Deltas	TR544	Azimuth	?	H.Dist	?	V.Dist	?		
Point	CG1 D	HA	30°31'25"	VA	86°04'58"	SD	205.400	Code	TRG
Std Errors		HA	0°00'03"	VA	0°00'03"	SD	3.000		
Target height	2.000	Prism constant	-30.0mm						
Point	CG1 E	HA	30°31'27"	VA	86°05'04"	SD	205.391	Code	SS
Std Errors		HA	0°00'03"	VA	0°00'03"	SD	3.000		
Target height	2.000	Prism constant	-30.0mm						

Point	MH1	HA	278°10'50"	VA	86°39'15"	SD	109.923	Code	SS
Std Errors		HA	0°00'03"	VA	0°00'03"	SD	3.000		
Target height	2.000	Prism constant	-30.0mm						
Point	MH1 C	HA	278°10'49"	VA	86°38'57"	SD	109.923	Code	SS
Std Errors		HA	0°00'03"	VA	0°00'03"	SD	3.000		
Target height	2.000	Prism constant	-30.0mm						
Point	MH1 D	HA	278°10'44"	VA	86°39'10"	SD	109.922	Code	SS
Std Errors		HA	0°00'03"	VA	0°00'03"	SD	3.000		
Target height	2.000	Prism constant	-30.0mm						

Instr
ume
nt

Instrument type	Unknown
EDM Refractive Index	275.0
EDM Carrier Wavelength	79.5
Horizontal Circle Mode	Set to azimuth

Horizontal Angle Precision	0°00'03"
Vertical Angle Precision	0°00'03"
EDM precision	3000mm +2ppm

Atm
osp
here

Pressure 1013.00mbar **Temperature** 20.0°C **ppm** 0.3

Curvature correction **Refraction const.** **Refraction correction** 0.142

Station setup

Station	36K9	Instrument height	1.690	Station type	Station setup	Scale factor	1.00000000	Std Error	?
----------------	------	--------------------------	-------	---------------------	---------------	---------------------	------------	------------------	---

Orientation

Station	36K9	Backsight point	TR124	Orientation correction	0°00'00"	Orient. Std Err	?		
Point (B.S.)	TR124	HA	129°57'27"	VA	86°51'40"	SD	?	Code	TRG
Std Errors		HA	0°00'03"	VA	0°00'03"	SD	?		
Target height	?	Prism constant	-30.0mm						
Point	TR544	HA	125°36'06"	VA	85°49'52"	SD	?	Code	TRG

Std Errors		HA	0°00'03"	VA	0°00'03"	SD	?		
Target height	?	Prism constant	-30.0mm						
Deltas	TR544	Azimuth	?	H.Dist	?	V.Dist	?		
Point	GCP1	HA	311°50'10"	VA	82°51'46"	SD	151.374	Code	GCP
Std Errors		HA	0°00'03"	VA	0°00'03"	SD	3.000		
Target height	2.000	Prism constant	-30.0mm						
Point	GCP11	HA	235°52'19"	VA	96°23'35"	SD	36.755	Code	GCP
Std Errors		HA	0°00'03"	VA	0°00'03"	SD	3.000		
Target height	2.000	Prism constant	-30.0mm						
Point	GCP2	HA	129°16'18"	VA	86°36'18"	SD	164.960	Code	GCP
Std Errors		HA	0°00'03"	VA	0°00'03"	SD	3.000		
Target height	2.000	Prism constant	-30.0mm						
Point	GCP12	HA	222°16'54"	VA	95°48'16"	SD	162.234	Code	GCP
Std Errors		HA	0°00'03"	VA	0°00'03"	SD	3.000		

Target height	2.000	Prism constant	-30.0mm						
----------------------	-------	-----------------------	---------	--	--	--	--	--	--

Instrument

Instrument type	Unknown
EDM Refractive Index	275.0
EDM Carrier Wavelength	79.5
Horizontal Circle Mode	Set to azimuth
Horizontal Angle Precision	0°00'03"
Vertical Angle Precision	0°00'03"
EDM precision	3000mm +2ppm

Atmosphere

--	--	--	--	--	--	--	--	--	--

Pressure 1013.00mbar **Temperature** 20.0°C **ppm** 0.3

Curvature Refraction Refraction
 Yes Yes 0.142 **correction**
correction const.

Station setup

Station	33K9	Instrument height	1.658	Station type	Station setup	Scale factor	1.00000000	Std Error	?
----------------	------	--------------------------	-------	---------------------	---------------	---------------------	------------	------------------	---

Orientation

--	--	--	--	--	--	--	--	--	--

Station	33K9	Backsight point	TR544	Orientation correction	0°00'00"	Orient. Std Err	?		
Point (B.S.)	TR544	HA	121°41'13"	VA	85°29'17"	SD	?	Code	TRG
Std Errors		HA	0°00'03"	VA	0°00'03"	SD	?		
Target height	?	Prism constant	-30.0mm						
Point	TR116	HA	354°46'05"	VA	67°23'41"	SD	?	Code	TRG
Std Errors		HA	0°00'03"	VA	0°00'03"	SD	?		
Target height	?	Prism constant	-30.0mm						
Deltas	TR116	Azimuth	?	H.Dist	?	V.Dist	?		
Point	GCP9	HA	91°10'10"	VA	87°15'35"	SD	24.287	Code	GCP
Std Errors		HA	0°00'03"	VA	0°00'03"	SD	3.000		
Target height	2.000	Prism constant	-30.0mm						

Instrument

Instrument type	Unknown
EDM Refractive Index	275.0
EDM Carrier	79.5

Wavelength	
Horizontal Circle Mode	Set to azimuth
Horizontal Angle Precision	0°00'03"
Vertical Angle Precision	0°00'03"
EDM precision	3000mm +2ppm

Instrument

Instrument type	Unknown
EDM Refractive Index	275.0
EDM Carrier Wavelength	79.5
Horizontal Circle Mode	Set to azimuth
Horizontal Angle Precision	0°00'03"
Vertical Angle Precision	0°00'03"
EDM precision	3000mm +2ppm

Instrument

Instrument type	Unknown
EDM Refractive Index	275.0

EDM Carrier	79.5
Wavelength	
Horizontal Circle Mode	Set to azimuth
Horizontal Angle Precision	0°00'03"
Vertical Angle Precision	0°00'03"
EDM precision	3000mm +2ppm

Atmosphere

Pressure	1013.00mbar	Temperature	20.0°C	ppm	0.3				
Curvature correction	Yes	Refraction correction	Yes	Refraction const.	0.142				

Station setup

Station	33K9	Instrument height	1.658	Station type	Station setup	Scale factor	1.00000000	Std Error	?
----------------	------	--------------------------	-------	---------------------	---------------	---------------------	------------	------------------	---

Orientation

Station	33K9	Backsight point	TR544	Orientation correction	0°00'00"	Orient. Std Err	?		
Point (B.S.)	TR544	HA	121°41'13"	VA	85°25'19"	SD	?	Code	TRG
Std Errors		HA	0°00'03"	VA	0°00'03"	SD	?		

Target height	?	Prism constant	-30.0mm						
Point	TR116	HA	354°46'10"	VA	67°24'30"	SD	?	Code	TRG
Std Errors		HA	0°00'03"	VA	0°00'03"	SD	?		
Target height	?	Prism constant	-30.0mm						
Deltas	TR116	Azimuth	?	H.Distance	?	V.Distance	?		
Point	GCP23	HA	240°42'06"	VA	91°11'35"	SD	175.917	Code	GCP
Std Errors		HA	0°00'03"	VA	0°00'03"	SD	3.000		
Target height	2.000	Prism constant	-30.0mm						

Instrument

Instrument type	Unknown
EDM Refractive Index	275.0
EDM Carrier Wavelength	79.5
Horizontal Circle Mode	Set to azimuth
Horizontal Angle Precision	0°00'03"

Vertical Angle Precision	0°00'03"
EDM precision	3000mm +2ppm

Atmosphere

Pressure	1013.00mbar	Temperature	20.0°C	ppm	0.3				
Curvature correction	Yes	Refraction correction	Yes	Refraction const.	0.142				

Station setup

Station	13K9	Instrument height	1.915	Station type	Station setup	Scale factor	1.00000000	Std Error	?
----------------	------	--------------------------	-------	---------------------	---------------	---------------------	------------	------------------	---

Orientation

Station	13K9	Backsight point	TR544	Orientation correction	0°00'00"	Orient. Std Err	?		
Point (B.S.)	TR544	HA	126°31'49"	VA	86°00'48"	SD	?	Code	TRG
Std Errors		HA	0°00'03"	VA	0°00'03"	SD	?		
Target height	?	Prism constant	-30.0mm						
Point	TR124	HA	131°10'28"	VA	86°57'50"	SD	?	Code	TRG
Std Errors		HA	0°00'03"	VA	0°00'03"	SD	?		
Target height	?	Prism constant	-30.0mm						

Deltas	TR124	Azimuth	?	H.Dist	?	V.Dist	?		
Point	GCP13	HA	309°06'04"	VA	92°55'21"	SD	111.075	Code	GCP13
Std Errors		HA	0°00'03"	VA	0°00'03"	SD	3.000		
Target height	2.000	Prism constant	-30.0mm						
Point	GCP13C	HA	309°06'03"	VA	92°55'19"	SD	111.079	Code	GCP13
Std Errors		HA	0°00'03"	VA	0°00'03"	SD	3.000		
Target height	2.000	Prism constant	-30.0mm						

Instrument

Instrument type	Unknown
EDM Refractive Index	275.0
EDM Carrier Wavelength	79.5
Horizontal Circle Mode	Set to azimuth
Horizontal Angle Precision	0°00'03"
Vertical Angle Precision	0°00'03"
EDM precision	3000mm +2ppm

Atmosphere

Pressure	1013.00mbar	Temperature	20.0°C	ppm	0.3				
Curvature correction	Yes	Refraction correction	Yes	Refraction const.	0.142				

Station setup

Station	45J8	Instrument height	1.725	Station type	Station setup	Scale factor	1.00000000	Std Error	?
----------------	------	--------------------------	-------	---------------------	---------------	---------------------	------------	------------------	---

Orientation

Station	45J8	Backsight point	TR124	Orientation correction	0°00'00"	Orient. Std Err	?		
Point (B.S.)	TR124	HA	129°25'17"	VA	85°55'15"	SD	?	Code	TRG
Std Errors		HA	0°00'03"	VA	0°00'03"	SD	?		
Target height	?	Prism constant	-30.0mm						
Point	TR544	HA	124°24'44"	VA	84°48'32"	SD	?	Code	TRG
Std Errors		HA	0°00'03"	VA	0°00'03"	SD	?		
Target height	?	Prism constant	-30.0mm						
Deltas	TR544	Azimuth	?	H.Dist	?	V.Dist	?		
Point	GCP3	HA	339°31'24"	VA	83°48'02"	SD	103.552	Code	GCP
Std		HA	0°00'03"	VA	0°00'03"	SD	3.000		

Errors									
Target height	2.000	Prism constant	-30.0mm						
Point	GCP6	HA	91°05'16"	VA	87°58'43"	SD	106.417	Code	GCP
Std Errors		HA	0°00'03"	VA	0°00'03"	SD	3.000		
Target height	2.000	Prism constant	-30.0mm						
Point	GCP6C	HA	91°03'26"	VA	87°58'54"	SD	106.405	Code	GCP
Std Errors		HA	0°00'03"	VA	0°00'03"	SD	3.000		
Target height	2.000	Prism constant	-30.0mm						
Point	GCP6D	HA	91°03'26"	VA	87°58'53"	SD	106.408	Code	GCP
Std Errors		HA	0°00'03"	VA	0°00'03"	SD	3.000		
Target height	2.000	Prism constant	-30.0mm						
Point	GCP7	HA	285°15'42"	VA	91°26'35"	SD	67.228	Code	GCP
Std Errors		HA	0°00'03"	VA	0°00'03"	SD	3.000		
Target height	2.000	Prism constant	-30.0mm						
Point	GCP10	HA	304°01'41"	VA	86°10'31"	SD	210.243	Code	GCP

Std Errors		HA	0°00'03"	VA	0°00'03"	SD	3.000		
Target height	2.000	Prism constant	-30.0mm						
Point	MH 45J	HA	118°49'15"	VA	89°22'51"	SD	30.894	Code	SS
Std Errors		HA	0°00'03"	VA	0°00'03"	SD	3.000		
Target height	2.000	Prism constant	-30.0mm						

Instrument

Instrument type	Unknown
EDM Refractive Index	275.0
EDM Carrier Wavelength	79.5
Horizontal Circle Mode	Set to azimuth
Horizontal Angle Precision	0°00'03"
Vertical Angle Precision	0°00'03"
EDM precision	3000mm +2ppm

Atmosphere

Pressure	1013.00mbar	Temperature	20.0°C	ppm	0.3				
-----------------	-------------	--------------------	--------	------------	-----	--	--	--	--

Curvature correction	Yes	Refraction correction	Yes	Refraction const.	0.142				
-----------------------------	-----	------------------------------	-----	--------------------------	-------	--	--	--	--

Station setup

Station	46J8	Instrument height	1.698	Station type	Station setup	Scale factor	1.00000000	Std Error	?
----------------	------	--------------------------	-------	---------------------	---------------	---------------------	------------	------------------	---

Orientation

Station	46J8	Backsight point	TR124	Orientation correction	0°00'00"	Orient. Std Err	?		
Point (B.S.)	TR124	HA	130°27'44"	VA	85°40'30"	SD	?	Code	TRG
Std Errors		HA	0°00'03"	VA	0°00'03"	SD	?		
Target height	?	Prism constant	-30.0mm						
Point	TR544	HA	125°06'15"	VA	84°26'10"	SD	?	Code	TRG
Std Errors		HA	0°00'03"	VA	0°00'03"	SD	?		
Target height	?	Prism constant	-30.0mm						
Deltas	TR544	Azimuth	?	H.Dist	?	V.Dist	?		
Point	GCP5	HA	108°15'20"	VA	91°11'57"	SD	68.439	Code	GCP
Std Errors		HA	0°00'03"	VA	0°00'03"	SD	3.000		

Target height	2.000	Prism constant	-30.0mm						
Point	GCP4	HA	74°22'22"	VA	87°50'40"	SD	90.154	Code	GCP
Std Errors		HA	0°00'03"	VA	0°00'03"	SD	3.000		
Target height	2.000	Prism constant	-30.0mm						
Point	GCP6 FINAL	HA	319°13'54"	VA	84°25'45"	SD	86.146	Code	GCP
Std Errors		HA	0°00'03"	VA	0°00'03"	SD	3.000		
Target height	2.000	Prism constant	-30.0mm						
Point	MH HALF 46J8	HA	289°31'18"	VA	87°31'05"	SD	76.269	Code	SS
Std Errors		HA	0°00'03"	VA	0°00'03"	SD	3.000		
Target height	2.000	Prism constant	-30.0mm						
Point	MH 46J8	HA	226°17'45"	VA	85°02'23"	SD	4.068	Code	SS
Std Errors		HA	0°00'03"	VA	0°00'03"	SD	3.000		

Target height	2.000	Prism constant	-30.0mm						
----------------------	-------	-----------------------	---------	--	--	--	--	--	--

Instrument

Instrument type	Unknown								
EDM Refractive Index	275.0								
EDM Carrier Wavelength	79.5								
Horizontal Circle Mode	Set to azimuth								
Horizontal Angle Precision	0°00'03"								

Vertical Angle Precision 0°00'03"

EDM precision 3000mm +2ppm

Atmosphere

Pressure	1013.00mb	Temperature	20.0°C	ppm	0.3				
Curvature correction	Yes	Refraction correction	Yes	Refraction const.	0.142				

Station setup

Station	51K8	Instrument height	1.735	Station type	Station setup	Scale factor	1.0000000	Std Error	?
----------------	------	--------------------------	-------	---------------------	---------------	---------------------	-----------	------------------	---

Orientation

Station	51K8	Backsight point	TR124	Orientation correction	0°00'00"	Orientation. Std Err	?		
Point (B.S.)	TR124	HA	123°10'33"	VA	85°55'02"	SD	?	Cod e	TR G
Std Errors		HA	0°00'03"	VA	0°00'03"	SD	?		
Target height	?	Prism constant	-30.0mm						
Point	TR544	HA	118°55'02"	VA	84°52'51"	SD	?	Cod e	TR G
Std Errors		HA	0°00'03"	VA	0°00'03"	SD	?		
Target height	?	Prism constant	-30.0mm						
Deltas	TR544	Azimuth	?	H.Distance	?	V.Distance	?		
Point	GCP8	HA	53°15'02"	VA	85°40'56"	SD	194.562	Cod e	GC P
Std Errors		HA	0°00'03"	VA	0°00'03"	SD	3.000		
Target height	2.500	Prism constant	-30.0mm						
Point	GCP8C	HA	53°15'05"	VA	85°40'53"	SD	194.559	Cod e	GC P
Std		HA	0°00'03"	VA	0°00'03"	SD	3.000		

Errors									
Target height	2.500	Prism constant	-30.0mm						
Point	MH 51K8	HA	46°37'45"	VA	85°57'22"	SD	44.631	Code	SS
Std Errors		HA	0°00'03"	VA	0°00'03"	SD	3.000		
Target height	2.000	Prism constant	-30.0mm						
Point	STP 51K9 INS	HA	64°52'17"	VA	88°02'16"	SD	16.099	Code	SS
Std Errors		HA	0°00'03"	VA	0°00'03"	SD	3.000		
Target height	2.000	Prism constant	-30.0mm						
Point	GCP21	HA	327°32'38"	VA	86°34'00"	SD	77.012	Code	GCP
Std Errors		HA	0°00'03"	VA	0°00'03"	SD	3.000		
Target height	2.000	Prism constant	-30.0mm						
Point	GCP20	HA	271°37'14"	VA	89°59'40"	SD	85.214	Code	GCP
Std Errors		HA	0°00'03"	VA	0°00'03"	SD	3.000		
Errors	2.000	Prism constant	-30.0mm						

Target height									
Point	GCP17	HA	152°15'54"	VA	93°50'10"	SD	166.351	Cod e	GC P
Std Errors		HA	0°00'03"	VA	0°00'03"	SD	3.000		
Target height	2.540	Prism constant	-30.0mm						
Point	GCP19	HA	213°28'50"	VA	93°02'05"	SD	131.469	Cod e	GC P
Std Errors		HA	0°00'03"	VA	0°00'03"	SD	3.000		
Target height	2.000	Prism constant	-30.0mm						

Instrument

Instrument type	Unknown
EDM Refractive Index	275.0
EDM Carrier Wavelength	79.5
Horizontal Circle Mode	Set to azimuth
Horizontal Angle Precision	0°00'03"
Vertical Angle Precision	0°00'03"

EDM precision	3000mm +2ppm
----------------------	--------------

Atmosphere

Pressure	1013.00mbar	Temperature	20.0°C	ppm	0.3				
Curvature correction	Yes	Refraction correction	Yes	Refraction const.	0.142				

Station setup

Station	52K8	Instrument height	1.665	Station type	Station setup	Scale factor	1.00000000	Std Error	?
----------------	------	--------------------------	-------	---------------------	---------------	---------------------	------------	------------------	---

Orientation

Station	52K8	Backsight point	TR124	Orientation correction	0°00'00"	Orient. Std Err	?		
Point (B.S.)	TR124	HA	122°59'20"	VA	85°40'55"	SD	?	Code	TRG
Std Errors		HA	0°00'03"	VA	0°00'03"	SD	?		
Target height	?	Prism constant	-30.0mm						

Instrument

Instrument type	Unknown
EDM Refractive Index	275.0
EDM Carrier Wavelength	79.5

Horizontal Circle Mode	Set to azimuth
Horizontal Angle Precision	0°00'03"
Vertical Angle Precision	0°00'03"
EDM precision	3000mm +2ppm

Atmosphere

Pressure	1013.00mbar	Temperature	20.0°C	ppm	0.3				
-----------------	-------------	--------------------	--------	------------	-----	--	--	--	--

Curvature Yes Refraction Yes Refraction 0.142 correction const.

Station setup

Station	50K8	Instrument height	1.665	Station type	Station setup	Scale factor	1.00000000	Std Error	?
----------------	------	--------------------------	-------	---------------------	---------------	---------------------	------------	------------------	---

Orientation

Station	50K8	Backsight point	TR544	Orientation correction	0°00'00"	Orient. Std Err	?		
Point (B.S.)	TR544	HA	118°52'53"	VA	84°31'21"	SD	?	Code	TRG
Std Errors		HA	0°00'03"	VA	0°00'03"	SD	?		
Target height	?	Prism constant	-30.0mm						

Point	TR124	HA	123°23'22"	VA	85°30'02"	SD	?	Code	TRG
Std Errors		HA	0°00'03"	VA	0°00'03"	SD	?		
Target height	?	Prism constant	-30.0mm						
Deltas	TR124	Azimuth	?	H.Distance	?	V.Distance	?		
Point	GCP16	HA	192°22'04"	VA	92°52'34"	SD	194.297	Code	GCP
Std Errors		HA	0°00'03"	VA	0°00'03"	SD	3.000		
Target height	2.000	Prism constant	-30.0mm						
Point	MH 50K8	HA	11°05'18"	VA	85°21'11"	SD	9.697	Code	SS
Std Errors		HA	0°00'03"	VA	0°00'03"	SD	3.000		
Target height	2.000	Prism constant	-30.0mm						
Point	GCP15	HA	160°30'51"	VA	93°23'30"	SD	164.596	Code	GCP
Std Errors		HA	0°00'03"	VA	0°00'03"	SD	3.000		
Target height	2.000	Prism constant	-30.0mm						
Point	GCP15C	HA	160°31'04"	VA	93°23'54"	SD	164.598	Code	GCP
Std		HA	0°00'03"	VA	0°00'03"	SD	3.000		

Errors									
Target height	2.000	Prism constant	-30.0mm						
Point	GCP14	HA	116°02'06"	VA	91°26'48"	SD	76.013	Code	GCP
Std Errors		HA	0°00'03"	VA	0°00'03"	SD	3.000		
Target height	2.000	Prism constant	-30.0mm						

Instrument

Instrument type	Unknown
EDM Refractive Index	275.0
EDM Carrier Wavelength	79.5
Horizontal Circle Mode	Set to azimuth
Horizontal Angle Precision	0°00'03"

Vertical Angle Precision 0°00'03"

EDM precision 3000mm +2ppm

Atmosphere

Pressure	1013.00mbar	Temperature	20.0°C	ppm	0.3				
-----------------	-------------	--------------------	--------	------------	-----	--	--	--	--

Curvature correction	Yes	Refraction correction	Yes	Refraction const.	0.142				
-----------------------------	-----	------------------------------	-----	--------------------------	-------	--	--	--	--

Station setup

Station	33K9	Instrument height	1.695	Station type	Station setup	Scale factor	1.00000000	Std Error	?
----------------	------	--------------------------	-------	---------------------	---------------	---------------------	------------	------------------	---

Orientation

Station	33K9	Backsight point	TR116	Orientation correction	0°00'00"	Orient. Std Err	?		
----------------	------	------------------------	-------	-------------------------------	----------	------------------------	---	--	--

Point (B.S.)	TR116	HA	354°46'01"	VA	72°38'51"	SD	?	Code	TRG
Std Errors		HA	0°00'03"	VA	0°00'03"	SD	?		
Target height	?	Prism constant	-30.0mm						

Instrument

Instrument type	Unknown
EDM Refractive Index	275.0
EDM Carrier Wavelength	79.5
Horizontal Circle Mode	Set to azimuth
Horizontal Angle Precision	0°00'03"

Vertical Angle Precision	0°00'03"
EDM precision	3000mm +2ppm

Atmosphere

Pressure	1013.00mbar	Temperature	20.0°C	ppm	0.3				
Curvature correction	Yes	Refraction correction	Yes	Refraction const.	0.142				

Station setup

Station	33K9	Instrument height	1.695	Station type	Station setup	Scale factor	1.00000000	Std Error	?
----------------	------	--------------------------	-------	---------------------	---------------	---------------------	------------	------------------	---

Orientation

Station	33K9	Backsight point	TR116	Orientation correction	0°00'00"	Orient. Std Err	?		
Point (B.S.)	TR116	HA	354°46'01"	VA	67°30'27"	SD	?	Code	TRG
Std Errors		HA	0°00'03"	VA	0°00'03"	SD	?		
Target height	?	Prism constant	-30.0mm						
Point	TR544	HA	121°40'59"	VA	85°26'58"	SD	?	Code	TRG
Std Errors		HA	0°00'03"	VA	0°00'03"	SD	?		
Target height	?	Prism constant	-30.0mm						

Deltas	TR544	Azimuth	?	H.Dist	?	V.Dist	?		
Point	STP 33K9R	HA	72°37'06"	VA	86°35'23"	SD	12.499	Code	TRG
Std Errors		HA	0°00'03"	VA	0°00'03"	SD	3.000		
Target height	2.000	Prism constant	-30.0mm						
Point	STP 33K9L	HA	85°09'19"	VA	87°17'17"	SD	19.048	Code	TRG
Std Errors		HA	0°00'03"	VA	0°00'03"	SD	3.000		
Target height	2.000	Prism constant	-30.0mm						
Point	SWR 33K9	HA	131°17'51"	VA	88°35'53"	SD	17.857	Code	SS
Std Errors		HA	0°00'03"	VA	0°00'03"	SD	3.000		
Target height	2.000	Prism constant	-30.0mm						

**Survey Controller
Reduced Points**

Point	50K8	Y	52249.780	X	3756200.870	Z	28.637	Code	TSM
Point	51K8	Y	52092.620	X	3756290.070	Z	36.189	Code	TSM
Point	52K8	Y	51939.640	X	3756376.750	Z	42.039	Code	TSM
Point	TR124	Y	54807.360	X	3754515.220	Z	275.800	Code	TRG

Point	TR125	Y	54853.460	X	3754583.190	Z	289.000	Code	TRG
Point	TR544	Y	55123.370	X	3754615.780	Z	352.300	Code	TRG
Point	1	Y	52224.444	X	3756034.001	Z	18.652	Code	SS
Point	2	Y	52170.340	X	3756033.740	Z	20.014	Code	SS
Point	3	Y	52278.305	X	3756088.181	Z	20.695	Code	SS
Point	4	Y	52224.124	X	3756087.912	Z	21.241	Code	SS
Point	5	Y	52170.050	X	3756087.553	Z	22.759	Code	SS
Point	6	Y	52115.860	X	3756087.309	Z	24.018	Code	SS
Point	8	Y	52278.008	X	3756142.091	Z	23.439	Code	SS
Point	10	Y	52169.710	X	3756141.521	Z	24.304	Code	SS
Point	11	Y	52115.558	X	3756141.239	Z	25.644	Code	SS
Point	12	Y	52061.398	X	3756140.919	Z	27.238	Code	SS
Point	15	Y	52223.545	X	3756195.707	Z	29.527	Code	SS
Point	16	Y	52115.233	X	3756195.098	Z	29.001	Code	SS
Point	17	Y	52061.127	X	3756194.768	Z	29.339	Code	SS
Point	18	Y	52006.961	X	3756194.489	Z	29.066	Code	SS
Point	19	Y	52006.961	X	3756194.488	Z	29.068	Code	SS
Point	23	Y	52169.103	X	3756249.311	Z	32.978	Code	SS
Point	24	Y	52114.961	X	3756249.015	Z	34.299	Code	SS

Point	25	Y	52060.793	X	3756248.691	Z	32.937	Code	SS
Point	26	Y	52006.670	X	3756248.392	Z	32.355	Code	SS
Point	28	Y	51898.403	X	3756247.826	Z	34.063	Code	SS
Point	33	Y	52114.665	X	3756302.895	Z	37.083	Code	SS
Point	34	Y	52060.547	X	3756302.542	Z	37.005	Code	SS
Point	36	Y	51896.910	X	3756302.011	Z	39.158	Code	SS
Point	44	Y	52060.242	X	3756356.445	Z	40.924	Code	SS
Point	45	Y	52006.099	X	3756356.181	Z	39.581	Code	SS

Point	46	Y	51952.035	X	3756355.894	Z	40.878	Code	SS
Point	47	Y	51897.819	X	3756355.543	Z	43.802	Code	SS
Point	56	Y	52005.822	X	3756410.054	Z	46.999	Code	SS
Point	57	Y	51951.659	X	3756409.753	Z	43.332	Code	SS
Point	58	Y	51897.510	X	3756409.446	Z	46.723	Code	SS
Point	66	Y	52005.533	X	3756463.946	Z	47.244	Code	SS
Point	36K9	Y	52125.170	X	3756762.460	Z	77.830	Code	TSM
Point	93	Y	52274.752	X	3756734.944	Z	93.501	Code	SS
Point	94	Y	52220.655	X	3756734.641	Z	84.996	Code	SS
Point	95	Y	52166.472	X	3756734.325	Z	79.691	Code	SS

Point	96	Y	52112.325	X	3756734.029	Z	74.962	Code	SS
Point	97	Y	52058.182	X	3756733.725	Z	68.954	Code	SS
Point	98	Y	52004.061	X	3756733.446	Z	66.820	Code	SS
Point	100	Y	52166.195	X	3756788.248	Z	90.642	Code	SS
Point	101	Y	52112.022	X	3756787.918	Z	84.589	Code	SS
Point	102	Y	52057.880	X	3756787.623	Z	81.012	Code	SS
Point	104	Y	52057.587	X	3756841.513	Z	94.739	Code	SS
Point	105	Y	52003.435	X	3756841.231	Z	91.278	Code	SS
Point	88	Y	52275.038	X	3756681.033	Z	90.157	Code	SS
Point	89	Y	52221.146	X	3756680.449	Z	84.389	Code	SS
Point	90	Y	52166.785	X	3756680.397	Z	77.611	Code	SS
Point	91	Y	52112.638	X	3756680.143	Z	70.210	Code	SS
Point	92	Y	52058.489	X	3756679.843	Z	64.275	Code	SS
Point	46J8	Y	52655.070	X	3756350.990	Z	50.750	Code	TSM
Point	38	Y	52709.964	X	3756360.095	Z	52.205	Code	SS
Point	50	Y	52601.334	X	3756413.396	Z	58.574	Code	SS
Point	59	Y	52601.048	X	3756467.248	Z	65.938	Code	SS
Point	51	Y	52547.209	X	3756413.057	Z	56.490	Code	SS
Point	52	Y	52493.062	X	3756412.765	Z	55.298	Code	SS

Point	45J8	Y	52492.830	X	3756417.850	Z	55.320	Code	TSM
Point	60	Y	52546.915	X	3756466.982	Z	65.967	Code	SS
Point	61	Y	52492.790	X	3756466.700	Z	61.217	Code	SS
Point	62	Y	52438.642	X	3756466.343	Z	56.848	Code	SS
Point	63	Y	52385.714	X	3756467.359	Z	56.074	Code	SS
Point	67	Y	52492.486	X	3756520.547	Z	70.049	Code	SS
Point	68	Y	52438.354	X	3756520.288	Z	66.562	Code	SS
Point	69	Y	52384.240	X	3756519.970	Z	66.078	Code	SS
Point	70	Y	52330.092	X	3756519.687	Z	65.397	Code	SS
Point	71	Y	52275.187	X	3756520.928	Z	66.066	Code	SS
Point	33K9	Y	52052.400	X	3756511.480	Z	53.240	Code	TSM
Point	53K8	Y	52111.260	X	3756489.060	Z	54.460	Code	TSM
Point	73	Y	52167.642	X	3756518.760	Z	61.129	Code	SS
Point	74	Y	52113.494	X	3756518.475	Z	58.636	Code	SS
Point	75	Y	52059.342	X	3756518.177	Z	53.507	Code	SS
Point	81	Y	52113.196	X	3756572.362	Z	64.676	Code	SS
Point	80	Y	52167.349	X	3756572.659	Z	69.288	Code	SS
Point	78	Y	52275.627	X	3756573.252	Z	75.037	Code	SS

Point	65	Y	52057.991	X	3756466.033	Z	50.066	Code	SS
Point	85	Y	52167.079	X	3756626.534	Z	75.658	Code	SS
Point	TT1	Y	52236.407	X	3756413.537	Z	50.536	Code	CTRL
Point	TT1C	Y	52236.404	X	3756413.549	Z	50.521	Code	CTRL
Point	TTT1	Y	52236.406	X	3756413.430	Z	50.528	Code	CP
Point	40	Y	52330.923	X	3756357.792	Z	43.990	Code	SS
Point	41	Y	52276.816	X	3756357.642	Z	44.861	Code	SS
Point	42	Y	52222.622	X	3756357.266	Z	45.626	Code	SS
Point	54	Y	52276.496	X	3756411.433	Z	49.114	Code	SS
Point	29	Y	52327.444	X	3756303.744	Z	39.574	Code	SS
Point	30	Y	52277.073	X	3756303.634	Z	39.741	Code	SS
Point	43	Y	52168.495	X	3756356.970	Z	43.738	Code	SS
Point	31	Y	52222.907	X	3756303.379	Z	39.261	Code	SS
Point	31a	Y	52222.908	X	3756303.378	Z	38.763	Code	SS
Point	32	Y	52168.757	X	3756303.085	Z	39.877	Code	SS
Point	53	Y	52327.628	X	3756406.198	Z	48.740	Code	SS
Point	34K9	Y	52059.620	X	3756622.320	Z	60.790	Code	TSM
Point	35K9	Y	52048.510	X	3756717.250	Z	66.560	Code	TSM
Point	103	Y	52003.746	X	3756787.342	Z	79.535	Code	SS
Point	86	Y	52112.900	X	3756626.238	Z	69.213	Code	SS

Point	87	Y	52058.772	X	3756625.964	Z	60.964	Code	SS
Point	99	Y	52220.284	X	3756788.499	Z	91.392	Code	SS
Point	2J9	Y	52530.410	X	3756594.930	Z	81.711	Code	TSM
Point	13K9	Y	52306.180	X	3756702.700	Z	93.814	Code	TSM
Point	14K9	Y	52376.180	X	3756643.250	Z	89.214	Code	TSM
Point	TT2	Y	52259.524	X	3756558.651	Z	72.851	Code	CTRL
Point	TT3	Y	52259.524	X	3756558.649	Z	72.851	Code	CTRL
Point	76	Y	52383.892	X	3756573.875	Z	74.736	Code	SS
Point	TT2C	Y	52259.523	X	3756558.593	Z	72.859	Code	CTRL
Point	TT2D	Y	52259.521	X	3756558.608	Z	72.868	Code	CTRL
Point	TTT2	Y	52259.524	X	3756558.622	Z	72.855	Code	CP
Point	77	Y	52329.746	X	3756573.563	Z	74.151	Code	SS
Point	83	Y	52275.313	X	3756627.168	Z	83.887	Code	SS
Point	84	Y	52221.135	X	3756626.835	Z	80.266	Code	SS
Point	79	Y	52221.478	X	3756572.963	Z	72.416	Code	SS
Point	72	Y	52221.773	X	3756519.772	Z	65.250	Code	SS
Point	82	Y	52329.459	X	3756627.452	Z	86.194	Code	SS
Point	7	Y	52332.150	X	3756142.384	Z	25.013	Code	SS
Point	9	Y	52223.818	X	3756141.807	Z	24.251	Code	SS
Point	35	Y	52006.376	X	3756302.298	Z	36.699	Code	SS

Point	105 CHECK	Y	52003.451	X	3756841.227	Z	91.290	Code	TRG
Point	105 CHECK2	Y	52003.455	X	3756841.228	Z	91.289	Code	TRG
Point	TR116	Y	51849.200	X	3758730.110	Z	985.900	Code	TRG
Point	CG1	Y	52043.710	X	3756553.252	Z	55.796	Code	SS
Point	CG1 C	Y	52043.712	X	3756553.249	Z	55.806	Code	SS
Point	CG1 D	Y	52043.705	X	3756553.250	Z	55.786	Code	TRG
Point	CG1 E	Y	52043.703	X	3756553.242	Z	55.780	Code	SS

Point	MH1	Y	51831.048	X	3756392.361	Z	48.167	Code	SS
Point	MH1 C	Y	51831.048	X	3756392.360	Z	48.177	Code	SS
Point	MH1 D	Y	51831.049	X	3756392.357	Z	48.170	Code	SS
Point	GCP1	Y	52013.282	X	3756862.627	Z	96.326	Code	GCP
Point	GCP11	Y	52094.958	X	3756741.983	Z	73.431	Code	GCP
Point	GCP2	Y	52252.629	X	3756658.241	Z	87.289	Code	GCP
Point	GCP12	Y	52016.600	X	3756643.067	Z	61.118	Code	GCP
Point	GCP9	Y	52076.625	X	3756510.985	Z	54.058	Code	GCP
Point	GCP23	Y	51899.042	X	3756425.425	Z	49.238	Code	GCP
Point	GCP13	Y	52220.116	X	3756772.645	Z	88.068	Code	GCP13

Point	GCP13C	Y	52220.112	X	3756772.648	Z	88.069	Code	GCP13
Point	GCP3	Y	52456.827	X	3756514.266	Z	66.225	Code	GCP
Point	GCP6	Y	52599.135	X	3756415.832	Z	58.798	Code	GCP
Point	GCP6C	Y	52599.123	X	3756415.889	Z	58.792	Code	GCP
Point	GCP6D	Y	52599.126	X	3756415.888	Z	58.793	Code	GCP
Point	GCP7	Y	52428.021	X	3756435.533	Z	53.353	Code	GCP
Point	GCP10	Y	52318.996	X	3756535.226	Z	69.070	Code	GCP
Point	MH 45J	Y	52519.870	X	3756402.972	Z	55.379	Code	SS
Point	GCP5	Y	52720.023	X	3756329.564	Z	49.017	Code	GCP
Point	GCP4	Y	52741.803	X	3756375.251	Z	53.838	Code	GCP
Point	GCP6 FINAL	Y	52599.100	X	3756415.904	Z	58.808	Code	GCP
Point	MH HALF 46J8	Y	52583.279	X	3756376.443	Z	53.750	Code	SS
Point	MH 46J8	Y	52652.161	X	3756348.210	Z	50.797	Code	SS
Point	GCP8	Y	52248.052	X	3756406.135	Z	50.073	Code	GCP
Point	GCP8C	Y	52248.051	X	3756406.130	Z	50.075	Code	GCP
Point	MH 51K8	Y	52124.962	X	3756320.623	Z	39.069	Code	SS
Point	STP 51K9	Y	52107.160	X	3756296.890	Z	36.474	Code	SS

	INS								
Point	GCP21	Y	52051.380	X	3756354.913	Z	40.534	Code	GCP
Point	GCP20	Y	52007.468	X	3756292.479	Z	35.933	Code	GCP
Point	GCP17	Y	52169.852	X	3756143.183	Z	24.258	Code	GCP
Point	GCP19	Y	52020.211	X	3756180.591	Z	28.967	Code	GCP
Point	GCP16	Y	52208.222	X	3756011.344	Z	18.557	Code	GCP
Point	MH 50K8	Y	52251.633	X	3756210.326	Z	29.085	Code	SS
Point	GCP15	Y	52304.580	X	3756045.996	Z	18.568	Code	GCP
Point	GCP15C	Y	52304.571	X	3756045.993	Z	18.549	Code	GCP
Point	GCP14	Y	52318.033	X	3756167.529	Z	26.384	Code	GCP
Point	STP 33K9R	Y	52064.279	X	3756515.199	Z	53.677	Code	TRG
Point	STP 33K9L	Y	52071.330	X	3756513.084	Z	53.835	Code	TRG
Point	SWR 33K9	Y	52065.789	X	3756499.718	Z	53.371	Code	SS

Quality Report



Generated with Pix4Dmapper version 4.6.4

! **Important:** Click on the different icons for:

- ?** Help to analyze the results in the Quality Report
- i** Additional information about the sections

💡 Click [here](#) for additional tips to analyze the Quality Report

Summary

Project	Biff_100m
Processed	2021-07-09 15:04:35
Camera Model Name(s)	FC6310_8.8_4864x3648 (RGB)
Average Ground Sampling Distance (GSD)	2.91 cm / 1.14 in
Area Covered	0.531 km ² / 53.1160 ha / 0.21 sq. mi. / 131.3205 acres

Quality Check

? Images	median of 56184 key points per image	✓
? Dataset	385 out of 385 images calibrated (100%), all images enabled	✓
? Camera Optimization	0.81% relative difference between initial and optimized internal camera parameters	✓
? Matching	median of 30701.2 matches per calibrated image	✓
? Georeferencing	yes, 18 GCPs (18 3D), mean RMS error = 0.005 m	✓

? **Preview**

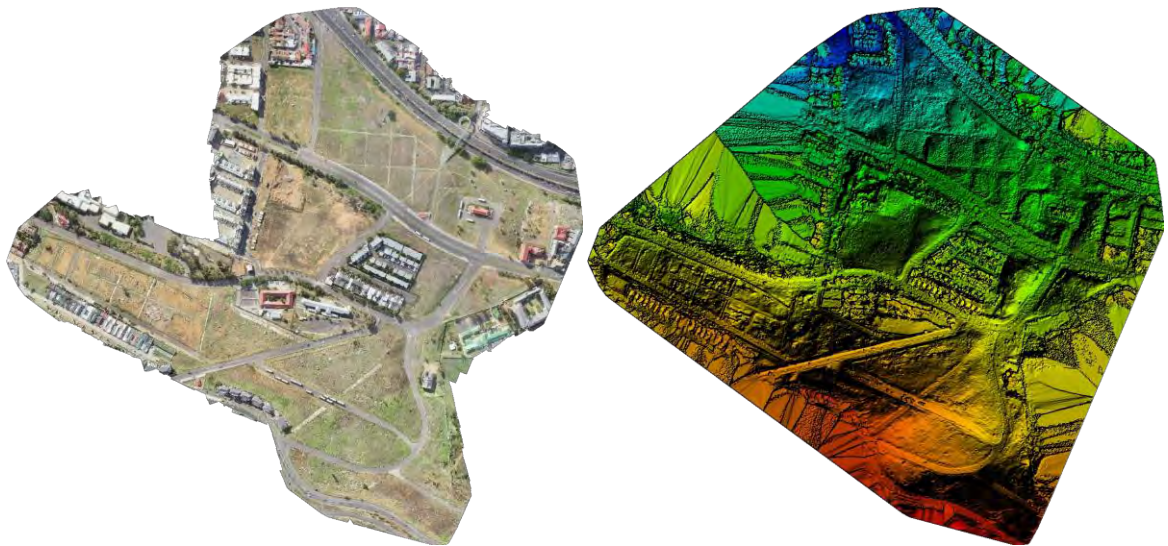


Figure 1: Orthomosaic and the corresponding sparse Digital Surface Model (DSM) before densification.

Calibration Details

Number of Calibrated Images	385 out of 385
Number of Geolocated Images	385 out of 385

🔍 Initial Image Positions

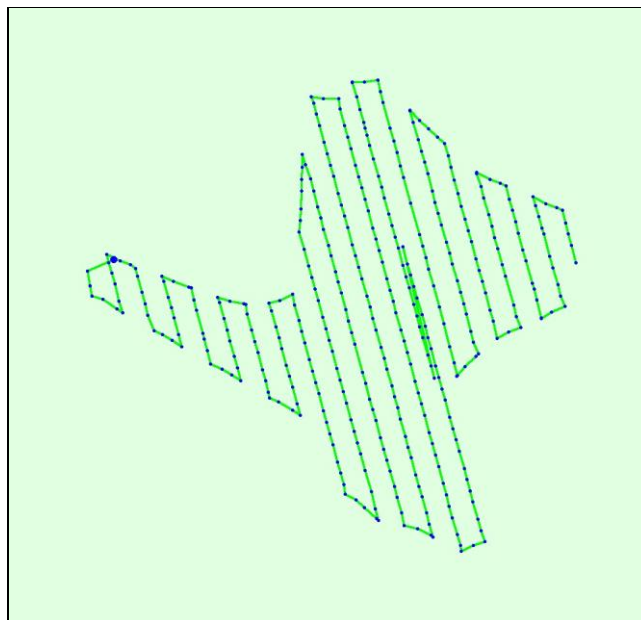
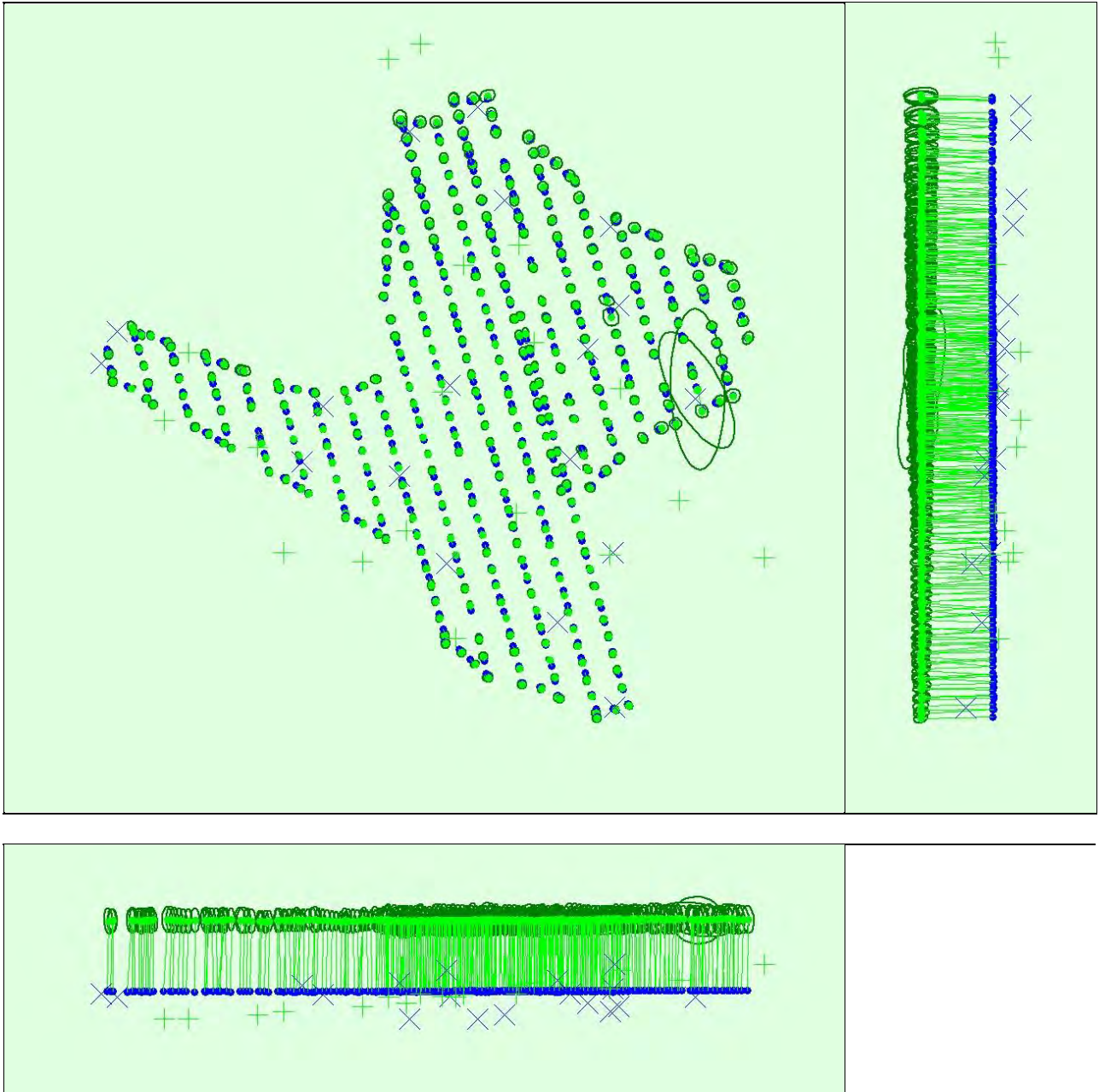


Figure 2: Top view of the initial image position. The green line follows the position of the images in time, starting from the large blue dot.

Computed Image/GCPs/Manual Tie Points Positions



Uncertainty ellipses 500x magnified

Figure 3: Offset between initial (blue dots) and computed (green dots) image positions as well as the offset between the GCP's initial positions (blue crosses) and their computed positions (green crosses) in the top-view (XY plane), front-view (XZ plane), and side-view (YZ plane). Dark green ellipses indicate the absolute position uncertainty of the bundle block adjustment result.

Absolute camera position and orientation uncertainties

X [m]	Y [m]	Z [m]	Omega [degree]	Phi [degree]	Kappa [degree]
-------	-------	-------	----------------	--------------	----------------

Mean	0.012	0.014	0.034	0.007	0.006	0.002
Sigma	0.007	0.014	0.007	0.007	0.004	0.001

🔍 Overlap

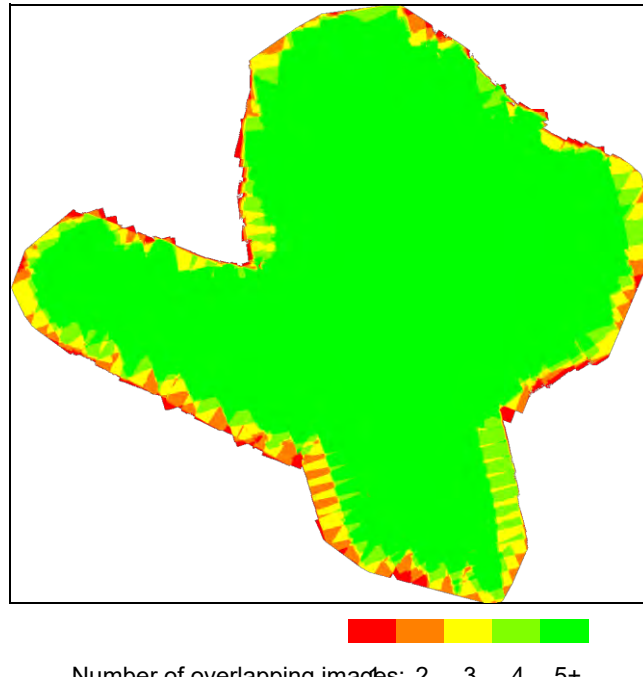


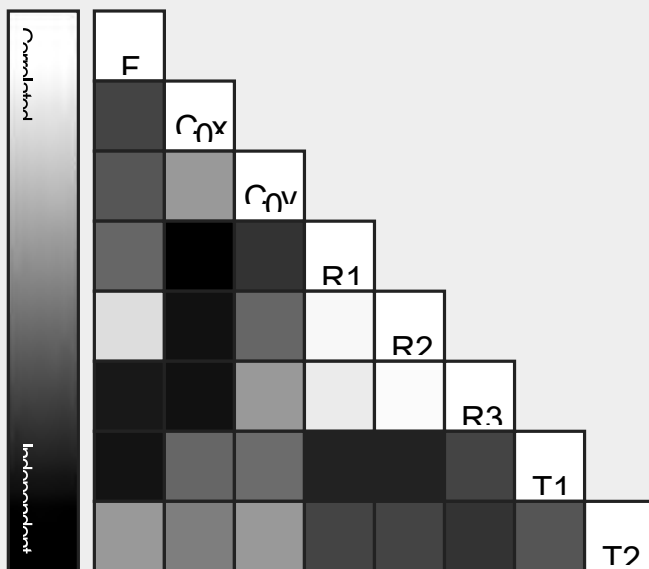
Figure 4: Number of overlapping images computed for each pixel of the orthomosaic. Red and yellow areas indicate low overlap, for which poor results may be generated. Green areas indicate an overlap of over 5 images for every pixel. Good quality results will be generated as long as the number of keypoint matches is also sufficient for these areas (see Figure 5 for keypoint matches).

Bundle Block Adjustment Details

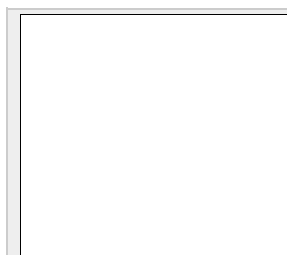
Number of 2D Keypoint Observations for Bundle Block Adjustment	11720038
Number of 3D Points for Bundle Block Adjustment	3772215
Mean Reprojection Error [pixels]	0.150

Internal Camera Parameters FC6310_8.8_4864x3648 (RGB).
Sensor Dimensions: 11.407 [mm] x 8.556 [mm]
 EXIF ID: FC6310_8.8_4864x3648

	Focal Length	Principal Point x	Principal Point y	R1	R2	R3	T1	T2
Initial Values	3666.955 [pixel] 8.600 [mm]	2432.001 [pixel] 5.704 [mm]	1823.999 [pixel] 4.278 [mm]	0.004	- 0.017	0.019	- 0.000	0.000
Optimized Values	3696.881 [pixel] 8.670 [mm]	2427.465 [pixel] 5.693 [mm]	1849.787 [pixel] 4.338 [mm]	0.005	- 0.019	0.020	0.001	0.000
Uncertainties (Sigma)	1.179 [pixel] 0.003 [mm]	0.098 [pixel] 0.000 [mm]	0.097 [pixel] 0.000 [mm]	0.000	0.000	0.000	0.000	0.000



The correlation between camera internal parameters determined by the bundle adjustment. White indicates a full correlation between the parameters, i.e., any change in one can be fully compensated by the other. Black indicates that the parameter is completely independent and is not affected by other parameters.



The number of Automatic Tie Points (ATPs) per pixel, averaged over all images of the is colour coded between black and white. White indicates that, on average, more than 16 have been extracted at the pixel location. Black indicates that, on average, 0 ATPs have been the pixel location. Click on the image to see the average direction and magnitude projection error for each pixel. Note that the vectors are scaled for better visualization. The indicates the magnitude of 1 pixel.

2D Keypoints Table

	Number of 2D Keypoints per Image	Number of Matched 2D Keypoints per Image
Median	56184	30701
Min	25508	51
Max	85671	52506
Mean	56291	30442

🔍 3D Points from 2D Keypoint Matches

	Number of 3D Points Observed
In 2 Images	2305756
In 3 Images	666546
In 4 Images	286219
In 5 Images	155532
In 6 Images	97983
In 7 Images	65832
In 8 Images	47276
In 9 Images	35036
In 10 Images	26838
In 11 Images	20162
In 12 Images	15912
In 13 Images	12275
In 14 Images	9413

In 15 Images	7488
In 16 Images	5679
In 17 Images	4270
In 18 Images	3282
In 19 Images	2555
In 20 Images	1689
In 21 Images	1167
In 22 Images	626
In 23 Images	338
In 24 Images	191
In 25 Images	90
In 26 Images	48
In 27 Images	11
In 28 Images	1

2D Keypoint Matches

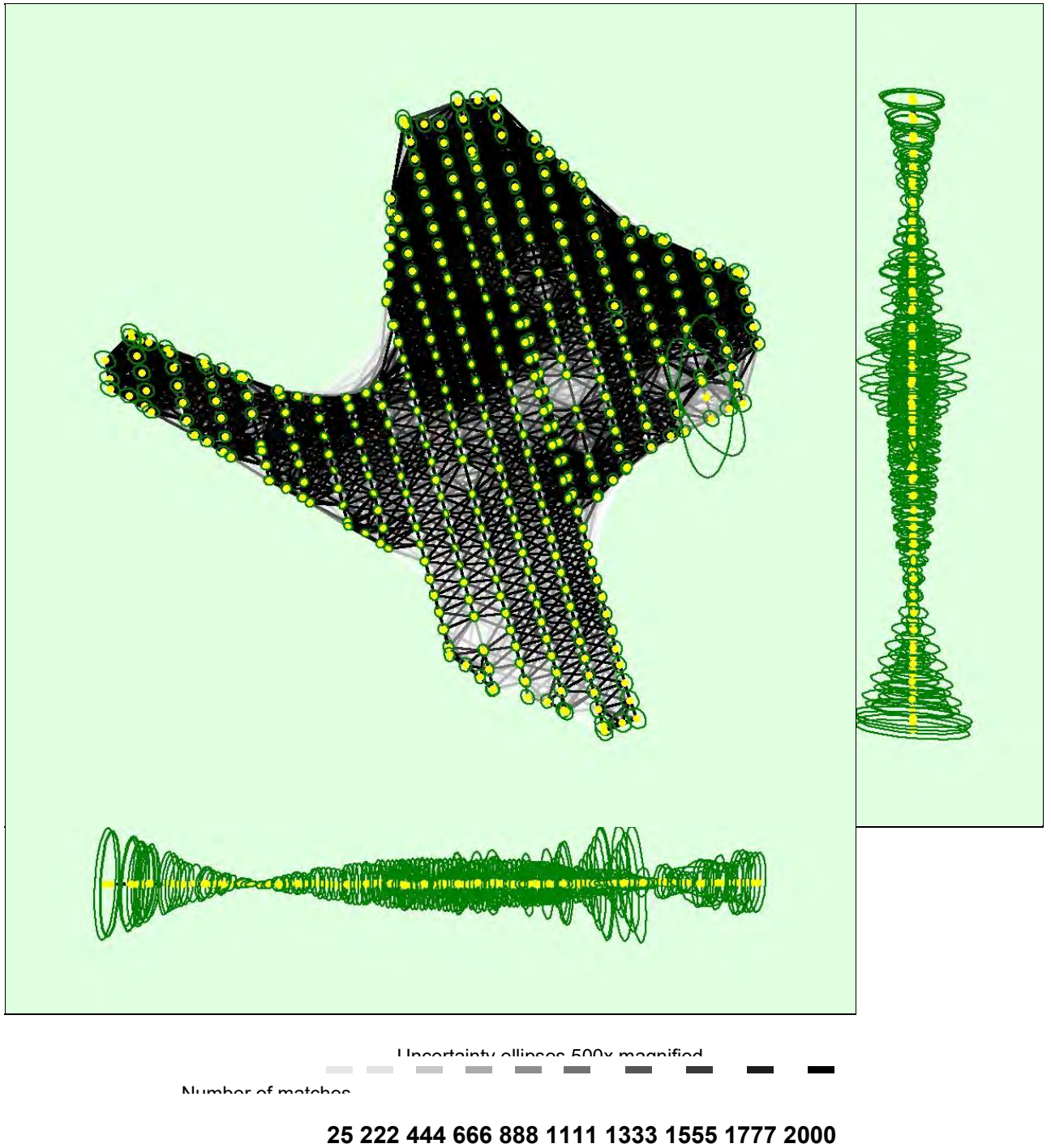


Figure 5: Computed image positions with links between matched images. The darkness of the links indicates the number of matched 2D keypoints between the images. Bright links indicate weak links and require manual tie points or more images. Dark green ellipses indicate the relative camera position uncertainty of the bundle block adjustment result.

Relative camera position and orientation uncertainties

	X [m]	Y [m]	Z [m]	Omega [degree]	Phi [degree]	Kappa [degree]
Mean	0.015	0.017	0.048	0.020	0.019	0.003
Sigma	0.007	0.014	0.029	0.013	0.010	0.001

Geolocation Details

? Ground Control Points

GCP Name	Accuracy XY/Z [m]	Error X [m]	Error Y [m]	Error Z [m]	Projection Error [pixel]	Verified/Marked
GCP1 (3D)	0.020/ 0.020	0.002	-0.001	-0.004	0.384	6 / 6
GCP2 (3D)	0.020/ 0.020	-0.005	0.007	-0.001	0.125	6 / 6
GCP3 (3D)	0.020/ 0.020	0.006	0.009	0.000	0.127	14 / 14
GCP4 (3D)	0.020/ 0.020	-0.001	-0.003	-0.002	0.037	8 / 8
GCP5 (3D)	0.020/ 0.020	-0.001	0.002	0.000	0.038	9 / 9
GCP7 (3D)	0.020/ 0.020	0.006	-0.003	0.010	0.101	13 / 13
GCP8 (3D)	0.020/ 0.020	0.002	-0.006	0.009	0.108	12 / 12
GCP9 (3D)	0.020/ 0.020	-0.005	0.007	-0.000	0.060	23 / 23
GCP10 (3D)	0.020/ 0.020	0.007	0.001	-0.004	0.036	11 / 11

GCP11 (3D)	0.020/ 0.020	-0.004	0.002	0.004	0.028	6 / 6
GCP12 (3D)	0.020/ 0.020	-0.007	0.002	-0.001	0.056	4 / 4
GCP15 (3D)	0.020/ 0.020	-0.005	-0.006	0.002	0.184	15 / 15
GCP16 (3D)	0.020/ 0.020	0.002	0.006	0.007	0.062	10 / 10
GCP17 (3D)	0.020/ 0.020	0.002	0.001	-0.012	0.113	21 / 21
GCP19 (3D)	0.020/ 0.020	-0.002	-0.003	0.017	0.040	18 / 18
GCP20 (3D)	0.020/ 0.020	0.006	-0.009	-0.006	0.089	18 / 18
GCP21 (3D)	0.020/ 0.020	0.004	0.001	-0.016	0.097	13 / 13
GCP23 (3D)	0.020/ 0.020	-0.009	-0.003	0.006	0.064	12 / 12
Mean [m]		- 0.000039	0.000103	0.000591		
Sigma [m]		0.004852	0.004852	0.007569		
RMS Error [m]		0.004852	0.004853	0.007592		

Localisation accuracy per GCP and mean errors in the three coordinate directions. The last column counts the number of calibrated images where the GCP has been automatically verified vs manually marked.

🔍 Absolute Geolocation Variance

Min Error [m]	Max Error [m]	Geolocation Error X [%]	Geolocation Error Y [%]	Geolocation Error Z [%]
-	-15.00	0.00	0.26	0.00
-15.00	-12.00	0.00	0.00	0.00
-12.00	-9.00	0.00	3.38	0.00
-9.00	-6.00	1.04	11.95	0.00
-6.00	-3.00	4.68	13.51	0.00
-3.00	0.00	37.14	18.96	53.25
0.00	3.00	56.36	22.34	46.75
3.00	6.00	0.52	12.47	0.00
6.00	9.00	0.26	11.69	0.00
9.00	12.00	0.00	5.45	0.00
12.00	15.00	0.00	0.00	0.00
15.00	-	0.00	0.00	0.00
Mean [m]		0.025326	0.463727	-99.925102
Sigma [m]		5.532518	1.903074	1.159643
RMS Error [m]		5.532576	1.958758	99.931831

Min Error and Max Error represent geolocation error intervals between -1.5 and 1.5 times the maximum accuracy of all the images. Columns X, Y, and Z show the percentage of images with geolocation errors within the predefined error intervals. The geolocation error is the difference between the initial and computed image positions.

Note that the image geolocation errors do not correspond to the accuracy of the observed 3D points.

Geolocation Bias	X	Y	Z
Translation [m]	-0.463722	-0.025306	-99.925106

Bias between image initial and computed geolocation given in output coordinate system.

? Relative Geolocation Variance

Relative Geolocation Error	Images X [%]	Images Y [%]	Images Z [%]
[-1.00, 1.00]	96.62	58.70	100.00
[-2.00, 2.00]	100.00	96.62	100.00
[-3.00, 3.00]	100.00	99.74	100.00
Mean of Geolocation Accuracy [m]	5.000000	5.000000	10.000000
Sigma of Geolocation Accuracy [m]	0.000000	0.000000	0.000000

Images X, Y, and Z, represent the percentage of images with a relative geolocation error in X, Y, and Z.

Geolocation Orientational Variance	RMS [degree]
Omega	1.255
Phi	0.642
Kappa	7.537

Geolocation RMS error of the orientation angles given by the difference between the initial and computed image orientation angles.

Initial Processing Details

System Information

Hardware	CPU: Intel(R) Ie(Ii7-8565U CPU @ 1.80GHz RAM: 16GB GPU: Inl(R) UHD Graphics 620 (Driver: 26.20.100.8141)
Operating System	Windows 10 Home Single Language, 64-bit

Coordinate Systems

Image Coordinate System	WGS 84 (EGM 96 Geoid)
Ground Control Point (GCP) Coordinate System	Hartebeesthoek94 / Lo19 (EGM 96 Geoid)
Output Coordinate System	Hartebeesthoek94 / Lo19 (EGM 96 Geoid)

Processing Options

Detected Template	No Template Available
Keypoints Image Scale	Full, Image Scale: 1
Advanced: Matching Image Pairs	Aerial Grid or Corridor
Advanced: Matching Strategy	Use Geometrically Verified Matching: no
Advanced: Keypoint Extraction	Targeted Number of Keypoints: Automatic
Advanced: Calibration	Calibration Method: Standard Internal Parameters Optimization: All External Parameters Optimization: All Rematch: Auto, yes

Point Cloud Densification details

Processing Options

Image Scale	multis $\frac{1}{2}$ e, 1/2 (Half image size, Default)
-------------	--

Point Density	Optimal
Minimum Number of Matches	3
3D Textured Mesh Generation	yes
3D Textured Mesh Settings:	Resolution: Medium Resolution (default) Colour Balancing: no
LOD	Generated: no
Advanced: 3D Textured Mesh Settings	Sample Density Divider: 1
Advanced: Image Groups	group1
Advanced: Use Processing Area	yes
Advanced: Use Annotations	yes
Time for Point Cloud Densification	01h:26m:32s
Time for Point Cloud Classification	NA
Time for 3D Textured Mesh Generation	33m:48s

Results

Number of Processed Clusters	3
Number of Generated Tiles	4
Number of 3D Densified Points	47513891
Average Density (per m ³)	103.47

DSM. Orthomosaic and Index Details

Processing Options

DSM and Orthomosaic Resolution	1 x GSD (2.91 [cm/pixel])
DSM Filters	Noise Filtering: yes Surface Smoothing: yes, Type: Sharp
Raster DSM	Generated: yes Method: Inverse Distance Weighting Merge Tiles: yes
Orthomosaic	Generated: yes Merge Tiles: yes GeoTIFF Without Transparency: no Google Maps Tiles and KML: no
Grid DSM	Generated: yes, Spacing [cm]: 500
Time for DSM Generation	01h:31m:32s
Time for Orthomosaic Generation	01h:58m:53s
Time for DTM Generation	00s
Time for Contour Lines Generation	00s
Time for Reflectance Map Generation	00s

Time for Index Map Generation	00s
----------------------------------	-----



Quality Report

Generated with Pix4Dmapper version 4.6.4

! **Important:** Click on the different icons for:

- ?** Help to analyze the results in the Quality Report
- i** Additional information about the sections

💡 Click [here](#) for additional tips to analyze the Quality Report

Summary

Project	Biff_120m
Processed	2021-07-12 09:11:00
Camera Model Name(s)	FC6310_8.8_4864x3648 (RGB)
Average Ground Sampling Distance (GSD)	3.43 cm / 1.35 in
Area Covered	0.583 km ² / 58.3159 ha / 0.23 sq. mi. / 144.1763 acres

Quality Check

? Images	median of 62711 key points per image	✔
? Dataset	290 out of 290 images calibrated (100%), all images enabled	✔
? Camera Optimization	0.09% relative difference between initial and optimized internal camera parameters	✔
? Matching	median of 34682 matches per calibrated image	✔
? Georeferencing	yes, 18 GCPs (18 3D), mean RMS error = 0.006 m	✔

? **Preview**

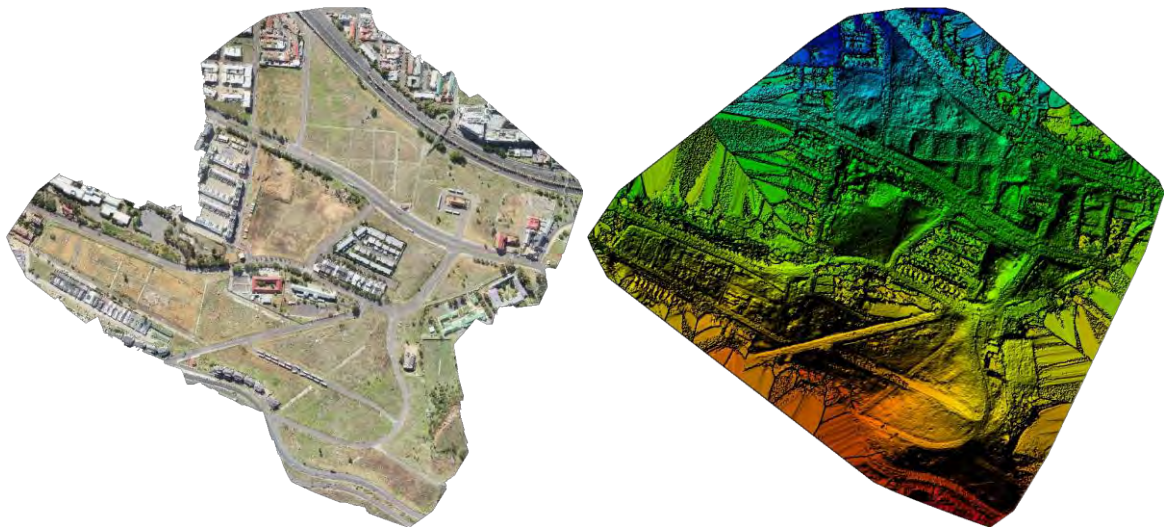


Figure 1: Orthomosaic and the corresponding sparse Digital Surface Model (DSM) before densification.

Calibration Details

Number of Calibrated Images	290 out of 290
Number of Geolocated Images	290 out of 290

? **Initial Image Positions**

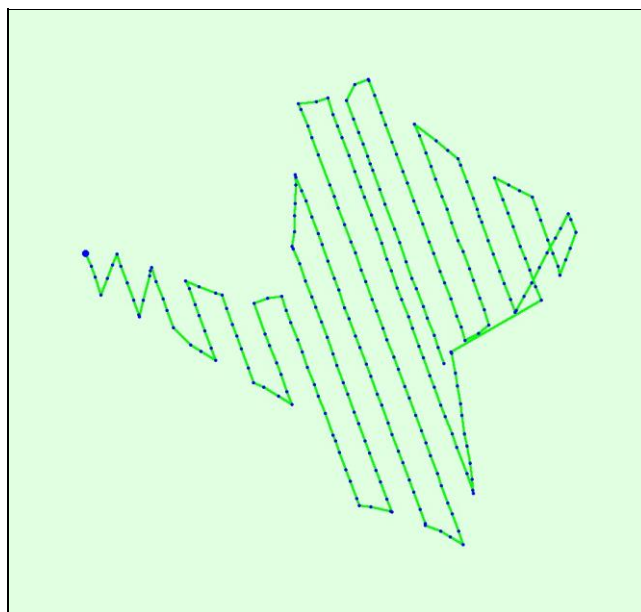
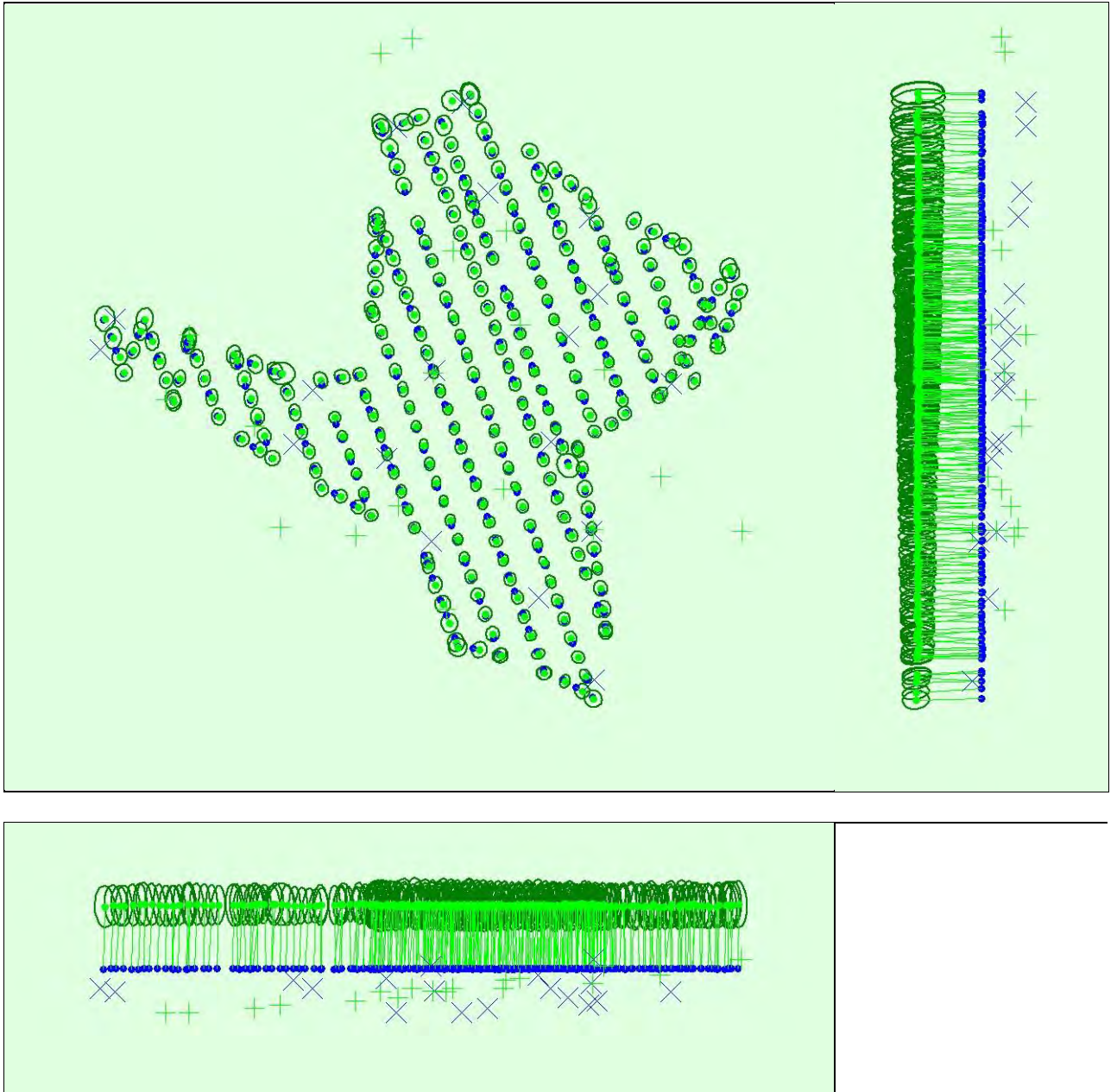


Figure 2: Top view of the initial image position. The green line follows the position of the images in time, starting from the large blue dot.

Computed Image/GCPs/Manual Tie Points Positions



Uncertainty ellipses 1000x magnified

Figure 3: Offset between initial (blue dots) and computed (green dots) image positions as well as the offset between the GCP's initial positions (blue crosses) and their computed positions (green crosses) in the top-view (XY plane), front-view (XZ plane), and side-view (YZ plane). Dark green ellipses indicate the absolute position uncertainty of the bundle block adjustment result.

Absolute camera position and orientation uncertainties

	X [m]	Y [m]	Z [m]	Omega [degree]	Phi [degree]	Kappa [degree]
--	-------	-------	-------	----------------	--------------	----------------

Mean	0.010	0.011	0.030	0.005	0.004	0.001
Sigma	0.002	0.002	0.005	0.001	0.001	0.000

🔍 Overlap

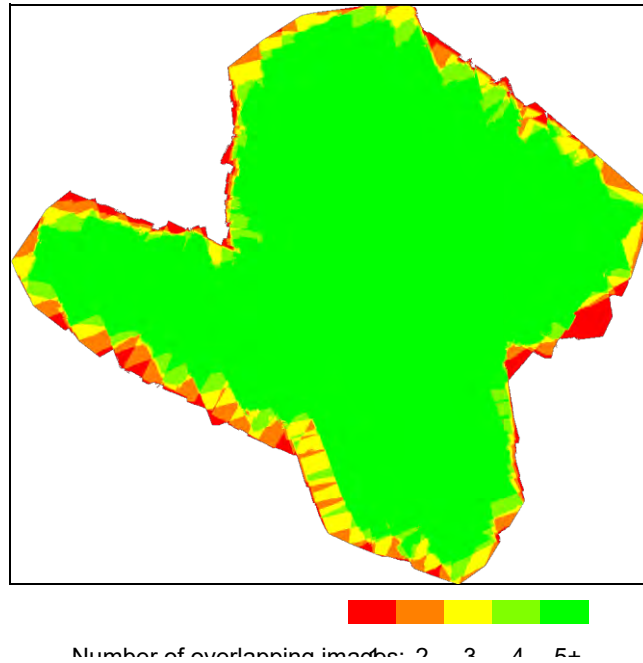


Figure 4: Number of overlapping images computed for each pixel of the orthomosaic.

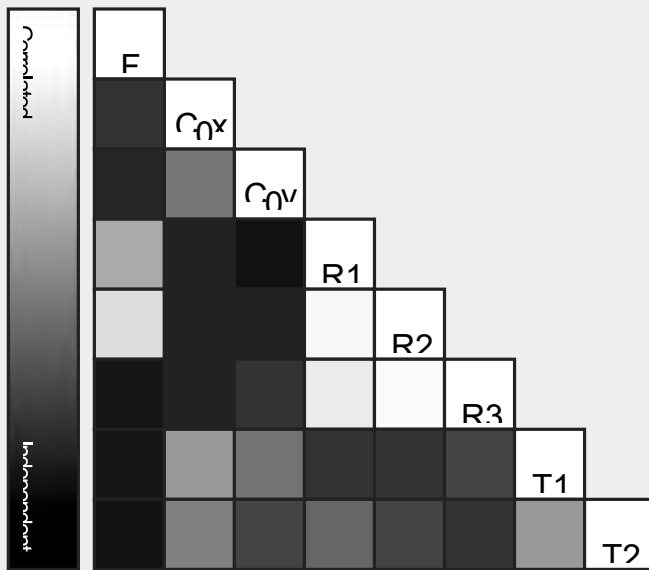
Red and yellow areas indicate low overlap, for which poor results may be generated. Green areas indicate an overlap of over 5 images for every pixel. Good quality results will be generated as long as the number of keypoint matches is also sufficient for these areas (see Figure 5 for keypoint matches).

Bundle Block Adjustment Details

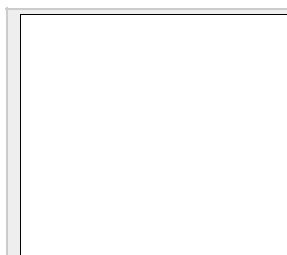
Number of 2D Keypoint Observations for Bundle Block Adjustment	10000016
Number of 3D Points for Bundle Block Adjustment	3281281
Mean Reprojection Error [pixels]	0.156

Internal Camera Parameters FC6310_8.8_4864x3648 (RGB).
Sensor Dimensions: 11.407 [mm] x 8.556 [mm]
 EXIF ID: FC6310_8.8_4864x3648

	Focal Length	Principal Point x	Principal Point y	R1	R2	R3	T1	T2
Initial Values	3666.955 [pixel] 8.600 [mm]	2432.001 [pixel] 5.704 [mm]	1823.999 [pixel] 4.278 [mm]	0.004	- 0.017	0.019	- 0.000	0.000
Optimized Values	3663.452 [pixel] 8.592 [mm]	2427.336 [pixel] 5.693 [mm]	1849.048 [pixel] 4.337 [mm]	0.005	- 0.018	0.018	0.001	0.000
Uncertainties (Sigma)	0.885 [pixel] 0.002 [mm]	0.083 [pixel] 0.000 [mm]	0.080 [pixel] 0.000 [mm]	0.000	0.000	0.000	0.000	0.000



The correlation between camera internal parameters determined by the bundle adjustment. White indicates a full correlation between the parameters, i.e., any change in one can be fully compensated by the other. Black indicates that the parameter is completely independent and is not affected by other parameters.



The number of Automatic Tie Points (ATPs) per pixel, averaged over all images of the camera is colour coded between black and white. White indicates that, on average, more than 16 have been extracted at the pixel location. Black indicates that, on average, 0 ATPs have been extracted at the pixel location. Click on the image to see the average direction and magnitude projection error for each pixel. Note that the vectors are scaled for better visualization. The indicates the magnitude of 1 pixel.

2D Keypoints Table

	Number of 2D Keypoints per Image	Number of Matched 2D Keypoints per Image
Median	62711	34682
Min	32974	5727
Max	86080	57115
Mean	63590	34483

🔍 3D Points from 2D Keypoint Matches

	Number of 3D Points Observed
In 2 Images	2003621
In 3 Images	589484
In 4 Images	255831
In 5 Images	138190
In 6 Images	86158
In 7 Images	57389
In 8 Images	40068
In 9 Images	29239
In 10 Images	21431
In 11 Images	16331
In 12 Images	12532
In 13 Images	9565
In 14 Images	6817

In 15 Images	5126
In 16 Images	3291
In 17 Images	2188
In 18 Images	1651
In 19 Images	1191
In 20 Images	650
In 21 Images	287
In 22 Images	146
In 23 Images	60
In 24 Images	24
In 25 Images	6
In 26 Images	5

2D Keypoint Matches

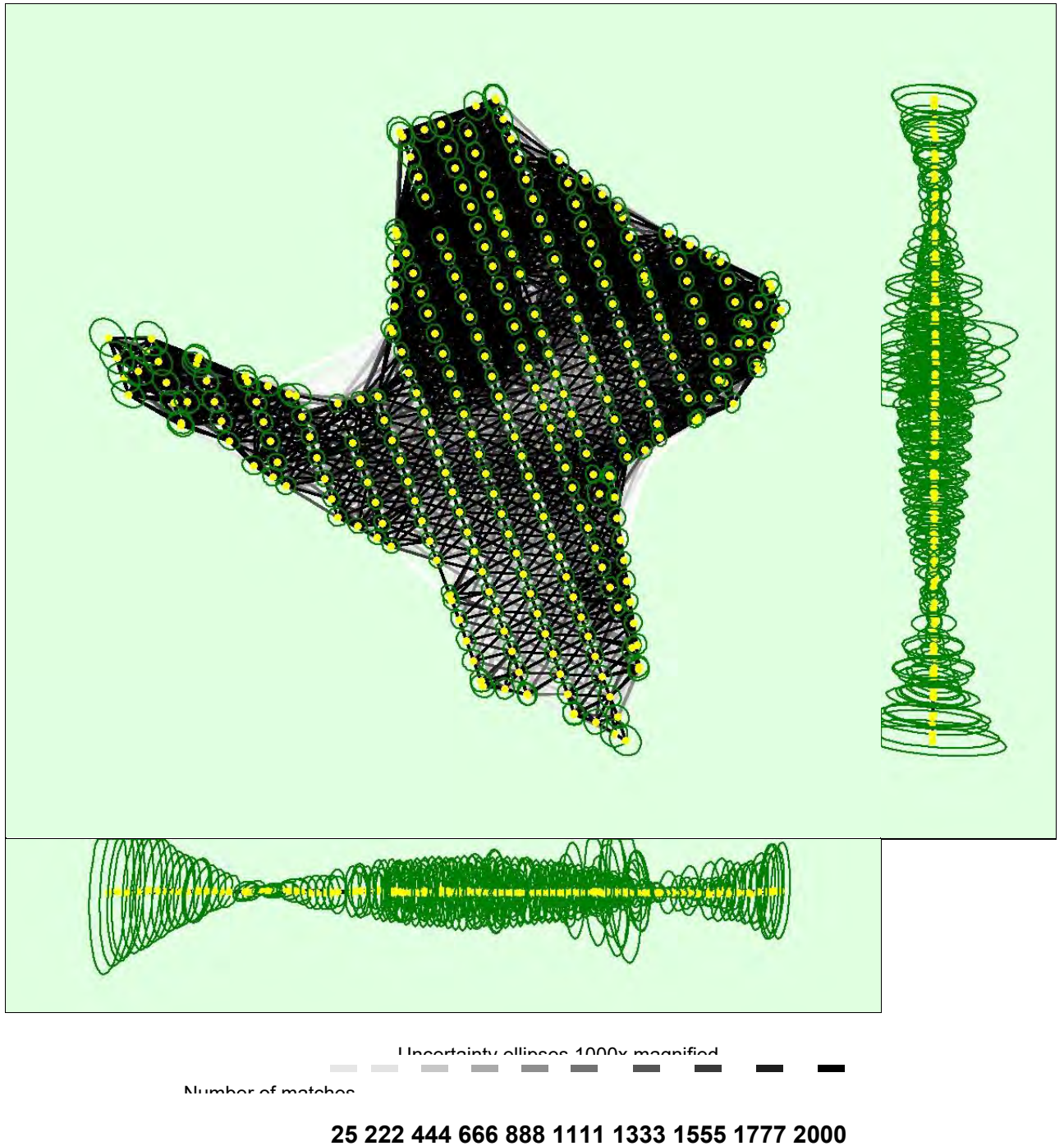


Figure 5: Computed image positions with links between matched images. The darkness of the links indicates the number of matched 2D keypoints between the images. Bright links indicate weak links and require manual tie points or more images. Dark green ellipses indicate the relative camera position uncertainty of the bundle block adjustment result.

Relative camera position and orientation uncertainties

	X [m]	Y [m]	Z [m]	Omega [degree]	Phi [degree]	Kappa [degree]
Mean	0.012	0.013	0.032	0.014	0.013	0.002
Sigma	0.003	0.003	0.019	0.007	0.007	0.001

Geolocation Details

? Ground Control Points

GCP Name	Accuracy XY/Z [m]	Error X [m]	Error Y [m]	Error Z [m]	Projection Error [pixel]	Verified/Marked
GCP1 (3D)	0.020/ 0.020	-0.000	-0.000	-0.006	0.161	5 / 5
GCP2 (3D)	0.020/ 0.020	-0.005	0.017	-0.000	0.097	6 / 6
GCP3 (3D)	0.020/ 0.020	0.011	0.013	0.002	0.110	10 / 10
GCP4 (3D)	0.020/ 0.020	-0.001	0.002	-0.005	0.069	8 / 8
GCP5 (3D)	0.020/ 0.020	0.003	-0.004	0.012	0.049	7 / 7
GCP7 (3D)	0.020/ 0.020	0.009	0.005	-0.008	0.289	7 / 7
GCP8 (3D)	0.020/ 0.020	0.004	-0.008	-0.006	0.531	12 / 12
GCP9 (3D)	0.020/ 0.020	-0.002	-0.003	-0.001	0.128	18 / 18
GCP10 (3D)	0.020/ 0.020	0.002	0.002	0.001	0.125	12 / 12

GCP11 (3D)	0.020/ 0.020	-0.009	0.004	0.001	0.112	8 / 8
GCP12 (3D)	0.020/ 0.020	-0.013	-0.004	-0.003	0.124	8 / 8
GCP15 (3D)	0.020/ 0.020	0.006	0.003	-0.013	0.282	10 / 10
GCP16 (3D)	0.020/ 0.020	0.007	-0.001	0.007	0.104	10 / 10
GCP17 (3D)	0.020/ 0.020	0.001	-0.001	0.002	0.064	21 / 21
GCP19 (3D)	0.020/ 0.020	-0.004	-0.007	0.005	0.067	14 / 14
GCP20 (3D)	0.020/ 0.020	0.003	-0.005	-0.000	0.109	17 / 17
GCP21 (3D)	0.020/ 0.020	0.003	-0.003	-0.010	0.071	15 / 15
GCP23 (3D)	0.020/ 0.020	-0.004	-0.009	-0.000	0.056	13 / 13
Mean [m]		0.000614	- 0.000011	- 0.001415		
Sigma [m]		0.006157	0.006484	0.006047		
RMS Error [m]		0.006188	0.006484	0.006210		

Localisation accuracy per GCP and mean errors in the three coordinate directions. The last column counts the number of calibrated images where the GCP has been automatically verified vs manually marked.

🔍 Absolute Geolocation Variance

Min Error [m]	Max Error [m]	Geolocation Error X [%]	Geolocation Error Y [%]	Geolocation Error Z [%]
-	-15.00	0.00	0.00	0.00
-15.00	-12.00	0.00	0.00	0.00
-12.00	-9.00	0.00	5.86	0.00
-9.00	-6.00	2.07	10.00	0.00
-6.00	-3.00	6.21	13.10	0.69
-3.00	0.00	38.97	22.41	45.52
0.00	3.00	43.45	19.31	53.79
3.00	6.00	9.31	11.38	0.00
6.00	9.00	0.00	11.72	0.00
9.00	12.00	0.00	5.17	0.00
12.00	15.00	0.00	1.03	0.00
15.00	-	0.00	0.00	0.00
Mean [m]		-0.560739	1.586192	-92.999350
Sigma [m]		5.590619	2.416829	1.265604
RMS Error [m]		5.618670	2.890860	93.007961

Min Error and Max Error represent geolocation error intervals between -1.5 and 1.5 times the maximum accuracy of all the images. Columns X, Y, and Z show the percentage of images with geolocation errors within the predefined error intervals. The geolocation error is the difference between the initial and computed image positions. Note that the image geolocation errors do not correspond to the accuracy of the observed 3D points.

Geolocation Bias	X	Y	Z
Translation [m]	-1.586192	0.560739	-92.999350

Bias between image initial and computed geolocation given in output coordinate system.

? Relative Geolocation Variance

Relative Geolocation Error	Images X [%]	Images Y [%]	Images Z [%]
[-1.00, 1.00]	97.24	58.97	100.00
[-2.00, 2.00]	100.00	92.07	100.00
[-3.00, 3.00]	100.00	100.00	100.00
Mean of Geolocation Accuracy [m]	5.000000	5.000000	10.000000
Sigma of Geolocation Accuracy [m]	0.000000	0.000000	0.000000

Images X, Y, and Z, represent the percentage of images with a relative geolocation error in X, Y, and Z.

Geolocation Orientational Variance	RMS [degree]
Omega	0.712
Phi	0.757
Kappa	6.785

Geolocation RMS error of the orientation angles given by the difference between the initial and computed image orientation angles.

Initial Processing Details

System Information

Hardware	CPU: Intel Core(TM) i7-8565U CPU @ 1.80GHz
----------	--

	RAM: 16IGPU: Intel(R) UHD Graphics 620 (Driver: 26.20.100.8141)
Operating System	Windows 10 Home Single Language, 64-bit

Coordinate Systems

Image Coordinate System	WGS 84 (EGM 96 Geoid)
Ground Control Point (GCP) Coordinate System	Hartebeesthoek94 / Lo19 (EGM 96 Geoid)
Output Coordinate System	Hartebeesthoek94 / Lo19 (EGM 96 Geoid)

Processing Options

Detected Template	No Template Available
Keypoints Image Scale	Full, Image Scale: 1
Advanced: Matching Image Pairs	Aerial Grid or Corridor
Advanced: Matching Strategy	Use Geometrically Verified Matching: no
Advanced: Keypoint Extraction	Targeted Number of Keypoints: Automatic
Advanced: Calibration	Calibration Method: Standard Internal Parameters Optimization: All External Parameters Optimization: All Rematch: Auto, yes

Point Cloud Densification details

Processing Options

Image Sc ^{1/2}	multiscale, 1/2 (Half image size, Default)
Point Density	Optimal
Minimum Number of Matches	3

3D Textured Mesh Generation	yes
3D Textured Mesh Settings:	Resolution: Medium Resolution (default) Colour Balancing: no
LOD	Generated: no
Advanced: 3D Textured Mesh Settings	Sample Density Divider: 1
Advanced: Image Groups	group1
Advanced: Use Processing Area	yes
Advanced: Use Annotations	yes
Time for Point Cloud Densification	01h:30m:11s
Time for Point Cloud Classification	NA
Time for 3D Textured Mesh Generation	18m:30s

Results

Number of Processed Clusters	2
Number of Generated Tiles	4
Number of 3D Densified Points	36348581
Average Density (per m ³)	64.95

DSM. Orthomosaic and Index Details

Processing Options

DSM and Orthomosaic Resolution	1 x GSD (3.43 [cm/pixel])
DSM Filters	Noise Filtering: yes Surface Smoothing: yes, Type: Sharp

Raster DSM	Generated: yes Method: Inverse Distance Weighting Merge Tiles: yes
Orthomosaic	Generated: yes Merge Tiles: yes GeoTIFF Without Transparency: no Google Maps Tiles and KML: no
Grid DSM	Generated: yes, Spacing [cm]: 500
Time for DSM Generation	48m:14s
Time for Orthomosaic Generation	59m:02s
Time for DTM Generation	00s
Time for Contour Lines Generation	00s
Time for Reflectance Map Generation	00s
Time for Index Map Generation	00s

Quality Report



Generated with Pix4Dmapper version 4.6.4

! **Important:** Click on the different icons for:

- ?** Help to analyze the results in the Quality Report
- i** Additional information about the sections

💡 Click [here](#) for additional tips to analyze the Quality Report

Summary

Project	Biff_140m
Processed	2021-07-08 19:02:19
Camera Model Name(s)	FC6310_8.8_4864x3648 (RGB)
Average Ground Sampling Distance (GSD)	3.88 cm / 1.53 in
Area Covered	0.583 km ² / 58.3100 ha / 0.23 sq. mi. / 144.1617 acres

Quality Check

? Images	median of 47784 key points per image	✓
? Dataset	212 out of 212 images calibrated (100%), all images enabled	✓
? Camera Optimization	0.09% relative difference between initial and optimized internal camera parameters	✓
? Matching	median of 29094.9 matches per calibrated image	✓

<p>Georeferencing</p>	<p>yes, 18 GCPs (18 3D), mean RMS error = 0.005 m</p>	<p>✓</p>
------------------------------	---	----------

Preview

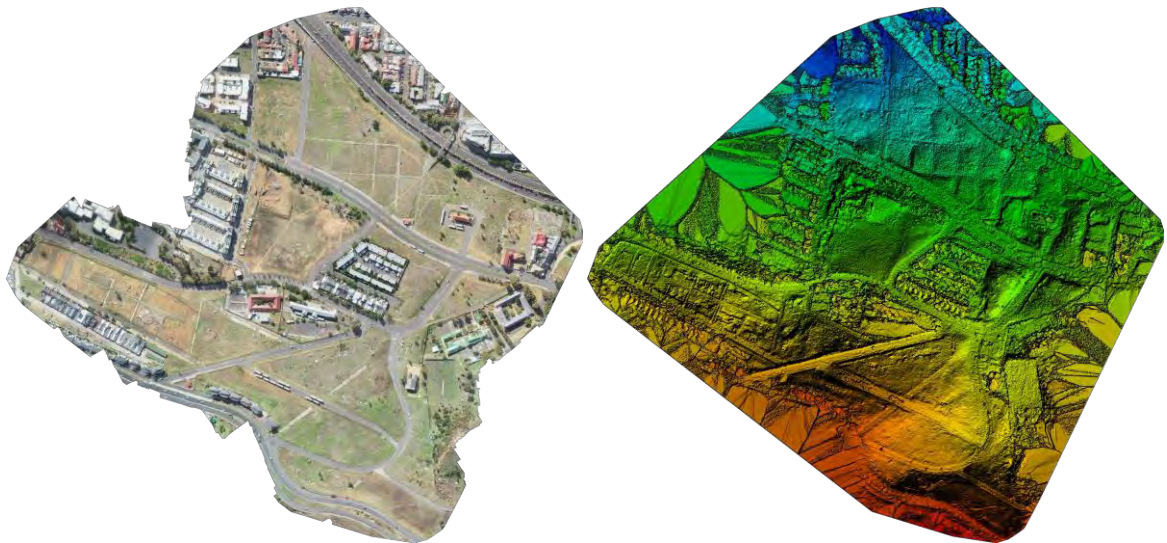


Figure 1: Orthomosaic and the corresponding sparse Digital Surface Model (DSM) before densification.

Calibration Details

Number of Calibrated Images	212 out of 212
Number of Geolocated Images	212 out of 212

Initial Image Positions

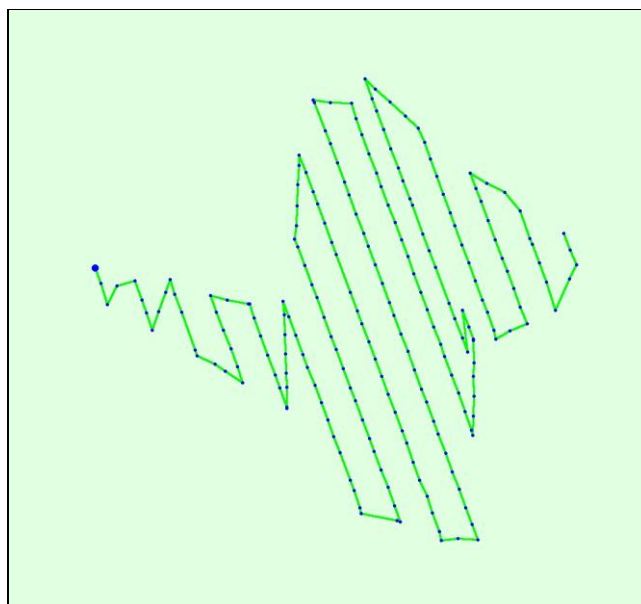
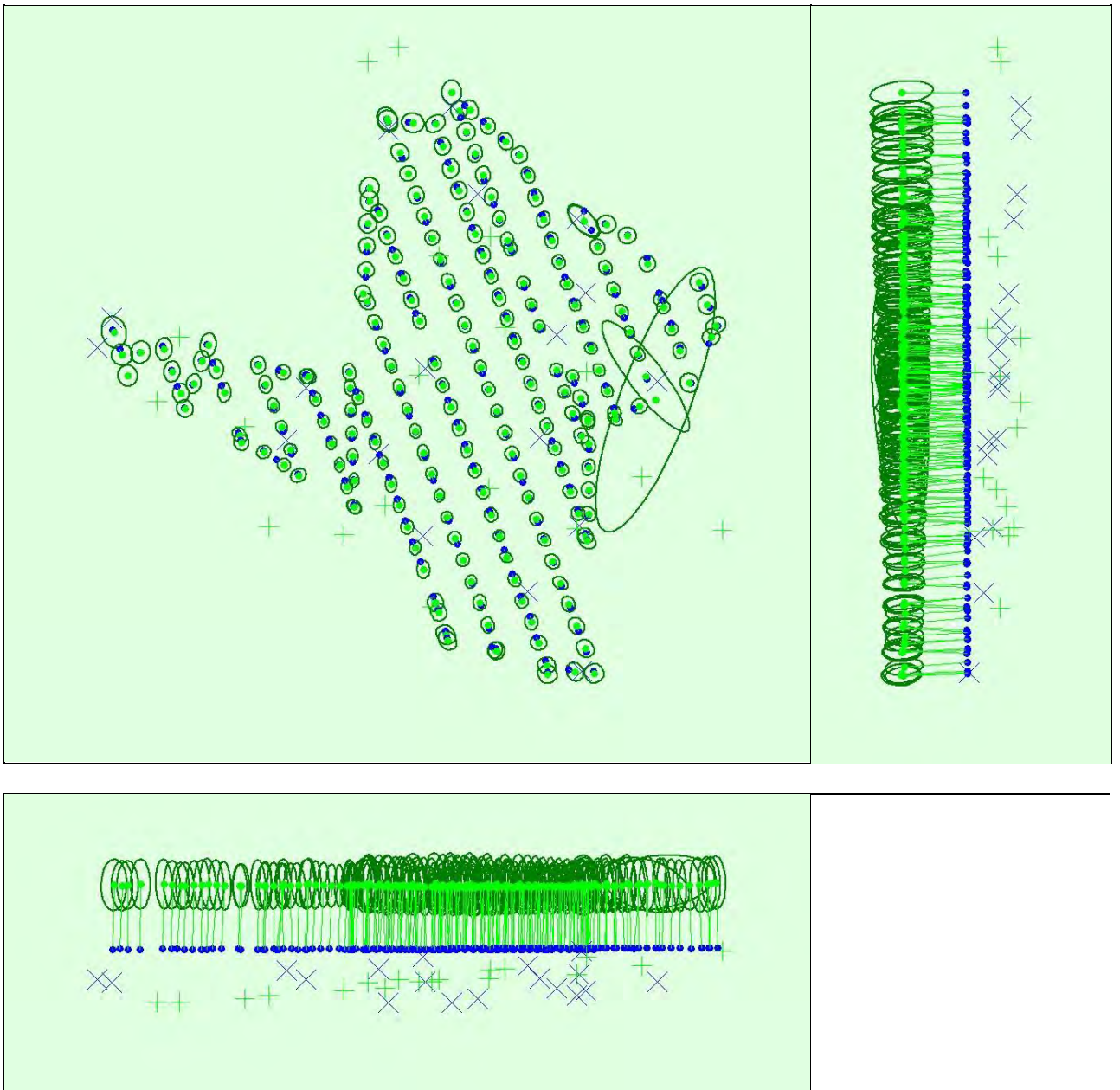


Figure 2: Top view of the initial image position. The green line follows the position of the images in time, starting from the large blue dot.

Computed Image/GCPs/Manual Tie Point Positions



Uncertainty ellipses 1000x magnified

Figure 3: Offset between initial (blue dots) and computed (green dots) image positions as well as the offset between the GCP's initial positions (blue crosses) and their computed positions (green crosses) in the top-view (XY plane), front-view (XZ plane), and side-view (YZ plane). Dark green ellipses indicate the absolute position uncertainty of the bundle block adjustment result.

Absolute camera position and orientation uncertainties

	X [m]	Y [m]	Z [m]	Omega [degree]	Phi [degree]	Kappa [degree]
Mean	0.012	0.014	0.037	0.005	0.005	0.001
Sigma	0.007	0.014	0.005	0.003	0.005	0.001

? Overlap

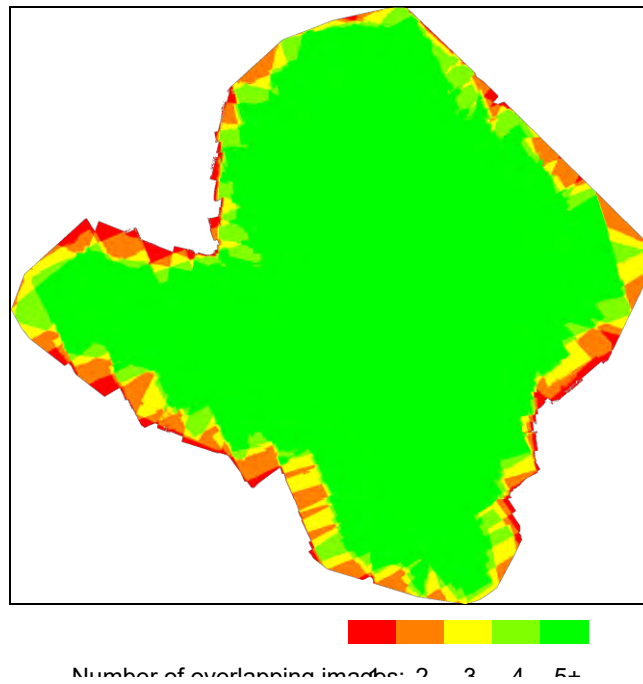


Figure 4: Number of overlapping images computed for each pixel of the orthomosaic.

Red and yellow areas indicate low overlap, for which poor results may be generated. Green areas indicate an overlap of over 5 images for every pixel. Good quality results will be generated as long as the number of keypoint matches is also sufficient for these areas (see Figure 5 for keypoint matches).

Bundle Block Adjustment Details

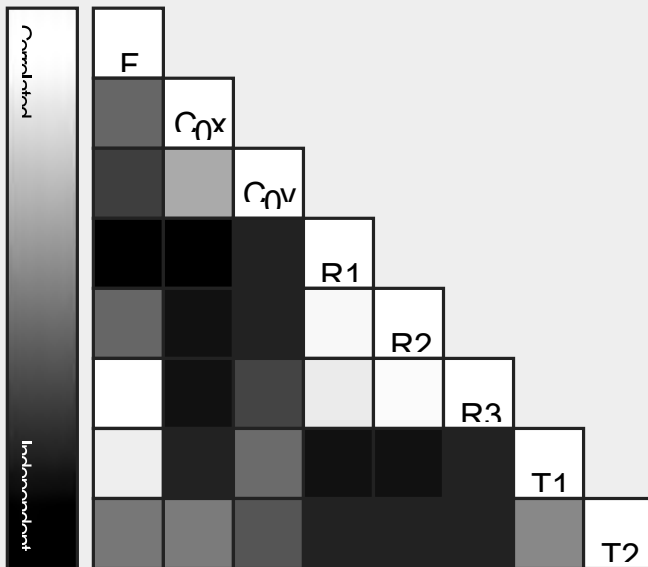
Number of 2D Keypoint Observations for Bundle Block Adjustment	6095996
Number of 3D Points for Bundle Block Adjustment	1917610
Mean Reprojection Error [pixels]	0.145

? Internal Camera Parameters

FC6310_8.8_4864x3648 (RGB). Sensor Dimensions: 11.407 [mm] x 8.556 [mm]

EXIF ID: FC6310_8.8_4864x3648

	Focal Length	Principal Point x	Principal Point y	R1	R2	R3	T1	T2
Initial Values	3666.955 [pixel] 8.600 [mm]	2432.001 [pixel] 5.704 [mm]	1823.999 [pixel] 4.278 [mm]	0.004	- 0.017	0.019	- 0.000	0.000
Optimized Values	3670.396 [pixel] 8.608 [mm]	2428.207 [pixel] 5.695 [mm]	1849.344 [pixel] 4.337 [mm]	0.003	- 0.019	0.020	0.001	0.000
Uncertainties (Sigma)	0.948 [pixel] 0.002 [mm]	0.098 [pixel] 0.000 [mm]	0.098 [pixel] 0.000 [mm]	0.000	0.000	0.000	0.000	0.000



The correlation between camera internal parameters determined by the bundle adjustment. White indicates a full correlation between the parameters, i.e., any change in one can be fully compensated by the other. Black indicates that the parameter is completely independent and is not affected by other parameters.

	<p>The number of Automatic Tie Points (ATPs) per nival, averaged over all images of the camera, is colour coded between black and white. White indicates that, on average, more than 16 have been extracted at the nival location. Black indicates that, on average, 0 ATPs have been extracted at the nival location. Click on the image to see the average direction and magnitude of the projection error for each nival. Note that the vectors are scaled for better visualization. The length of the vector indicates the magnitude of 1 nival.</p>
--	--

2D Keypoints Table

	Number of 2D Keypoints per Image	Number of Matched 2D Keypoints per Image
Median	47784	29095
Min	26183	169
Max	69340	46255
Mean	48823	28755

3D Points from 2D Keypoint Matches

	Number of 3D Points Observed
In 2 Images	1106002
In 3 Images	347786
In 4 Images	164581
In 5 Images	93802
In 6 Images	61542
In 7 Images	41047
In 8 Images	29283
In 9 Images	21286
In 10 Images	16083

In 11 Images	11250
In 12 Images	7610
In 13 Images	5872
In 14 Images	4005
In 15 Images	2913
In 16 Images	1775
In 17 Images	1120
In 18 Images	719
In 19 Images	462
In 20 Images	290
In 21 Images	103
In 22 Images	63
In 23 Images	15
In 26 Images	1

2D Keypoint Matches

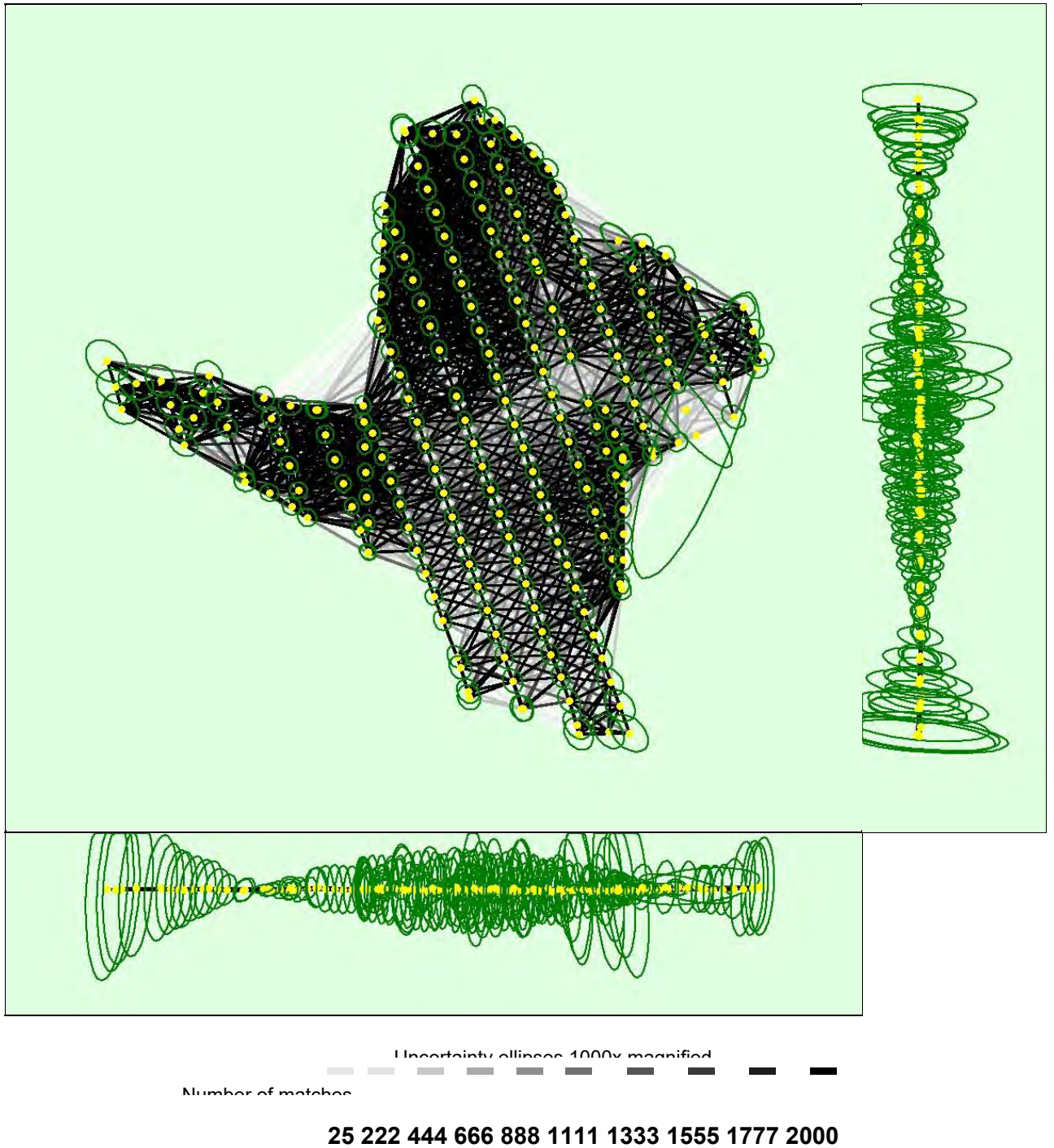


Figure 5: Computed image positions with links between matched images. The darkness of the links indicates the number of matched 2D keypoints between the images. Bright links indicate weak links and require manual tie points or more images. Dark green ellipses indicate the relative camera position uncertainty of the bundle block adjustment result.

Relative camera position and orientation uncertainties

	X [m]	Y [m]	Z [m]	Omega [degree]	Phi [degree]	Kappa [degree]
Mean	0.014	0.016	0.036	0.016	0.015	0.002
Sigma	0.007	0.014	0.023	0.009	0.009	0.001

Geolocation Details

? Ground Control Points

GCP Name	Accuracy XY/Z [m]	Error X [m]	Error Y [m]	Error Z [m]	Projection Error [pixel]	Verified/Marked
GCP1 (3D)	0.020/ 0.020	-0.004	-0.002	-0.009	0.459	5 / 5
GCP2 (3D)	0.020/ 0.020	-0.006	0.002	-0.001	0.056	6 / 6
GCP3 (3D)	0.020/ 0.020	0.001	0.007	-0.003	0.039	12 / 12
GCP4 (3D)	0.020/ 0.020	0.003	-0.007	0.020	0.035	5 / 5
GCP5 (3D)	0.020/ 0.020	0.006	-0.005	0.027	0.011	3 / 3
GCP7 (3D)	0.020/ 0.020	0.005	0.006	-0.005	0.105	15 / 15
GCP8 (3D)	0.020/ 0.020	-0.001	-0.000	0.005	0.074	11 / 11
GCP9 (3D)	0.020/ 0.020	-0.004	-0.003	0.002	0.062	17 / 17
GCP10 (3D)	0.020/ 0.020	-0.002	-0.000	0.002	0.026	15 / 15

GCP11 (3D)	0.020/ 0.020	-0.001	0.006	-0.001	0.083	11 / 11
GCP12 (3D)	0.020/ 0.020	-0.003	-0.005	-0.006	0.077	10 / 10
GCP15 (3D)	0.020/ 0.020	0.004	0.005	-0.005	0.069	8 / 8
GCP16 (3D)	0.020/ 0.020	0.002	0.001	-0.008	0.116	13 / 13
GCP17 (3D)	0.020/ 0.020	0.003	-0.002	0.002	0.067	21 / 21
GCP19 (3D)	0.020/ 0.020	0.001	-0.006	-0.004	0.107	13 / 13
GCP20 (3D)	0.020/ 0.020	0.002	-0.007	0.008	0.090	15 / 15
GCP21 (3D)	0.020/ 0.020	0.001	-0.001	0.001	0.029	14 / 14
GCP23 (3D)	0.020/ 0.020	-0.001	-0.004	-0.004	0.116	11 / 11
Mean [m]		0.000349	- 0.000747	0.001114		
Sigma [m]		0.003212	0.004441	0.009068		
RMS Error [m]		0.003231	0.004503	0.009137		

Localisation accuracy per GCP and mean errors in the three coordinate directions. The last column counts the number of calibrated images where the GCP has been automatically verified vs manually marked.

🔍 Absolute Geolocation Variance

Min Error [m]	Max Error [m]	Geolocation Error X [%]	Geolocation Error Y [%]	Geolocation Error Z [%]
-	-15.00	0.00	0.47	0.00
-15.00	-12.00	0.00	0.47	0.00
-12.00	-9.00	0.94	8.49	0.00
-9.00	-6.00	1.89	8.49	0.00
-6.00	-3.00	8.96	13.21	6.60
-3.00	0.00	35.85	17.45	38.68
0.00	3.00	41.51	19.81	52.83
3.00	6.00	10.38	12.74	1.89
6.00	9.00	0.00	12.74	0.00
9.00	12.00	0.00	5.66	0.00
12.00	15.00	0.47	0.47	0.00
15.00	-	0.00	0.00	0.00
Mean [m]		-1.359551	1.117315	-94.852556
Sigma [m]		6.041455	2.696257	1.696007
RMS Error [m]		6.192541	2.918595	94.867717

Min Error and Max Error represent geolocation error intervals between -1.5 and 1.5 times the maximum accuracy of all the images. Columns X, Y, and Z show the percentage of images with geolocation errors within the predefined error intervals. The geolocation error is the difference between the initial and computed image positions. Note that the image geolocation errors do not correspond to the accuracy of the observed 3D points.

Geolocation Bias	X	Y	Z
Translation [m]	-1.117315	1.359551	-94.852556

Bias between image initial and computed geolocation given in output coordinate system.

? Relative Geolocation Variance

Relative Geolocation Error	Images X [%]	Images Y [%]	Images Z [%]
[-1.00, 1.00]	95.28	53.77	100.00
[-2.00, 2.00]	99.06	91.98	100.00
[-3.00, 3.00]	100.00	99.53	100.00
Mean of Geolocation Accuracy [m]	5.000000	5.000000	10.000000
Sigma of Geolocation Accuracy [m]	0.000000	0.000000	0.000000

Images X, Y, and Z, represent the percentage of images with a relative geolocation error in X, Y, and Z.

Geolocation Orientational Variance	RMS [degree]
Omega	1.014
Phi	0.679
Kappa	7.601

Geolocation RMS error of the orientation angles given by the difference between the initial and computed image orientation angles.

Initial Processing Details

System Information

Hardware	CPU: Intel(R) Core(TM) i7-8565U CPU @ 1.80GHz
----------	---

	RAM: 16GB GPU: Intel(R) UHD Graphics 620 (Driver: 26.20.100.8141)
Operating System	Windows 10 Home Single Language, 64-bit

Coordinate Systems

Image Coordinate System	WGS 84 (EGM 96 Geoid)
Ground Control Point (GCP) Coordinate System	Hartebeesthoek94 / Lo19 (EGM 96 Geoid)
Output Coordinate System	Hartebeesthoek94 / Lo19 (EGM 96 Geoid)

Processing Options

Detected Template	No Template Available
Keypoints Image Scale	Full, Image Scale: 1
Advanced: Matching Image Pairs	Aerial Grid or Corridor
Advanced: Matching Strategy	Use Geometrically Verified Matching: no
Advanced: Keypoint Extraction	Targeted Number of Keypoints: Automatic
Advanced: Calibration	Calibration Method: Standard Internal Parameters Optimization: All External Parameters Optimization: All Rematch: Auto, yes

Point Cloud Densification details

Processing Options

Image Scale	multiscale, 1/2 (Half image size, Default)
Point Density	Optimal

Minimum Number of Matches	3
3D Textured Mesh Generation	yes
3D Textured Mesh Settings:	Resolution: Medium Resolution (default) Colour Balancing: no
LOD	Generated: no
Advanced: 3D Textured Mesh Settings	Sample Density Divider: 1
Advanced: Image Groups	group1
Advanced: Use Processing Area	yes
Advanced: Use Annotations	yes
Time for Point Cloud Densification	50m:11s
Time for Point Cloud Classification	NA
Time for 3D Textured Mesh Generation	13m:18s

Results

Number of Generated Tiles	1
Number of 3D Densified Points	26581472
Average Density (per m ³)	50.83

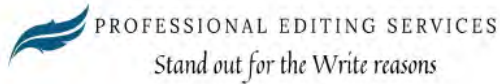
DSM. Orthomosaic and Index Details

Processing Options

DSM and Orthomosaic Resolution	1 x GSD (3.88 [cm/pixel])
DSM Filters	Noise Filtering: yes

	Surface Smoothing: yes, Type: Sharp
Raster DSM	Generated: yes Method: Inverse Distance Weighting Merge Tiles: yes
Orthomosaic	Generated: yes Merge Tiles: yes GeoTIFF Without Transparency: no Google Maps Tiles and KML: no
Grid DSM	Generated: yes, Spacing [cm]: 500
Time for DSM Generation	40m:45s
Time for Orthomosaic Generation	44m:01s
Time for DTM Generation	00s
Time for Contour Lines Generation	00s
Time for Reflectance Map Generation	00s
Time for Index Map Generation	00s

Appendix H Editor's Certificate



Gerald T du Preez
PhD

22 Clivia Avenue
Brantwood, Kuils River, 7580
+27 (21) 903-3145 | +27 (83) 325 1842
gerald9@gmail.com

Certificate of Editing

This serves to confirm that copy-editing and proofreading services were rendered to
for a master's thesis entitled

An assessment of UAV-generated digital elevation model using ground surveying techniques

by

Thabani Thuse

with final word count of 50 015 on 1 August 2022

I am a member of the Professional Editors' Guild (member number DUP015) and commit to the following codes of practice (among others):

- *I have completed the work independently and did not sub-contract it out*
- *I kept to the agreed deadlines and/or communicated changes within reasonable time frames*
- *I treated all work as confidential and maintained objectivity in editing*
- *I did not accept work that could be considered unlawful, dishonest or contrary to public interest*

I uphold the following editing standards:

- *proofreading for mechanical errors such as spelling, punctuation, grammar*
- *copy-editing that includes commenting on, but not correcting, structure, organisation and logical flow of content, formatting (headings, page numbers, table of contents, etc.), eliminating unnecessary repetition*
- *checking citation style is correct, punctuating as needed and flagging missing or incorrect references*
- *commenting on suspected plagiarism and missing sources*
- *returning the document with track changes for the author to accept*

I confirm that I have met the above standards of editing and professional ethical practice. The content of the work edited remains that of the student.

Gerald T du Preez, PhD

Membership: Southern African Freelancers' Association and Professional Editors' Guild (Membership #DUP015)

Appendix I Plagiarism Report

